

---

**Analysis, Optimization and Application  
of AAV Capsid Assembly using *Escherichia coli***

---

**Dissertation**

Zur Erlangung des akademischen Grades

*Doctor rerum naturalium (Dr. rer. nat.)*

Zelluläre und Molekulare Biotechnologie

Technische Fakultät

Universität Bielefeld

vorgelegt von

**Dinh To Le**

geboren in Binh Dinh, Vietnam

Bielefeld

2021



Die vorliegende Arbeit entstand in der Zeit von  
Oktober 2017 bis Februar 2021  
in der Arbeitsgruppe  
- Zelluläre und Molekulare Biotechnologie -  
an der Technische Fakultät der Universität Bielefeld  
unter Leitung von  
**Herrn Prof. Dr. Kristian M. Müller**

1. Gutachter: Prof. Dr. Kristian M. Müller  
Arbeitsgruppe Zelluläre und Molekulare Biotechnologie,  
Technische Fakultät, Universität Bielefeld
2. Gutachter: Prof. Dr. Alexander Grünberger  
Arbeitsgruppe Multiscale Bioengineering,  
Technische Fakultät, Universität Bielefeld



## Acknowledgements

First of all, I would like to thank my supervisor Prof. Kristian Müller for giving me the opportunity to work in the ZMB lab. Prof. Müller supported and inspired me throughout the years of my study.

I am thankful to Prof. Alexander Grünberger for accepting to review this thesis, Prof. Karl Friehs and Dr. Raimund Hoffrogge for being part of the examining board.

My special thank goes to Marco Radukic for supporting me during the years. It was lucky to work with Marco on our projects.

I want to thank my colleagues Rebecca Feiner, Julian Teschner, Kathrin Teschner, Lennard Karsten, Claire Rothschild, Georg Falck, Charlotte Mann, Marius Schöller, Thilo Pohle and Philipp Borchert for their help and insightful discussions of my work, the students Lukas Becker, Lucas Krause, Albin Thaqi, Jassin Hamidi for their assistance, and AG Zellkulturtechnik members for their kind help.

Many thanks to Dr. Olaf Behrsing, Ann-Christin Moritzer, Prof. Dario Anselmetti, Dr. Yvonne Hannappel for the great collaborations.

Many thanks also go to Prof. Nguyen Duc Hoang for supporting me to apply for the DAAD scholarship, Thanh Thao 08CS, Thanh Quang 08CS for their kind support during the scholarship application procedure, Linh and Thung for being friends and helping me in Bielefeld, Tan Le for his kind assistance in Vietnam.

Finally, I would like to thank my father, my mother, my sisters and especially my wife for supporting me in pursuing my doctoral thesis in Germany.



## Publications

**Dinh To Le**, Marco T. Radukic, Kristian M. Müller. Adeno-associated virus capsid protein expression in *Escherichia coli* and chemically defined capsid assembly. *Scientific Reports*, Volume 9, Issue 1, 18631 (2019). doi.org/10.1038/s41598-019-54928-y.

**Dinh To Le**, Marco T. Radukic, Kristian M. Müller. AAV Capsid Assembly Using *Escherichia coli*. *Molecular Therapy*, Volume 28, Issue 4, Supplement 1, Page 79 (2020). doi.org/10.1016/j.ymthe.2020.04.019.

**Dinh To Le** and Kristian Müller. *In vitro* assembly of virus-like particles and their applications. *Life*, Volume 11, Issue 4, 334 (2021). doi.org/10.3390/life11040334.

**Dinh To Le**, Olaf Behrsing, Claire Rothschild, Marco T. Radukic, Katja M. Arndt, Kristian M. Müller. AAV capsid proteins fused with SARS-CoV-2 RBD or RBM: Expression in *E. coli*, *in-vitro* assembly, and characterization. *Molecular Therapy*, Volume 29, Issue 4, Supplement 1, Page 357 (2021). doi.org/10.1016/j.ymthe.2021.04.019.

**Dinh To Le**, Marco T. Radukic, Kathrin Teschner, Lukas Becker, Kristian M. Müller. Expression and concomitant assembly of adeno-associated virus-like particles in *Escherichia coli*. (In preparation).

Marco T. Radukic, **Dinh To Le**, Kristian M. Müller. Nucleic Acid Sequence Composition of the Oxford – AstraZeneca Vaccine ChAdOx1 nCoV-19 (AZD1222, Vaxzevria). *Research Square* (2021). 10.21203/rs.3.rs-799338/v1.

## Posters

**Dinh To Le**, Marco T. Radukic, Kristian M. Müller. Adeno-associated virus capsid protein expression in *Escherichia coli* and assembly *in vitro*. The 1st International Conference on Microbiology and One Health, VNUHCM-University of Science, Vietnam, 227 Nguyen Van Cu, District 5, Ho Chi Minh City, Vietnam, 2018.

**Dinh To Le**, Marco T. Radukic, Kristian M. Müller. AAV Capsid Assembly Using *Escherichia coli*. The American Society of Gene & Cell Therapy's 23rd Annual Meeting, Boston, MA, US, May 12-15, 2020.

**Dinh To Le**, Olaf Behrsing, Claire Rothschild, Marco T. Radukic, Katja M. Arndt, Kristian M. Müller. AAV Capsid Proteins Fused with SARS-CoV-2 RBD or RBM: Expression in *E. coli*, *In-vitro* Assembly, and Characterization. The American Society of Gene & Cell Therapy's 24th Annual Meeting, May 11-14, 2021.



# Contents

1. Abstract .....	1
2. Introduction .....	3
2.1. Adeno-associated virus vectors .....	3
2.1.1. AAV biology .....	3
2.1.2. rAAV applications and production .....	4
2.2. Virus-like particles .....	4
2.2.1. Capsid protein production .....	5
2.2.1.1. Protein refolding .....	5
2.2.2. Assembly of virus-like particles .....	6
2.2.2.1. <i>In vivo</i> assembly of VLPs .....	6
2.2.2.2. <i>In vitro</i> assembly of VLPs .....	7
2.2.3. Virus-like particle characterization .....	9
2.2.4. Virus-like particle applications .....	10
2.2.4.1. Vaccine development .....	10
2.2.4.2. Nucleic acid and drug delivery .....	10
3. Aim .....	13
4. Results and Discussion .....	15
4.1. AAV2 capsid protein expression and <i>in vitro</i> assembly .....	15
4.1.1. AAV2 VP3 capsid protein expression and purification .....	15
4.1.2. AAV2 VP3 VLP assembly <i>in vitro</i> and characterization .....	16
4.1.3. <i>In-vitro</i> AAV2 VLP assembly yield improvement by AAP2 supplement .....	19
4.1.4. <i>In-vitro</i> AAV2 VLP modification .....	21
4.2. Expression and concomitant assembly of AAV5 VLPs inside <i>E. coli</i> .....	23
4.2.1. AAV5 VP3 capsid protein expression and concomitant assembly in <i>E. coli</i> .....	23
4.2.2. AAV5 VP3 VLP purification and characterization .....	24
4.2.3. Co-expression of AAV5 VP3 and AAP5 in <i>E. coli</i> improved capsid assembly yields .....	26
4.3. Applications of <i>in vitro</i> AAV assembly .....	27
4.3.1. AAV2 VP3 capsid proteins fused with SARS-CoV-2 RBD or RBM: Expression in <i>E. coli</i> , <i>in-vitro</i> assembly and functional characterization .....	28
4.3.1.1. AAV2 VP3_RBM and VP3_RBD expression in <i>E. coli</i> and purification .....	28
4.3.1.2. <i>In vitro</i> refolding and concomitant assembly of AAV2 VP3_RBM and VP3_RBD proteins to VLPs, and VLP characterization .....	29
4.3.1.3. Expression of GFP fused with RBD protein in 293-F cells .....	31
4.3.1.4. Immunization of mice and immune response .....	32
4.3.2. <i>In vitro</i> encapsidation of DNA into AAV VLPs .....	36
4.3.2.1. Arginine-rich motif (ARM) fused with AAV5 VP3 capsid protein expression, purification and <i>in vitro</i> assembly .....	36
4.3.2.2. ssDNA production .....	37

4.3.2.3.	DNA encapsidation into ARM_VP3 VLPs.....	38
4.3.3.	<i>In vitro</i> AAV VLP chemical conjugation for imaging.....	40
4.3.3.1.	AAV2 VP3 VLP and FITC conjugation.....	40
4.3.3.2.	Internalization of FITC-conjugated VLPs .....	40
5.	Conclusion and Outlook.....	43
6.	Materials and Methods.....	45
6.1.	Materials .....	45
6.1.1.	Equipment.....	45
6.1.2.	Consumables.....	47
6.1.3.	Software and web servers .....	48
6.1.4.	Chemicals .....	48
6.1.5.	Buffers and solutions .....	51
6.1.6.	Phage, <i>E. coli</i> strains and eukaryotic cell lines.....	54
6.1.7.	Media .....	54
6.1.8.	Antibodies.....	55
6.1.9.	Kits.....	55
6.1.10.	Enzymes .....	56
6.1.11.	Ladders.....	56
6.1.12.	Oligonucleotides .....	56
6.1.13.	Plasmids .....	58
6.2.	Methods.....	58
6.2.1.	Molecular genetic methods.....	58
6.2.1.1.	Cultivation and storage of <i>E. coli</i> .....	58
6.2.1.2.	Preparation and heat shock transformation of chemically competent <i>E. coli</i> cells	58
6.2.1.3.	General cloning procedures.....	59
6.2.1.4.	ssDNA production .....	60
6.2.2.	Methods in protein biochemistry .....	60
6.2.2.1.	Recombinant protein expression and purification in <i>E. coli</i> and 293-F cells	60
6.2.2.2.	SDS-PAGE and western blot.....	61
6.2.3.	Biophysical measurements .....	62
6.2.3.1.	Dynamic light scattering .....	62
6.2.3.2.	Atomic force microscopy .....	62
6.2.3.3.	Transmission electron microscopy .....	62
6.2.4.	Cell culture techniques .....	62
6.2.4.1.	Cultivation and cryopreservation of eukaryotic cells .....	62
6.2.4.2.	Counting of eukaryotic cells.....	63
6.2.4.3.	ssDNA transfection.....	63
6.2.4.4.	Generation of transient HEK-293 cells displaying hACE2 receptors.....	63
6.2.5.	VLP and virological methods.....	63

6.2.5.1.	<i>In vitro and in vivo</i> assembly of AAV VLPs.....	63
6.2.5.2.	rAAV production in adherent HEK-293 cells .....	64
6.2.5.3.	AAV VLP and rAAV purification .....	64
6.2.5.4.	Dot blot assay.....	64
6.2.5.5.	ELISA.....	65
6.2.5.6.	AAV VLP internalization assay .....	65
6.2.5.7.	Cell binding assay .....	66
6.2.5.8.	DNA encapsidation into AAV VLP and ARM_VP3 VLP formation.....	66
6.2.5.9.	Determination of rAAV genomic titers and AAV VLP encapsidated DNA .....	66
6.2.5.10.	Cell transduction assay.....	67
6.2.5.11.	FITC conjugation to AAV VLPs, VLP agarose gel electrophoresis and FITC-labeled AAV VLP internalization.....	67
6.2.6.	Mouse experiment.....	68
6.2.6.1.	Mouse immunization and serum collection.....	68
6.2.6.2.	Serum ELISA.....	68
7.	References.....	69
8.	Appendix .....	95
8.1.	Supplementary information to section 4.1.....	95
8.2.	Supplementary information to section 4.2.....	96
8.3.	Appendix: Publications.....	98



## List of abbreviations

a.a.	amino acid
AAP	assembly-activating protein
AAV	adeno-associated virus
AAVR	adeno-associated virus receptor
AAV2	adeno-associated virus serotype 2
AAV5	adeno-associated virus serotype 5
ABTS	2,2'-326 Azinobis [3-ethylbenzothiazoline-6-sulfonic acid]-diammonium salt
ACE2	angiotensin-converting enzyme 2
AFM	atomic force microscopy
APS	ammonium persulfate
ARM	arginine-rich motif
BFDV	beak and feather disease virus
bp	base pair
BSA	Bovine serum albumin
B19	parvovirus B19 (primate erythroparvovirus 1)
CCMV	cowpea chlorotic mottle virus
DAPI	4',6-Diamidino-2-phenylindole
DLS	dynamic light scattering
DNA	deoxyribonucleic acid
DTT	dithiothreitol
EDTA	ethylenediaminetetraacetic acid
ELISA	enzyme-linked immunosorbent assay
EMA	The European Medicines Agency
FACS	fluorescence-activated cell sorting
FDA	The U.S. Food and Drug Administration
FCS	fetal calf serum
FITC	fluorescein 5-isothiocyanate
gc	genomic copies
GFP	green fluorescent protein
GuHCl	guanidine hydrochloride
HBSS	Hank's balanced salt solution

HBV	hepatitis B virus
HCV	hepatitis C virus
HEV	hepatitis E virus
HIV	human immunodeficiency virus
HPV	human papillomavirus
HSV	herpes simplex virus
HRP	horseradish peroxidase
IEX	ion-exchange chromatography
IMAC	immobilized metal-ion affinity chromatography
IPTG	isopropyl $\beta$ -D-thiogalactopyranoside
ITR	inverted terminal repeat
kb	Kilobase
kDa	Kilo-Dalton
LB	Lysogeny Broth (from Luri and Bertani)
MOI	multiplicities of infection
OD	optical density
ORF	open reading frame
PAGE	polyacrylamide gel electrophoresis
PBS	phosphate-buffered saline
PCR	polymerase chain reaction
PEI	polyethylenimine
PKD	polycystic kidney disease
RBD	receptor binding domain
RSV	human respiratory syncytial virus
RV	rotavirus
SARS-CoV-2	severe acute respiratory syndrome coronavirus 2
SV40	simian virus 40
sfGFP	superfolder green fluorescent protein
TEM	transmission electron microscopy
TBS	tris-buffered saline
VLP	virus-like particle
VP	viral protein

Commonly used abbreviations and SI units are not separately listed.

## 1. Abstract

Recombinant adeno-associated viruses (rAAV) are leading drugs in gene therapy with three products approved by the European Medicines Agency (EMA) and the Food and Drug Administration (FDA). Currently, rAAV vectors are evaluated in many ongoing clinical trials for treating rare genetic diseases and other therapies. Mammalian and insect cells have been utilized for rAAV production, but scaling to for the rapidly growing demand for rAAV in clinical trials remains challenging. Thus, a new AAV production technology is urgently needed. Meanwhile, AAV empty capsids as virus-like particles (VLP) produced in mammalian cells have raised increasing interest for vaccine development and drug delivery. This thesis established a new approach to produce AAV VLPs using *E. coli* and *in vitro* capsid formation. The use of these AAV VLPs for vaccine development and therapeutic delivery was also studied and strategies for DNA encapsidation were tested.

Among 13 known human and nonhuman primate AAV serotypes, AAV serotype 2 (AAV2) is the most studied and AAV serotype 5 (AAV5) is the most genetically divergent serotype. To analyze AAV capsid assembly, AAV2 and AAV5 VP3 capsid proteins were expressed in *E. coli*. AAV2 VP3 proteins formed inclusion bodies in *E. coli*, which were successfully purified and assembled into AAV2 VLPs in a chemically defined reaction. Contrary, AAV5 VP3 developed AAV5 VLPs inside *E. coli* cells. Recovery of the assembled AAV5 VLPs was straightforward via a one-step purification. Moreover, the supplement of AAV assembly-activating protein (AAP) into the AAV2 VLP assembly *in vitro* and the AAV5 VLP assembly in *E. coli* led to an increase of capsid formation yield. These findings provide the first evidence that AAV2 capsids can be developed in a defined reaction and AAV5 capsids can be formed inside *E. coli* cells.

The SARS-CoV-2 spike protein, in particular, its receptor-binding domain (RBD) containing the receptor-binding motif (RBM) mediates virus binding to the host cell receptor, and therefore RBD and RBM are lead candidates for SARS-CoV-2 subunit vaccine development. VLPs have been widely used in vaccine research due to their ability to strongly induce an immune response compared to the subunit protein alone. To assess the potential of AAV VLPs in vaccine research, RBD and RBM fused with AAV2 VP3 capsid proteins were expressed in *E. coli*. These fusion proteins were purified, then refolded and concomitantly assembled to VLPs. The refolded samples of AAV2 VP3\_RBD and VP3\_RBM containing VLPs were imaged by atomic force microscopy (AFM). AAV2 VP3\_RBD VLPs were recognized by an antibody binding the folded RBD. Immunization of mice with VP3\_RBM VLPs resulted in a high level of RBD-specific antibodies indicating SARS-CoV-2 specificity. However, VP3\_RBD VLPs induced strong antibody responses against the VP3 VLP scaffold, but a relatively low level of RBD-specific antibodies. These data suggest that VP3\_RBM VLP is a promising vaccine candidate for SARS-CoV-2.

## 1 Abstract

Packaging of DNA in AAV is proposed as an only partially understood active procedure in which the DNA enters formed capsids with the help of proteins. *In vitro*, passive encapsidation would be easier and thus an arginine-rich motif (ARM), a DNA-binding domain known to passively aid DNA packaging of many viruses, was incorporated at the N-terminus of the AAV5 VP3 capsid protein. AAV ssDNA was produced using phagemids and M13 helper phage. The produced circular ssDNA with an expression cassette flanked by AAV inverted terminal repeat sequences (ITRs) mediated protein expression in CHO-K1 cells. The ARM\_VP3 fusion protein was successfully obtained from *E. coli* and the *in-vitro* capsid assembly and DNA encapsidation resulted in VLPs and in protection of DNA from DNase I. However, these VLPs did not mediate protein expression in CHO-K1 cells. More studies are needed to productively encapsidate DNA in AAV capsids *in vitro*.

Fluorescent VLPs provide a tool for the analysis of VLP-cell interaction. In this study, FITC was chemically conjugated onto the formed particles via covalent bonds to visualize and image the AAV VLPs. The labeled VLPs internalized into human HeLa cells. This success opens opportunities to chemically couple a drug to AAV VLPs and label rAAV for different biological applications.

In summary, these studies show the first evidence that AAV capsids can be assembled in a chemically defined reaction or inside *E. coli* cells. The potentials of AAV VLPs for vaccine development, DNA encapsidation and imaging were also explored. These findings pave the way for using AAV VLPs in many different biological applications in the future.

## 2. Introduction

### 2.1. Adeno-associated virus vectors

#### 2.1.1. AAV biology

Adeno-associated virus (AAV) is a non-enveloped, 4.7 kb-single-stranded DNA (ssDNA) virus of 60 capsid proteins arranged in a T=1 icosahedral symmetry (20-25 nm in diameter, **Figure 1a**) and a member of the *Parvoviridae* family genus *Dependoparvovirus*. It is dependent on other helper viruses, such as adenovirus or herpes simplex virus (HSV) for replication. In the absence of helper viruses, AAV is known to integrate into a specific site in the human chromosome 19q13.4.<sup>1</sup>

Among currently 13 human and nonhuman primate serotypes, AAV serotype 2 (AAV2) is the best-studied member,<sup>2</sup> and AAV serotype 5 (AAV5) is the most genetically divergent AAV.<sup>3,4</sup> The AAV2 genome consists of two open-reading-frame (ORF) cassettes flanked by inverted terminal repeat (ITR) sequences (**Figure 1c**). The REP ORF cassette of AAV2 codes for four non-structural Rep proteins (Rep 78, Rep 68, Rep 52, and Rep 40), which are responsible for AAV DNA replication, transcriptional regulation, packaging of DNA genome into the preformed capsid, and site-specific integration.<sup>5-8</sup> The CAP ORF cassette codes for three capsid proteins VP1, VP2 and VP3 (VP proteins) with apparent molecular masses of 87 kDa, 73 kDa, and 62 kDa, respectively.<sup>9</sup> These proteins, which only differ in their N-terminus, are produced by alternative splicing and leaky scanning from one reading frame to achieve a molar ratio of VP1:VP2:VP3=1:1:10.<sup>10</sup> VP3 is the main structural protein (**Figure 1b**) and can form VP3-only capsids.<sup>11</sup>

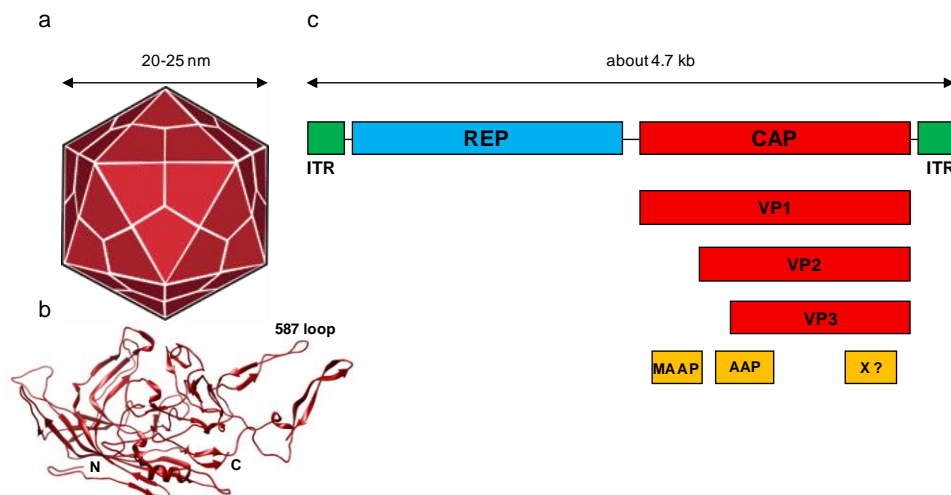


**Figure 1.** Schematic representation of AAV capsid and genome. (a) AAV capsid with a size of 20-25 nm arranged in a T=1 icosahedral symmetry. (b) Ribbon diagram of AAV2 VP3 capsid protein (PDB ID: 1LP3). (c) 4.7-kb ssDNA AAV2 genome comprises two open-reading frame cassettes (REP and CAP) flanked by two inverted terminal repeat sequences (ITRs). CAP ORF codes for three capsid proteins (VP1, VP2, VP3) and accessory proteins (AAP, MAAP and X).

The CAP ORF cassette also codes in a different reading frame for the assembly-activating protein (AAP), which promotes capsid assembly by increasing capsid protein stability and VP-VP interactions.<sup>12,13</sup> Furthermore, the AAP of AAV2 (AAP2) also plays a role in transporting the capsid proteins to the nucleolus for assembly.<sup>14</sup> Interestingly, AAV4, AAV5 and AAV11 can assemble without AAP, whereas the other AAV serotypes require AAP to form capsids.<sup>4</sup> Recently, a membrane-associated accessory protein (MAAP) coded by the CAP ORF was discovered.<sup>15</sup> One group demonstrated that the CAP ORF also codes for X protein, which is involved in AAV replication,<sup>16</sup> however, X gene has not been detected using a Frameshift Score in another study.<sup>15</sup>

### 2.1.2. rAAV applications and production

AAV vectors have had increasing successes in many recent clinical gene therapy trials among with approved products on the market,<sup>17</sup> such as Luxturna (Voretigene neparvovec) based on AAV2 for the treatment of patients with an inherited form of vision loss approved by the U.S. Food and Drug Administration (FDA) in 2017,<sup>18</sup> Zolgensma (Onasemnogene abeparvovec) based on AAV9 for the treatment of children with spinal muscular atrophy approved by FDA in 2019<sup>19</sup> and Glybera (Alipogene tiparvovec) based on AAV1 approved by the European Medicines Agency (EMA) in 2012 to treat patients with lipoprotein lipase deficiency.<sup>20</sup> Mammalian cell (HEK-293) and insect cell (Sf9) based systems are the two most commonly used methods for rAAV production, though they have difficulties to meet a high demand for AAV in clinical trials.<sup>21</sup> HEK-293 cell culture is difficult to scale, specifically when using adherent cells, post-translational modifications of rAAV lead to charge heterogeneity,<sup>22</sup> and process- and product-related impurities occur.<sup>23</sup> While AAV production in Sf9 cells has drawbacks related to the genetic instability of baculovirus stocks during the expansion phase, the difficulty to produce infectious AAV particles with a correct capsid protein ratio and the requirement to remove baculoviruses and its components.<sup>24,25</sup> Yeast has also been explored for AAV production. However, low vector yields hinder its application.<sup>26</sup> AAV empty capsids can also be formed via *in vitro* assembly of viral protein expressed in the baculovirus system.<sup>27</sup> Also, the *in-vitro* packaging of AAV has been studied in the presence of cell extracts.<sup>28,29</sup> Thus, *in vitro* assembly of AAV from capsid protein produced in high-expression hosts and *in vitro* encapsidation of AAV genomes into capsids in a chemically defined reaction could be a feasible strategy for rAAV production.

## 2.2. Virus-like particles

Virus-like particles (VLPs) are highly structured protein complexes that resemble the native virus capsid. Due to the lack of viral genomes, the particles are non-infectious.<sup>30</sup> These particles are a class of nanoparticle delivery systems that comprise a variety of nano-scale size materials.<sup>31</sup> They can be either enveloped or non-enveloped, assembled from single or multiple capsid proteins.<sup>32</sup>

### 2.2.1. Capsid protein production

VLPs are formed by self-assembly of capsid protein subunits that can be obtained either by expression and purification from different hosts, cell-free protein synthesis (CFPS) systems or via a disassembly procedure from *in-vivo* formed VLPs.

*E. coli* is a preferred host for high capsid protein expression.<sup>33</sup> Depending on the viral protein structure and expression method, proteins are either expressed in soluble form, which is normally favorable for capsid assembly, or as aggregates forming inclusion bodies within *E. coli*. To obtain more soluble proteins, different factors such as the choice of the host, the expression vector, the expression temperature, the induction condition and the medium can be optimized.<sup>34</sup> Besides, tags can be added to the protein terminus at the genetic level to aid protein folding or purification. Since the additional tag may interfere with capsid formation, a protease cleavage site can be added and used before assembly.<sup>35-37</sup>

Other favorable hosts for capsid protein production are Sf9 insect cells using baculovirus vectors and yeast, which offer advantages related to the ability to scale up and expression of post-translationally modified proteins.<sup>27,38,39</sup> Lastly, cell-free protein synthesis systems can also be used to produce viral capsid proteins in defined transcription/translation reactions.<sup>40-42</sup>

In some cases, capsid proteins have also been obtained from VLPs assembled inside the expression hosts that may contaminate cell components. Different methods have been used to disassemble the VLPs. Bacteriophage MS2 VLPs produced in *E. coli* were disassembled at low pH, while human papillomavirus (HPV) VLPs obtained from insect cells were dissociated with a carbonate buffer at pH 9.6.<sup>43,44</sup> Cowpea chlorotic mottle virus (CCMV) assembled in plants can be denatured in a high-salt concentration, neutral pH buffer.<sup>45-47</sup> Urea is commonly used to disassemble the formed VLPs. Bacteriophage Q $\beta$  VLPs were disassembled in 6 M urea,<sup>48</sup> whereas 2.5 M urea was sufficient to denature hepatitis B core protein (HBc) VLPs.<sup>49</sup> Reducing and chelating agents can also be used in VLP disassembly.<sup>44,50-55</sup> The capsid proteins can be then used to reassemble with a cargo of interest.

#### 2.2.1.1. Protein refolding

Capsid proteins also tend to form inclusion bodies during expression in *E. coli* owing to the incorrect folding.<sup>56</sup> This aggregate can be easily obtained with high yields using strong denaturing conditions like 6 M GuHCl or 6-8 M urea.<sup>57-61</sup> GuHCl is usually preferable to urea due to its stronger chaotropic activity. Also, urea solutions may contain isocyanates that can react with free amino acid groups of proteins to form carbamyl derivatives.<sup>62,63</sup> For proteins containing cysteine, reducing reagents can be used to reduce disulfide bonds during inclusion body solubilization.<sup>64</sup> Gel filtration, ion-exchange chromatography (IEX) and immobilized metal-ion affinity chromatography

(IMAC) could be used to purify proteins in the presence of a denaturant.<sup>62</sup> Taken into account that GuHCl may interfere with protein binding to an ion-exchange column during purification.

*In vitro* protein refolding has been attained by the removal of the denaturants from solubilized protein solutions. In order to avoid protein aggregates and/or misfolded protein, the choice of solubilization agent, the protein concentration, refolding conditions and refolding methods should be optimized.<sup>65</sup> Various chemical additives that can act as protein stabilizers, refolding enhancers or aggregation inhibitors have been added to aid *in vitro* protein renaturation.<sup>66</sup> Dilution and dialysis are the most commonly used methods to refold proteins. The latter method has been shown a better yield than the dilution approach. Column refolding can be used to not only renature proteins but also separate the folded proteins from other protein aggregates, this might reduce costs at the industrial scale.<sup>62,65-67</sup> Microfluidic chips and urease-mediated refolding have also been studied for recovery of folded proteins from inclusion bodies.<sup>68,69</sup>

### 2.2.2. Assembly of virus-like particles

The capsid self-assembly is driven by Brownian motion and interactions between subunits, subunits and other viral, non-viral components to minimize free energy in higher structures. The capsid assembly is proposed to occur in three steps. First, a nucleus, a small capsid fragment, is formed from capsid proteins in the nucleation phase. Afterwards, building blocks (a protein monomer, or larger capsid fragment) are added to the nucleus during the growth phase. Finally, the last building block is inserted to complete the capsid.<sup>70-72</sup> VLPs can be assembled *in vivo* inside host cells or via *in vitro* assembly in a chemically defined reaction (**Figure 2**).

#### 2.2.2.1. *In vivo* assembly of VLPs

For *in vivo* capsid assembly, capsid proteins are expressed and concomitantly assembled into particles in the host cells. The *in-vivo* particles have been produced using different expression systems, such as mammalian cells, insect cells, plant cells, yeast and bacteria.<sup>30</sup> Among them, bacteria, in particular, *E. coli* has been frequently used for VLP production due to its low cost and high yield.<sup>33</sup> Compare to a defined *in-vitro* assembly, capsid assembly inside the host cells offers an opportunity for large-scale production, and the *in-vivo* VLPs can be obtained directly from the cells by direct purification.<sup>73-75</sup> However, as the capsid assembly occurs within the hosts, possible contaminations of host-related components may impede capsid applications, especially for vaccine development.<sup>76</sup> In some cases, capsid proteins tend to aggregate during expression, forming inclusion bodies in the cells,<sup>27,77</sup> therefore *in vitro* capsid assembly is needed.

2.2.2.2. *In vitro* assembly of VLPs

*In vitro* assembly of VLPs occurs in a cell-free, defined and controllable reaction. The assembly process is complex and highly dependent on the viral protein structure and experimental conditions. There are main factors that affect *in vitro* assembly.

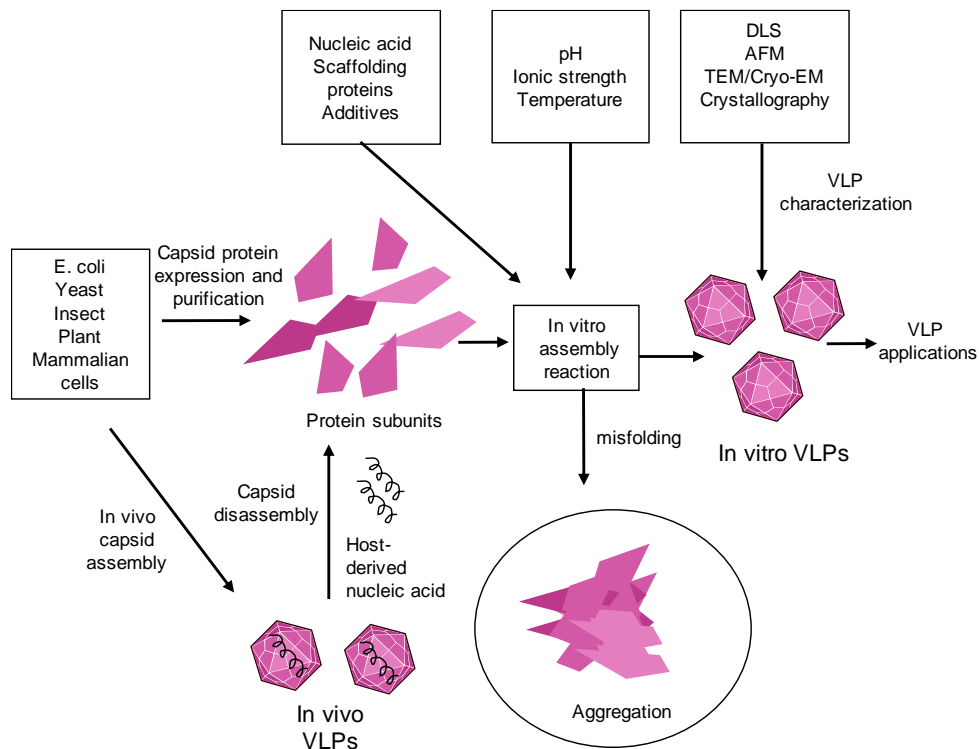


Figure 2. Schematic representation of *in vitro* and *in vivo* capsid assembly (adapted from Le et al. <sup>78</sup>).

pH plays an important role for *in vitro* assembly since it effects the capsid protein charge. Most *in-vitro* assembly reactions were optimized at a physiological pH.<sup>36,58,79</sup> Interestingly, some particles are formed during an assembly reaction at an acidic or alkaline pH. The *in-vitro* assembly of CCMV showed that the attraction among capsid proteins was optimal at about pH 5 and decreased sharply with an increase of pH.<sup>80</sup> Rotavirus (RV) VLPs were also able to be developed *in vitro* at an acidic pH.<sup>61</sup> Contrary, *in vitro* assembly results of *Potato virus X* indicated that the alkaline pH (pH 8.5) was the most suitable condition to form VLPs.<sup>81</sup> Besides pH, ionic strength is also the main factor affecting capsid assembly *in vitro*. Salts interact with charges on the protein surface, influence the water shell and disfavor hydrophobic exposure and ultimately affect protein stability.<sup>82</sup> To optimize *in-vitro* capsid assembly reactions, various ionic strengths need to be optimized along with the change of pH.<sup>36,58,79</sup> In addition, the effect of temperature on the capsid assembly also needs to be evaluated. Low temperatures are normally favorable due to avoiding protein aggregation and chemical degradation. For example, the *in-vitro* assembly of primate

## 2 Introduction

erythroparvovirus 1 (B19) at 4°C showed a better yield than that at 37°C.<sup>58</sup> In contrast, near-physiological temperatures promoted the Rous Sarcoma Virus capsid formation *in vitro* described by Jaballah et al.<sup>83</sup> Another report on Hepatitis virus assembly revealed that temperature regulated capsid assembly *in vitro*.<sup>84</sup>

The *in-vitro* assembly of some capsids is highly influenced by the presence of nucleic acids. Cowpea chlorotic mottle virus (CCMV), a single-stranded RNA virus, is a well-studied model. Garmann et al. demonstrated that the assembly of CCMV depended on the balance of capsid protein (CP) – CP interactions relative to CP-RNA interactions.<sup>85</sup> Furthermore, a high CP/RNA mass ratio was required to assemble CCMV VLPs.<sup>86</sup> Recently, CCMV showed the ability to encapsidate both single-stranded DNA (ssDNA) and double-stranded DNA (dsDNA), resulting in the formation of spherical or rod-like VLPs, respectively.<sup>87</sup> Other RNA viruses also require nucleic acids for *in vitro* assembly. The assembly of Gag protein into HIV1 VLPs in a defined system was directly supported by RNA.<sup>88</sup> Similarly, the *in-vitro* assembly of Hepatitis C virus (HCV) nucleocapsid-like particles required structured RNA as reported by Kunkel et al.<sup>89</sup> Bacteriophage MS2 was also assembled *in vitro* in the presence of nucleic acids.<sup>43</sup> The assembly of the beak and feather disease virus (BFDV), a member of the circular ssDNA circovirus family, is regulated by its ssDNA genomes. The highly positive charged N-terminal arginine-rich motif (ARM) of capsid proteins directly interacted with ssDNA during *in vitro* capsid assembly.<sup>90</sup> dsDNA viruses, such as simian virus 40 (SV40) and human papillomavirus (HPV), also needed DNA for *in vitro* capsid assembly.<sup>51,91</sup>

Scaffolding proteins are not a component of a mature capsid. These proteins are involved in capsid assembly by assisting capsid formation. Providing a scaffolding protein to *in-vitro* capsid assembly reactions in many cases increased the yield of capsid formation. The assembly of different bacteriophages was highly dependent on a scaffolding protein, which promoted the polymerization of the major capsid proteins.<sup>92–96</sup> The Herpes Simplex Virus procapsid assembly reaction from purified major capsid proteins has been reported by Newcomb et al. to require the scaffolding protein and to form small procapsids at a low concentration of the scaffolding protein.<sup>97</sup> In addition, small molecule additives can be used to aid capsid assembly. L-arginine improved the solubility of assembled VLPs by preventing aggregation during protein refolding.<sup>59,98</sup> In a study performed by Lampel et al., chemical chaperones, such as methylamines enhanced HIV-1 *in vitro* assembly.<sup>99</sup> Other reagents can be combined with capsid proteins during *in vitro* assembly leading to new hybrid materials. For example, CCMV capsid proteins have been explored in combination with different supramolecular templates. Organo-Pt (II) monomers were added to CCMV capsid assembly to form icosahedral and non-icosahedral (rod-like) CCMV VLPs.<sup>100</sup> Micelles and DNA micelles were packaged inside CCMV VLPs that offer new drug delivery systems, especially for hydrophobic drugs.<sup>101,102</sup> Polymers were also incorporated into CCMV VLPs during *in vitro* assembly.<sup>103,104</sup>

### 2.2.3. Virus-like particle characterization

To analyze the formed VLPs, different biochemical and biophysical methods have been used. Standard methods are SDS-PAGE to determine size and purity, western blot to confirm the identity and UV-visible spectroscopy, which monitors amino acids (phenylalanine, tyrosine and tryptophan) and nucleotides with an absorbance spectrum of about 240-300 nm to determine concentration.<sup>50,105,106</sup> Other protein quantitation methods, such as Bicinchoninic acid (BCA) assay and Bradford assay have also been employed.<sup>50,58,107</sup> Size exclusion chromatography (SEC) and dynamic light scattering (DLS) are widely used to characterize the size of VLPs.<sup>59,108–110</sup> The latter method provides the heterogeneity of the VLP samples and the mean of particle hydrodynamic diameter, which is normally greater than the physical diameter. Stability has been assessed using techniques such as differential scanning calorimetry.<sup>111</sup> Structural integrity has been verified by circular dichroism spectroscopy (CD) and Fourier-transform infrared spectroscopy (FT-IR).<sup>112</sup> The nucleic-capsid protein interactions have been determined by gel retardation assay, optical tweezers (OT) and acoustic force spectroscopy (AFS).<sup>86,91</sup> VLP morphology and possible intermediate aggregates formed during assembly can be visualized using transmission electron microscopy (TEM) or atomic force microscopy (AFM). Moreover, TEM can also be used to discriminate between empty and encapsulated VLPs,<sup>86,92</sup> AFM can assess the VLP height profile.<sup>59,113,114</sup> A VLP high-resolution structure can be determined using Cryo-EM<sup>85</sup> or crystallography.<sup>90</sup> Mass spectrometry has been used to identify VLP composition.<sup>115</sup> ELISAs with an intact-particle antibody help to confirm VLP conformation.<sup>59</sup>

Understanding capsid self-assembly pathways will help to elucidate the mechanisms of virus infection and replication that can be implied for therapeutic applications. Different methods have been used to characterize intermediate assemblies and the assembly pathways of virus capsids, such as electron microscopy,<sup>116–119</sup> X-ray crystallography,<sup>90</sup> atomic force microscopy,<sup>90,91,118</sup> small-angle X-ray scattering,<sup>120–125</sup> mass spectrometry,<sup>126–128</sup> size-exclusion chromatography,<sup>117</sup> resistive-pulse sensing,<sup>117,129</sup> interferometric scattering microscopy,<sup>130</sup> single-molecule fluorescence correlation spectroscopy,<sup>131</sup> optical tweezers in combination with confocal fluorescence microscopy and acoustic force spectroscopy.<sup>91,132</sup> Recently, high-speed atomic force microscopy (HS-AFM), a powerful single-molecule technique for real-time visualization of biomolecules in dynamic action,<sup>133</sup> has been used to visualize self-assembly of HIV capsid protein lattice.<sup>114</sup> This physical virology technique enables real-time capsid assembly studies of other viruses in the future.

### 2.2.4. Virus-like particle applications

#### 2.2.4.1. Vaccine development

VLPs are composed of protein monomer units in a repetitively ordered structure that is appropriate for vaccination. With a size of 20-200 nm in diameter, VLPs are able to induce a strong immune response.<sup>76</sup> Compared to subunit peptides or proteins, VLPs present a natural epitope conformation that benefits an antiviral B- and T-cell immune response. Moreover, due to the highly repetitive epitope presentations, VLPs can induce a strong B cell response even without adjuvants.<sup>134-136</sup> Another advantage is that a foreign epitope can be chemically or genetically incorporated onto the VLP surface, offering a flexible platform to create different vaccine candidates.<sup>137-140</sup>

VLP-based vaccine development has significantly progressed in the clinic in recent years along with approved products on the market.<sup>141</sup> These vaccine candidates have been produced *in vivo* or by a cell-free system. *In-vivo* VLP-based vaccines against Hepatitis B virus (HBV) have been produced in CHO cells.<sup>141,142</sup> Recently, *in-vivo* VLP vaccine candidates produced in plants have been developed against influenza viruses and SARS-CoV-2.<sup>143,144</sup> Compared to *in-vivo* VLP production, which potentially contaminates host-derived components resulting in unpredictable immune responses, a cell-free VLP technology offers a better control during production with many vaccines on the market (Cervarix,<sup>145</sup> Gardasil and Gardasil 9,<sup>112,146</sup> and Cecolin<sup>147,148</sup> for human papillomavirus (HPV), ENGERIX B, Fendix<sup>149,150</sup> and Recombivax HB<sup>151,152</sup> for Hepatitis B virus (HBV), Hecolin for Hepatitis E Virus (HEV)<sup>111,153-155</sup>) and many candidates currently in clinical trials (HPV 9-valent vaccine candidate,<sup>156</sup> SARS-CoV-2 vaccine candidate,<sup>110,157</sup> influenza virus vaccine candidate,<sup>158,159</sup> and human respiratory syncytial virus (RSV) vaccine candidate.<sup>38,160,161</sup>).

#### 2.2.4.2. Nucleic acid and drug delivery

VLPs are attractive candidates to deliver nucleic acids, drugs or small molecules due to their biocompatibility, biodegradability and targeted delivery.<sup>162,163</sup> Different cargo-loading strategies have been explored with both *in-vivo* and *in-vitro* VLPs.<sup>164</sup> Nucleic acids have been packaged by different *in-vitro* approaches, which occur via disassembly/reassembly of the formed VLPs or during *in vitro* assembly of purified proteins into VLPs. CCMV has widely been exploited in nucleic acid encapsidation and delivery. CCMV particles produced in plant or *E. coli* can be disassembled in a high salt concentration, neutral pH buffer, and afterwards nucleic acids were added and dialyzed into a low salt concentration or acidic buffer.<sup>45,46,87</sup> The nucleic acids were encapsidated into CCMV VLPs via the electrostatic interaction to capsid proteins during capsid assembly. Simian virus 40 (SV40) and human papillomavirus (HPV) VLPs were also used for gene delivery.<sup>51-53,55,165,166</sup> These VLPs produced in insect or human cells were dissociated in the presence of a metal chelator

(EDTA, EGTA) and a reducing agent (DTT). Afterwards, dsDNA encapsidation and capsid reassembly occurred in a buffer containing  $MgCl_2$  and  $CaCl_2$ . Additionally, VLPs were also used for RNA delivery. Bacteriophage MS2 produced in *E. coli* was disassembled in glacial acetic acid, then RNA or an RNA-conjugated drug was encapsidated into the particles by dialyzing into a pH-6 assembly buffer.<sup>43,167</sup> Nucleic acids can also be packaged into VLPs via *in vitro* assembly of purified capsid proteins and nucleic acids. The capsid protein of the beak and feather disease virus (BFDV) was expressed in soluble form in *E. coli* and purified by IMAC and size exclusion chromatography. After that, purified capsid proteins and ssDNA were mixed to form DNA-encapsidated VLPs.<sup>90</sup>

VLPs have also been explored in drug delivery with different approaches.<sup>163,168</sup> Capsid proteins have been chemically conjugated with drugs via primary amino acids with amide bonds. Doxorubicin (DOX), a chemotherapy drug, was incorporated into Rotavirus (RV) and Cowpea chlorotic mottle virus (CCMV) capsid proteins. The DOX-conjugated VLPs assembled via *in vitro* assembly were used for therapeutic delivery.<sup>61,169</sup> Besides, genetic modification of VLPs could be used in drug delivery. In this method, a peptide or protein can be genetically fused to capsid proteins. For example, tumor-targeting peptide RGD was incorporated into Hepatitis B core VLPs for targeting cancer cells.<sup>49</sup> A nanobody can be genetically inserted into the hepatitis B virus VLPs.<sup>170</sup> Moreover, drugs can also be encapsidated into formed VLPs by diffusion<sup>171</sup> or during a VLP self-assembly reaction.<sup>172</sup> With similar strategies, fluorescent VLPs can be generated for visualization and imaging of the particles, analysis of VLP-host interaction and also tracking drug-conjugated VLPs *in vivo*. To do this, fluorophores have been labeled by a non-covalent, covalent attachment, or genetically fused to capsid proteins.<sup>173,174</sup> Another widely used labeling method for medical imaging is encapsidation of nanoparticle templates, such as quantum dots, gold nanoparticles or other magnetic nanoparticles into VLPs via *in-vitro* assembly reactions.<sup>175–178</sup>



### 3. Aim

Vectors based on the adeno-associated virus have emerged as leading candidates in gene therapy with three approved products by EMA and FDA and many ongoing clinical trials. Currently, rAAV production in HEK-293 and Sf9 cells remains challenging due to the very high demand for rAAV vectors in research and clinical trials. AAV vectors have been used for a large number of gene therapy applications, though the AAV capsid assembly mechanism is still unclear. Meanwhile, empty capsids or VLPs, which lack DNA genomes, have been widely used for various applications including vaccine development with many products on the market, drug delivery and materials science. VLPs also offer a potential platform for genetic payloads in gene therapy.

Therefore, the main aim of the thesis is to establish a new method to assemble AAV capsids using *E. coli* for a feasible rAAV production method based on AAV VLP *in vitro* assembly and DNA encapsidation. This also contributes to a better understanding of the AAV capsid assembly biology. At the same time, AAV VLPs can be applied for different biological applications. To do this, the expression and assembly of the VP3 protein of the most-studied AAV serotype AAV2 and the most genetically divergent serotype AAV5 should be studied. An effect of AAP protein during capsid assembly is also to be evaluated.

VLPs have been commonly produced for vaccines with many products on the market. AAV VLPs produced in mammalian cells have also been studied for vaccine development. Mammalian cell-based AAV VLP production is expensive and may contaminate cellular components. This thesis will therefore focus on expression of SARS-CoV-2 receptor-binding domain (RBD) and receptor-binding motif (RBM) fused to AAV2 VP3 in *E. coli*, formation and characterization of modified AAV VLPs, and immunogenicity of AAV VLPs comprising RBD and RBM.

In addition, to explore the application of *E. coli* AAV VLPs in gene therapy that might help to address the bottleneck of current rAAV production systems, the encapsidation of ssDNA into the assembled AAV capsids is of great interest. To test this hypothesis, ssDNA will be produced and assembled with modified AAV5 VP3 proteins containing a DNA-binding domain in a chemically defined buffer condition. Finally, to visualize and image AAV VLPs, fluorophore conjugation of VLPs and the cellular uptake of the VLPs should be studied.



## 4. Results and Discussion

### 4.1. AAV2 capsid protein expression and *in vitro* assembly

Results of this work were published in Scientific Reports journal with the title “Adeno-associated virus capsid protein expression in *Escherichia coli* and chemically defined capsid assembly” and are summarized in this chapter. The original publication is included in the appendix (8.3).

AAV has emerged as the most prominent candidate for gene therapy approaches. However, several steps of AAV capsid assembly remain unclear. At the same time, an effective method to produce AAV is needed, which should address the issues of current production systems.<sup>179</sup> AAV assembly has been proposed to occur in two steps. Empty capsids form and are then filled with their single-stranded DNA genome.<sup>7</sup> Hence, production of empty capsids from *E. coli* might not only help to elucidate the AAV biology aspect in capsid assembly, but also provide a feasible strategy for future AAV production. In this chapter, capsid proteins were produced in *E. coli* and AAV2 capsids formed in a chemically defined assembly reaction.

#### 4.1.1. AAV2 VP3 capsid protein expression and purification

AAV2 VP3 wild type (VP3wt) protein is known to form VP3-only capsids.<sup>11</sup> Therefore, the codon usage of the VP3wt gene was optimized for *E. coli* and cloned as a synthetic gene into a pET vector downstream of a T7 promoter without an additional tag (**Figure 3a**). We tested different expression conditions in shake flasks with the BL21(DE3) host, such as temperature (37°C, 25°C and 18°C), OD at induction (OD<sub>600</sub> of 0.6, 1.5 and 2.5) and duration of cultivation after induction (6 h, 18 h) to obtain soluble protein. However, only inclusion bodies were obtained due to suspected folding problems and growth-limiting effects of VP3wt protein to *E. coli*. Consequently, we settled with overexpression with the T7 system in inclusion body form at 18°C and induction of expression at an OD<sub>600</sub> of 1.5 for 18 h (**Figure 3b**, lane 5). The identity of the VP3 protein was confirmed by western blot analysis using the antibody B1. Interestingly, in addition to a strong band at the expected size of VP3wt (theoretical mass 60.06 kDa), the B1 antibody identified four weaker and smaller bands. This suggests that VP3wt is unstable during expression (**Figure 3c**, lane 2 and lane 4). Capsid proteins were then solubilized under a denaturing condition (8 M Urea) and purified by denaturing anion-exchange chromatography (IEX). SDS-PAGE analysis of purified protein showed a major protein band at about 60 kDa which is in agreement with the theoretical mass of VP3wt (**Figure 3d**). The purified protein yield with one degradation band around 50 kDa was around 10 mg per liter of culture with an estimated final purity of the correct-mass protein of 79 % (by SDS-PAGE).

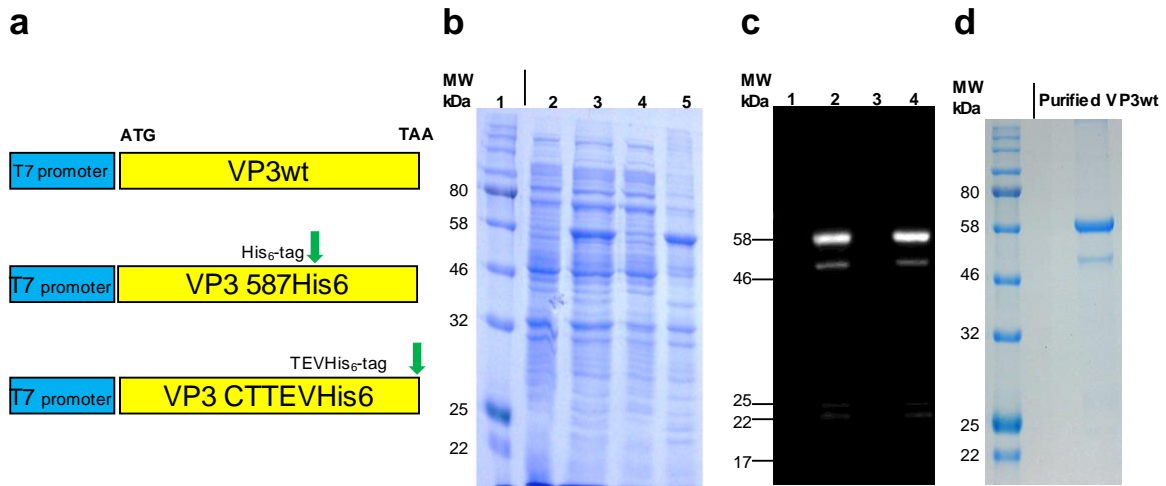


Figure 3. Expression of AAV2 VP3wt protein in *E. coli*. (a) Schematic representation of VP3wt protein expression constructs downstream of a T7 promoter. Either a His<sub>6</sub>-tag coding sequence was incorporated at the a.a. 587 coding position or a TEV<sub>cleavage\_site</sub>-His<sub>6</sub>-tag coding sequence was cloned 3' of the VP3wt gene. (b) Coomassie stained SDS-PAGE of VP3wt expression; lane 1, protein standard; lane 2, whole-cell protein of *E. coli* BL21(DE3) before induction; lane 3, whole-cell protein 18 h post-induction with IPTG; lane 4, soluble fraction of intracellular protein 18 h post-induction; lane 5, insoluble fraction of intracellular protein. (c) Western blot analysis; lane 1-4, samples corresponding to lane 2-5 (b) detected with B1 antibody. (d) SDS-PAGE of VP3wt protein after IEX purification. The black vertical line divides two different crops of the same gel.

*E. coli* is one of the most attractive hosts to produce recombinant proteins, because of well-established protocols and low cost. Due to the high level of expression in *E. coli*, heterologous proteins tend to aggregate and form inclusion bodies with a lack of biological activity. For proteins that can be refolded *in vitro*, however, especially for toxic or unstable proteins or proteins with potential protease activity, inclusion body formation can be advantageous due to the high volumetric yield and easy purification.<sup>180</sup> In addition, viral particles forming in *E. coli* might encapsidate bacterial polymers such as DNA or RNA, which are then difficult to remove and not desired for human application. In this study, VP3wt protein expression blocked *E. coli* growth at physiological temperatures and no useful amounts of VP3 were obtained in soluble form even at low temperatures. However, VP3 was effectively expressed in inclusion bodies and subsequently easily purified by a one-step purification using IEX. The presence of VP3 was confirmed during expression with the B1 antibody, which recognizes a C-terminal epitope of VP3.<sup>181</sup> Next to the major VP3 band, additional lower molecular weight bands were detected in western blots. We suppose that VP3 is proteolytically degraded, possibly by an intrinsic protease activity as found in AAV2 particles,<sup>182</sup> or cleaved by *E. coli* proteases.

#### 4.1.2. AAV2 VP3 VLP assembly *in vitro* and characterization

VP3wt proteins in denaturing buffer were used as the starting material for refolding and concomitant *in vitro* assembly to VLPs. In other studies, capsid formation from denatured protein was initiated by the removal of denaturant.<sup>98,183</sup> To test this strategy, the AAV2 VP3wt sample, which was concentrated and re-buffered in denaturing buffer with 5 M guanidine/HCl and 1 mM DTT as

## 4 Results and Discussion

reducing agent, was dialyzed against PBS buffer containing 0.2 mol/l L- arginine at different pH conditions (pH 6, pH 7.5, pH 8.5, and pH 9). Significant amounts of VP3wt protein precipitated at pH 6 and pH 7.5. At pH 8.5 and pH 9, however, precipitation decreased. At these pH values, after removal of aggregates by centrifugation and filtration, the yield of soluble protein was around 36% at pH 8.5 and 70% at pH 9. Since particles aggregated when going back to the neutral pH, the samples were used at pH 9 for further characterization.

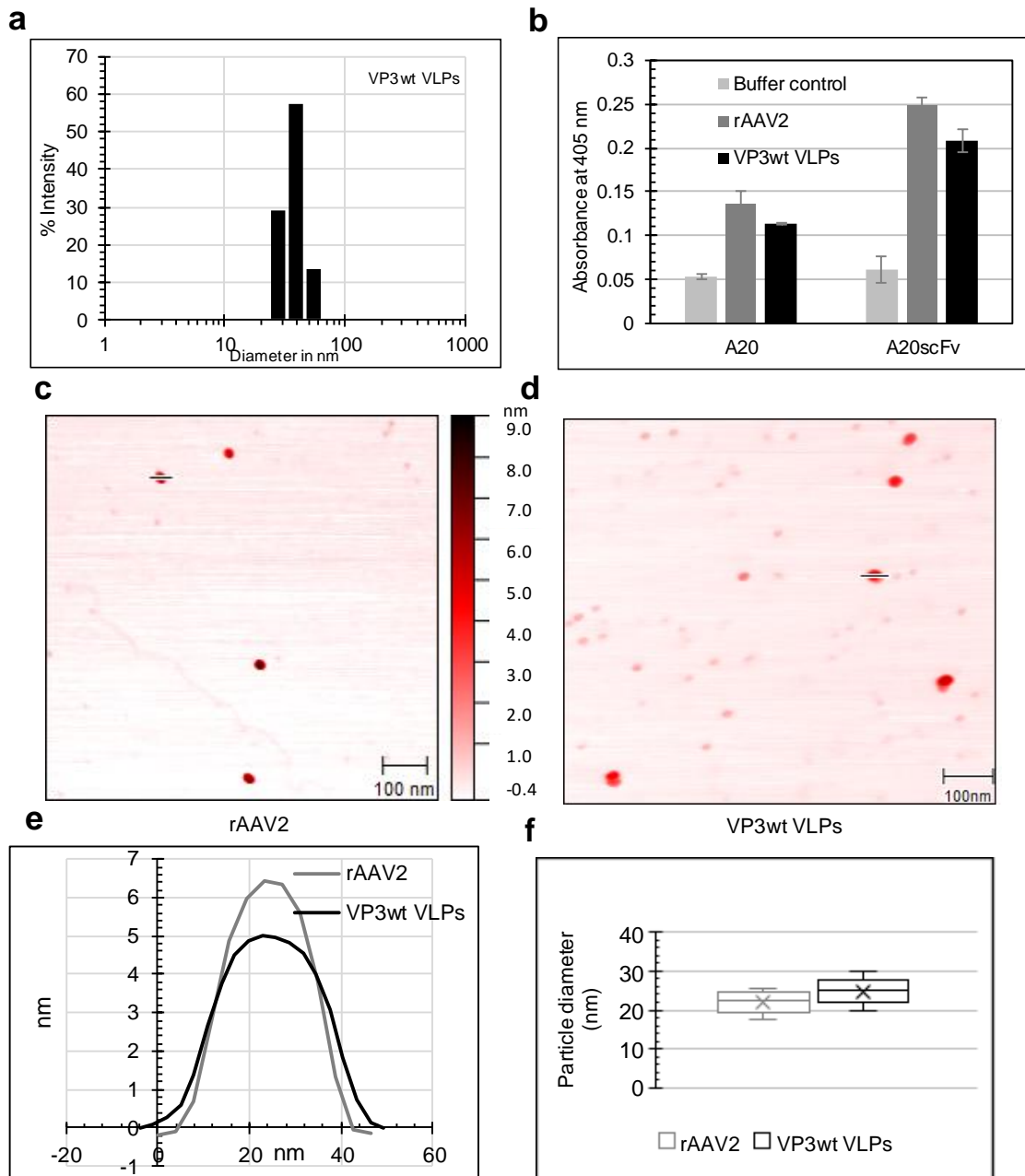


**Figure 4.** Characterization of AAV2 VP3wt VLPs. (a) Size distribution of VP3wt VLP determined by DLS at pH 9.0. (b) ELISA detected with anti-intact-capsid AAV2 antibodies (A20 mAb or A20 scFv-Fc); samples were rAAV2 particles ( $1.6 \times 10^9$  particles/ml) and VP3wt VLPs (50  $\mu$ g/ml). (c, d) AFM images of rAAV2 and VP3wt VLPs, respectively. Scale bars are 100 nm. (e) AFM height profiles of rAAV2 and VP3wt VLPs. (f) Box plot of the size distribution of rAAV2 particles and VP3wt VLPs determined by AFM ( $n=9$ , mean  $\pm$  SD, box from first to third quartile, cross median marker).

First, the presence of VLPs and/or their intermediate forms was analyzed by dynamic light scattering (DLS) at pH 9. The dialyzed VP3wt sample showed a mean hydrodynamic diameter of 37.7

## 4 Results and Discussion

nm and a polydispersity of 0.22 indicating homogeneity and the assembly of VLPs (**Figure 4a**). Note that the hydrodynamic size is always greater than the physical size, and that this result is consistent with the hydrodynamic size of rAAV measured by DLS from other reports (34.4 nm or 38.2 nm).<sup>184,185</sup>

Next, the AAV2 VP3wt VLP conformation was assessed by ELISA with the A20 monoclonal antibody (mAb), which only binds to assembled AAV2 capsids.<sup>181</sup> Parallel to the A20 antibody, we also used a recombinant A20 single-chain Fv fragment Fc fusion antibody variant (A20 scFv-Fc) cloned in our lab and produced in HEK-293 cells.<sup>186</sup> The ELISA signals indicated correctly assembled VLPs (**Figure 4b**). We compared the ELISA result to a sample of rAAV2 with known capsid concentration and estimated the ratio of correctly assembled particles to be 1 VLP per 5000 theoretical VLPs based on VP3wt concentration (i.e. protein concentration divided by 60). The total yield from 0.23 mg denatured protein was  $5 \times 10^9$  correctly assembled VLPs in 1.5 ml. With the protein production yield of about 10 mg per liter culture, we estimate the yield of AAV2 VLPs would be  $2.2 \times 10^{11}$  VLPs per liter LB culture. Compared to AAV2 VLP production yield using adherent HEK-293 cells in our lab that is estimated about  $2 \times 10^{11}$  AAV2 VLPs per 100 ml culture (using plasmid pΔRepCap, derived from plasmid pZMB0216 (**Table 14**)), or about  $1.1 \times 10^{11}$  AAV2 VLPs per 100 ml culture (using a pcDNA5 vector, pZMB0602) (data unpublished), the production in *E. coli* could offer a cheaper method for AAV2 VLP production.

The physical size and height profile of the particles were measured by atomic force microscopy (AFM). Recombinant AAV2 produced in HEK-293 cells was used for comparison. The shape and diameter of rAAV2 and VP3wt VLPs were similar, spherical and around 22 nm in diameter (**Figure 4c, d, e, f**), which is expected for AAV.<sup>187</sup> In the AFM images of the *in-vitro* assembly, we found other particles with a smaller diameter, which we attribute to assembly intermediates or protein monomers. The mechanism of capsid assembly of an icosahedral virus is known to involve the formation of intermediate forms, and our observation correlates with those obtained for *in vitro* production of other icosahedral capsids.<sup>98,118</sup>

We used HeLa cells to evaluate cellular uptake and thereby biological activity of VP3wt VLPs, as these cells are known to have a high density of AAV2's primary receptor heparan sulfate proteoglycan.<sup>188</sup> Using a fluorophore-tagged A20 antibody (red fluorescent signal), we were able to identify rAAV2 and VP3wt VLPs inside HeLa cells by fluorescence microscopy after 2 h of coincubation and subsequent fixation and permeabilization (**Figure 5**). No red fluorescent background signal was seen in the buffer control treated with the detection antibody (**Figure 5a**). The distribution of rAAV2 was shifted towards the nucleus (**Figure 5b**), while VP3wt VLPs were widely distributed in

the cytoplasm, potentially in endosomes (**Figure 5c**). We attribute this to the known nuclear translocation role of VP1, however, most of rAAV2 particles were still located in the cytoplasm after 2 h. This result indicates that VP3wt VLPs are biologically active and can internalize into cells.

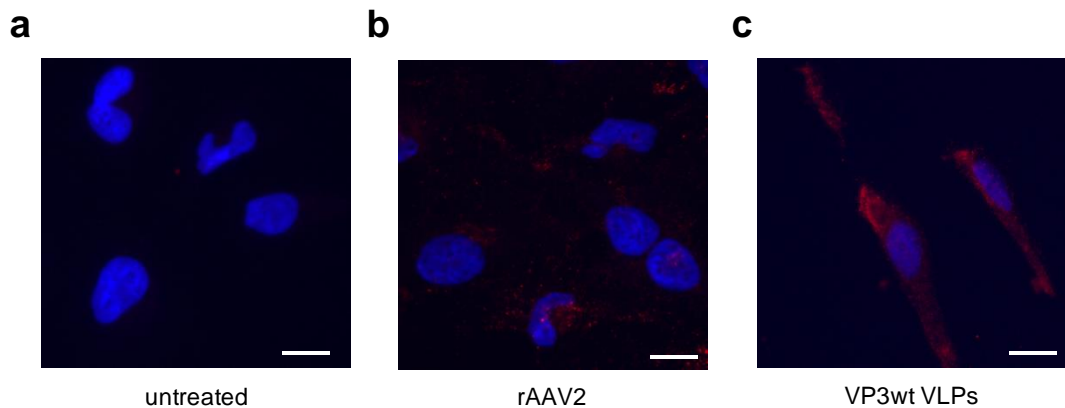


*Figure 5. Fluorescent microscopy images of rAAV2 and VP3wt VLPs internalization. HeLa cells were incubated with either (a) medium, (b) rAAV2 ( $3 \times 10^4$  particles/cell) or (c) VP3wt VLPs (final concentration of  $50 \mu\text{g/ml}$ ) at  $37^\circ\text{C}$ . After 2 h, cells were fixed, permeabilized and stained with A20 antibody followed DyLight 594 conjugated secondary antibody (red) as well as with DAPI (blue) and imaged with a  $40\times$  objective. Scale bars are  $10 \mu\text{m}$ .*

AAV2 binds to permissive cells using heparan sulfate proteoglycan (HSPG)<sup>189</sup> and other surface proteins including human fibroblast growth factor receptor 1 (FGFR1)<sup>190</sup> and hepatocyte growth factor receptor (MET)<sup>191</sup> as the putative co-receptors. Recently, a universal AAV receptor was identified with high affinity to multiple AAV serotypes.<sup>192</sup> These receptor-virus interfaces all lie within the VP3-only capsid. After attachment to the cell membrane, AAV2 internalizes by receptor-mediated endocytosis. Endosomal escape and nuclear entry, the next steps in infection, are attributed to the VP1 capsid protein.<sup>193,194</sup> Therefore, VP3wt VLPs should be able to enter cells that express the corresponding receptors but should not be able to translocate to the nucleus. We show that 2 h after transduction with the given buffer conditions, VP3wt VLPs internalized and distributed granular in the cytosol without nuclear preference, which is compatible with expectations of endosomal confinement. rAAV2 from mammalian production showed a similar appearance albeit with a shift towards the nucleus. These observations are consistent with a previously described distribution of rAAV2 and rAAV2 with deleted VP1 after infection of HeLa cells,<sup>195</sup> which supports the finding of biological activity of our VLPs. Further work will elucidate the internalization pathway of the particles.

#### 4.1.3. *In-vitro* AAV2 VLP assembly yield improvement by AAP2 supplement

AAP2 plays a critical role in AAV2 assembly. To investigate the impact of AAP2 on the production of AAV2 VLPs *in vitro*, we expressed AAP2 in *E. coli*. For detection and purification, we added a C-

## 4 Results and Discussion

terminal His-tag (**Figure 6a**), as a modification at this position does not interfere with AAP function.<sup>196</sup> As for VP3, we tested various expression temperatures, such as 37°C, 25°C and 18°C, to acquire AAP2 in soluble form. At 18°C, AAP2 was expressed as a soluble protein, however, most proteins degraded during expression. Therefore, we settled with an inclusion body production at 37°C and convenient purification by immobilized metal ion affinity chromatography (IMAC) under denaturing conditions (**Figure 6b**). Under these conditions, AAP was stable. We observed an apparent molecular weight of AAP2 of about 28 kDa, which is consistent with AAP2 produced in HEK-293 cells.<sup>4</sup> AAP2 was then added to the *in-vitro* assembly reaction in the presence of 5 M guanidine with VP3wt:AAP2 ratios of 1:2 or 2.5:1 and the refolding and assembly was performed as described. After dialysis, analysis by ELISA revealed that even though VP3wt only can form capsids on its own, AAP2 enhanced the *in-vitro* assembly (**Figure 6c**). Specifically, at a ratio of VP3wt:AAP2 of 1:2, the ELISA signal of VLP particles was 1.9 times greater than that of the VP3wt-only assembly reaction. This suggests that the yield of *in vitro* assembly increases in the presence of AAP2.

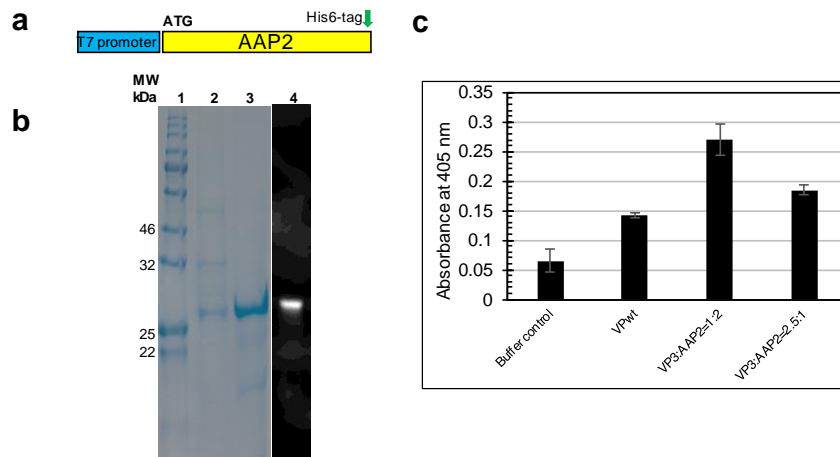


**Figure 6.** Impact of AAP2 on AAV2 *in vitro* assembly. (a) Schematic representation of AAP2 expression construct. A His6-tag coding sequence was added 3' of the AAP2 gene. (b) Coomassie SDS-PAGE (1) protein standard; (2) insoluble fraction of intracellular protein before purification; (3) IMAC purified protein; (4) Western blot of the insoluble fraction detected with anti-His-tag antibody. (c) ELISA after *in vitro* assembly using the same final protein concentration (50 µg/ml) with different ratios of VP3wt:AAP2.

Our study provides evidence that AAV2 VP3 proteins can form capsids *in vitro*, even in the complete absence of AAP2. AAP2 likely acts as a chaperone and/or a scaffold that directly or indirectly binds the luminal surface of VP proteins and plays a role in VP stability and in VP oligomerization during assembly.<sup>13,197</sup> However, the exact action mode of AAP2 in AAV2 assembly remains unclear. Our initial results of AAP2-free assembly agree with the previous report from Steinbach et al.,<sup>27</sup> although the authors of this study used HeLa cell extract for assembly. Here, by using a chemically defined reaction, we present direct evidence that the ability to form a capsid is entirely a property of VP3. To further investigate the role of AAP2 in capsid assembly, we expressed it in *E. coli* as inclusion bodies. Subsequent addition of solubilized AAP to our assembly reaction resulted in a

1.9-fold increase of mAb A20 positive particles over the AAP2-free assembly reaction. Although the complexity of the experiment provides a challenge for interpretation, the result indicates that AAP2 directly aides in capsid assembly, next to its before described function in VP stabilization by inhibition of proteasomal, lysosomal or autophagosomal degradation and nuclear translocalization.<sup>13,14</sup>

#### 4.1.4. *In-vitro* AAV2 VLP modification

Incorporation of peptides into the capsid is an important strategy in AAV retargeting<sup>198</sup> and also gains interest in vaccine development.<sup>199,200</sup> To evaluate the effect of small peptide insertions on *in vitro* assembly, we chose two sites for modification. We genetically incorporated either a tag containing a TEV protease cleavage site followed by a His-tag at the C-terminus (VP3 CTTEVHis<sub>6</sub>) or a His-tag into the 587-loop (VP3 587His<sub>6</sub>) of VP3wt protein (**Figure 7a, Figure 8a**). The two sites were previously described to tolerate insertions *in vivo*.<sup>198,201</sup> We found that neither insertion of the tag at the C-terminus nor the 587-loop affected protein expression in *E. coli*. *In vitro* assembly of both modified proteins formed VLPs according to DLS, AFM and TEM measurements (**Figure 7b, c, Figure 8b, c, d**).

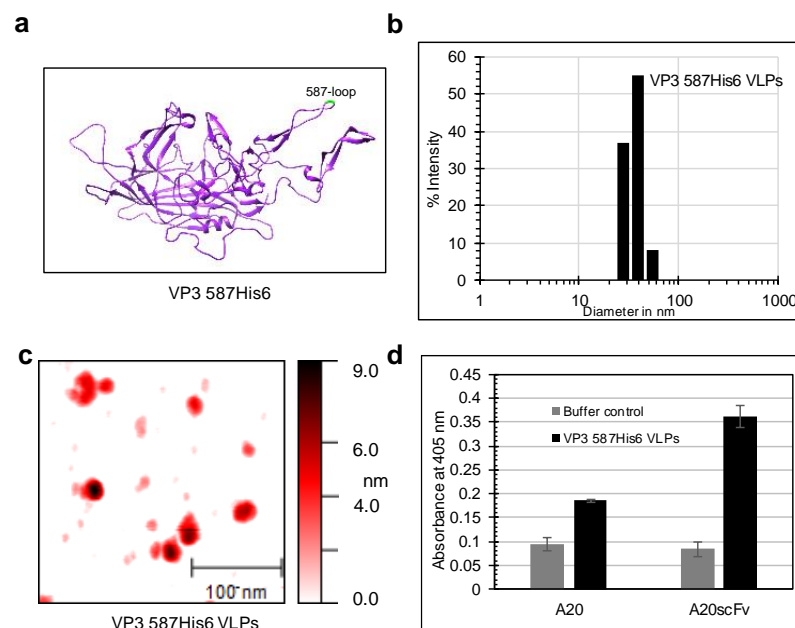
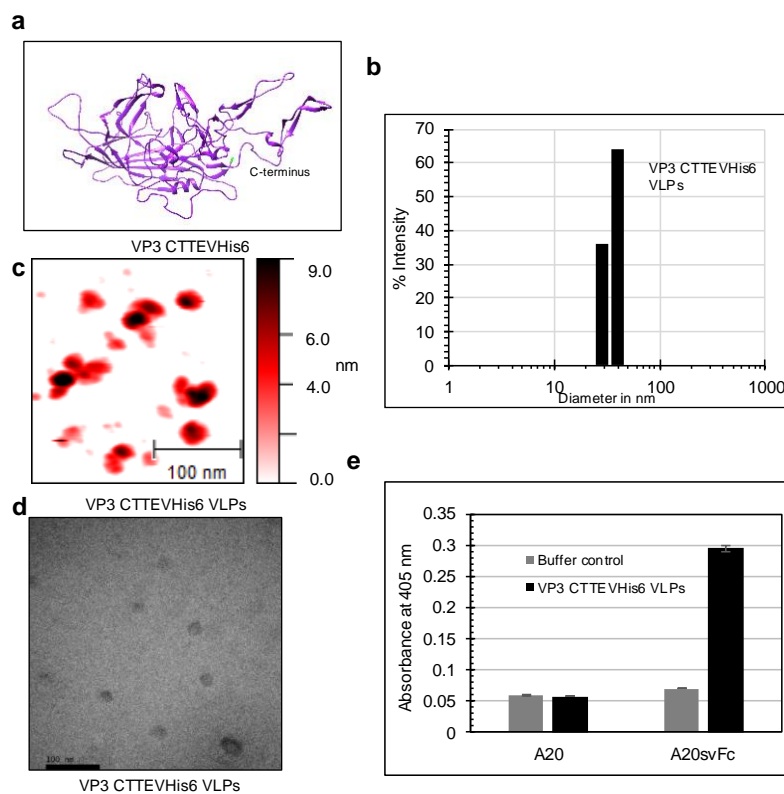


Figure 7. The effect of incorporation of a small peptide into the 587-loop on AAV2 *in vitro* assembly. (a) Representations of VP3wt protein structure (PDB ID: 1LP3) with highlighted 587-loop. (b) DLS size distribution of VP3 587His6 VLPs ( $35.7 \pm 7.5$  nm). (c) AFM image of VP3 587His6 VLPs. Scale bars are 100 nm. (d) ELISA of VP3 587His6 VLPs using either A20 mAb or A20 scFv-Fc antibody for detection.

In ELISA, the anti-capsid A20 antibody did recognize VP3 587His6 particles as did the A20 scFv-Fc recombinant antibody construct (**Figure 7d**) indicating wt-identical VLP assembly. Interestingly, ELISA results also showed that the A20 monoclonal antibody did not bind to VP3 CTTEVHis<sub>6</sub> VLPs

## 4 Results and Discussion

although particles were present (**Figure 8c, d, e**). In contrast, the A20 scFv-Fc readily recognized VP3 CTTEVHis6 VLPs. These findings suggest a more flexible binding mode of this antibody construct. The broader binding of the single-chain construct can possibly be attributed to its general structural flexibility, allowing binding of slightly distorted capsids. One group found that a VP3 C-terminal His-tag is compatible with biological function<sup>201</sup> and another found that the tag interferes with capsid assembly *in vivo*.<sup>202</sup> From our data, we can conclude that a C-terminal His-tag is compatible with forming particles which are very similar in shape and diameter to wt capsids, but show subtle structural differences revealed by A20 mAb recognition. The results also show that the 587-loop of VP3 is a potential position for capsid modification of particles assembled in a chemically defined reaction. As the capsid is known to tolerate these modifications *in vivo*,<sup>198,201</sup> our result hints that the *in-vitro* assembly process in general reflects the cellular process. Since the loop-region is exposed on the capsid surface, this opens the possibility to produce VLPs with modified tropism. Furthermore, these modified VLPs could be used to display functional proteins and act as antigen carriers for vaccination as described before for other virus particles.<sup>33,203</sup>



**Figure 8.** The effect of incorporation of a small peptide at the C-terminus of VP3wt on AAV2 *in vitro* assembly. (a) Representations of VP3wt protein structure (PDB ID: 1LP3) with highlighted C-terminus. (b) DLS size distribution of CTTEVHis6 VLPs ( $35.9 \pm 5.5$  nm). (c) AFM image of VP3 CTTEVHis6 VLPs. (d) TEM image of VP3 CTTEVHis6 VLPs. Scale bars are 100 nm. (e) ELISA of VP3 CTTEVHis6 VLPs using either A20 mAb or A20 scFv-Fc antibody for detection.

#### 4.2. Expression and concomitant assembly of AAV5 VLPs inside *E. coli*

Results of this project were mainly summarized in a manuscript with the title “Expression and concomitant assembly of adeno-associated virus-like particles inside *Escherichia coli*”. This work was also presented partially at the American Society Gene and Cell Therapy 23<sup>rd</sup> Annual Meeting and published in *Molecular Therapy* with the title “AAV Capsid Assembly Using *Escherichia Coli*”.<sup>204</sup> The manuscripts are included in the appendix (8.3).

To obtain more AAV capsids for therapeutic applications, AAV5 was chosen for VLP production in *E. coli*. Among 13 known human and nonhuman primate AAV serotypes, AAV serotype 5 is the most genetically divergent AAV and its capsid can assemble without AAP.<sup>3,4</sup> This project aimed to produce AAV5 VLPs, based on the straightforward expression of capsid proteins in *E. coli* and subsequent direct purification of VLPs from the soluble protein fraction as described in **Figure 9**.

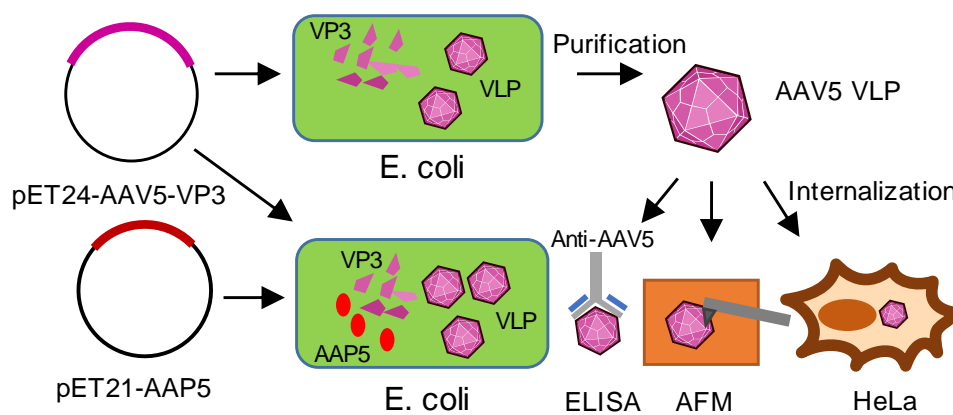


Figure 9. Schematic representation of AAV5 VLP production in *E. coli*.

##### 4.2.1. AAV5 VP3 capsid protein expression and concomitant assembly in *E. coli*

As AAV is able to form capsids with only VP3 proteins,<sup>11</sup> we optimized the codon usage of the AAV5 VP3 (VP3) gene for *E. coli* expression using the GeneArt online software tool (Thermo Fisher Scientific) and cloned it into a pET vector (**Figure 10a**). To assess the expression level, we tested two different expression temperatures (at 37°C and 18°C) and performed a western blot analysis with the B1 antibody, which recognizes unassembled VP proteins. As a result, VP3 protein was observed with an apparent mass of about 60 kDa at both 37°C and 18°C, which is consistent with its theoretical molecular weight (59.55 kDa) (**Figure 10b**). At 37°C, VP3 protein mainly formed inclusion bodies (**Figure 10b**, lane 1, 2, 3), conversely, VP3 protein was highly soluble at 18°C (**Figure 10b**, lane 4, 5, 6). We attribute this to the impact of temperature to reduce protein misfolding during expression in *E. coli*. It is known that aggregation is favored at higher temperatures during protein folding due to the temperature dependence of hydrophobic interaction.<sup>205,206</sup> Interestingly, in addition to the full-size VP3 protein band, other bands with lower molecular weight were

## 4 Results and Discussion

also detected by the antibody. The B1 antibody specifically recognizes an epitope at the C-terminus of VP proteins,<sup>181</sup> indicating that AAV5 VP3 protein was not stable during expression. This occurrence is possibly due to either an intrinsic protease activity of the protein or *E. coli* protease activity, a phenomenon we also observed during AAV2 VP3 expression in *E. coli*.<sup>59</sup>

Since a large part of the VP3 protein was soluble with the 18°C expression protocol, we analyzed whether VLPs spontaneously formed during capsid protein expression. To detect VLPs in the supernatant lysed *E. coli* extract, we performed a dot blot using an anti-intact-AAV5 antibody (ADK5a), which only binds AAV5-assembled capsids but not unassembled capsid proteins.<sup>207</sup> The results shown in **Figure 10c** indicate the presence of VLPs in *E. coli* harboring the pET24-AAV5-VP3 vector after induction and expression (**Figure 10c**, lane 2), while there was no particle detected in the control sample of cell extracts from untransformed *E. coli* (**Figure 10c**, lane 1).

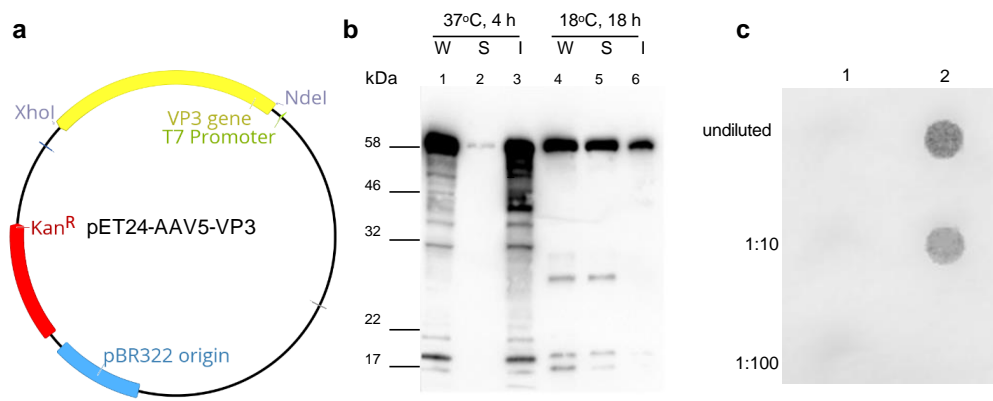


Figure 10. Expression of AAV5 VP3 protein in *E. coli*. (a) Plasmid map of pET24-AAV5-VP3. (b) Western blot analysis of VP3 expression with B1 antibody (whole-cell proteins (W), soluble fraction (S) and insoluble fraction (I) of intracellular proteins); Lane 1, 2, 3: expression for 4 h at 37°C; Lane 4, 5, 6: expression for 18 h at 18°C. (c) Dot blot of *E. coli* cell extracts with anti-AAV5 (intact capsid) antibody (ADK5a); lane 1, *E. coli* BL21(DE3) cell extracts; lane 2, *E. coli* BL21(DE3) containing pET24-AAV5-VP3 vector cell extracts.

### 4.2.2. AAV5 VP3 VLP purification and characterization

We next tested to purify the assembled particles by POROS AAVX affinity resin which contains a single-domain [V<sub>H</sub>H] antibody fragment known for AAV-capsid specific binding.<sup>208</sup> The SDS-PAGE of the purified sample displayed a band with the expected size of VP3 protein (**Figure 11a**, lane 2), which was also identified by the B1 antibody (**Figure 11b**), even though other contaminating proteins remained.

To detect the purified VLPs, we performed an ELISA with the ADK5a antibody. Besides the VLPs, we used rAAV5 produced in HEK-293 and also purified by POROS AAVX resin as control. Our ELISA data in **Figure 11c** reaffirmed the presence of AAV5 VLPs after purification. To detect possible encapsidation of host nucleic acid polymers (DNA/RNA) during VLP production in *E. coli*, an agarose gel electrophoresis of heated rAAV5 and VLPs was performed. After staining with SYBR Gold,

## 4 Results and Discussion

no nucleic acid polymers were found inside VLPs, while a DNA band, potentially rAAV5 genomes, was detected within rAAV5 (**Figure 11d**). Within the limits of this analysis, we conclude that capsids should mostly be empty and this finding offers the prospect of loading of genetic materials into the empty VLPs either within *E. coli* cells or in an *in-vitro* reaction.

Furthermore, we used atomic force microscopy (AFM) to analyze the size and morphology of the purified particles. We found homogeneous particles with a size of about 25 nm and a height of around 15 nm in both rAAV5 and VLP samples (**Figure 11e, f, g, h**). This is characteristic of AAV particles and consistent with a previous report.<sup>209</sup> Notably, the previous reports showed that the insertion of a peptide onto a loop of AAV5 capsid did not interfere with capsid formation in HEK-293 production.<sup>210,211</sup> Thus, the AAV5 capsids produced in *E. coli* can be used for an antigen display in vaccination.

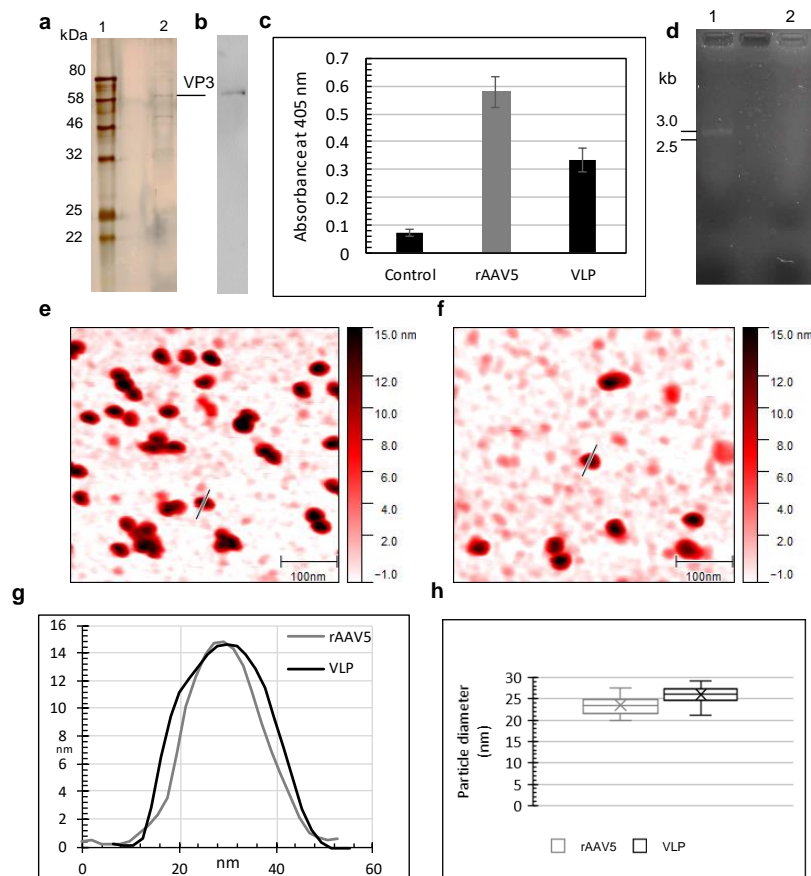


**Figure 11.** Purification and characterization of AAV5 VLPs. (a) SDS-PAGE of purified VLPs; lane 1, protein ladder; lane 2, sample after purification by POROS AAVX resin column. (b) Western blot analysis of sample after purification (Figure 11a (lane 2)) with B1 antibody. (c) ELISA probed with anti-AAV5 (intact capsid) antibody (ADK5a). (d) Agarose gel electrophoresis (rAAV5 and VLPs were heated at 95°C for 10 min, run in 1% Agarose gel, TAE buffer and stained by SYBR Gold; lane 1, rAAV5 ( $4 \times 10^{10}$  rAAV particles/well); lane 2, VLPs (about  $4 \times 10^{10}$  VLPs/well)). (e) AFM image of rAAV5 produced in HEK-293. (f) AFM image of AAV5 VLPs produced in *E. coli*. (g) Height profile of rAAV5 and VLPs. (h) Box plot of the size distribution of rAAV5 and VLPs determined by AFM ( $n = 20$ , mean  $\pm$  SD, box from first to third quartile, cross median marker).

## 4 Results and Discussion

We used HeLa cells to assess the cellular uptake of VLPs and thereby their biological activity. HeLa cells were incubated with rAAV5 and AAV5 VLPs, fixed, permeabilized and stained with the ADK5a antibody and a fluorescent coupling secondary antibody. After 2 h of incubation, both rAAV5 and VLPs were found inside the cells (**Figure 12b, c**), while no signal was detectable in the buffer control (**Figure 12a**). The particle distribution after 2h was in line with the previous reports of rAAV5 internalization into HeLa cells.<sup>212,213</sup> AAV5 enters into the cell by receptor-mediated endocytosis. The particles initially bind to  $\alpha$ 2-3 sialic acid on the cell surface as a primary receptor,<sup>214</sup> then interact with the platelet-derived growth factor receptor (PDGFR)<sup>215</sup> and the polycystic kidney disease 1 (PKD1) domain of the AAV receptor.<sup>192,216</sup> Since the recognized domains of AAV5 are present on the VP3-only capsid exterior, VP3-only AAV5 capsids are able to internalize into cells. This finding demonstrated the biological activity of VLPs and offers an application of VLPs in drug delivery into human cells.

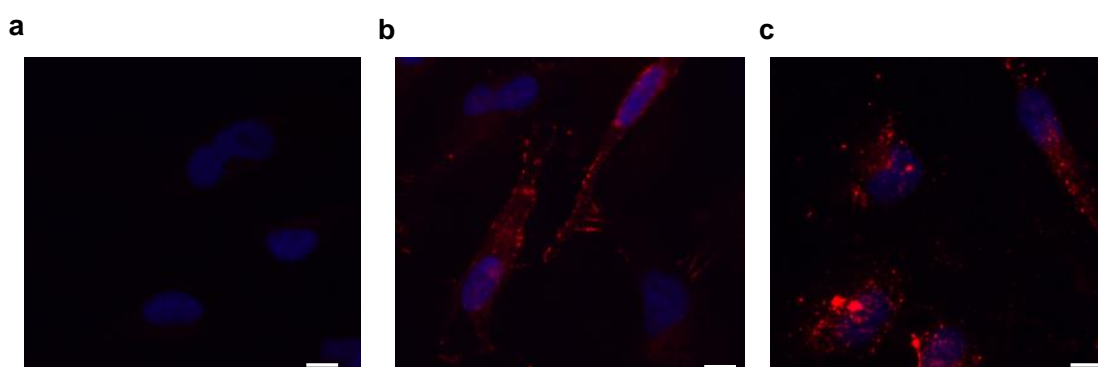


Figure 12. Internalization of rAAV5 and VLPs. HeLa cells were treated with (a) buffer, (b) rAAV5 or (c) VLPs. Samples were stained with the ADK5a antibody followed by a Dylight 594 conjugated secondary antibody (red) and DAPI (blue). Scale bars are 10  $\mu$ m.

### 4.2.3. Co-expression of AAV5 VP3 and AAP5 in *E. coli* improved capsid assembly yields

rAAV5 is able to form capsids without AAP5 in HEK-293 cells, although the supply of AAP5 *in trans* improves rAAV production significantly.<sup>4</sup> Therefore, we cloned AAP5 with a His-tag coding sequence 3' of the gene into another pET vector (pET21-AAP5, **Figure 13a**) and co-transformed *E. coli* with this vector and pET24-AAV5-VP3 vector (**Figure 10a**). The addition of a tag at the C-terminus of the AAP protein has previously been shown not to interfere with AAP function,<sup>196</sup> and allows the detection of AAP5 expression. AAP5 was successfully co-expressed with VP3 in *E. coli* as proven by western blot analysis (**Figure 13b, c**). Notably, in addition to the experimentally expected band of AAP5 (about 33 kDa),<sup>4</sup> degraded fragments were also visible (**Figure 13b**), which is in agreement with a previous report of AAP5 expression in HEK-293 cells.<sup>217</sup> Furthermore, the expression of VP3 protein in *E. coli* expressing also AAP5 was lower compared to VP3 expression

## 4 Results and Discussion

in *E. coli* harboring VP3 only (**Figure 13c**). However, even though a reduced amount of VP3 protein was observed, the assembled particles significantly increased in the co-expression system as shown by western blot analysis with the B1 antibody of POROS AAVX purified particles (**Figure 13d**) and about 3.6-fold by sandwich ELISA with PKD1 as a capture agent (produced in *E. coli*) and the ADK5a antibody as detection antibody (**Figure 13e**). This is the first evidence that AAP5 helps to improve the capsid production in *E. coli* and hints again on the fundamental chaperone activity of AAP, which was reported during AAV capsid production using mammalian cells,<sup>12</sup> yeast<sup>26</sup> and *in vitro* assembly.<sup>59</sup>

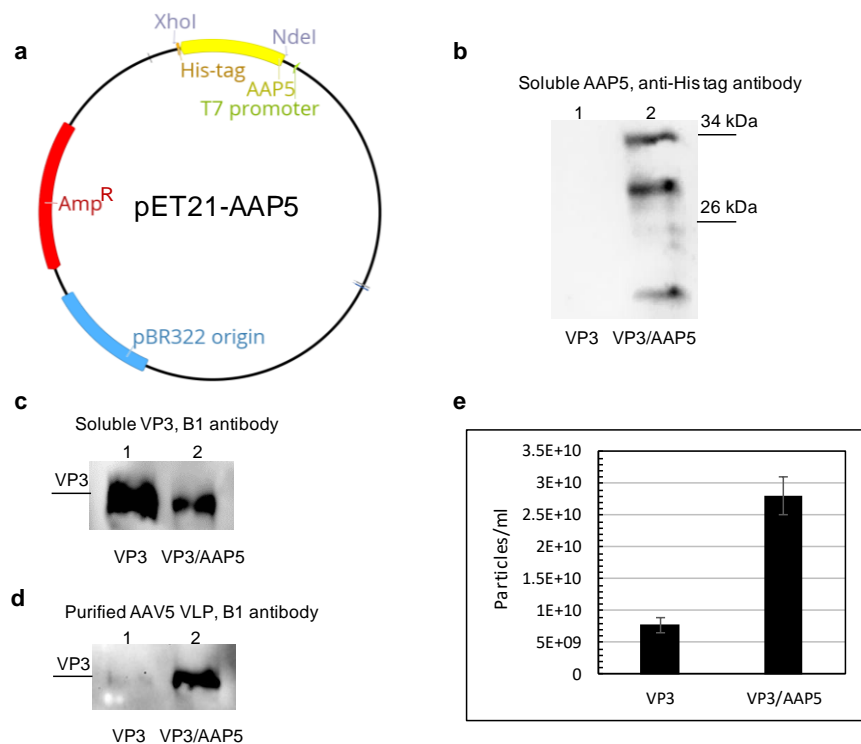


**Figure 13.** Co-expression of AAP5 and AAV5 VP3 in *E. coli*. (a) Plasmid map of pET21-AAP5. A His6-tag was inserted at the C-terminus of AAP5. (b) Western blot with the anti-His-tag antibody of the soluble fraction of intracellular proteins after induction and expression; lane 1, *E. coli* harboring pET24-AAV5-VP3; lane 2, *E. coli* harboring pET24-AAV5-VP3 and pET21-AAP5. (c) Western blot of the soluble fraction of intracellular proteins with the B1 antibody after induction and expression; lane 1, *E. coli* harboring pET24-AAV5-VP3; lane 2, *E. coli* harboring pET24-AAV5-VP3 and pET21-AAP5. (d) Western blot of the purified VLPs with the B1 antibody; lane 1, *E. coli* harboring pET24-AAV5-VP3; lane 2, *E. coli* harboring pET24-AAV5-VP3 and pET21-AAP5. (e) A number of purified VLPs estimated by sandwich ELISA using PKD1 protein and the ADK5a antibody with qPCR-titered rAAV5 from HEK-293-production taken as reference.

### 4.3. Applications of *in vitro* AAV assembly

In this chapter, *in-vitro* AAV VLPs were utilized for vaccine development against SARS-CoV-2, packaging DNA for therapeutic delivery and labeling with a fluorophore for imaging.

### 4.3.1. AAV2 VP3 capsid proteins fused with SARS-CoV-2 RBD or RBM: Expression in *E. coli*, *in-vitro* assembly and functional characterization

This work was presented at the American Society Gene and Cell Therapy 24<sup>th</sup> Annual Meeting and published in *Molecular Therapy* with the title “AAV Capsid Proteins Fused with SARS-CoV-2 RBD or RBM: Expression in *E. coli*, *In-Vitro* Assembly, and Characterization”.<sup>218</sup>

In the current COVID-19 pandemic, the SARS-CoV-2 virus has infected over hundred million people and contributed to millions of deaths. Receptor-binding domain (RBD) in the SARS-CoV-2 spike protein (S protein), in particular its receptor-binding motif (RBM), is responsible for virus binding to the cellular receptor angiotensin-converting enzyme 2 (ACE2) and subsequent viral internalization (**Figure 14**),<sup>219</sup> therefore they are promising candidates for SARS-CoV-2 subunit vaccine development. VLPs have been widely used for vaccine development due to their ability to induce a strong immune response and AAV VLPs produced in mammalian cells have been tested as a scaffold for presenting antigens.<sup>199,200</sup> However, mammalian cell culture is expensive and VLPs may contaminate cellular components. As described in chapter 4.1, AAV2 VP3 capsid protein produced in *E. coli* can be assembled to AAV2 VLPs *in vitro*, and the incorporation of a His6-tag into the 587-loop of VP3 protein was compatible with capsid assembly. Thus, to explore the potential of our *in-vitro* AAV2 VLPs in vaccine development, SARS-CoV-2 RBM and RBD were incorporated into the AAV2-VP3 587-loop. The fusion proteins VP3 and RBM (VP3\_RBM), VP3 and RBD (VP3\_RBD) were produced in *E. coli* and used for VLP assembly *in vitro* to generate VLP-based vaccine candidates.

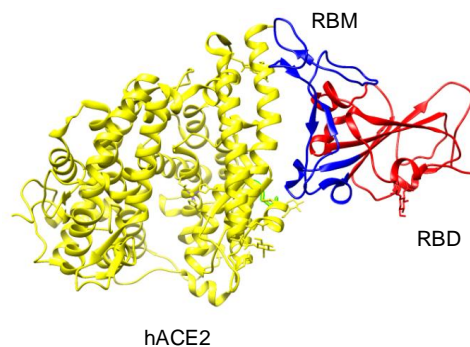


Figure 14. Structure of SARS-CoV-2 RBD, core subdomain (red) and RBM (blue), in complex with its human ACE2 (hACE2) receptor (yellow) (PDB: 6LZG).

#### 4.3.1.1. AAV2 VP3\_RBM and VP3\_RBD expression in *E. coli* and purification

AAV2 VP3\_RBM and AAV2 VP3\_RBD sequences containing a His6-tag were cloned into pET24 vectors and introduced into *E. coli* cells (**Figure 15a**). These proteins were then expressed at 18°C or 37°C. As a result, VP3\_RBD and VP3\_RBM fusion proteins aggregated into inclusion bodies during expression, and both proteins were successfully purified by IMAC under denaturing conditions of 8 M urea. VP3\_RBM and VP3\_RBD proteins were observed with an apparent mass of about 68.8

## 4 Results and Discussion

and 86.4 kDa, respectively (**Figure 15b**). The *E. coli* expression of RBM and RBD-fused AAV2 VP3 is similar to that of AAV2 VP3 protein only (**Figure 3**) that formed inclusion bodies even at the low expression temperature (18°C). A recent study on expression of SARS-CoV-2 RBD fused with capsid proteins of norovirus in *E. coli* also resulted in inclusion bodies.<sup>220</sup> The reducing environment in *E. coli* cytoplasm could cause the aggregation of RBD protein, which comprises four pairs of disulfide bonds in the structure.<sup>221</sup> In addition, N-terminus-degraded fragments of VP3\_RBM and VP3\_RBD proteins were also found during expression in *E. coli* (**Figure 15b**) that was observed during the expression of AAV2 VP3 proteins only (**4.1.1**). The obtained proteins were used for *in vitro* refolding and concomitant assembly.

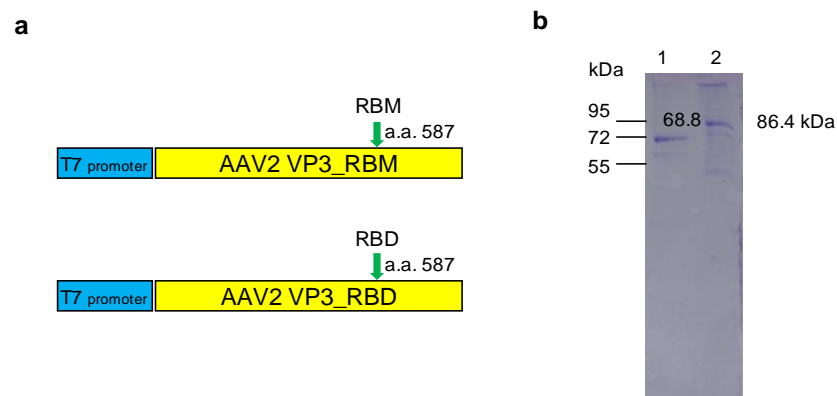


Figure 15. AAV2 VP3\_RBM and AAV2 VP3\_RBD expression in *E. coli* and purification. (a) Schematic representation of AAV2 VP3\_RBM and AAV2 VP3\_RBD protein expression construct downstream of a T7 promoter. RBM and RBD coding sequences were incorporated at the a.a. 587 coding position of the AAV2 VP3 gene. (b) Protein expression in *E. coli* and purification under denaturing conditions. Lane 1, AAV2 VP3\_RBM after IMAC purification; lane 2, AAV2 VP3\_RBD after IMAC purification.

### 4.3.1.2. *In vitro* refolding and concomitant assembly of AAV2 VP3\_RBM and VP3\_RBD proteins to VLPs, and VLP characterization

Refolding and concomitant *in vitro* assembly of AAV2 VP3\_RBM VLPs or VP3\_RBD VLPs was attained by serially dialyzing initial denatured proteins against different buffers containing 4, 2, 1, 0.5, and finally 0 M urea. After dialysis, the refolded protein samples were measured by AFM. **Figure 16** shows that VP3\_RBM VLPs and VP3\_RBD VLPs were found under AFM with the expected size of about 24 nm and 32 nm, respectively. Though irregular formations and smaller structures, potentially single or intermediate assemblies, were observed in both samples. The AFM-recorded formations are similar to those of AAV2 VP3 587His6 VLP after *in vitro* assembly (**Figure 7**), hinting that the incorporation of RBM or RBD into the 587-loop did not interfere with *in vitro* AAV2 VLP capsid assembly. The size of *in-vitro* AAV2 VP3 VLPs was about 22 nm (**Figure 4d, e**), therefore we attribute the slightly larger size of VP3\_RBD VLPs (32 nm) to the introduction of a 26-kDa RBD protein on the AAV2-VP3 587-loop. The incorporation of a protein into the 587-loop of AAV2 led to an increase of particle size was also observed during production in HEK-293 cells by our working group.<sup>222</sup>

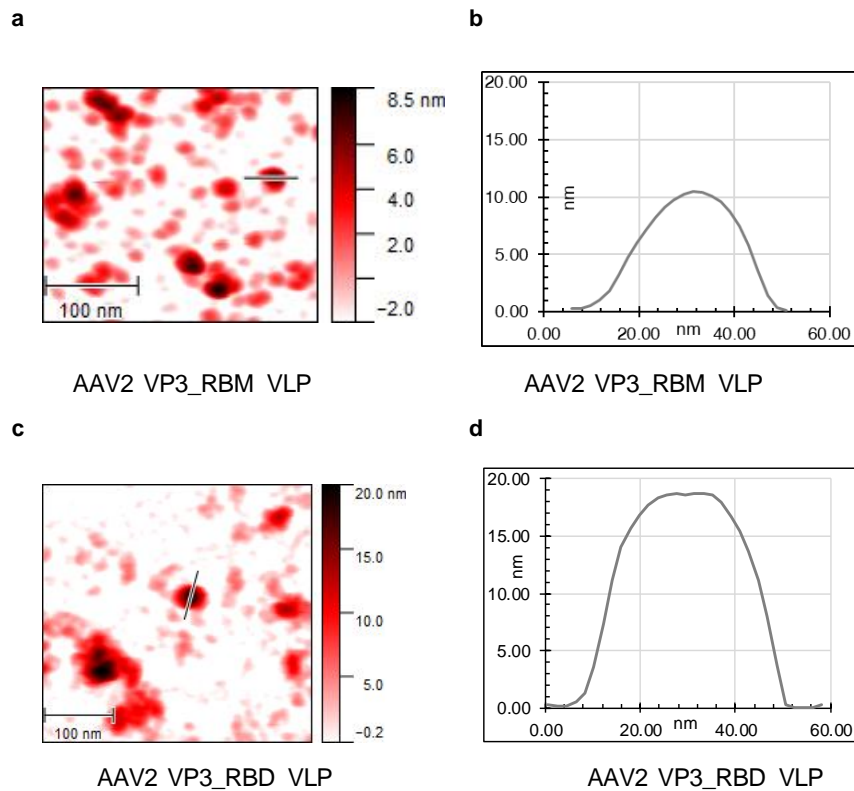


Figure 16. AFM images and height profiles of AAV2 VP3\_RBM and VP3\_RBD VLPs after assembly. (a) and (b) AFM image and height profile of VP3\_RBM VLPs. (c) and (d) AFM image and height profile of VP3\_RBD VLPs. Scale bars are 100 nm.

Next, ELISA with a conformational RBD antibody was performed to assess a correct conformation of RBD presented on the VP3\_RBD VLPs after assembly. The results presented in **Figure 17** confirmed the conformation of the refolded RBD that fused to the 587-loop of AAV2 VP3, indicating at least partial correct folding of VP3\_RBD. This finding is the first evidence that the refolded RBD from inclusion bodies in *E. coli* was readily recognized by the conformational RBD nanobody.

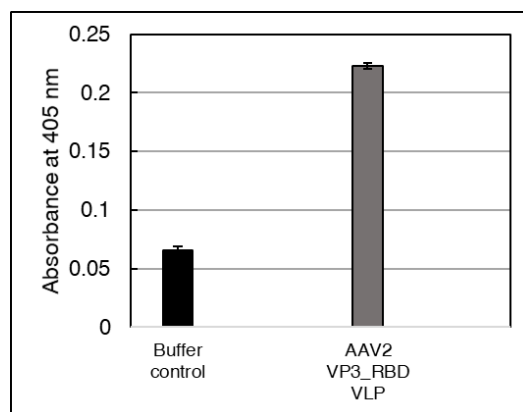


Figure 17. ELISA probed with an anti-conformational RBD antibody.

### 4.3.1.3. Expression of GFP fused with RBD protein in 293-F cells

SARS-CoV-2 enters human cells via the interaction between SARS-CoV-2 RBD and the hACE2 receptor, therefore, to block the SARS-CoV-2 entry, induced antibodies from vaccine recipients are required to specifically bind to conformational RBD proteins. Therefore, as a control for SARS-CoV-2 specificity, we sought to produce the conformational RBD in 293-F cells. To do this, we used a pcDNA3-SARS-CoV-2-S-RBD-sfGFP plasmid (No. 141184, Addgene) that contains a GFP-fused RBD (RBD\_GFP) sequence downstream of a signal peptide sequence from influenza hemagglutinin (HA) and a CMV promoter for protein expression. A His6-tag was then cloned at 3' of the RBD\_GFP sequence to aid protein purification. The incorporation of a fluorescent protein into RBD proteins allows us to assess the RBD functionality. Superfolder GFP (sfGFP) was preferred due to its folding ability when fused to other proteins.<sup>223</sup> The RBD\_GFP fusion protein was then expressed in 293-F cells and the secreted protein was subsequently purified by an IMAC column. The results presented in **Figure 18a, b** demonstrate that the RBD\_GFP protein was successfully purified from 293-F cultures with an apparent band of about 50 kDa (lane 3, **Figure 18b**), and the GFP protein folded properly as observed under UV light (**Figure 18a**).

Next, we aimed to generate HEK-293 cells expressing the SARS-CoV-2 receptor hACE2 and assess the binding ability of the produced RBD to the expressed hACE2 receptor to prove RBD functionality. The expression of the membrane protein hACE2 receptor on the HEK-293 cell surfaces was described before by Moore et al.<sup>224</sup> In this work, HEK-293 cells were transfected with a pcDNA3.1-hACE2 plasmid (No. 1786, Addgene), which consists of an hACE2 DNA sequence downstream of a CMV promoter, and subsequently incubated for 48 h prior to analysis. Afterwards, the purified RBD\_GFP proteins at different concentrations (50 nM, 100 nM, 200 nM) were applied onto HEK-293 cells expressing the hACE2 receptor (**Figure 18c**). As a negative control, the RBD\_GFP proteins were also incubated with untransfected HEK cells. After washing to remove non-specific binding, the binding ability of RBD to hACE2 was evaluated via GFP-positive cells by FACS. **Figure 18d** indicates that the RBD protein produced in 293-F cells specifically bound to hACE2 receptor-expressed cells but not untransfected cells, and thereby proven its functionality. These data also suggest that the untransfected HEK cells did not present detectable hACE2 receptors, about 80% of the transfected HEK-293 cell population displayed hACE2 on their surfaces, and 50 nM RBD\_GFP was sufficient to entirely bind to the receptors. The direct binding of RBD\_GFP protein to the hACE2 receptor expressed on the HEK-293 cell surfaces also offers a feasible model to assess neutralizing antibodies induced by vaccine candidates.

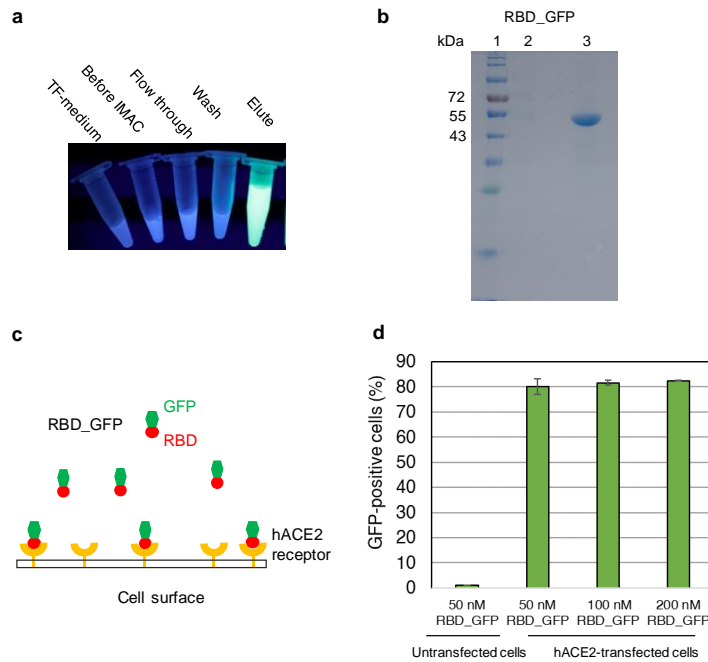


Figure 18. RBD\_GFP protein expression in 293-F cells and purification. (a) Samples before and after IMAC purification under UV light. (b) SDS-PAGE gel of RBD\_GFP purification. Lane 1, protein ladder; lane 2, medium sample before IMAC purification; lane 3, samples after IMAC purification. (c) Schematic representation of RBD\_GFP binding to the hACE2 receptors. (d) Binding assay of RBD\_GFP to HEK-293 displaying hACE2 receptors. RBD\_GFP (50 nM, 100 nM, 200 nM) was applied to hACE2 plasmid-transfected HEK-293 cells. 50 nM RBD\_GFP was also applied to untransfected cells as a negative control. The percentage of GFP-positive cells was calculated using FACS.

#### 4.3.1.4. Immunization of mice and immune response

Mouse experiments were conducted by Dr. Olaf Behrsing, Molecular Biotechnology, Institute for Biochemistry and Biology, University of Potsdam, Germany with proteins provided by me. VP3\_RBM and VP3\_RBD VLPs mixed with/without complete Freund's adjuvants (CFA) were used to immunize. Mice were vaccinated with VP3\_RBM VLP antigens and CFA for the first immunization, then with antigens only (without CFA) for the boosters. For VP3\_RBD VLP immunization, one mouse was injected with antigens only for the first immunization, while another mouse was immunized with VP3\_RBD VLP antigens mixed with CFA. After that VP3\_RBD VLP antigens only were used for the boosters. Serum was collected at various timepoints (**Figure 19**). The immune response was examined by ELISA with coated antigens (VP3\_RBM and VP3\_RBD VLPs), VP3 VLP scaffolds, GFP proteins as well as RBD\_GFP produced in 293-F cells (**4.3.1.3**) as a control for SARS-CoV-2 specificity.

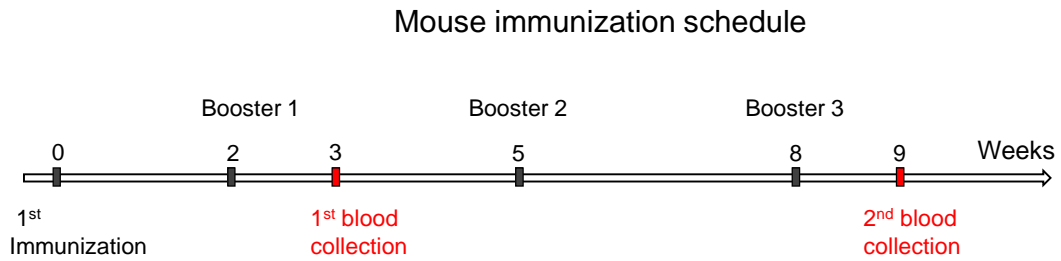


Figure 19. Mouse immunization schedule.

The results of mouse immunization with AAV2 VP3\_RBM VLP and VP3\_RBD VLP presented in **Figure 20** and **Figure 21** (yellow bars) showed that both VP3\_RBM VLPs and VP3\_RBD VLPs elicited immune responses against the injected antigens. Notably, a mouse injected with VP3\_RBD VLPs without the adjuvants (mouse 1, **Figure 21**) also showed a strong immune response. This finding is in agreement with the immunization of VLPs that are known to be high immunogenic.<sup>225,226</sup> Complete Freund's adjuvants (CFA), which consists of killed *Mycobacterium tuberculosis* and is known to enhance an immune response in mice,<sup>227</sup> were mixed and vaccinated with the particles for the first immunizations that could also contribute to the observed strong immune responses.

Importantly, the vaccination of AAV2 VP3\_RBM VLP resulted in a relatively high level of RBD\_GFP-specific antibodies, especially in the sera from the second blood collection (blue bars, **Figure 20**), besides, the generated antibodies did not bind to the GFP control (green bars, **Figure 20**). This indicates the SARS-CoV-2-RBD specificity of the induced antibodies. The RBD-specific antibodies have shown a strong correlation to viral neutralization,<sup>228–230</sup> hinting great potential of VP3\_RBM VLP vaccine candidates for preventing SARS-CoV-2 infection. Also, **Figure 20** suggests that the amount of RBD-specific antibodies in the second serum collection (**b, d**) were much higher than those presented in the first collection (**a, c**). Thus, the longer intervals and additional boosters of the particles benefit the RBD-specific antibody generation.

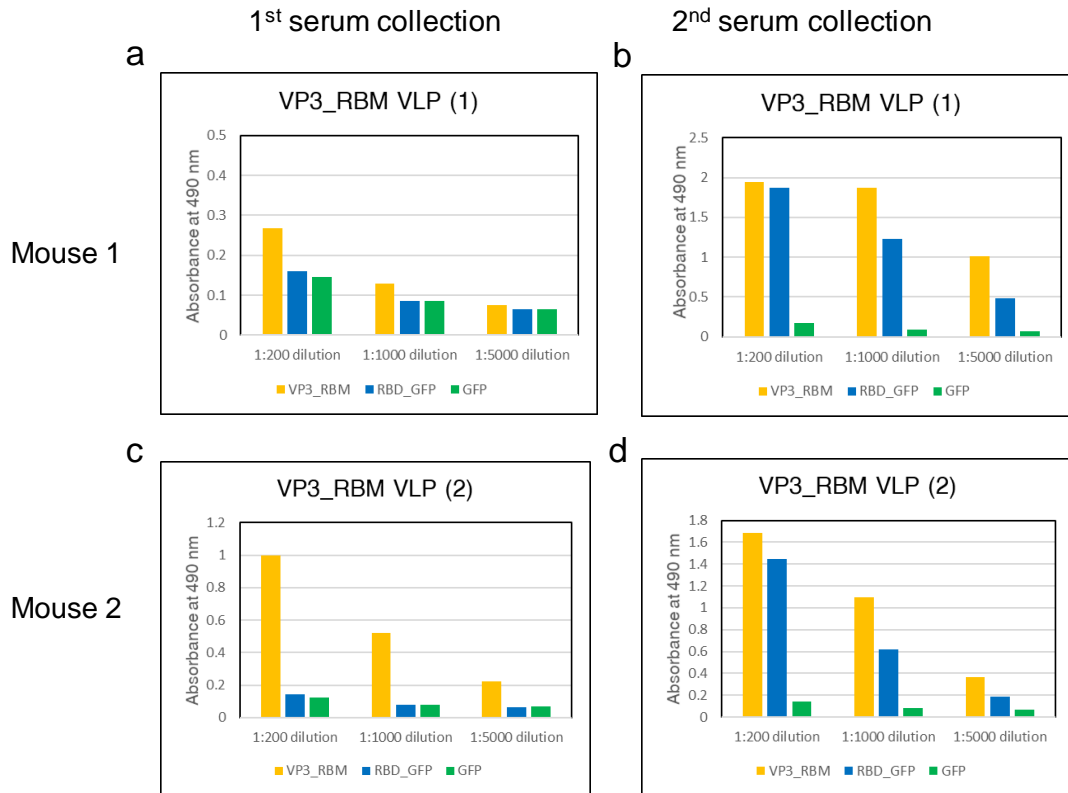


Figure 20. Mouse vaccination with AAV2 VP3\_RBM VLPs. Antigen-specific IgG antibodies in sera from the immunized mice were measured by ELISA. Sera (1:200, 1:1000, 1:5000 dilution) were applied on a plate captured with AAV2 VP3\_RBM VLPs (yellow), RBD\_GFP (blue), GFP only (green).

Unexpectedly, even though AAV2 VP3\_RBD VLPs induced a strong immune response against the vaccinated antigen AAV2 VP3\_RBD VLPs, the induced antibodies mainly targeted the AAV2 VP3 VLP scaffolds (red bars), but not SARS-CoV-2 RBD proteins (blue bars) (Figure 21). This suggests a small amount of AAV2 VP3\_RBD VLPs comprising a correct RBD conformation presented in the injected samples that may not be enough for the RBD-specific antibody generation. The protein expression in *E. coli* resulted in the absence of glycosylation of RBD that was present at two sites N331 and N343 when expressed in human cells.<sup>231</sup> This modification may disturb the RBD conformation.<sup>232</sup> Also, the larger size of RBD (26 kDa), compared to its motif (RBM) (8.3 kDa), could hinder the correct RBD-structure formation during *in vitro* capsid assembly of VP3\_RBD VLPs. To increase RBD refolding efficiency, RBD with different flexible linkers could be incorporated into the 587-loop of VP3 protein in the future. Moreover, the AFM results of VLP assembly (Figure 16) indicate the presence of other contaminated structures in the injected antigens, therefore *in-vitro* assembly optimization and further purifications of VLPs will improve the antigen-directed immune responses.

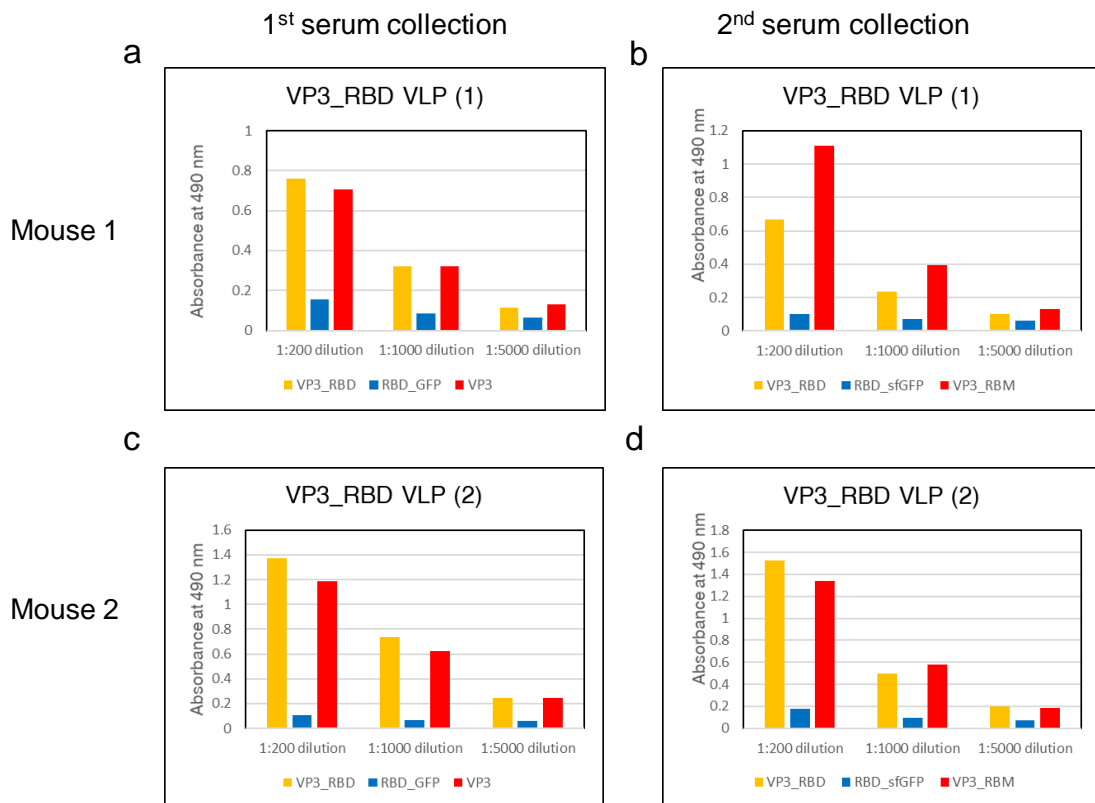


Figure 21. Mouse vaccination with AAV2 VP3\_RBD VLPs. Mouse 1 was vaccinated with VP3\_RBD antigens only. Mouse 2 was vaccinated with VP3\_RBD antigens mixed with CFA for the first immunization, VP3\_RBD antigens only for the boosters. Antigen-specific IgG antibodies in sera from the immunized mice were measured by ELISA. Sera (1:200, 1:1000, 1:5000 dilution) were applied on a plate captured with AAV2 VP3\_RBD VLPs (yellow), RBD\_GFP (blue) and VLP scaffolds (red).

Currently, SARS-CoV-2 spike protein (S protein) and RBD have been tested as favorable candidates for many SARS-CoV-2 protein subunit vaccine candidates.<sup>233</sup> However, RBM, the small motif of RBD, which interacts directly with the cell receptor hACE2,<sup>221</sup> is less attractive for vaccination due to its low immunogenicity. VLPs have a size of 20-200 nm and repeated structures known to be high immunogenic, therefore, they have been used for presenting peptides of interest on the VLP surfaces to enhance peptide-directed immune responses.<sup>234</sup> Herein, for the first time, *in-vitro* AAV VLPs were used to display antigens on their surfaces. As a result, AAV2 VP3\_RBM VLP elicited the strong SARS-CoV-2-specific antibody response. Since we immunized mice with VLPs presenting RBM, the generated antibodies that bound to conformational RBD in the serum ELISA are RBM-directed. As reported before, most SARS-CoV-2 neutralizing antibodies bind directly to RBM and thereby block virus-receptor interaction,<sup>235</sup> suggesting the neutralizing potential of the antibodies induced by VP3\_RBM VLPs. In addition, the prevalence of anti-AAV2 antibodies has been reported between 30% and more than 60% of the human population.<sup>236</sup> Interestingly, a previous study on the immunogenicity of AAV2 VLPs presenting L2 epitopes (HPV) demonstrated that pre-existing

anti-AAV2 antibodies rather boost than prevent the antigen-directed immune response.<sup>200</sup> Even though more studies are still needed, our data suggest that AAV2 VP3\_RBM VLP is a promising vaccine candidate for SARS-CoV-2 and our *in-vitro* AAV VLPs bear potential as vaccine scaffolds.

### 4.3.2. *In vitro* encapsidation of DNA into AAV VLPs

#### 4.3.2.1. Arginine-rich motif (ARM) fused with AAV5 VP3 capsid protein expression, purification and *in vitro* assembly

AAV packaging was proposed as an active process, in which AAV capsid forms followed by an AAV genome encapsidation.<sup>7</sup> As yet the viral packaging model and components remain unclear, we attempted to incorporate an arginine-rich motif (ARM) into AAV capsid protein for packaging of DNA into AAV capsids. ARM has been proven to aid virus packaging passively by interacting with negatively charged DNA genomes.<sup>237</sup> ARM also contains a nuclear localization signal (NLS) sequence,<sup>90</sup> which is needed for the delivery of a gene to the cell nucleus for expression. As described in **4.2.1**, we demonstrated that AAV5 VP3 capsid protein was able to form *in-vivo* AAV5 VLPs during protein expression in *E. coli*, however, the majority of soluble VP3 protein was still unassembled and the protein could be obtained for *in vitro* assembly. We therefore incorporated the ARM into the N-terminus of AAV5 VP3 (VP3\_ARM) and then cloned the VP3\_ARM sequence into a pET24 expression vector (**Figure 22a**). A His6-tag was also added to VP3\_ARM to aid protein purification. The fusion protein VP3\_ARM was expressed in *E. coli* at 18°C overnight and purified by an IMAC column. Purification buffers with the high-salt concentration (1 M NaCl) were used to get rid of possible contaminating nucleic acids bound to the ARM as has been reported before.<sup>90</sup> The results in **Figure 22b** indicate that the protein was expressed in soluble form with an evident band of about 65 kDa and successfully purified by IMAC. This is similar with the expression result of AAV5 VP3 only in *E. coli* (**4.2.1**), implying that the introduction of the ARM did not interfere with protein expression in *E. coli*. VP3\_ARM fusion protein in high salt concentration was subsequently dialyzed into an assembly buffer (**6.2.5.8**) to assemble capsids. As a result, ARM\_VP3 VLPs were found by AFM measurement (**Figure 22c, d**). The VP3\_ARM VLPs were similar in diameter (about 28 nm) and height to AAV5 VP3 particles assembled inside *E. coli* (**4.2.2**), even though small assemblies were also observed. The insertion of ARM at VP3 N-terminus therefore did not hinder the AAV5 VLP formation.

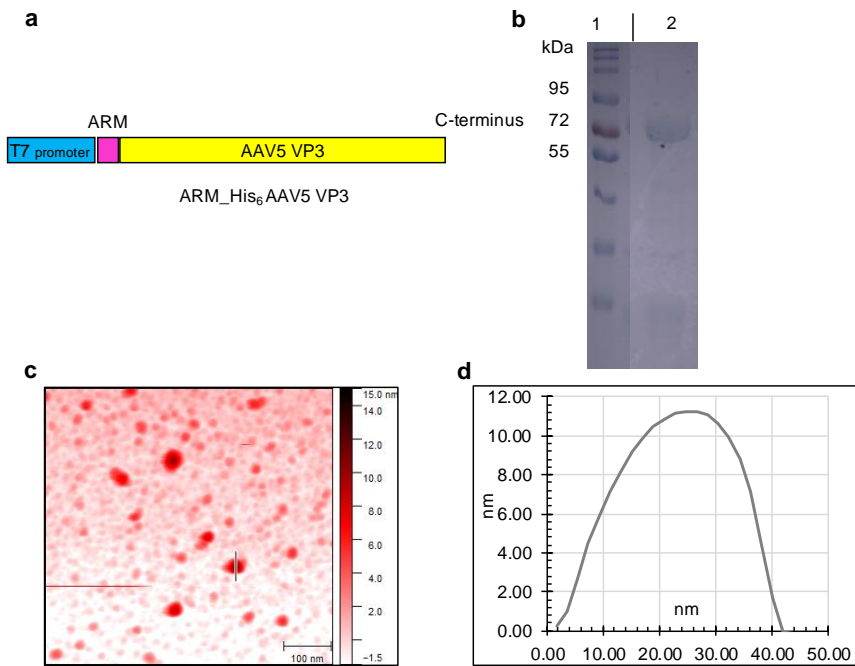


Figure 22. ARM\_VP3 production and in vitro assembly. (a) Schematic representation of ARM\_VP3 expression construct. ARM sequence was cloned 5' of the AAV5-VP3 sequence. (b) ARM\_VP3 production in *E. coli*. Lane 1, protein ladder; lane 2, ARM\_VP3 protein was purified by IMAC column. (c) AFM image of ARM\_VP3 VLPs. Scale bar is 100 nm. (d) Height profile of ARM\_VP3 VLPs by AFM measurement. The black vertical line divides two different crops of the same gel.

#### 4.3.2.2. ssDNA production

AAV has a single-stranded DNA genome of about 4.7 kb, therefore we sought to produce ssDNA with a similar size for an *in-vitro* encapsidation into AAV VLPs. An ITR-mKate plasmid containing the mKate-protein expression cassette flanked by ITR sequences (**Figure 23a**) was transformed into *E. coli* ER2738, after that the helper phage M13KO7 was added to the transformed *E. coli* culture for ssDNA production. **Figure 23b** demonstrates that we successfully produced ssDNA using a phagemid and the helper phage. CHO-K1 cells were transfected with the produced circular ssDNA to assess protein expression. Fluorescence microscopy was used for mKate detection. **Figure 23c, d** reveals that mKate protein was highly expressed in CHO-K1 cells. Once circular ssDNA enters the cells, ITR sequences may play a role in DNA transcription for gene expression. The expression of a protein from circular ssDNA containing ITR sequences was also observed before with the hybrid vector AAV/phage,<sup>238</sup> even though the mechanism of ITR sequences involved remains unclear. The produced ssDNA can be used for *in vitro* encapsidation or as a DNA template for AAV genome production if a digestion reaction to remove the plasmid backbone becomes possible.

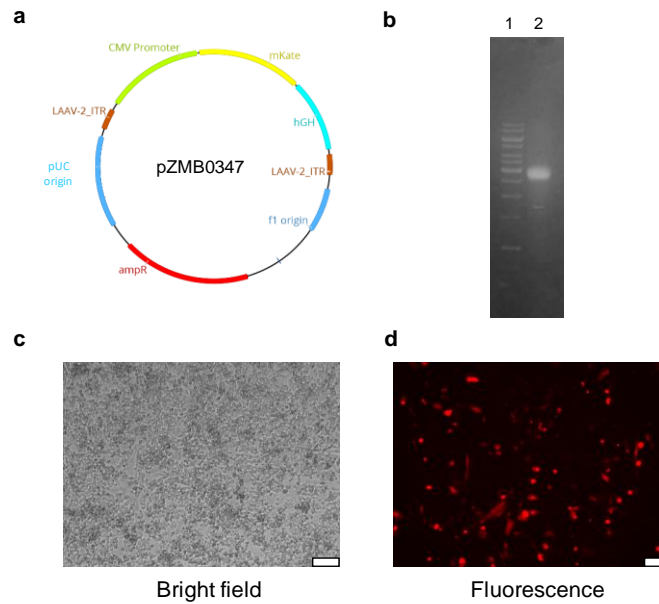


Figure 23. ssDNA production. (a) Plasmid map of pZMB0347 (pUC19bb\_ITR\_EXS\_pCMV\_mKate2\_hGH). The mKate-gene expression cassette is flanked with AAV2\_ITR sequences. The plasmid contains pUC and f1 origin for its replication in *E. coli* and packaging in phages. (b) *cssDNA* produced in phage on an agarose gel. Lane 1, DNA ladder; Lane 2, ssDNA. (c, d) ssDNA transfection results in CHO-K1 cells under bright light (c) and fluorescent channel for the detection of mKate expression (d). Scale bars are 100  $\mu$ m.

#### 4.3.2.3. DNA encapsidation into ARM\_VP3 VLPs

To perform the encapsidation, ssDNA was mixed with ARM\_VP3 protein with a molar ratio of about 1 DNA per capsid (60 proteins). The encapsidation result was first examined by qPCR to detect possible DNA protected by the VLPs from DNase I digestion. As a control, the mixture of VP3\_ARM and ssDNA was preheated at 95°C, 5 min. Prior to qPCR, samples were digested with DNase I to remove unprotected DNA. The result in **Figure 24a** shows that ssDNA was protected by VLPs during digestion compared to the control.

The arginine-rich motif (ARM) showed the ability to aid *in vitro* capsid formation of the beak and feather disease virus (BFDV) by interaction with its ssDNA genome.<sup>90</sup> Thus, to examine the effect of our produced ssDNA on AAV capsid assembly *in vitro*, we performed capsid ELISA with an anti-AAV5, intact-capsid antibody, which recognizes assembled capsids only. The ELISA results indicate that the addition of ssDNA into the assembly reaction did not improve capsid assembly yield compared to the assembly of VP3\_ARM only, though VLPs were detected (**Figure 24b**).

Since CHO-K1 cells shown sufficient *in-vitro* transduction efficacy with rAAV5,<sup>239</sup> we used this cell line to evaluate the transduction ability of our possible DNA-encapsidated VLPs via expression of the fluorescent protein. rAAV5 produced in HEK-293 cells was also used as a positive control. In **Figure 24c**, rAAV5 showed the ability to transduce the cells at the MOI of  $10^5$  particles as indicated by the expression of the AAV transgene (mVenus). Contrary, there was no fluorescent signal detected in the VLP sample, suggesting that VLPs did not transduce the cells. Meanwhile, 1.3 kb-dsDNA (short CMV promoter\_mVenus\_polyA derived from pZMB0522 vector by PCR) and 2.2 kb-

## 4 Results and Discussion

dsDNA (CMV promoter\_mKate\_polyA derived from pZMB0347 by digestion with PvuII) were also used for packaging into ARM\_VP3 capsids. The encapsidation results were similar to those of ssDNA, ARM\_VP3 was able to protect DNA from attack by DNase but not mediate protein expression in CHO-K1 cells. Conformational differences between the circular ssDNA, dsDNA used and the linear ssDNA AAV genome could hinder DNA packaging into VLPs. We cannot rule out that the *in-vitro* assembly and passive packaging efficacy was too low as shown by the small number of capsids formed (ELISA results, **Figure 24b**), even though AFM confirmed the presence of VLPs after DNA packaging reactions. AAP improved capsid assembly *in vitro*,<sup>59</sup> hence AAP can be added into packaging reactions in the future. Other tasks will be the generation of linear ssDNA AAV genome, optimization of packaging reactions with different buffer conditions. Other DNA-binding domains could also be incorporated into VP3 capsid proteins to support *in vitro* packaging.

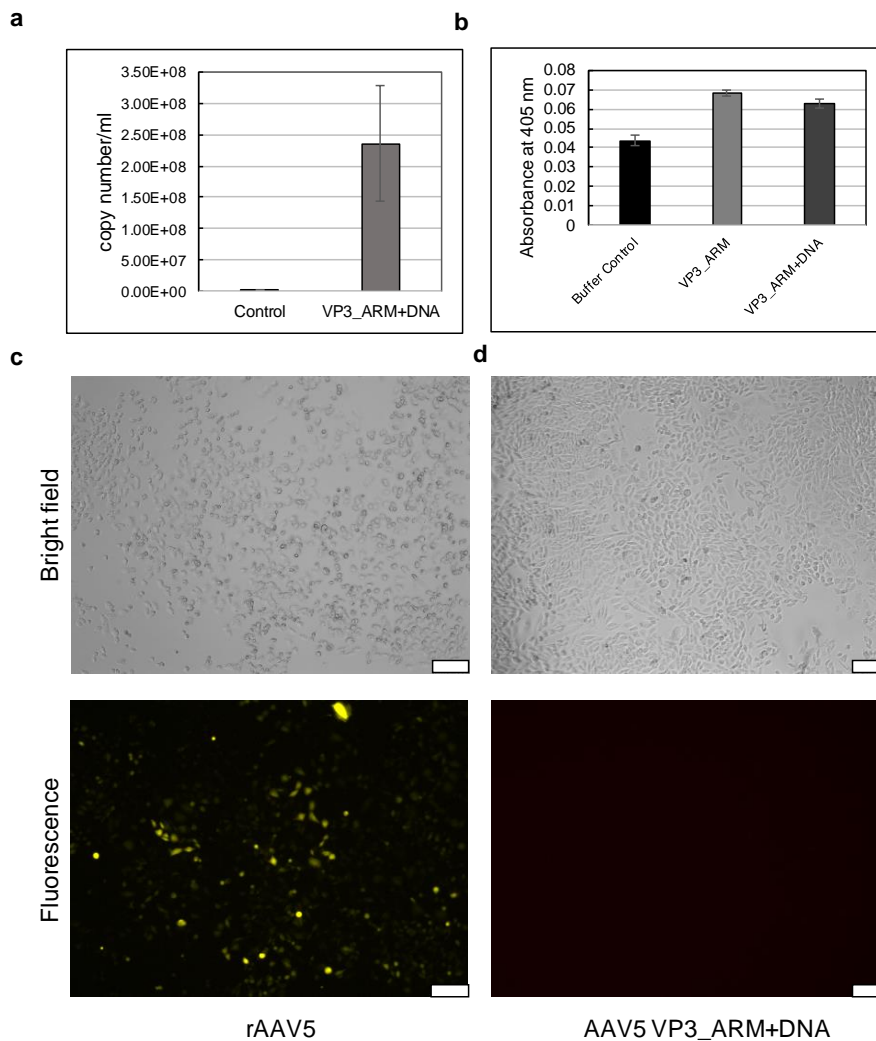


Figure 24. ssDNA encapsidation results. (a) qPCR determined DNA protected by ARM\_VP3 protein. (b) ELISA probed with ADK5a antibody (anti-intact AAV5 capsids). (c) rAAV5 transduction results with an MOI of  $10^5$  AAV particles under bright field and fluorescence. (d) Results of DNA-encapsidated VLP transduction under bright field and fluorescence. Scale bars are 100  $\mu$ m.

4.3.3. *In vitro* AAV VLP chemical conjugation for imaging

## 4.3.3.1. AAV2 VP3 VLP and FITC conjugation

For AAV2 VLP imaging, FITC was chosen to conjugate to the VLPs via primary amines. FITC reacts with primary lysine amino acids on the AAV2 VLP surface to form a covalent bond.<sup>240</sup> After FITC conjugation, labeled VLPs were analyzed by dynamic light scattering (DLS) and native agarose electrophoresis. The DLS measurement shown in **Figure 25a** indicates that after labeling the AAV particles remained with an expected hydrodynamic diameter of 33.98 nm, which is similar to the size of AAV2 VLPs before conjugation (**Figure 8b**). The particles were then separated in an agarose gel, examined under the blue light table ( $\lambda=470$  nm) for FITC detection and stained by Coomassie to confirm the FITC-conjugation. As a result, FITC-labeled VLPs were visualized under the blue light with a defined band (**Figure 25b**), which is in line with the Coomassie staining result. Thus, FITC was successfully conjugated to AAV2 VLPs via covalent amide bonds. As primary lysine amino acids also present on the surface of AAV vectors, this conjugation method can be used to label different AAV vectors for various applications.

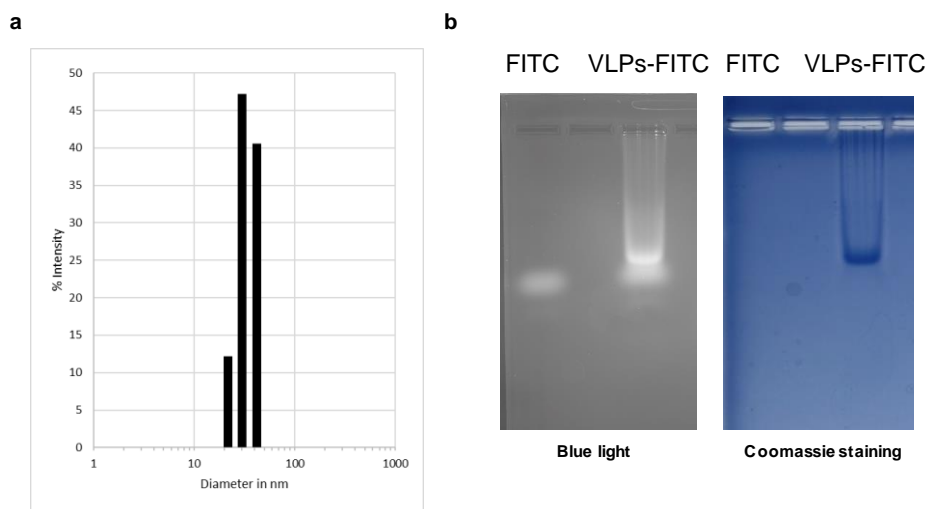


Figure 25. AAV2 VLP-FITC conjugation. (a) Dynamic light scattering (DLS) of VLPs after FITC conjugation. (b) Native AAV2 VLP agarose electrophoresis visualized under blue light and stained with Coomassie.

## 4.3.3.2. Internalization of FITC-conjugated VLPs

Next, the intracellular trafficking of FITC-labeled AAV VLPs was studied using HeLa cells by a confocal microscope. The labeled VLPs and buffer samples were incubated with HeLa cells for 2 h before visualizing under microscopy. The cell nucleus was stained with Hoechst 33342 (blue), and FITC-labeled VLPs were directly detected (green). The results shown in **Figure 26** indicate that our labeled VLPs were able to internalize into HeLa cells after 2-h incubation (**Figure 26b, c**) compared to the buffer control (**Figure 26a**), which is consistent with the cellular uptake of *in-vitro* AAV2 VLPs detected by A20 antibody as described above (**4.1.3**) and that of FITC-labeled AAV2 reported by Mevel et al.<sup>240</sup> This finding reveals that the incorporation of FITC to AAV2 VLPs was compatible

## 4 Results and Discussion

with AAV2 VLP internalization and opens chances for tracking AAV VLPs and rAAV vectors *in vitro* and *in vivo*. Moreover, potential drugs can be conjugated to AAV VLPs via surface lysine residues for therapeutic delivery.

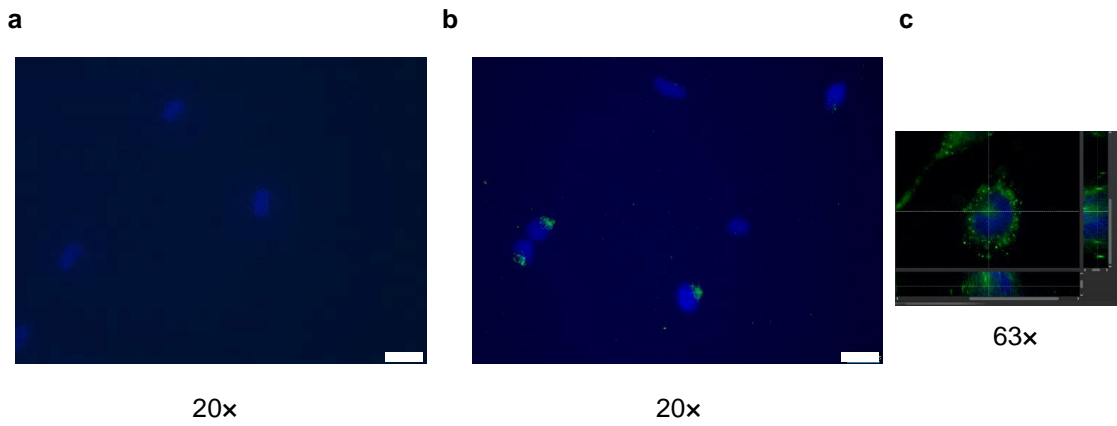


Figure 26. Internalization of FITC-labeled AAV2 VLPs. HeLa cells were treated with (a) buffer, (b) FITC-labeled AAV2 VLPs (20×), (c) FITC-labeled AAV2 VLPs (63×). FITC (green) and DAPI (blue), scale bars are 25 μm.



## 5. Conclusion and Outlook

The demand for rAAV in gene therapy clinical trials has significantly increased and approaches the limits of the current production systems using HEK-293 and insect cells. This thesis sought to establish an AAV assembly protocol via a defined reaction or inside *E. coli* that may offer a new strategy to produce rAAV if an *in-vitro* AAV genome encapsidation becomes possible. The potential applications of AAV VLPs for vaccine development and therapeutic delivery have also been explored.

The assembly protocol of AAV2, the most extensively studied AAV serotype, was successfully established in a chemically defined reaction. *In vitro* capsid assembly of AAV2 resulted in AAV2 VLPs as well as other small intermediate structures and larger aggregates, leading to a low yield of capsid formation. Thus, assembly protocol and buffer conditions need to be optimized in the future. In contrast, the assembly of the most divergent AAV serotype AAV5 was concomitant with capsid protein expression inside *E. coli*. The *E. coli* assembled AAV5 VLPs were directly obtained from *E. coli* with a better yield compared to *in vitro* AAV2 assembly. Different expression conditions would improve an AAV5 capsid formation yield in *E. coli*.

AAV particles were used to present the RBM or RBD to induce a strong immune response against SARS-CoV-2. RBM and RBD-fused VP3 capsid proteins were able to express in *E. coli*. The *in-vitro* assembly of fusion proteins resulted in particles among other structures. The mouse immunization of AAV2 VP3\_RBM VLPs resulted in a high level of RBD-specific antibodies, suggesting that the particle is a promising vaccine candidate for SARS-CoV-2. A serum virus neutralization assay, T cell responses and testing on larger animals will be needed in the future. Contrary, the AAV2 VP3\_RBD VLPs induced a low level of SARS-CoV-2 specific antibodies but a high level of VP3 VLP scaffold-directed antibodies, indicating the incorrect conformation of RBD presented on the VLPs after refolding. Future work on optimization of VP3\_RBD VLP assembly will be needed.

In addition, circular ssDNA was produced using the phagemid/helper phage system for an AAV *in-vitro* packaging reaction. Arginine-rich motif (ARM) for helping DNA passive packaging was fused to AAV5 VP3 protein, and the fusion protein was successfully obtained from *E. coli*. After the *in-vitro* packaging reaction, the assembled ARM\_VP3 VLPs showed the ability to protect ssDNA but not mediate protein expression in CHO-K1 cells. The future work will be the generation of AAV linear ssDNA genomes, incorporation of other DNA-binding domains into capsid proteins, and optimization of *in vitro* passive packaging reactions. An active packaging of AAV *in vitro* will also be tested.

## **5 Conclusion and Outlook**

Furthermore, AAV VLPs were labeled with FITC via amide bonds. The success of FITC-AAV VLP chemical conjugation opens opportunities to track the labeled AAV VLPs in further experiments, label rAAV vectors and chemically couple other drugs with a similar strategy.

## 6. Materials and Methods

### 6.1. Materials

#### 6.1.1. Equipment

Table 1. Equipment used in this work.

Device	Specification	Manufacturer
Agarose electrophoresis chamber	PerfectBlue Gelsystem Mini (S, M, L)	Peqlab
Analytical camera system	Fusion Fx7	Vilber
Atomic force microscope	Multimode 8 AFM with Tap300AI-G cantilevers	Brucker
Autoclave	GE6612	Getinge
Autoclave	FVS 2	Integra Bioscience
Automated cell counter	LUNA	Logos Biosystems
Bio-Dot® Apparatus	96-well	Bio-Rad
Blue light table (470 nm)	Serva blue light table	Serva Electrophoresis GmbH
Camera	EOS 600D (EFS 18-55 mm)	Canon
Cell Sorter	S3e™	Bio-Rad
Centrifuge	Megafuge 1.0	Heraeus Instruments
Centrifuge	Pico17	Thermo Scientific
Clean bench	LaminAir Model 1.2	Holten
Clean bench	LaminAir HB 2448	Heraeus Instruments
CO <sub>2</sub> Incubator	CB E6	Binder GmbH
Cryo-TEM	JEM-2200FS	JEOL
DynaPro 99		Wyatt/ Protein Solutions
Electroporator	MicroPulser™	Bio-Rad
Fluorescence Microscope	DMI 6000 B, Filters: 405 (EX: 375-435, DC: 455, EM: 445-495), YFP (EX: 490-510, DC: 515, EM: 520-550), TX2 (EX: 540-580, DC: 595, EM: 607-683)	Leica Microsystems
Freezer (-150°C)	MDF-2156VAN	Panasonic
Freezer (-80°C)	KM-DU 73Y1	Panasonic
Freezer (-20°C)		Bosch

## 6 Materials and Methods

French press	SLM AMINCO	SLM Instruments
French Pressure Cell	FA-032	Thermo Fisher Scientific
Fridge (4°C)		Bosch
Ice machine	UBE 50-35	Ziegra Eismaschinen
Incubator	B 6120	Heraeus Instruments
Light microscope	Axiovert 25	Zeiss
Magnetic stirrer	RCT	Ikamag
Microplate reader	PowerWare HT	BioTek
Microwave	HF 22043	Siemens
Milli-Q water system		Millipore
Mixing Block	MB102	Bioer
Orbital shaker	ES-X	Kühner
pH electrode	InLab Expert Pt1000	Mettler Toledo
pH meter	SevenCompact S220	Mettler Toledo
Pipetboy	Comfort	Integra
Pipette	Research® plus	Eppendorf
Power supply	EV231	Consort
Precision scale	CP 224 S	Sartorius
Precision scale	XA205 DualRange	Mettler Toledo
Real-time PCR system	Lightcycler 480 II	Roche
Refrigerated centrifuge	Multifuge X1R	Thermo Scientific
Refrigerated centrifuge	RC5C (SS-34 and GS-3 rotors)	Sorvall Instruments
Refrigerated centrifuge	Centrifuge 5424R	Eppendorf
Rocking shaker	Dou Max 1030	Star Lab
Scale	BP 2100 S	Sartorius
SDS PAGE chamber	SE260	Hoefer
SDS PAGE gel caster	Multiple gel caster	Hoefer
Semi-dry blotting apparatus	Semi-Dry-Blotter	VWR
Shaking platform	SI-600 R	Lab. Companion
Shaking platform	Sky Line	ELMI
Spectrophotometer	NanoDrop 2000c UV/Vis	Thermo Scientific
Tecan plate reader	Infinite® M Plex	Tecan Trading AG
Thermocycler	Peqstar 96x Universal gradient	Peqlab
UV-Transilluminator	ECX-F20.M	Vilber Lourmat

Vacuum Manifold	QIAvac 24 Plus	Qiagen
Vortex	Vortex Genie 2	Scientific Instruments
Water bath		GFL
White light table LED	LP-400N	Universal Electronics Industries
Äkta™ start	Protein purification system	GE Healthcare Life Science

### 6.1.2. Consumables

Table 2. Consumables used in this work.

Name	Specification	Manufacturer
Adhesive film for real-time PCR Plates	Ultra clear (A26979)	GeneOn
Amicon Ultra-4 centrifugal filters	10 kDa, 30 kDa, 100 kDa NMWL	Merck
Bijou sample containers	7 ml, sterile, PS	Sci Labware Limited
Blotting paper	2 mm	Bio-Rad
Cell culture dishes	100-mm diameter	Sarstedt
Cell scraper	25 cm	Sarstedt
Cryogenic plastic vessel	1.8 ml	Star Lab
Carbon-coated copper grid	200 mesh	Science Services
Cover glass		Thermo Scientific
Cuvette	10 mm, plastic	Sarstedt
Electroporation cuvette	10 mm	Bio-Rad
Lightcycler Plate	96-well, white	Sarstedt
LUNA Cell Counting Slide	Two-chamber slide	Logos Biosystems
MaxiSorp plate	96-well, flat-bottom	Nunc
Mica for AFM	50×76 mm, 0.2 mm thick	PLANO
Microscopy slide		Marienfeld
Multi-well plates	6-, 12-, 24-, 96-well	Sarstedt
Nitrocellulose membrane	0.45 µm	Thermo Scientific
Petri dishes	90×16 mm	Sarstedt
Pipette tips	0.01 ml, 0.1 ml, 1 ml, 5 ml	Star lab
Pipette tips (cell culture)	TipOne Filter Tips	Star lab
Reaction tube	15 ml, PP	Sarstedt
Reaction tube	50 ml, PP	Sarstedt
Reaction tube	50 ml, 25K×g	VWR

Reaction vessels	0.5 ml, 1.5 ml, 2 ml	Sarstedt
Reaction vessel (PCR)	0.2 ml	Star Lab
Scalpel blades	S123	Hartenstein
Shaker flask	250 ml	Sarstedt
Spectra/Por membrane	MWCO 6-8000 Da	Spectrum Medical Industries
Syringe	1 ml, 5 ml, 10 ml, 50 ml	B. Braun
T-flask	25 cm <sup>2</sup> , 75 cm <sup>2</sup> , 150 cm <sup>2</sup>	Sarstedt

### 6.1.3. Software and web servers

Table 3. Software and web servers used in this work.

Software	Developer
Dynamics, Ver. 5.25.44	Protein Solutions
FlowJo™, Ver. 10.6.1	Becton Dickinson
FUSION-FX	Vilber
GeneArt online tool	Thermo Fisher Scientific
Geneious, Ver. 9.1.8	Biomatters Ltd.
Gwyddion, Ver. 2.49	David Nečas et al.
i-control™, Ver. 2.0	Tecan
ImageJ, Ver. 1.52a	Wayne Rasband, National Institutes of Health, USA
KC4, Ver. 3.3	BioTek
Leica Application Suit X, Ver. 3.3.0.16799	Leica Microsystems
LightCycle 480II, Ver. 1.5.0	Roche
Mendeley Desktop, Ver. 1.19.4	Mendeley Ltd.
Microsoft office 2016	Microsoft
NanoDrop 2000/200c, Ver. 1.5	Thermo Fisher Scientific
NEBio Calculator, Ver. 1.12.0	NEB
Soft Imaging Viewer	Olympus
UCSF Chimera, Ver. 1.12	University of California San Francisco, USA
UNICORN™ start, Ver. 1.0	GE Healthcare Life Science

### 6.1.4. Chemicals

Table 4. Chemicals used in this work.

Chemicals	Supplier
ABTS	A1008,0001, AppliChem

## 6 Materials and Methods

Acetic acid	20104.334, VWR
Accutase	6964-100ML, Sigma-Aldrich
Acrylamid-Bisacrylamid 30% solution (29:1)	A3574, Sigma-Aldrich
Agar-Agar	6494.2, Carl Roth
Agarose	M3044.0500, Genaxxon Bioscience
Ammonium sulfate	3746.1, Carl Roth
Ampicillin sodium salt	K029.4, Carl Roth
APS	A1142,0250, AppliChem
BH <sub>2</sub> NaO <sub>4</sub>	A10189, Alfa Aesar
Boric acid	0588, AMRESCO
Brilliant Blue R-250	27816-25G, Sigma-Aldrich
Bromophenol blue	A512.1, Carl Roth
BSA	A2153-10G, Sigma-Aldrich
CaCl <sub>2</sub>	C/1400/53, Fisher Scientific
CFA (complete Freund's adjuvant)	0638-59, Difco laboratories
Citric acid	244.1000, Merck
Chloramphenicol	3886.3, Carl Roth
Dabco	0738, Carl Roth
DTT	A1101,0005, AppliChem
EDTA	8043.2, Carl Roth
Ethanol	20821.296, VWR
Fluorescein isothiocyanate, Isomer I (FITC)	F7250, Sigma-Aldrich
FCS	P4333, Sigma-Aldrich
Formaldehyde 37% (v/v)	410731000, Thermo Fisher
Glucose	X997.2, Carl Roth
Glutamine	G7513-100ML, Sigma-Aldrich
Glycerol	158920010, Fisher Scientific
Glycine	3908.2, Carl Roth
GuHCl	0037.1, Carl Roth
HBSS	H6648-500ML, Sigma-Aldrich
HCl	H/1200/PB15, Fisher Scientific
HEPES	9105.4, Carl Roth
Hoechst 33342	62249, Thermo Scientific
Imidazole	I5513-100G, Sigma-Aldrich

## 6 Materials and Methods

IPTG	2316.4, Carl Roth
Kanamycin sulfate	60615-5G, Sigma-Aldrich
KCl	26764.298, VWR
KH <sub>2</sub> PO <sub>4</sub>	60220, Fluka
L-Arginine	A3675,0500, Applichem
Lipofectamine 2000	11668-027, Invitrogen
Mowiol 4-88	0713.1, Carl Roth
MgCl <sub>2</sub> .6H <sub>2</sub> O	141396.1211, Applichem
NaCl	27810.295, VWR
NaH <sub>2</sub> PO <sub>4</sub>	2370.1, Carl Roth
Na <sub>2</sub> CO <sub>3</sub>	A135.2, Carl Roth
NaHCO <sub>3</sub>	27778.293, VWR
NaOH	S/4920/60, Fisher Scientific
NCS (newborn calf serum)	NCS-1A, Capricorn
Non-fat milk powder	A0830,0500, AppliChem
PEI Max (Polyethylenimine "Max", MW 40000)	24765, Polysciences
Penicillin-Streptomycin	P4333, Sigma-Aldrich
OptiMEM	11058021, Gibco, Thermo Fisher Scientific
Poly-D-Lysine hydrobromide	P6407-5MG, Sigma-Aldrich
POROS™ CaptureSelect AAVX Affinity Resin	A36739, Thermo Fisher Scientific
Protino Ni-NTA Agarose	745400.25, Macherey-Nagel
ROTIgelStain	3865.1, Carl Roth
SDS	4360.2, Carl Roth
Silver nitrate	209139, Sigma-Aldrich
Sodium thiosulfate pentahydrate	1615107, Sigma-Aldrich
SYPR Gold nucleic acid gel stain	S11494, Thermo Fisher Scientific
TEMED	CK37762132 735, Merck
Tetracycline	87128-25G, Sigma-Aldrich
Tris	T1503-1KG, Sigma-Aldrich
Tris-HCl	9090.3, Carl Roth
Triton X-100	T8787-50ML, Sigma-Aldrich
Tween 20	9127.2, Carl Roth
Trypan blue	T8154, Sigma-Aldrich
Trypsin/EDTA	T4049-100ML, Sigma-Aldrich

Tryptone/ Peptone	8952.2, Carl Roth
Uranyl acetate	E22405, Science Services
Urea	3941.1, Carl Roth
Yeast extract	2363.1, Carl Roth

### 6.1.5. Buffers and solutions

Table 5. Buffers and solutions used in this work.

Name	Composition
AAV lysis buffer	50 mM Tris 150 mM NaCl 2 mM MgCl <sub>2</sub> pH 7.5 – 8.0
ABTS solution	3.25 mM BH <sub>2</sub> NaO <sub>4</sub> 40 mM Citric acid 60 mM Na <sub>2</sub> HPO <sub>4</sub> pH 4.5 1g/L ABTS
Agarose gel with ROTIGelStain	1% (w/v) Agarose 0.005% (w/v) ROTIGelStain in TAE buffer
Ampicillin stock solution (1000×)	100 mg/ml Ampicillin sodium salt in MilliQ water
APS solution	1.5% (w/v) APS
Blocking buffer (ELISA)	0.8% (w/v) BSA in PBS
CaCl <sub>2</sub> solution	100 mM CaCl <sub>2</sub> , 300 mM CaCl <sub>2</sub>
CaCl <sub>2</sub> solution with glycerol	85 mM CaCl <sub>2</sub> 15% (v/v) Glycerol
Chloramphenicol stock solution (1000×)	20 mg/ml Chloramphenicol in Ethanol
Coomassie staining solution	0.1% (w/v) Brilliant Blue R-250 40% (v/v) Ethanol 10% (v/v) Acetic acid
Destaining solution	10% (v/v) Acetic acid
<i>E. coli</i> lysis buffer	50 mM NaH <sub>2</sub> PO <sub>4</sub> 300 mM NaCl pH 8
Elution buffer (POROS AAVX column)	100 mM Citric acid

## 6 Materials and Methods

	pH 2.0
HBS buffer (2×)	50 mM HEPES 1.5 mM NaH <sub>2</sub> PO <sub>4</sub> 280 mM NaCl pH 7.05
IEX buffer A	20 mM Tris-HCl 8 M Urea pH 8.0
IEX Buffer B	20 mM Tris-HCl 1 M NaCl 8 M Urea pH 8.0
IMAC elution buffer	50 mM NaH <sub>2</sub> PO <sub>4</sub> 300 mM NaCl 250 mM Imidazole pH 8.0 (6 M GuHCl or 8 M Urea)
IMAC equilibration buffer	50 mM NaH <sub>2</sub> PO <sub>4</sub> 300 mM NaCl 10 mM Imidazole pH 8.0 (6 M GuHCl or 8 M Urea)
IMAC washing buffer	50 mM NaH <sub>2</sub> PO <sub>4</sub> 300 mM NaCl 27 mM Imidazole pH 8.0 (6 M GuHCl or 8 M Urea)
IPTG stock solution	1 M IPTG in MilliQ water
Kanamycin stock solution (1000×)	50 mg/ml Kanamycin in MilliQ water
Neutralization buffer (POROS AAVX column)	1 M Tris-HCl (pH 8.7)
PBS buffer	137 mM NaCl 2.6 mM KCl 10 mM Na <sub>2</sub> HPO <sub>4</sub> 1.8 mM KH <sub>2</sub> PO <sub>4</sub>

## 6 Materials and Methods

	pH 7.2
PBST buffer	0.05% (v/v) Tween 20 in PBS buffer
Laemmli sample buffer (5×)	0.05% (w/v) Bromophenol blue 20% (v/v) Glycerol 10% (w/v) SDS 0.2 M Tris-HCl 25 mM DTT pH 6.8
SDS running buffer	25 mM Tris-HCl 192 mM Glycine 0.1% (w/v) SDS pH 8.3
Semi-dry transfer buffer	25 mM Tris-HCl 192 mM Glycine 20% (v/v) Ethanol pH 8.2
Separating gel buffer	1.5 M Tris pH 8.8
Carbonate-Bicarbonate buffer	0.091 M NaHCO <sub>3</sub> 0.009 M Na <sub>2</sub> CO <sub>3</sub> pH 9.0
Solubilization buffer	5 M GuHCl 20 mM Tris-HCl 0.15 M NaCl 1 mM EDTA 1 mM DTT pH 8.0
Stacking gel buffer	0.5 M Tris pH 6.8
TAE buffer (1×)	40 mM Tris 1 mM EDTA 20 mM Acetic acid pH 8.0
TBE buffer (1×)	89 mM Tris 89 mM Boric acid

	2 mM EDTA pH 8.0
Tetracycline stock solution (1000×)	10 mg/ml Tetracycline in Ethanol
TBS buffer	50 mM Tris-HCl 150 mM NaCl pH 7.6
TBST buffer	0.05% (v/v) Tween 20 0.2% Triton X-100 in TBS buffer

### 6.1.6. Phage, *E. coli* strains and eukaryotic cell lines

Table 6. Phage and *E. coli* strains used in this work.

Strain	Source
M13KO7 Helper Phage	NEB
DH10β	Invitrogen
DH5α	Fermentation Technology Group, Bielefeld University, Germany
ER2738	NEB
BL21(DE3)	Fermentation Technology Group, Bielefeld University, Germany
RV308	DSMZ

Table 7. Human and animal cell lines used in this work.

Eukaryotic cell lines	Source
HeLa	DSMZ
HEK-293	DSMZ
FreeStyle 293-F	Thermo Fisher Scientific
CHO-K1	DSMZ

### 6.1.7. Media

Table 8. Media used in this work.

Name	Composition
LB medium (Lennox, Carl Roth)	1% (w/v) Tryptone 0.5% (w/v) NaCl 0.5% (w/v) Yeast extract pH 7.0
LB-Agar	LB medium 1.5% (w/v) Agar

SOC medium	2% (w/v) Tryptone/Peptone 0.5% (w/v) Yeast extract 10 mM NaCl 2.5 mM KCl 10 mM MgCl <sub>2</sub> 20 mM Glucose
DMEM	DMEM (Sigma-Aldrich) 10% FCS (Sigma-Aldrich) 1% P/S (Sigma-Aldrich)
HEK-TF	HEK-TF (Xell AG) 8 mM Glutamine (Sigma-Aldrich)
DMEM/Ham's F-12	DMEM/Ham's F-12 (Merck Milipore) 10% FCS (Sigma-Aldrich) 1% P/S (Sigma-Aldrich) 2 mM Glutamine (Sigma-Aldrich)

### 6.1.8. Antibodies

Table 9. Antibodies used in this work.

Antibody (dilution)	Supplier
Anti-AAV VP1/VP2/VP3 mouse monoclonal, B1 (1: 100)	65158, Progen
Anti-AAV2 (intact particle) mouse monoclonal, A20 (1: 250)	61055, Progen
Anti-AAV5 (intact particle) mouse monoclonal, ADK5a (1:250)	610148, Progen
Anti-human IgG1 (gamma 1 chain specific), mouse antibody, HRP (1: 2500)	AM08151HR-N, Acris Antibodies
Goat anti-mouse IgG (H+L), HRP conjugated secondary antibody (1: 2500)	31430, Thermo Fisher Scientific
Goat anti-Mouse IgG (H+L) Secondary Antibody, Dylight 594 (1: 500)	35510, Thermo Fisher Scientific
SARS-CoV-2 Spike RBD Nanobody (1: 10000)	CSB-RA33245A2GMY, Cusabio
Tetra-His (1: 2000)	34670, Qiagen

### 6.1.9. Kits

Table 10. Kits used in this work.

Kits	Supplier
Gibson Assembly® Master Mix	E2611S, NEB
GoTaq® qPCR Master Mix	A600.1, Promega

NucleoSpin® Gel and PCR Clean-up	740609.250, Macherey-Nagel
NucleoSpin® Plasmid	746588.250, Macherey-Nagel
NucleoSpin® Xtra Midi	740410.50, Macherey-Nagel
SuperSignal™ WEST Pico PLUS	34580, Thermo Scientific

### 6.1.10. Enzymes

Table 11. Enzymes used in this work.

Enzyme	Supplier
Benzonase nuclease	Sigma-Aldrich
DNase I	NEB
Phusion High-Fidelity DNA Polymerase	NEB
Protease K	Sigma-Aldrich
Restriction enzymes	NEB
T4 ligase	Thermo Fisher Scientific

### 6.1.11. Ladders

Table 12. DNA and protein ladders.

DNA and protein ladder	Supplier
GeneRuler 1kb DNA Ladder	SM0311, Thermo Fisher Scientific
Color Prestained Protein Standard, Broad Range	P7712, P7719, NEB

### 6.1.12. Oligonucleotides

Table 13. Oligonucleotides used in this work.

Name	Sequence
T7pro_Seq	CCACGATGCGTCCGGCGTAG
qPCR-hGH_F	CTCCCCAGTG CCTCTCT
qPCR-hGH_R	ACTTGCCCCCTTGCTCCATAC
qPCR-CMV_F	GGGACTTTCCTACTTGCA
qPCR-CMV_R	GGCGGAGTTGTTACGACA
AAV2 VP3_Seq1	AACTGTTTAATATCCAGGTG
AAV2 VP3_Seq2	CCGTGTTATCGTCAGCAGCG
AAV2 VP3_F	ATATAGAATTCAAATATCTAGACATATGGCAACCGGTTTCAG
AAV2 VP3_R	TATATCTGCAGTATATACTAGTAAGCTTCTC
AAV2 VP3_TEV_His6_F	ATATAGAATTCAAATATCTAGACATATGGCAACCGGTTTCAG
AAV2 VP3_TEV_His6_R	ATATACTCGAGTTACAGATTACGTGTCAGATAGCGGG
AAV2 VP3_His6 <sup>587</sup> _F	CATCATCACCATCATCATCGTCAGGCAGCAACCGCAG

## 6 Materials and Methods

AAV2 VP3_His6 <sup>587</sup> _R	ATGATGATGGTGTATGATGATTACCACGTTGCAGATTG
AAP2_F	ATATACATATGGAGACGCAGACTCAGTA
AAP2_R	ATATACTCGAG- TTAATGATGATGGTGTATGATGGGGTGAGGTATCCATACTG
AAV5 VP3_Seq1	CCACGATGCGTCCGGCGTAG
AAV5 VP3_Seq2	CGTATGTTGTTGGCAATGG
AAV5 VP3_Seq3	CAGCCTGCAAATCCGGGTAC
AAP5_F	ATATAATATACATATGGACCCAGCGGATCCAG
AAP5_R	ATATACTCGAGTTAATGATGATGGTGTATGATGGCGTCGCGTAACCG- TACTGC
AAP5_Seq	CCACGATGCGTCCGGCGTAG
AAV5 VP3_His6_F	ATATACATATGCATCATCACCATCATCACATGTCTGCAGGTGGTGGTGG
AAV5 VP3_His6_R	ATATACTCGAGTTACAGCGGACGG
AAV5 VP3_ARM_F	ATACATATGATTCGTCGTCGTTATGCACGTCCG- TATCGTCGTCGCCATATTCGTCGC- TATCGTCGCCGTCGTCGTCATTTTCGCCGTCGCCGTTTTACCACACATCAT CACCATCATCAC
AAV5 VP3_ARM_R	ATATACTCGAGTTACAGCGGACGG
ssDNA_F	CGATGTACGGGCCAGATATA
ssDNA_R	CTAGTATCTGTGGCCAGCT
RBD_F	TCATCATCACCATCATCATGGCGGCAGCGGCAGAGTCC
RBD_R	CTGCGGTTGCTGCCTGACGGCCGCTGCCGCCGAAATTG
RBD_AAV2 VP3_F	ATGATGATGGTGTATGATGATTACCACG
RBD_AAV2 VP3_R	CGTCAGGCAGCAACCGCAG
RBD_AAV5 VP3_F	TCCCCTCTAGAAATAATTTTGTT
RBD_AAV5 VP3_R	ATATACTCGAGTTAGAAATTGACACATTTGTTTTAAC
0701_His6_F	GTGGGCCCAAAAAGGGATCC
0701_His6_R	ATATACTCGAGTTATCAGTGTATGGTGGTGGTGTATGTTT- GTAGAGCTCATCCATGCC
0701_Seq1	CCACTGCTTACTGGCTTATC
0701_Seq2	GGCAGTACGCCATGTAACG
0701_Seq3	CTACAAGACGCGTGCTGAAG
His6_RBD_F	TCCCCTCTAGAAATAATTTTGTT
His6_RBD_R	ATATACTCGAGTTAGAAATTGACACATTTGTTTTAAC

## 6.1.13. Plasmids

Table 14. Plasmids used in this work.

Number	Name	Source
pZMB0088	pHelper	Agilent
pZMB0216	pSB1C3_001_Rep_VP123_453_587wt_p5tataless	ZMB
pZMB0347	pUC19bb_ITR_EXS_pCMV_mKate2_hGH	ZMB
pZMB0522	pUC19bb_ITR_EXS_pCMV_mVenus_hGHPolyA	ZMB
pZMB0452	pET24b_AAV2_VP3_TEV_His6	This work
pZMB0458	pJKME_AAV2_VP3_TEV_His6	This work
pZMB0580	pET24b_AAV2_VP3	This work
pZMB0581	pET24b_AAV2_VP3 His6 <sup>587</sup>	This work
pZMB0582	pET24b_AAP2	This work
pZMB0611	pET24b_AAV5_VP3	This work
pZMB0647	Rep2Cap5	Penn Vector Core
pZMB0649	pJKME_AAV5_VP3	This work
pZMB0668	pET21a_AAP5	This work
pZMB0669	pET24b_His6_AAV5 VP3	This work
pZMB0670	pET24b_ARM_His6_AAV5 VP3	This work
pZMB0701	pcDNA3_SARS-CoV-2_S-RBD-sfGFP	Addgene
pZMB0702	pcDNA3.1_CMV_hACE2	Addgene
pZMB0706	pET24b_AAV2_VP3_587 His6_RBD	This work
pZMB0711	pcDNA3_SARS-CoV-2_S-RBD-sfGFP_His6	This work
pZMB0728	pET24b-His6_RBD_AAV5 VP3	This work
pZMB0733	pET24b-His6_RBD	This work

## 6.2. Methods

## 6.2.1. Molecular genetic methods

6.2.1.1. Cultivation and storage of *E. coli*

*E. coli* was cultivated using LB medium or LB Agar supplemented with appropriate antibiotics (**Table 5, Table 8**). Cultures were stored at 4°C for a short period of time on agar plates. For long-time storage, 650 µl of liquid culture was mixed with 350 µl of glycerol 80% and stored at -80°C.

6.2.1.2. Preparation and heat shock transformation of chemically competent *E. coli* cells

Chemical competent *E. coli* cells were prepared using a standard CaCl<sub>2</sub> protocol.<sup>241</sup> To do a transformation, 5 µl of a ligation mixture or 1 µl of isolated DNA plasmid was added to a 50-µl aliquot

## 6 Materials and Methods

of *E. coli* competent cells and incubated on ice for 30 min. After a heat shock at 42°C for 45 s, *E. coli* cells were put on ice again for 2 min. Afterwards, 1 ml of SOC medium (**Table 8**) was added and incubated at 37°C, 200 rpm for 1h. Then, 100 µl of transformed *E. coli* was plated on agar plates containing appropriate antibiotics. For the transformation of a plasmid containing the ampicillin resistance gene, *E. coli* was directly plated on an agar plate without recovery step in SOC medium.

### 6.2.1.3. General cloning procedures

Plasmid DNA was isolated from *E. coli* cells using the NucleoSpin Plasmid kit (Macherey-Nagel) for a small amount of DNA isolation. For the larger one, NucleoBond Xtra Midi (Macherey-Nagel) was used. The extraction protocols were performed as described by the manufacturer. DNA concentration was then determined using the NanoDrop 200c UV/Vic spectrophotometer (Thermo Fisher Scientific). Afterwards, the plasmid DNA was used as a template for a PCR (**Table 15**) or a digestion reaction (**Table 16**). For agarose gel electrophoresis, 1% w/v agarose gel in TAE buffer (**Table 5**) was used. ROTIGelStain was added into the gel to detect DNA (**Table 5**). DNA ligation of two compatible DNA fragments was done using T4 DNA ligase as described in **Table 16**. Insert: vector molar ratios were calculated using NEBio Calculator (Ver. 1.12.0, NEB). The fragments could also be ligated using Gibson Assembly Master Mix (E2611, NEB, following the manufacturer's protocol). Finally, the cloned DNA sequences were confirmed by sequencing at the Sequencing Core Facility, CeBiTec, Bielefeld University, Germany.

Table 15. PCR reaction (Phusion High-Fidelity Polymerase, NEB).

Components		Thermal cycling condition	
5×GC buffer	10 µl	Initial denaturation	98°C, 3 min
10 mM dNTPs	1 µl	30 cycles	
10 µM forward primer ( <b>Table 13</b> )	2.5 µl	Denaturation	98°C, 30 s
10 µM revert primer ( <b>Table 13</b> )	2.5 µl	Annealing	45°C-72°C, 20 s
DMSO	0.5 µl	Extension	72°C, 30 s/kb
MgCl <sub>2</sub>	2 µl		
Polymerase	0.5 µl	Final extension	72°C, 5 min
Plasmid template	1 pg-10 ng	Store	8°C
MilliQ	to 50 µl		

Table 16. Digestion and ligation reaction.

Digestion reaction		DNA ligation reaction	
CutSmart buffer (10×)	5 µl	T4 buffer (10×)	2 µl
Restriction endonuclease	1 µl	T4 DNA ligase	1 µl
	1 µg	Insert DNA	3:1 or 5:1 molar ratio over plasmid

DNA	to 50 $\mu$ l	Plasmid DNA	100 ng
MilliQ	37°C, 1 h	MilliQ	to 20 $\mu$ l
			Room temperature, 1h

#### 6.2.1.4. ssDNA production

ssDNA was produced using bacteriophage M13. Briefly, *E. coli* ER2738 was transformed with plasmid pZMB0347 (ITR-mKate plasmid) using the electroporation method (1.8 kV, MicroPulser, Bio-Rad).<sup>242</sup> After overnight culture in LB medium containing Ampicillin and Tetracycline, *E. coli* was transferred to a 50-ml fresh medium and cultured to OD<sub>600</sub> of 0.6. Helper phage M13KO7 was then added to the *E. coli* culture with a concentration of  $5 \times 10^9$  phages/ml and incubated for 4 h at 37°C, 180 rpm. Afterwards, the culture was centrifuged at 5000 $\times$ g, 10 min (2 times), and the supernatant fraction containing phages was transferred to a new tube. Glacial acetic acid was added to the supernatant (10  $\mu$ l acetic acid per 1 ml culture) and incubated for 2 min. After that, ssDNA was then isolated from the supernatant using NucleoSpin Plasmid kit (Macherey-Nagel).

### 6.2.2. Methods in protein biochemistry

6.2.2.1. Recombinant protein expression and purification in *E. coli* and 293-F cells  
BL21(DE3) and a pET expression vector were used to express recombinant proteins in *E. coli*. Transformed *E. coli* was cultured in LB medium containing appropriate antibiotics at 37°C to an OD<sub>600</sub> of 1.2-1.5, then isopropyl  $\beta$ -D-thiogalactopyranoside (IPTG) was added to a concentration of 0.4 mM, and the culture was subsequently incubated at 37°C, 4h or 18°C, 18 h at 180 rpm. Cells were harvested at 5000 $\times$ g, 4°C for 15 min. Pelleted cells were resuspended in a lysis buffer (50 mM NaH<sub>2</sub>PO<sub>4</sub>, 300 mM NaCl, pH 8) supplemented with 1 mg/ml lysozyme and lysed by sonication on ice (Branson Sonifier 250 with micro tip, power setting 70%, constant duty, 10 cycles, 30 s each) or by a French press at 1000 psi.

For the recombinant proteins that formed inclusion bodies, cell debris and inclusion bodies were collected by centrifugation at 20000 $\times$ g, 4°C for 30 min. Ion-exchange chromatography was used to purify proteins without a purification tag using the Äkta start purification system (UNICORN software). In brief, the remaining pellet was solubilized in IEX buffer A (20 mM Tris-HCl, 8M Urea, pH 8). A 2-ml Q Sepharose resin (GE Healthcare) packed column was equilibrated with IEX Buffer A. The column was then loaded with sample and washed with IEX Buffer A. Bound proteins were eluted with a gradient of IEX Buffer B (20 mM Tris-HCl, 1M NaCl 8M, Urea, pH 8). Fractions containing target proteins were collected and concentrated with centrifugal filter units. Other proteins containing a His6-tag, the proteins were purified by immobilized metal-ion affinity chromatography (IMAC). Briefly, a column with 2 ml of Ni-NTA Agarose (Macherey-Nagel) was equilibrated with IMAC buffer A (50 mM NaH<sub>2</sub>PO<sub>4</sub>, 300 mM NaCl, 10 mM imidazole, 8 M Urea, pH 8), then sample was loaded and washed with five-column volumes of IMAC buffer A containing 7%

## 6 Materials and Methods

IMAC buffer B (50 mM NaH<sub>2</sub>PO<sub>4</sub>, 300 mM NaCl, 250mM imidazole, 8 M Urea, pH 8). Afterwards, bound proteins were eluted with 100% IMAC buffer B.

For recombinant proteins expressed in soluble form in *E. coli*, the supernatant from cell lysate was separated and collected. Protein purification was performed as described above but under non-denaturing conditions (without urea and GuHCl). Notably, to obtain ARM\_AAV5 VP3 protein that was expressed in soluble form in *E. coli*, IMAC purification in high salt concentration buffer (1 M NaCl) was used.

FreeStyle 293-F cells were used to produce RBD\_GFP protein. Briefly, 50 ml of cells in HEK-TF medium (3 × 10<sup>6</sup> cells/ml) in a 250-ml flask was washed with 1× PBS. Afterwards, 120 µg RBD\_GFP plasmid DNA (pZMB0711) was mixed with PEI in a 1:4 DNA: PEI ratio (w/w) and added to the cells in 75 ml HEK-TF medium. After 4 h incubation at 185 rpm, 37°C, 75 ml fresh HEK-TF medium was added to the culture. After that, the culture was split into two 250-ml shaking flasks and cultivated for 6 days. The cell culture supernatant containing recombinant proteins was collected by centrifuging at 2000×g for 10 min. Since a His6-tag was inserted at the C-terminus of RBD\_GFP, the protein purification was performed using an IMAC column as described above. Buffers for protein purification were listed in **Table 5**.

### 6.2.2.2. SDS-PAGE and western blot

Samples of protein were separated on an acrylamide gel using the Hoefer SE 260 system.<sup>243</sup> The polyacrylamide gel consisted of 12% separating and 4% stacking gels. Gel components were listed in **Table 17**.

Table 17. Composition of 12% separating and 4% stacking gels.

Components (Table 5)	12% gel solution	4% gel solution
MilliQ	13 ml	8.17 ml
Separating gel buffer	12.5 ml	-
Stacking gel buffer	-	3.78 ml
10% SDS solution	0.5 ml	0.15 ml
Acrylamid-Bisacrylamid 30% solution (29:1)	20 ml	3.35 ml
TEMED	0.025 ml	0.015 ml
1.5% APS solution	4 ml	0.9 ml
<b>Total volume (for 4 gels)</b>	<b>50.025 ml</b>	<b>16.365 ml</b>

Protein ladders (**Table 12**) and protein mixed with the Laemmli sample buffer (5×) were loaded to the gel then separated using a Hoefer SE 260 chamber filled with the running buffer (**Table 5**).

## 6 Materials and Methods

After that, protein staining was either performed with silver nitrate<sup>244</sup> or Coomassie. For western blot, protein was transferred to nitrocellulose membranes (88018, Thermo Fisher Scientific, 0.45  $\mu\text{m}$ ) equilibrated in the transfer buffer (**Table 5**) using a semi-dry blotting apparatus (VWR). After blocking with 10% (w/v) non-fat dry milk (Applichem) in TBS buffer, the membranes were incubated for 1 h at room temperature with a primary antibody (**Table 9**). Detection was achieved using a secondary antibody coupled to horseradish peroxidase (**Table 9**), SuperSignal™ West Pico PLUS Chemiluminescent Substrate (34580, Thermo Fisher Scientific) and a Fusion FX camera system (Vilber).

### 6.2.3. Biophysical measurements

#### 6.2.3.1. Dynamic light scattering

Dynamic light scattering (DLS) was performed on a DynaPro 99 (Wyatt/Protein Solutions) instrument (Dynamics software). Samples were filtered through 0.22  $\mu\text{m}$  PVDF syringe filters (Millipore) and centrifuged at 18000 $\times$ g for 30 min before measurement. Measurements for each sample were averaged of at least 20 acquisitions.

#### 6.2.3.2. Atomic force microscopy

A multimode 8 AFM (Bruker) with Tap300AI-G cantilevers (BudgetSensors) in tapping mode in air was used to measure the particles. Briefly, particles in buffer were spotted onto freshly cleaved mica and incubated for three minutes. Then, wash the mica with distilled water and dry it under a gentle nitrogen flow. The AFM images and particle height profiles were generated using Gwyddion 2.49 software.

#### 6.2.3.3. Transmission electron microscopy

3  $\mu\text{l}$  of VLP samples was applied to a carbon-coated grid (200 mesh, Electron Microscopy Science) treated with oxygen plasma and incubated for 2 min. Excess liquid was removed with filter papers, the grid was dried at room temperature and washed with three drops of distilled water. To perform negative staining, 3  $\mu\text{l}$  of 2% (v/v) uranyl acetate (Science Services) was added and incubated for 1 min. Excess liquid was drained off and the grids were dried again. VLP samples were visualized with a Cryo-TEM. Images were analyzed using the Soft Imaging Viewer (Olympus).

### 6.2.4. Cell culture techniques

#### 6.2.4.1. Cultivation and cryopreservation of eukaryotic cells

All cell lines were maintained at 37°C with 5% CO<sub>2</sub>, 95% humidity. Adherent cells were cultivated in T-flasks or 10-cm Petri dishes, suspension cells were maintained in Erlenmeyer cell culture flasks on an orbital shaking platform at 185 rpm, 5-cm amplitude. HeLa and HEK-293 cell lines were cultivated in DMEM supplemented with 10% FCS, 1% P/S. DMEM/Ham's F-12 containing 2 mM

Glutamine was used to cultivate CHO-K1 cell line. Cultivation of 293-F cells (a suspension cell line) was carried out in HEK-TF medium with the supplement of 8 mM Glutamine (**Table 8**).

Cells can be cryopreserved in the growth medium supplemented with 10% DMSO at -150°C. Initially, cells were counted, pelleted (150×g, 5 min) and resuspended to a concentration of  $1 \times 10^7$  cells/ml. Cells were then aliquoted to 1-ml cryogenic vials and frozen slowly at 1°C/min in an insulated freezing container in a -80°C freezer. The vials were transferred to a -150 freezer for long-term storage. For thawing, a frozen vial was placed in a 37°C water bath, the cells were then suspended in the growth medium and transferred to the culture flasks.

### 6.2.4.2. Counting of eukaryotic cells

The Luna Automated Cell Counter system was used to determine the number of mammalian and animal cells. 10 µl of cell samples was taken during passaging and mixed with 10 µl of 0.4% trypan blue solution (Sigma-Aldrich). The mixture was applied to a counting slide and inserted into the counting system. The total cell number and percentage of viability provided by the device were used for further experiments.

### 6.2.4.3. ssDNA transfection

CHO-K1 cells were seeded overnight prior to transfection in 24-well plates ( $3 \times 10^4$  cells/well). The transfection mixture was prepared by combining 1.6 µg ssDNA in 50 µl OptiMEM and 2 µl Lipofectamine 2000 (Thermo Fisher Scientific) in 50 µl OptiMEM, then incubated for 20 min. After that, 100 µl of transfection mixture was directly applied to each well. The cells were incubated for 48 to 72 h for further analysis.

### 6.2.4.4. Generation of transient HEK-293 cells displaying hACE2 receptors

The transfection was performed using the calcium phosphate protocol.<sup>245</sup> HEK-293 cells were seeded overnight prior to transfection in 24-well plates ( $1 \times 10^5$  cells/well). Afterwards, 1 µg hACE2 plasmid DNA (No. 1786, addgene) diluted in 0.3 M CaCl<sub>2</sub> was added dropwise into 2× HBS buffer. The mixture was vortexed thoroughly and added to the cells. The number of HEK-293 cells displaying the receptors was accessed after 48 h incubation.

## 6.2.5. VLP and virological methods

### 6.2.5.1. *In vitro and in vivo* assembly of AAV VLPs

*In vitro* AAV capsid assembly was carried out by dialyzing 1.5 mL of AAV2 VP3 and modified AAV2 VP3 proteins (0.15 mg/mL) in solubilization buffer (**Table 5**) five times against 100 ml of phosphate-buffered saline (PBS) pH 9 containing 0.2 M L-arginine at 4°C, changing buffer every 12 h over a 60-h period. To investigate the effect of AAP2 on *in vitro* assembly, purified VP3 protein (0.15 mg/ml) was mixed with a varying concentration of purified AAP2 (a VP3:AAP2 ratio of 1:2 or 2.5:1). Afterwards, capsid assembly was performed as mentioned above.

## 6 Materials and Methods

To form modified AAV2 VP3\_RBM and VP3\_RBD VLPs *in vitro*, 2 ml of RBM and RBD-fused VP3 proteins (0.2 mg/ml) in 8 M urea were gradually dialyzed into 100 ml buffers of 4, 2, 1, 0.5, 0 M Urea, 20 mM Tris-HCl, 500 mM NaCl, pH 9. The dialyzed samples were then centrifuged at 11000×g for 10 min and the supernatant was collected for further analysis.

For AAV5 assembly inside *E. coli*, the cells containing pET24-AAV5 VP3 were cultured in LB medium containing 50 µg/ml kanamycin at 37°C until OD<sub>600</sub> reached 1.5. Then, IPTG was added to a final concentration of 0.4 mM and the 1-liter medium was incubated in an orbital shaker with a speed of 170 rpm at 18°C for 18 h. To improve the *in-vivo* capsid assembly yield, pET21-AAP5 and pET24-AAV5-VP3 were co-transferred into *E. coli* BL21(DE3), and protein expression was performed using LB media containing 50 µg/ml kanamycin and 100 µg/ml ampicillin as described above.

### 6.2.5.2. rAAV production in adherent HEK-293 cells

Recombinant AAV (rAAV2 or rAAV5) was produced in HEK-293 cells with a three-plasmid system.<sup>246</sup> Briefly, HEK-293 cells were seeded with a density of  $3 \times 10^6$  cells per 10-cm dish and cultivated overnight. Cells were then transfected with 15 µg of total DNA per dish including Rep2Cap2 plasmid (pZMB0216) or Rep2Cap5 plasmid (pZMB0647), pHelper plasmid and ITR-containing plasmid (**Table 14**) with a molar ratio of 1:1:1 using calcium phosphate.<sup>245</sup> After 3-day incubation, the cells were harvested and rAAV was then purified for further uses.

### 6.2.5.3. AAV VLP and rAAV purification

AAV5 VLP formed inside *E. coli* was purified using POROS<sup>TM</sup> CaptureSelect<sup>TM</sup> AAVX Affinity resin (A36739, Thermo Fisher Scientific). Briefly, *E. coli* cells were harvested at 5000×g, 4°C for 10 min. Pelleted cells were washed, resuspended in PBS buffer (**Table 5**) and disrupted with a French press at 1000 psi. Afterwards, soluble proteins were obtained by centrifugation at 20000×g, 4°C for 20 min. Proteins were then precipitated from this solution by ammonium sulfate (12.52 g per 40 ml of sample, on ice 1 h) and VLPs were purified from the pellet using the AAVX Affinity resin column. Briefly, a 0.5-ml resin-packed column was equilibrated with 5 ml 1× PBS buffer plus 0.1 M NaCl, pH 7.4 at 1 ml/min. The column was then loaded with the sample and washed with 10 ml equilibration buffer at 1 ml/min. Bound particles were eluted using 5 ml citric acid (100 mM, pH 2) and neutralized with 1 M Tris-HCl (pH 8.7), concentrated and changed to 500 µl Hank's Balanced Salt Solution (HBSS) buffer with a centrifugal filter unit of 100 kDa molecular weight cut-off.

For rAAV purification, HEK-293 cells were resuspended in an AAV lysis buffer (50 mM Tris, 150 mM NaCl, 2 mM MgCl<sub>2</sub>, pH 7.5 - 8.0), and the particles were released from the cells by three freeze-thaw cycles. AAVX Affinity column was used to purify rAAV as described above.

### 6.2.5.4. Dot blot assay

Dot blot assay was used to detect the presence of AAV5 VLPs in *E. coli* cell extracts. Nitrocellulose membrane (88018, Thermo Fisher Scientific) was submerged in TBS buffer and mounted onto a

Dot-blot apparatus (Bio-Dot® Apparatus, Bio-Rad). *E. coli* cell extracts were diluted (10 and 100 times) in TBS buffer to 250 µl and applied to the membrane with a flow rate of 250 µl per 45 seconds. Afterwards, the membrane was removed from the apparatus and washed with TBS buffer for 10 min. The following steps were performed as described above for western blot analysis.

### 6.2.5.5. ELISA

Capsid ELISA with anti-intact-capsid antibodies was used to detect AAV particles. Briefly, VLP and rAAV samples were captured onto a Nunc MaxiSorp 96 well plate at 4°C overnight, and an anti-AAV2 (A20, Progen or A20 scFv-Fc antibody produced in our lab<sup>186</sup>) or anti-AAV5 (ADK5a antibody, Progen, **Table 9**) monoclonal antibody was used for detection of AAV2 or AAV5 particles. The wells were blocked with 0.8% BSA in PBS for 1 h, followed by incubation with the first antibody (1: 250 dilution, in blocking buffer) for 1 h at room temperature. The appropriate secondary antibody was an anti-mouse-HRP conjugate (31430, Thermo Fisher Scientific, 1: 2500 dilution) or anti-human-HRP conjugate (AM08151HR-N, Acris Antibodies, 1: 2500 dilution). After that, 1 g/L 2,2'-326 Azinobis [3-ethylbenzothiazoline-6-sulfonic acid]-diammonium salt (ABTS) in ABTS buffer (**Table 5**) was added and incubated for 30 min. Optical density was measured by a microplate reader (PowerWaveHT (KC4 software), BioTek or Infinite® M Plex (i-control software), Tecan) at 405 nm.

We used a sandwich ELISA with recombinant PKD1 domain of the AAV receptor for capture and an anti-AAV5 mouse monoclonal (ADK5a) antibody for detection to titer AAV5 particles. Briefly, PKD1 (200 ng/well) produced by our working group<sup>247</sup> was applied to a Nunc MaxiSorp 96 well plate and incubated at 4°C overnight. Then, 0.8% BSA was used to block the wells before adding AAV5 VLPs and ADK5a antibody, respectively. Further steps of the ELISA were performed as mentioned above.

To confirm the conformation of RBD after refolding from inclusion bodies of VP3\_RBD fusion proteins in *E. coli*, ELISA with a conformational RBD nanobody (CSB-RA33245A2GMY, CUSABIO, 1: 10000 dilution) was performed. AAV2 VP3\_RBD protein (0.4 µg/well) was captured on an ELISA plate overnight at 4°C. Anti-human-HRP conjugate was used as a secondary antibody. The ELISA protocol was carried out as described above.

### 6.2.5.6. AAV VLP internalization assay

Internalization of VLPs was studied using human HeLa cells. First, HeLa cells were seeded on L-lysine-coated coverslips (1.2 cm diameter) placed in 24-well plates with a density of  $3 \times 10^4$  cells/well overnight. Then, the cells were incubated with rAAV or VLPs for 2 h at 37°C, followed by fixation with 4% paraformaldehyde and permeabilization with 1% Triton X-100. BSA 1% was applied for blocking for 30 min and the A20 antibody for AAV2 and ADK5a antibody for AAV5

## 6 Materials and Methods

detection in blocking buffer was added and incubated at 4°C overnight. For detection, a fluorescently label antibody (Goat anti-Mouse IgG (H+L) Secondary Antibody, Dylight 594, 35510, Thermo Fisher Scientific, 1:500) was used. After washing, the cells were incubated with 4',6-diamidino-2-phenylindole (DAPI) for 10 min at room temperature and the coverslips were mounted on glass slides, followed by image acquisition on a Leica DMI6000 B microscopy.

### 6.2.5.7. Cell binding assay

Cell-binding assay was used to assess the functionality of RBD\_GFP produced in 293-F cells. Briefly, RBD\_GFP with different concentrations (50 nM, 100 nM, 200 nM) was diluted in DMEM medium (without FCS, without P/S), then applied onto the HEK-293 cells expressing hACE2 receptors washed with 1× PBS (in **6.2.4.4**), subsequently incubated for 30 min at 37°C. After washing 3 times with 1× PBS, 100 µl Accutase was added to each well for 2 min to detach the cells. The cells were then resuspended with 400 µl colorless RPMI, filtrated and transferred to a FACS tube. The binding assays were examined via GFP-positive cells using a FACSalibur system. At least 10000 events were measured and analyzed using a FlowJo software (Ver. 10.6.1).

### 6.2.5.8. DNA encapsidation into AAV VLP and ARM\_VP3 VLP formation

DNA samples were mixed with ARM\_VP3 protein in a high salt buffer of 1 M NaCl, then either directly diluted three times into a low salt concentration buffer (20 mM Tris-HCl, pH 8.0), incubated overnight or dialyzed into an assembly buffer of 20 mM Tris-HCl, 125 mM NaCl, pH 8.0. As a control, ARM\_VP3 protein only was dialyzed against the assembly buffer (20 mM Tris-HCl, 125 mM NaCl, pH 8.0). To do the dialysis, the lower part of a 0.5-ml reaction tube was cut off and the center of the tube lid was removed. A membrane with an MWCO of 6-8 kDa was then fixated between the tube and the lid. The tube in a piece of foam was put in a beaker of 200 mL assembly buffer. The prepared samples were then applied through the bottom side of the tube and dialyzed overnight at 4°C.

### 6.2.5.9. Determination of rAAV genomic titers and AAV VLP encapsidated DNA

qPCR was used to determine AAV genomic titers and the AAV VLP encapsidated DNA. Prior to qPCR, samples were treated with 5 U DNase I in a final volume of 25 µl reaction at 37°C, 30 min, followed by heat inactivation at 75°C, 20 min. Crude lysate samples were additionally incubated with 0.8 U Proteinase K at 37°C, 50 min before heat inactivation at 95°C, 20 min. 25-fold diluted samples in nuclease-free water were used as qPCR templates. The samples (5 µl) were mixed with 5 µl primer mix (2.5 µl forward primer, 2.5 µl revert primer at a concentration of 4µM) and 10 µl of 2× GoTag qPCR Mastermix (Promega). The qPCR cycling conditions were performed as described in **Table 18** with a LightCycler 480 II.

*Table 18. Thermal cycling conditions.*

Cycle step	Temperature	Time
Initial denaturation	95°C	10 min
40 cycles		
Denaturation	95°C	15 s
Annealing/Elongation	60°C (hGH primer set) or 58°C (CMV primer set)	1 min

The genomic titer was calculated based on a standard curve of 10 to 10<sup>6</sup> copies of the ITR plasmid and an internal control (10<sup>4</sup>-10<sup>5</sup> copies).

#### 6.2.5.10. Cell transduction assay

Transduction efficiency of rAAV5 and AAV5 VLPs was performed on CHO-K1 cells. rAAV5 samples in different multiplicities of infection (MOI) were applied on the cells that were seeded and settled for 1 h on a 12-well plate (3 × 10<sup>4</sup> cells in 500 µl medium per well). After overnight incubation, 500 µl of fresh medium was added to the wells. The cells were then incubated for 3 to 4 days for fluorescent protein reporter detection. Fluorescence was detected using a fluorescence microscope (Leica DMI6000 B).

#### 6.2.5.11. FITC conjugation to AAV VLPs, VLP agarose gel electrophoresis and FITC-labeled AAV VLP internalization

AAV2 VLP (VP3 CTTEVHis6 VLP) samples were dialyzed into 0.1 M Carbonate-Bicarbonate buffer (pH 9) (**Table 5**). Afterwards, FITC solution in DMSO (1 mg/ml) was added to the VLP samples with a ratio of 100 ng FITC per 1 µg VLP and incubated in the dark for 8 h at 4°C. To get rid of free FITC, the reaction was dialyzed into a 2-L PBS buffer.

To perform native VLP agarose gel electrophoresis, the FITC-labeled VLPs were loaded to 1.2% Agarose gel in 1× TBE buffer (**Table 5**). The electrophoresis was performed at 120 V for 1 h. The labeled VLPs were visualized using a BlueLight table. The agarose gel was then stained with the Coomassie solution (**Table 5**).

For an internalization assay, HeLa cells were seeded on a D-lysine-coated coverslip plated in a 24-well plate with a density of 10<sup>4</sup> cells/well and cultivated overnight. On the following day, the cells were pre-incubated with DMEM medium (without FCS) for 30 min. Afterwards, the labeled VLPs were applied to the wells and incubated at 37°C for 2 h. After 3 times washing with 1× PBS, the coverslips were stained with Hoechst 33342 solution for 20 min and mounted on a microscopy slide using Mowiol-Dabco solution. The samples were examined under a Leica DMI6000 B microscopy with different objectives.

### 6.2.6. Mouse experiment

Mouse experiments were conducted by Dr. Olaf Behrsing, Molecular Biotechnology, Institute for Biochemistry and Biology, University of Potsdam, Germany.

#### 6.2.6.1. Mouse immunization and serum collection

The immunogenicity of AAV2 VP3\_RBM and VP3\_RBD VLPs was evaluated in BALB/c mice (20 g) at the animal facility (Building 25, Karl-Liebknecht-Str. 24-25, D-14476 Potsdam-Golm), Molecular Biotechnology, Institute for Biochemistry and Biology, University of Potsdam. Mice were injected with either AAV2 VP3\_RBM VLPs or AAV2 VP3\_RBD VLPs (20 µg VLPs per dose) by intraperitoneal injection with the schedule described in **Figure 19**. For VP3\_RBM immunization, a mixture of adjuvants (CFA) and samples was inoculated for the first immunization, followed by sample-only injection for boosters. For VP3\_RBD immunization, one mouse was injected with VP3\_RBD only, another one was immunized with VP3\_RBD and CFA for the first vaccination followed by injection of VP3\_RBD antigens only for the boosters. Sera were collected around one week after the first and the third booster.

#### 6.2.6.2. Serum ELISA

Antigen-specific IgG antibodies in sera from the immunized mice were measured by ELISA. Briefly, injected antigens, VP3 VLP scaffolds, RBD\_GFP and GFP only in PBS buffer (2-5 µg/ml) were captured on 96-well ELISA plates for 2 h at room temperature. 5% newborn calf serum (NCS) in PBS was used to block for 30 min. Afterwards, sera (1: 200, 1: 1000 and 1: 5000 dilution) in blocking buffer (5% NCS in PBS) were applied onto the wells and incubated for 40 min at room temperature. HRP-labelled goat anti-mouse IgG antibody (0.2 µg/ml), and a substrate (o-phenylenediamine (OPD) (1 mg/ml) and H<sub>2</sub>O<sub>2</sub> (0.01%)) in substrate buffer (50 mM citric acid, 100 mM Na<sub>2</sub>HPO<sub>4</sub>, pH5.0) were used for detection. The reactions were stopped with 1 M H<sub>2</sub>SO<sub>4</sub> and 50 mM Na<sub>2</sub>SO<sub>3</sub>, and measured at 490 nm.

## 7. References

- (1) Balakrishnan, B.; Jayandharan, G. Basic Biology of Adeno-Associated Virus (AAV) Vectors Used in Gene Therapy. *Curr. Gene Ther.* **2014**, *14* (2), 86–100. <https://doi.org/10.2174/1566523214666140302193709>.
- (2) Agbandje-McKenna, M.; Schmidt, M.; Chiorini, J. A.; Afione, S.; Govindasamy, L.; Kaludov, N. Molecular Characterization of the Heparin-Dependent Transduction Domain on the Capsid of a Novel Adeno-Associated Virus Isolate, AAV(VR-942). *J. Virol.* **2008**, *82* (17), 8911–8916. <https://doi.org/10.1128/jvi.00672-08>.
- (3) Gao, G.; Vandenberghe, L. H.; Alvira, M. R.; Lu, Y.; Calcedo, R.; Zhou, X.; Wilson, J. M. Clades of Adeno-Associated Viruses Are Widely Disseminated in Human Tissues. *J. Virol.* **2004**, *78* (12), 6381–6388. <https://doi.org/10.1128/JVI.78.12.6381>.
- (4) Earley, L. F.; Powers, J. M.; Adachi, K.; Baumgart, J. T.; Meyer, N. L.; Xie, Q.; Chapman, M. S.; Nakai, H. Adeno-Associated Virus (AAV) Assembly-Activating Protein Is Not an Essential Requirement for Capsid Assembly of AAV Serotypes 4, 5, and 11. *J. Virol.* **2017**, *91* (3), e01980-16. <https://doi.org/10.1128/JVI.01980-16>.
- (5) Ward, P.; Elias, P.; Linden, R. M. Rescue of the Adeno-Associated Virus Genome from a Plasmid Vector: Evidence for Rescue by Replication. *J. Virol.* **2003**, *77* (21), 11480–11490. <https://doi.org/10.1128/JVI.77.21.11480-11490.2003>.
- (6) Pereira, D. J.; McCarty, D. M.; Muzyczka, N. The Adeno-Associated Virus (AAV) Rep Protein Acts as Both a Repressor and an Activator to Regulate AAV Transcription during a Productive Infection. *J. Virol.* **1997**, *71* (2), 1079–1088. <https://doi.org/10.1128/JVI.71.2.1079-1088.1997>.
- (7) King, J. A.; Dubielzig, R.; Grimm, D.; Kleinschmidt, J. A. DNA Helicase-Mediated Packaging of Adeno-Associated Virus Type 2 Genomes into Preformed Capsids. *EMBO J.* **2001**, *20* (12), 3282–3291. <https://doi.org/10.1093/emboj/20.12.3282>.
- (8) Surosky, R. T.; Urabe, M.; Godwin, S. G.; McQuiston, S. a; Kurtzman, G. J.; Ozawa, K.; Natsoulis, G. Adeno-Associated Virus Rep Proteins Target DNA Sequences to a Unique Locus in the Human Genome. *J. Virol.* **1997**, *71* (10), 7951–7959.
- (9) Rose, J. A.; Maizel, J. V; Inman, J. K.; Shatkin, A. J. Structural Proteins of Adenovirus-Associated Viruses. *J. Virol.* **1971**, *8* (5), 766–770. <https://doi.org/10.3109/03602537909046435>.
- (10) Becerra, S. P.; Koczot, F.; Fabisch, P.; Rose, J. A. Synthesis of Adeno-Associated Virus

## 7 References

- Structural Proteins Requires Both Alternative mRNA Splicing and Alternative Initiations from a Single Transcript. *J. Virol.* **1988**, *62* (8), 2745–2754. <https://doi.org/10.1128/JVI.62.8.2745-2754.1988>.
- (11) Sonntag, F.; Köther, K.; Schmidt, K.; Weghofer, M.; Raupp, C.; Nieto, K.; Kuck, A.; Gerlach, B.; Böttcher, B.; Müller, O. J.; et al. The Assembly-Activating Protein Promotes Capsid Assembly of Different Adeno-Associated Virus Serotypes  $\gamma$ . *J. Virol.* **2011**, *85* (23), 12686–12697. <https://doi.org/10.1128/JVI.05359-11>.
- (12) Sonntag, F.; Schmidt, K.; Kleinschmidt, J. A. A Viral Assembly Factor Promotes AAV2 Capsid Formation in the Nucleolus. *Proc. Natl. Acad. Sci. U. S. A.* **2010**, *107* (22), 10220–10225. <https://doi.org/10.1073/pnas.1001673107>.
- (13) Maurer, A. C.; Pacouret, S.; Cepeda Diaz, A. K.; Blake, J.; Andres-Mateos, E.; Vandenberghe, L. H. The Assembly-Activating Protein Promotes Stability and Interactions between AAV's Viral Proteins to Nucleate Capsid Assembly. *Cell Rep.* **2018**, *23* (6), 1817–1830. <https://doi.org/10.1016/j.celrep.2018.04.026>.
- (14) Nakai, H.; Dai, M.-S.; Sun, X.-X.; Adachi, K.; Earley, L. F.; Kawano, Y. Identification and Characterization of Nuclear and Nucleolar Localization Signals in the Adeno-Associated Virus Serotype 2 Assembly-Activating Protein. *J. Virol.* **2015**, *89* (6), 3038–3048. <https://doi.org/10.1128/jvi.03125-14>.
- (15) Ogden, P. J.; Kelsic, E. D.; Sinai, S.; Church, G. M. Comprehensive AAV Capsid Fitness Landscape Reveals a Viral Gene and Enables Machine-Guided Design. *Science (80-. )*. **2019**, *366* (6469), 1139–1143. <https://doi.org/10.1126/science.aaw2900>.
- (16) Cao, M.; You, H.; Hermonat, P. L. The X Gene of Adeno-Associated Virus 2 (AAV2) Is Involved in Viral DNA Replication. *PLoS One* **2014**, *9* (8), e104596. <https://doi.org/10.1371/journal.pone.0104596>.
- (17) Wang, D.; Tai, P. W. L.; Gao, G. Adeno-Associated Virus Vector as a Platform for Gene Therapy Delivery. *Nat. Rev. Drug Discov.* **2019**, *18* (5), 358–378. <https://doi.org/10.1038/s41573-019-0012-9>.
- (18) FDA Advisory Committee. *Spark Therapeutics Briefing Document*; 2017.
- (19) FDA. FDA approves innovative gene therapy to treat pediatric patients with spinal muscular atrophy, a rare disease and leading genetic cause of infant mortality <https://www.fda.gov/news-events/press-announcements/fda-approves-innovative-gene-therapy-treat-pediatric-patients-spinal-muscular-atrophy-rare-disease> (accessed

- Jun 6, 2019).
- (20) Ylä-Herttuala, S. Endgame: Glybera Finally Recommended for Approval as the First Gene Therapy Drug in the European Union. *Mol. Ther.* **2012**, *20* (10), 1831–1832. <https://doi.org/10.1038/mt.2012.194>.
- (21) Li, C.; Samulski, R. J. Engineering Adeno-Associated Virus Vectors for Gene Therapy. *Nat. Rev. Genet.* **2020**. <https://doi.org/10.1038/s41576-019-0205-4>.
- (22) Giles, A. R.; Sims, J. J.; Turner, K. B.; Govindasamy, L.; Alvira, M. R.; Lock, M.; Wilson, J. M. Deamidation of Amino Acids on the Surface of Adeno-Associated Virus Capsids Leads to Charge Heterogeneity and Altered Vector Function. *Mol. Ther.* **2018**, *26* (12), 2848–2862. <https://doi.org/10.1016/j.ymthe.2018.09.013>.
- (23) Wright, J. F. Product-Related Impurities in Clinical-Grade Recombinant AAV Vectors: Characterization and Risk Assessment. *Biomedicines* **2014**, *2* (1), 80–97. <https://doi.org/10.3390/biomedicines2010080>.
- (24) Kohlbrenner, E.; Aslanidi, G.; Nash, K.; Shklyae, S.; Campbell-Thompson, M.; Byrne, B. J.; Snyder, R. O.; Muzyczka, N.; Warrington, K. H.; Zolotukhin, S. Successful Production of Pseudotyped RAAV Vectors Using a Modified Baculovirus Expression System. *Mol. Ther.* **2005**, *12* (6), 1217–1225. <https://doi.org/10.1016/j.ymthe.2005.08.018>.
- (25) Clément, N.; Grieger, J. C. Manufacturing of Recombinant Adeno-Associated Viral Vectors for Clinical Trials. *Mol. Ther. - Methods Clin. Dev.* **2016**, *3* (November 2015), 16002. <https://doi.org/10.1038/mtm.2016.2>.
- (26) Barajas, D.; Aponte-Ubillus, J. J.; Akeefe, H.; Cinek, T.; Peltier, J.; Gold, D. Generation of Infectious Recombinant Adenoassociated Virus in *Saccharomyces Cerevisiae*. *PLoS One* **2017**, *12* (3), e0173010. <https://doi.org/10.1371/journal.pone.0173010>.
- (27) Steinbach, S.; Wistuba, A.; Bock, T.; Kleinschmidt, J. A. Assembly of Adeno-Associated Virus Type 2 Capsids in Vitro. *J. Gen. Virol.* **1997**, *78*, 1453–1462. <https://doi.org/10.1099/0022-1317-78-6-1453>.
- (28) Zhou, X.; Muzyczka, N. In Vitro Packaging of Adeno-Associated Virus DNA. *J. Virol.* **1998**, *72* (4), 3241–3247. <https://doi.org/10.1128/JVI.72.4.3241-3247.1998>.
- (29) Ding, L.; Lu, S.; Munshi, N. In Vitro Packaging of an Infectious Recombinant Adeno-Associated Virus 2. *Gene Ther.* **1997**, *4* (11), 1167–1172. <https://doi.org/10.1038/sj.gt.3300514>.

## 7 References

- (30) Zeltins, A. Construction and Characterization of Virus-like Particles: A Review. *Mol. Biotechnol.* **2013**, *53* (1), 92–107. <https://doi.org/10.1007/s12033-012-9598-4>.
- (31) Jeevanandam, J.; Barhoum, A.; Chan, Y. S.; Dufresne, A.; Danquah, M. K. Review on Nanoparticles and Nanostructured Materials: History, Sources, Toxicity and Regulations. *Beilstein J. Nanotechnol.* **2018**, *9* (1), 1050–1074. <https://doi.org/10.3762/bjnano.9.98>.
- (32) Lua, L. H. L.; Connors, N. K.; Sainsbury, F.; Chuan, Y. P.; Wibowo, N.; Middelberg, A. P. J. Bioengineering Virus-like Particles as Vaccines. *Biotechnol. Bioeng.* **2014**, *111* (3), 425–440. <https://doi.org/10.1002/bit.25159>.
- (33) Huang, X.; Wang, X.; Zhang, J.; Xia, N.; Zhao, Q. Escherichia Coli-Derived Virus-like Particles in Vaccine Development. *npj Vaccines* **2017**, *2* (1), 3. <https://doi.org/10.1038/s41541-017-0006-8>.
- (34) Ladd Effio, C.; Baumann, P.; Weigel, C.; Vormittag, P.; Middelberg, A.; Hubbuch, J. High-Throughput Process Development of an Alternative Platform for the Production of Virus-like Particles in Escherichia Coli. *J. Biotechnol.* **2016**, *219*, 7–19. <https://doi.org/10.1016/j.jbiotec.2015.12.018>.
- (35) Bajaj, S.; Banerjee, M. In Vitro Assembly of Polymorphic Virus-like Particles from the Capsid Protein of a Nodavirus. *Virology* **2016**, *496*, 106–115. <https://doi.org/10.1016/j.virol.2016.05.025>.
- (36) Xu, J.; Guo, H.-C. C.; Wei, Y.-Q. Q.; Dong, H.; Han, S.-C. C.; Ao, D.; Sun, D.-H. H.; Wang, H.-M. M.; Cao, S.-Z. Z.; Sun, S.-Q. Q.; et al. Self-Assembly of Virus-like Particles of Canine Parvovirus Capsid Protein Expressed from Escherichia Coli and Application as Virus-like Particle Vaccine. *Appl. Microbiol. Biotechnol.* **2014**, *98* (8), 3529–3538. <https://doi.org/10.1007/s00253-013-5485-6>.
- (37) Guo, H.; Zhu, J.; Tan, Y.; Li, C.; Chen, Z.; Sun, S.; Liu, G. Self-Assembly of Virus-like Particles of Rabbit Hemorrhagic Disease Virus Capsid Protein Expressed in Escherichia Coli and Their Immunogenicity in Rabbits. *Antiviral Res.* **2016**, *131*, 85–91. <https://doi.org/10.1016/j.antiviral.2016.04.011>.
- (38) Smith, G.; Raghunandan, R.; Wu, Y.; Liu, Y.; Massare, M.; Nathan, M.; Zhou, B.; Lu, H.; Boddapati, S.; Li, J.; et al. Respiratory Syncytial Virus Fusion Glycoprotein Expressed in Insect Cells Form Protein Nanoparticles That Induce Protective Immunity in Cotton Rats. *PLoS One* **2012**, *7* (11), e50852. <https://doi.org/10.1371/journal.pone.0050852>.
- (39) Acosta-Rivero, N.; Rodriguez, A.; Musacchio, A.; Falcón, V.; Suarez, V. M.; Martinez, G.;

- Guerra, I.; Paz-Lago, D.; Morera, Y.; De La Rosa, M. C.; et al. In Vitro Assembly into Virus-like Particles Is an Intrinsic Quality of *Pichia Pastoris* Derived HCV Core Protein. *Biochem. Biophys. Res. Commun.* **2004**, *325* (1), 68–74. <https://doi.org/10.1016/j.bbrc.2004.10.012>.
- (40) Bundy, B. C.; Swartz, J. R. Efficient Disulfide Bond Formation in Virus-like Particles. *J. Biotechnol.* **2011**, *154* (4), 230–239. <https://doi.org/10.1016/j.jbiotec.2011.04.011>.
- (41) Bundy, B. C.; Franciszkowicz, M. J.; Swartz, J. R. Escherichia Coli-Based Cell-Free Synthesis of Virus-like Particles. *Biotechnol. Bioeng.* **2008**, *100* (1), 28–37. <https://doi.org/10.1002/bit.21716>.
- (42) Spice, A. J.; Aw, R.; Bracewell, D. G.; Polizzi, K. M. Synthesis and Assembly of Hepatitis B Virus-Like Particles in a *Pichia Pastoris* Cell-Free System. *Front. Bioeng. Biotechnol.* **2020**, *8* (February), 72. <https://doi.org/10.3389/fbioe.2020.00072>.
- (43) Ashley, C. E.; Carnes, E. C.; Phillips, G. K.; Durfee, P. N.; Buley, M. D.; Lino, C. A.; Padilla, D. P.; Phillips, B.; Carter, M. B.; Willman, C. L.; et al. Cell-Specific Delivery of Diverse Cargos by Bacteriophage MS2 Virus-like Particles. *ACS Nano* **2011**, *5* (7), 5729–5745. <https://doi.org/10.1021/nn201397z>.
- (44) McCarthy, M. P.; White, W. I.; Palmer-Hill, F.; Koenig, S.; Suzich, J. A. Quantitative Disassembly and Reassembly of Human Papillomavirus Type 11 Virus like Particles In Vitro. *J. Virol.* **1998**, *72* (1), 32–41. <https://doi.org/10.1128/JVI.72.1.32-41.1998>.
- (45) Villagrana-Escareño, M. V.; Reynaga-Hernández, E.; Galicia-Cruz, O. G.; Durán-Meza, A. L.; De la Cruz-González, V.; Hernández-Carballo, C. Y.; Ruíz-García, J. VLPs Derived from the CCMV Plant Virus Can Directly Transfect and Deliver Heterologous Genes for Translation into Mammalian Cells. *Biomed Res. Int.* **2019**, *2019*, 4630891. <https://doi.org/10.1155/2019/4630891>.
- (46) Lam, P.; Steinmetz, N. F. Delivery of siRNA Therapeutics Using Cowpea Chlorotic Mottle Virus-like Particles. *Biomater. Sci.* **2019**, *7* (8), 3138–3142. <https://doi.org/10.1039/c9bm00785g>.
- (47) Comellas-Aragonès, M.; Engelkamp, H.; Claessen, V. I.; Sommerdijk, N. A. J. M.; Rowan, A. E.; Christianen, P. C. M.; Maan, J. C.; Verduin, B. J. M.; Cornelissen, J. J. L. M.; Nolte, R. J. M. A Virus-Based Single-Enzyme Nanoreactor. *Nat. Nanotechnol.* **2007**, *2* (10), 635–639. <https://doi.org/10.1038/nnano.2007.299>.
- (48) Fang, P. Y.; Ramos, L. M. G.; Holguin, S. Y.; Hsiao, C.; Bowman, J. C.; Yang, H. W.; Williams, L. D. Functional RNAs: Combined Assembly and Packaging in VLPs. *Nucleic Acids Res.* **2016**,

- 45 (6), 3519–3527. <https://doi.org/10.1093/nar/gkw1154>.
- (49) Ren, L.; Zhang, X.; Bi, S.; Shan, W.; Ye, S.; Hu, B.; Wu, Y.; Lv, X.; Zhang, D.; Zhou, X. Modularized Peptides Modified HBC Virus-like Particles for Encapsulation and Tumor-Targeted Delivery of Doxorubicin. *Nanomedicine Nanotechnology, Biol. Med.* **2017**, *14* (3), 725–734. <https://doi.org/10.1016/j.nano.2017.12.002>.
- (50) Lee, E. B.; Kim, J.-H.; Hur, W.; Choi, J. E.; Kim, S. M.; Park, D. J.; Kang, B.-Y.; Lee, G. W.; Yoon, S. K. Liver-Specific Gene Delivery Using Engineered Virus-Like Particles of Hepatitis E Virus. *Sci. Rep.* **2019**, *9* (1), 1616. <https://doi.org/10.1038/s41598-019-38533-7>.
- (51) Cerqueira, C.; Pang, Y.-Y. S.; Day, P. M.; Thompson, C. D.; Buck, C. B.; Lowy, D. R.; Schiller, J. T. A Cell-Free Assembly System for Generating Infectious Human Papillomavirus 16 Capsids Implicates a Size Discrimination Mechanism for Preferential Viral Genome Packaging. *J. Virol.* **2016**, *90* (2), 1096–1107. <https://doi.org/10.1128/JVI.02497-15>.
- (52) Cerqueira, C.; Thompson, C. D.; Day, P. M.; Pang, Y.-Y. S.; Lowy, D. R.; Schiller, J. T. Efficient Production of Papillomavirus Gene Delivery Vectors in Defined In Vitro Reactions. *Mol. Ther. - Methods Clin. Dev.* **2017**, *5* (June), 165–179. <https://doi.org/10.1016/j.omtm.2017.04.005>.
- (53) Touze, A.; Coursaget, P. In Vitro Gene Transfer Using Human Papillomavirus-like Particles. *Nucleic Acids Res.* **1998**, *26* (5), 1317–1323. <https://doi.org/10.1093/nar/26.5.1317>.
- (54) Colomar, M. C.; Degoumois-Sahli, C.; Beard, P. Opening and Refolding of Simian Virus 40 and in Vitro Packaging of Foreign DNA. *J. Virol.* **1993**, *67* (5), 2779–2786. <https://doi.org/10.1128/jvi.67.5.2779-2786.1993>.
- (55) Sandalon, Z.; Dalyot-Herman, N.; Oppenheim, A. B.; Oppenheim, A. In Vitro Assembly of SV40 Virions and Pseudovirions: Vector Development for Gene Therapy. *Hum. Gene Ther.* **1997**, *8* (7), 843–849. <https://doi.org/10.1089/hum.1997.8.7-843>.
- (56) Rudolph, R. Renaturation of Recombinant, Disulfide-Bonded Proteins from “Inclusion Bodies.” In *Modern Methods in Protein- and Nucleic Acid Research*; Tschesche, H., Ed.; De Gruyter: Berlin, Boston, 1990; pp 149–172. <https://doi.org/10.1515/9783110853537-009>.
- (57) Yazdani, R.; Shams-Bakhsh, M.; Hassani-Mehraban, A.; Arab, S. S.; Thelen, N.; Thiry, M.; Crommen, J.; Fillet, M.; Jacobs, N.; Brans, A.; et al. Production and Characterization of Virus-like Particles of Grapevine Fanleaf Virus Presenting L2 Epitope of Human Papillomavirus Minor Capsid Protein. *BMC Biotechnol.* **2019**, *19* (1), 81. <https://doi.org/10.1186/s12896-019-0566-y>.

- (58) Sánchez-Rodríguez, S. P.; Münch-Anguiano, L.; Echeverría, O.; Vázquez-Nin, G.; Mora-Pale, M.; Dordick, J. S.; Bustos-Jaimes, I. Human Parvovirus B19 Virus-like Particles: In Vitro Assembly and Stability. *Biochimie* **2012**, *94* (3), 870–878. <https://doi.org/10.1016/j.biochi.2011.12.006>.
- (59) Le, D. T.; Radukic, M. T.; Müller, K. M. Adeno-Associated Virus Capsid Protein Expression in Escherichia Coli and Chemically Defined Capsid Assembly. *Sci. Rep.* **2019**, *9* (1), 18631. <https://doi.org/10.1038/s41598-019-54928-y>.
- (60) Bin Mohamed Suffian, I. F.; Garcia-Maya, M.; Brown, P.; Bui, T.; Nishimura, Y.; Palermo, A. R. B. M. J.; Ogino, C.; Kondo, A.; Al-Jamal, K. T. Yield Optimisation of Hepatitis B Virus Core Particles in E. Coli Expression System for Drug Delivery Applications. *Sci. Rep.* **2017**. <https://doi.org/10.1038/srep43160>.
- (61) Zhang, L.; Zhang, J.; Zhang, Z.; Chen, Y.; Zhao, Q.; Chen, W. Self-Assembled Virus-Like Particles from Rotavirus Structural Protein VP6 for Targeted Drug Delivery. *Bioconjug. Chem.* **2011**, *22* (3), 346–352. <https://doi.org/10.1021/bc1002532>.
- (62) Rudolph, R.; Lilie, H. In Vitro Folding of Inclusion Body Proteins. *FASEB J.* **1996**, *10* (1), 49–56. <https://doi.org/10.1096/fasebj.10.1.8566547>.
- (63) Hagel, P.; Gerding, J. J. T.; Fieggen, W.; Bloemendal, H. Cyanate Formation in Solutions of Urea. *Biochim. Biophys. Acta - Protein Struct.* **1971**, *243* (3), 366–373. [https://doi.org/10.1016/0005-2795\(71\)90003-1](https://doi.org/10.1016/0005-2795(71)90003-1).
- (64) Schoemaker, J. M.; Brasnett, A. H.; Marston, F. A. Examination of Calf Prochymosin Accumulation in Escherichia Coli: Disulphide Linkages Are a Structural Component of Prochymosin-Containing Inclusion Bodies. *EMBO J.* **1985**, *4* (3), 775–780. <https://doi.org/10.1002/j.1460-2075.1985.tb03696.x>.
- (65) Singhvi, P.; Saneja, A.; Srichandan, S.; Panda, A. K. Bacterial Inclusion Bodies: A Treasure Trove of Bioactive Proteins. *Trends Biotechnol.* **2020**, *38* (5), 474–486. <https://doi.org/10.1016/j.tibtech.2019.12.011>.
- (66) Yamaguchi, S.; Yamamoto, E.; Mannen, T.; Nagamune, T.; Nagamune, T. Protein Refolding Using Chemical Refolding Additives. *Biotechnol. J.* **2013**, *8* (1), 17–31. <https://doi.org/10.1002/biot.201200025>.
- (67) Middelberg, A. P. J. Preparative Protein Refolding. *Trends Biotechnol.* **2002**, *20* (10), 437–443. [https://doi.org/10.1016/S0167-7799\(02\)02047-4](https://doi.org/10.1016/S0167-7799(02)02047-4).
- (68) Yamaguchi, H.; Miyazaki, M.; Briones-Nagata, M. P.; Maeda, H. Refolding of Difficult-to-

## 7 References

- Fold Proteins by a Gradual Decrease of Denaturant Using Microfluidic Chips. *J. Biochem.* **2010**, *147* (6), 895–903. <https://doi.org/10.1093/jb/mvq024>.
- (69) Okada, J.; Maruyama, T.; Motomura, K.; Kuroki, K.; Maenaka, K.; Sakono, M.; Goto, M. Enzyme-Mediated Protein Refolding. *Chem. Commun.* **2009**, No. 46, 7197. <https://doi.org/10.1039/b916225a>.
- (70) Perlmutter, J. D.; Hagan, M. F. Mechanisms of Virus Assembly. *Annu. Rev. Phys. Chem.* **2015**, *66*, 217–239. <https://doi.org/10.1146/annurev-physchem-040214-121637>.
- (71) Hagan, M. F. Modeling Viral Capsid Assembly. In *Advances in Chemical Physics*; Rice, S. A., Dinner, A. R., Eds.; Wiley: New Jersey USA, 2014; pp 1–68. <https://doi.org/10.1002/9781118755815.ch01>.
- (72) Hagan, M. F.; Elrad, O. M. Understanding the Concentration Dependence of Viral Capsid Assembly Kinetics—the Origin of the Lag Time and Identifying the Critical Nucleus Size. *Biophys. J.* **2010**, *98* (6), 1065–1074. <https://doi.org/10.1016/j.bpj.2009.11.023>.
- (73) Landry, N.; Pillet, S.; Favre, D.; Poulin, J.-F.; Trépanier, S.; Yassine-Diab, B.; Ward, B. J. Influenza Virus-like Particle Vaccines Made in *Nicotiana Benthamiana* Elicit Durable, Poly-Functional and Cross-Reactive T Cell Responses to Influenza HA Antigens. *Clin. Immunol.* **2014**, *154* (2), 164–177. <https://doi.org/10.1016/j.clim.2014.08.003>.
- (74) Li, H.; Onbe, K.; Liu, Q.; Iijima, M.; Tatematsu, K.; Seno, M.; Tada, H.; Kuroda, S. Ichi. Synthesis and Assembly of Hepatitis B Virus Envelope Protein-Derived Particles in *Escherichia Coli*. *Biochem. Biophys. Res. Commun.* **2017**, *490* (2), 155–160. <https://doi.org/10.1016/j.bbrc.2017.06.015>.
- (75) Powilleit, F.; Breinig, T.; Schmitt, M. J. Exploiting the Yeast L-A Viral Capsid for the In Vivo Assembly of Chimeric VLPs as Platform in Vaccine Development and Foreign Protein Expression. *PLoS One* **2007**, *2* (5), e415. <https://doi.org/10.1371/journal.pone.0000415>.
- (76) Mohsen, M. O.; Gomes, A. C.; Vogel, M.; Bachmann, M. F. Interaction of Viral Capsid-Derived Virus-like Particles (VLPs) with the Innate Immune System. *Vaccines* **2018**, *6* (3), 1–12. <https://doi.org/10.3390/vaccines6030037>.
- (77) Klikova, M.; Rhee, S. S.; Hunter, E.; Ruml, T. Efficient in Vivo and in Vitro Assembly of Retroviral Capsids from Gag Precursor Proteins Expressed in Bacteria. *J. Virol.* **1995**, *69* (2), 1093–1098. <https://doi.org/10.1128/JVI.69.2.1093-1098.1995>.
- (78) Le, D. T.; Müller, K. M. In Vitro Assembly of Virus-Like Particles and Their Applications. *Life* **2021**, *11* (4), 334. <https://doi.org/10.3390/life11040334>.

- (79) Barklis, E.; Alfadhli, A.; McQuaw, C.; Yalamuri, S.; Still, A.; Barklis, R. L.; Kukull, B.; López, C. S. Characterization of the In Vitro HIV-1 Capsid Assembly Pathway. *J. Mol. Biol.* **2009**, *387* (2), 376–389. <https://doi.org/10.1016/j.jmb.2009.01.058>.
- (80) Johnson, J. M.; Tang, J.; Nyame, Y.; Willits, D.; Young, M. J.; Zlotnick, A. Regulating Self-Assembly of Spherical Oligomers. *Nano Lett.* **2005**, *5* (4), 765–770. <https://doi.org/10.1021/nl050274q>.
- (81) Kwon, S.-J.; Park, M.-R.; Kim, K.-W.; Plante, C. A.; Hemenway, C. L.; Kim, K.-H. Cis-Acting Sequences Required for Coat Protein Binding and in Vitro Assembly of Potato Virus X. *Virology* **2005**, *334* (1), 83–97. <https://doi.org/10.1016/j.virol.2005.01.018>.
- (82) Dominy, B. N.; Perl, D.; Schmid, F. X.; Brooks, C. L. The Effects of Ionic Strength on Protein Stability: The Cold Shock Protein Family. *J. Mol. Biol.* **2002**, *319* (2), 541–554. [https://doi.org/10.1016/S0022-2836\(02\)00259-0](https://doi.org/10.1016/S0022-2836(02)00259-0).
- (83) Jaballah, S. A.; Bailey, G. D.; Desfosses, A.; Hyun, J.; Mitra, A. K.; Kingston, R. L. In Vitro Assembly of the Rous Sarcoma Virus Capsid Protein into Hexamer Tubes at Physiological Temperature. *Sci. Rep.* **2017**, *7* (1), 2913. <https://doi.org/10.1038/s41598-017-02060-0>.
- (84) Uetrecht, C.; Watts, N. R.; Stahl, S. J.; Wingfield, P. T.; Steven, A. C.; Heck, A. J. R. Subunit Exchange Rates in Hepatitis B Virus Capsids Are Geometry- and Temperature-Dependent. *Phys. Chem. Chem. Phys.* **2010**, *12* (41), 13368–13371. <https://doi.org/10.1039/c0cp00692k>.
- (85) Comas-Garcia, M.; Knobler, C. M.; Gelbart, W. M.; Gopal, A.; Garmann, R. F. The Assembly Pathway of an Icosahedral Single-Stranded RNA Virus Depends on the Strength of Inter-Subunit Attractions. *J. Mol. Biol.* **2013**, *426* (5), 1050–1060. <https://doi.org/10.1016/j.jmb.2013.10.017>.
- (86) Gelbart, W. M.; Garmann, R. F.; Cadena-Nava, R. D.; Comas-Garcia, M.; Knobler, C. M.; Rao, A. L. N. Self-Assembly of Viral Capsid Protein and RNA Molecules of Different Sizes: Requirement for a Specific High Protein/RNA Mass Ratio. *J. Virol.* **2011**, *86* (6), 3318–3326. <https://doi.org/10.1128/jvi.06566-11>.
- (87) de Ruyter, M. V.; van der Hee, R. M.; Driessen, A. J. M.; Keurhorst, E. D.; Hamid, M.; Cornelissen, J. J. L. M. Polymorphic Assembly of Virus-Capsid Proteins around DNA and the Cellular Uptake of the Resulting Particles. *J. Control. Release* **2019**, *307* (March), 342–354. <https://doi.org/10.1016/j.jconrel.2019.06.019>.
- (88) Comas-Garcia, M.; Kroupa, T.; Datta, S. A. K.; Harvin, D. P.; Hu, W.-S.; Rein, A. Efficient

## 7 References

- Support of Virus-like Particle Assembly by the HIV-1 Packaging Signal. *Elife* **2018**, *7*, e38438. <https://doi.org/10.7554/eLife.38438>.
- (89) Kunkel, M.; Lorinczi, M.; Rijnbrand, R.; Lemon, S. M.; Watowich, S. J. Self-Assembly of Nucleocapsid-Like Particles from Recombinant Hepatitis C Virus Core Protein. *J. Virol.* **2001**, *75* (5), 2119–2129. <https://doi.org/10.1128/jvi.75.5.2119-2129.2001>.
- (90) Sarker, S.; Terrón, M. C.; Khandokar, Y.; Aragão, D.; Hardy, J. M.; Radjainia, M.; Jiménez-Zaragoza, M.; de Pablo, P. J.; Coulibaly, F.; Luque, D.; et al. Structural Insights into the Assembly and Regulation of Distinct Viral Capsid Complexes. *Nat. Commun.* **2016**, *7* (1), 13014. <https://doi.org/10.1038/ncomms13014>.
- (91) van Rosmalen, M. G. M.; Kamsma, D.; Biebricher, A. S.; Li, C.; Zlotnick, A.; Roos, W. H.; Wuite, G. J. L. Revealing in Real-Time a Multistep Assembly Mechanism for SV40 Virus-like Particles. *Sci. Adv.* **2020**, *6* (16), eaaz1639. <https://doi.org/10.1126/sciadv.aaz1639>.
- (92) Medina, E. M.; Andrews, B. T.; Nakatani, E.; Catalano, C. E. The Bacteriophage Lambda GpNu3 Scaffolding Protein Is an Intrinsically Disordered and Biologically Functional Procapsid Assembly Catalyst. *J. Mol. Biol.* **2011**, *412* (4), 723–736. <https://doi.org/10.1016/j.jmb.2011.07.045>.
- (93) Motwani, T.; Lokareddy, R. K.; Dunbar, C. A.; Cortines, J. R.; Jarrold, M. F.; Cingolani, G.; Teschke, C. M. A Viral Scaffolding Protein Triggers Portal Ring Oligomerization and Incorporation during Procapsid Assembly. *Sci. Adv.* **2017**, *3* (7), e1700423. <https://doi.org/10.1126/sciadv.1700423>.
- (94) Wang, S.; Palasingam, P.; Nøkling, R. H.; Lindqvist, B. H.; Dokland, T. In Vitro Assembly of Bacteriophage P4 Procapsids from Purified Capsid and Scaffolding Proteins. *Virology* **2000**, *275* (1), 133–144. <https://doi.org/10.1006/viro.2000.0521>.
- (95) Cerritelli, M. E.; Studier, F. W. Assembly of T7 Capsids from Independently Expressed and Purified Head Protein and Scaffolding Protein. *J. Mol. Biol.* **1996**, *258* (2), 286–298. <https://doi.org/10.1006/jmbi.1996.0250>.
- (96) Fu, C.; Morais, M. C.; Battisti, A. J.; Rossmann, M. G.; Prevelige, P. E. Molecular Dissection of  $\phi$ 29 Scaffolding Protein Function in an in Vitro Assembly System. *J. Mol. Biol.* **2007**, *366* (4), 1161–1173. <https://doi.org/10.1016/j.jmb.2006.11.091>.
- (97) Newcomb, W. W.; Homa, F. L.; Thomsen, D. R.; Brown, J. C. In Vitro Assembly of the Herpes Simplex Virus Procapsid: Formation of Small Procapsids at Reduced Scaffolding Protein Concentration. *J. Struct. Biol.* **2001**, *133* (1), 23–31.

- <https://doi.org/10.1006/jsbi.2001.4329>.
- (98) Sánchez-Rodríguez, S. P.; Morán-García, A. del C.; Bolonduro, O.; Dordick, J. S.; Bustos-Jaimes, I. Enhanced Assembly and Colloidal Stabilization of Primate Erythroparvovirus 1 Virus-like Particles for Improved Surface Engineering. *Acta Biomater.* **2016**, *35*, 206–214. <https://doi.org/10.1016/j.actbio.2016.02.024>.
- (99) Lampel, A.; Bram, Y.; Levy-Sakin, M.; Bacharach, E.; Gazit, E. The Effect of Chemical Chaperones on the Assembly and Stability of HIV-1 Capsid Protein. *PLoS One* **2013**, *8* (4), 25–29. <https://doi.org/10.1371/journal.pone.0060867>.
- (100) Sinn, S.; Yang, L.; Biedermann, F.; Wang, D.; Kübel, C.; Cornelissen, J. J. L. M.; De Cola, L. Templated Formation of Luminescent Virus-like Particles by Tailor-Made Pt(II) Amphiphiles. *J. Am. Chem. Soc.* **2018**, *140* (6), 2355–2362. <https://doi.org/10.1021/jacs.7b12447>.
- (101) Millán, J. G.; Brasch, M.; Anaya-Plaza, E.; De La Escosura, A.; Velders, A. H.; Reinhoudt, D. N.; Torres, T.; Koay, M. S. T.; Cornelissen, J. J. L. M. Self-Assembly Triggered by Self-Assembly: Optically Active, Paramagnetic Micelles Encapsulated in Protein Cage Nanoparticles. *J. Inorg. Biochem.* **2014**, *136*, 140–146. <https://doi.org/10.1016/j.jinorgbio.2014.01.004>.
- (102) Kwak, M.; Minten, I. J.; Anaya, D. M.; Musser, A. J.; Brasch, M.; Nolte, R. J. M.; Müllen, K.; Cornelissen, J. J. L. M.; Herrmann, A. Virus-like Particles Templated by DNA Micelles: A General Method for Loading Virus Nanocarriers. *J. Am. Chem. Soc.* **2010**, *132* (23), 7834–7835. <https://doi.org/10.1021/ja101444j>.
- (103) Comellas-Aragonès, M.; de la Escosura, A.; Dirks, A. (Ton) J.; van der Ham, A.; Fusté-Cuñé, A.; Cornelissen, J. J. L. M.; Nolte, R. J. M. Controlled Integration of Polymers into Viral Capsids. *Biomacromolecules* **2009**, *10* (11), 3141–3147. <https://doi.org/10.1021/bm9007953>.
- (104) Sikkema, F. D.; Comellas-Aragonès, M.; Fokkink, R. G.; Verduin, B. J. M.; Cornelissen, J. J. L. M.; Nolte, R. J. M. Monodisperse Polymer-Virus Hybrid Nanoparticles. *Org. Biomol. Chem.* **2007**, *5* (1), 54–57. <https://doi.org/10.1039/b613890j>.
- (105) Mach, H.; Middaugh, C. R.; Lewis, R. V. Statistical Determination of the Average Values of the Extinction Coefficients of Tryptophan and Tyrosine in Native Proteins. *Anal. Biochem.* **1992**, *200* (1), 74–80. [https://doi.org/10.1016/0003-2697\(92\)90279-G](https://doi.org/10.1016/0003-2697(92)90279-G).
- (106) Mach, H.; Middaugh, C. R. Simultaneous Monitoring of the Environment of Tryptophan,

## 7 References

- Tyrosine, and Phenylalanine Residues in Proteins by Near-Ultraviolet Second-Derivative Spectroscopy. *Anal. Biochem.* **1994**, 222 (2), 323–331. <https://doi.org/10.1006/abio.1994.1499>.
- (107) Walker, J. M. The Bicinchoninic Acid (BCA) Assay for Protein Quantitation. *Methods Mol. Biol.* **1994**, 32 (Basic Protein and Peptide Protocols), 5–8. <https://doi.org/10.1385/0-89603-268-X:5>.
- (108) Dashti, N. H.; Abidin, R. S.; Sainsbury, F. Programmable in Vitro Coencapsulation of Guest Proteins for Intracellular Delivery by Virus-like Particles. *ACS Nano* **2018**, 12 (5), 4615–4623. <https://doi.org/10.1021/acsnano.8b01059>.
- (109) Glasgow, J. E.; Capehart, S. L.; Francis, M. B.; Tullman-Ercek, D. Osmolyte-Mediated Encapsulation of Proteins inside MS2 Viral Capsids. *ACS Nano* **2012**, 6 (10), 8658–8664. <https://doi.org/10.1021/nn302183h>.
- (110) Termini, E.; Description, F. P.; Street, D.; Id, B. S.; Schedule, E.; Code, F. F.; Funds, F.; Code, S. F.; Funds, S.; Funds, L.; et al. SARS-CoV-2 Spike Glycoprotein Vaccine Candidate NVX-CoV2373 Elicits Immunogenicity in Baboons and Protection in Mice. *bioRxiv* **2020**. <https://doi.org/10.1101/2020.06.29.178509>.
- (111) Zhang, X.; Wei, M.; Pan, H.; Lin, Z.; Wang, K.; Weng, Z.; Zhu, Y.; Xin, L.; Zhang, J.; Li, S.; et al. Robust Manufacturing and Comprehensive Characterization of Recombinant Hepatitis E Virus-like Particles in Hecolin®. *Vaccine* **2014**, 32 (32), 4039–4050. <https://doi.org/10.1016/j.vaccine.2014.05.064>.
- (112) European Medicines Agency. Gardasil : EPAR - Scientific discussion [https://www.ema.europa.eu/en/documents/scientific-discussion/gardasil-epar-scientific-discussion\\_en.pdf](https://www.ema.europa.eu/en/documents/scientific-discussion/gardasil-epar-scientific-discussion_en.pdf) (accessed Dec 20, 2020).
- (113) Zhao, Q.; Allen, M. J.; Wang, Y.; Wang, B.; Wang, N.; Shi, L.; Sitrin, R. D. Disassembly and Reassembly Improves Morphology and Thermal Stability of Human Papillomavirus Type 16 Virus-like Particles. *Nanomedicine Nanotechnology, Biol. Med.* **2012**, 8 (7), 1182–1189. <https://doi.org/10.1016/j.nano.2012.01.007>.
- (114) Valbuena, A.; Maity, S.; Mateu, M. G.; Roos, W. H. Visualization of Single Molecules Building a Viral Capsid Protein Lattice through Stochastic Pathways. *ACS Nano* **2020**, 14 (7), 8724–8734. <https://doi.org/10.1021/acsnano.0c03207>.
- (115) Ashcroft, A. E. Mass Spectrometry-Based Studies of Virus Assembly. *Curr. Opin. Virol.* **2019**, 36, 17–24. <https://doi.org/10.1016/j.coviro.2019.02.006>.

- (116) Prevelige, P. E.; Thomas, D.; King, J. Nucleation and Growth Phases in the Polymerization of Coat and Scaffolding Subunits into Icosahedral Procapsid Shells. *Biophys. J.* **1993**, *64* (3), 824–835. [https://doi.org/10.1016/S0006-3495\(93\)81443-7](https://doi.org/10.1016/S0006-3495(93)81443-7).
- (117) Li, C.; Kneller, A. R.; Jacobson, S. C.; Zlotnick, A. Single Particle Observation of SV40 VP1 Polyanion-Induced Assembly Shows That Substrate Size and Structure Modulate Capsid Geometry. *ACS Chem. Biol.* **2017**, *12* (5), 1327–1334. <https://doi.org/10.1021/acscchembio.6b01066>.
- (118) Medrano, M.; Fuertes, M. Á.; Valbuena, A.; Carrillo, P. J. P.; Rodríguez-Huete, A.; Mateu, M. G. Imaging and Quantitation of a Succession of Transient Intermediates Reveal the Reversible Self-Assembly Pathway of a Simple Icosahedral Virus Capsid. *J. Am. Chem. Soc.* **2016**, *138* (47), 15385–15396. <https://doi.org/10.1021/jacs.6b07663>.
- (119) Ignatiou, A.; Brasilès, S.; El Sadek Fadel, M.; Bürger, J.; Mielke, T.; Topf, M.; Tavares, P.; Orlova, E. V. Structural Transitions during the Scaffolding-Driven Assembly of a Viral Capsid. *Nat. Commun.* **2019**, *10* (1), 4840. <https://doi.org/10.1038/s41467-019-12790-6>.
- (120) Khaykelson, D.; Raviv, U. Studying Viruses Using Solution X-Ray Scattering. *Biophys. Rev.* **2020**, *12* (1), 41–48. <https://doi.org/10.1007/s12551-020-00617-4>.
- (121) Tuma, R.; Tsuruta, H.; French, K. H.; Prevelige, P. E. Detection of Intermediates and Kinetic Control during Assembly of Bacteriophage P22 Procapsid. *J. Mol. Biol.* **2008**, *381* (5), 1395–1406. <https://doi.org/10.1016/j.jmb.2008.06.020>.
- (122) Tresset, G.; Le Coeur, C.; Bryche, J.-F.; Tatou, M.; Zeghal, M.; Charpilienne, A.; Poncet, D.; Constantin, D.; Bressanelli, S. Norovirus Capsid Proteins Self-Assemble through Biphasic Kinetics via Long-Lived Stave-like Intermediates. *J. Am. Chem. Soc.* **2013**, *135* (41), 15373–15381. <https://doi.org/10.1021/ja403550f>.
- (123) Asor, R.; Selzer, L.; Schlicksup, C. J.; Zhao, Z.; Zlotnick, A.; Raviv, U. Assembly Reactions of Hepatitis B Capsid Protein into Capsid Nanoparticles Follow a Narrow Path through a Complex Reaction Landscape. *ACS Nano* **2019**, *13* (7), 7610–7626. <https://doi.org/10.1021/acsnano.9b00648>.
- (124) Chevreuil, M.; Law-Hine, D.; Chen, J.; Bressanelli, S.; Combet, S.; Constantin, D.; Degrouard, J.; Möller, J.; Zeghal, M.; Tresset, G. Nonequilibrium Self-Assembly Dynamics of Icosahedral Viral Capsids Packaging Genome or Polyelectrolyte. *Nat. Commun.* **2018**, *9* (1), 3071. <https://doi.org/10.1038/s41467-018-05426-8>.
- (125) Panahandeh, S.; Li, S.; Marichal, L.; Leite Rubim, R.; Tresset, G.; Zandi, R. How a Virus

## 7 References

- Circumvents Energy Barriers to Form Symmetric Shells. *ACS Nano* **2020**, *14* (3), 3170–3180. <https://doi.org/10.1021/acsnano.9b08354>.
- (126) Uetrecht, C.; Barbu, I. M.; Shoemaker, G. K.; van Duijn, E.; Heck, A. J. R. Interrogating Viral Capsid Assembly with Ion Mobility–Mass Spectrometry. *Nat. Chem.* **2011**, *3* (2), 126–132. <https://doi.org/10.1038/nchem.947>.
- (127) Lutomski, C. A.; Lykтей, N. A.; Pierson, E. E.; Zhao, Z.; Zlotnick, A.; Jarrold, M. F. Multiple Pathways in Capsid Assembly. *J. Am. Chem. Soc.* **2018**, *140* (17), 5784–5790. <https://doi.org/10.1021/jacs.8b01804>.
- (128) Shoemaker, G. K.; van Duijn, E.; Crawford, S. E.; Uetrecht, C.; Baclayon, M.; Roos, W. H.; Wuite, G. J. L.; Estes, M. K.; Prasad, B. V. V.; Heck, A. J. R. Norwalk Virus Assembly and Stability Monitored by Mass Spectrometry. *Mol. Cell. Proteomics* **2010**, *9* (8), 1742–1751. <https://doi.org/10.1074/mcp.M900620-MCP200>.
- (129) Harms, Z. D.; Selzer, L.; Zlotnick, A.; Jacobson, S. C. Monitoring Assembly of Virus Capsids with Nanofluidic Devices. *ACS Nano* **2015**, *9* (9), 9087–9096. <https://doi.org/10.1021/acsnano.5b03231>.
- (130) Garmann, R. F.; Goldfain, A. M.; Manoharan, V. N. Measurements of the Self-Assembly Kinetics of Individual Viral Capsids around Their RNA Genome. *Proc. Natl. Acad. Sci.* **2019**, *116* (45), 22485–22490. <https://doi.org/10.1073/pnas.1909223116>.
- (131) Borodavka, A.; Tuma, R.; Stockley, P. G. Evidence That Viral RNAs Have Evolved for Efficient, Two-Stage Packaging. *Proc. Natl. Acad. Sci.* **2012**, *109* (39), 15769–15774. <https://doi.org/10.1073/pnas.1204357109>.
- (132) Marchetti, M.; Kamsma, D.; Cazares Vargas, E.; Hernandez García, A.; van der Schoot, P.; de Vries, R.; Wuite, G. J. L.; Roos, W. H. Real-Time Assembly of Viruslike Nucleocapsids Elucidated at the Single-Particle Level. *Nano Lett.* **2019**, *19* (8), 5746–5753. <https://doi.org/10.1021/acs.nanolett.9b02376>.
- (133) Uchihashi, T.; Scheuring, S. Applications of High-Speed Atomic Force Microscopy to Real-Time Visualization of Dynamic Biomolecular Processes. *Biochim. Biophys. Acta - Gen. Subj.* **2018**, *1862* (2), 229–240. <https://doi.org/10.1016/j.bbagen.2017.07.010>.
- (134) Jegerlehner, A.; Storni, T.; Lipowsky, G.; Schmid, M.; Pumpens, P.; Bachmann, M. F. Regulation of IgG Antibody Responses by Epitope Density and CD21-Mediated Costimulation. *Eur. J. Immunol.* **2002**, *32* (11), 3305–3314. [https://doi.org/10.1002/1521-4141\(200211\)32:11<3305::AID-IMMU3305>3.0.CO;2-J](https://doi.org/10.1002/1521-4141(200211)32:11<3305::AID-IMMU3305>3.0.CO;2-J).

- (135) Chackerian, B.; Lenz, P.; Lowy, D. R.; Schiller, J. T. Determinants of Autoantibody Induction by Conjugated Papillomavirus Virus-Like Particles. *J. Immunol.* **2002**, *169* (11), 6120–6126. <https://doi.org/10.4049/jimmunol.169.11.6120>.
- (136) Zabel, F.; Mohanan, D.; Bessa, J.; Link, A.; Fettelschoss, A.; Saudan, P.; Kündig, T. M.; Bachmann, M. F. Viral Particles Drive Rapid Differentiation of Memory B Cells into Secondary Plasma Cells Producing Increased Levels of Antibodies. *J. Immunol.* **2014**, *192* (12), 5499–5508. <https://doi.org/10.4049/jimmunol.1400065>.
- (137) Peacey, M.; Wilson, S.; Baird, M. A.; Ward, V. K. Versatile RHDV Virus-like Particles: Incorporation of Antigens by Genetic Modification and Chemical Conjugation. *Biotechnol. Bioeng.* **2007**, *98* (5), 968–977. <https://doi.org/10.1002/bit.21518>.
- (138) Billaud, J.-N.; Peterson, D.; Barr, M.; Chen, A.; Sallberg, M.; Garduno, F.; Goldstein, P.; McDowell, W.; Hughes, J.; Jones, J.; et al. Combinatorial Approach to Hepadnavirus-Like Particle Vaccine Design. *J. Virol.* **2005**, *79* (21), 13656–13666. <https://doi.org/10.1128/JVI.79.21.13656-13666.2005>.
- (139) Marini, A.; Zhou, Y.; Li, Y.; Taylor, I. J.; Leneghan, D. B.; Jin, J.; Zaric, M.; Mekhaieel, D.; Long, C. A.; Miura, K.; et al. A Universal Plug-and-Display Vaccine Carrier Based on HBsAg VLP to Maximize Effective Antibody Response. *Front. Immunol.* **2019**, *10* (December), 02931. <https://doi.org/10.3389/fimmu.2019.02931>.
- (140) Zha, L.; Zhao, H.; Mohsen, M. O.; Hong, L.; Zhou, Y.; Li, Z.; Yao, C.; Guo, L.; Chen, H.; Liu, X.; et al. Development of a COVID-19 Vaccine Based on the Receptor Binding Domain Displayed on Virus-like Particles. *bioRxiv* **2020**, 10.1101/2020.05.06.079830. <https://doi.org/10.1101/2020.05.06.079830>.
- (141) Qian, C.; Liu, X.; Xu, Q.; Wang, Z.; Chen, J.; Li, T.; Zheng, Q.; Yu, H.; Gu, Y.; Li, S.; et al. Recent Progress on the Versatility of Virus-like Particles. *Vaccines* **2020**, *8* (1), 1–15. <https://doi.org/10.3390/vaccines8010139>.
- (142) Shouval, D.; Ilan, Y.; Adler, R.; Deepen, R.; Panet, A.; Even-Chen, Z.; Gorecki, M.; Gerlich, W. H. Improved Immunogenicity in Mice of a Mammalian Cell-Derived Recombinant Hepatitis B Vaccine Containing Pre-S1 and Pre-S2 Antigens as Compared with Conventional Yeast-Derived Vaccines. *Vaccine* **1994**, *12* (15), 1453–1459. [https://doi.org/10.1016/0264-410X\(94\)90155-4](https://doi.org/10.1016/0264-410X(94)90155-4).
- (143) Ward, B. J.; Makarkov, A.; Séguin, A.; Pillet, S.; Trépanier, S.; Dhaliwall, J.; Libman, M. D.; Vesikari, T.; Landry, N. Efficacy, Immunogenicity, and Safety of a Plant-Derived, Quadrivalent, Virus-like Particle Influenza Vaccine in Adults (18–64 Years) and Older Adults

## 7 References

- (≥65 Years): Two Multicentre, Randomised Phase 3 Trials. *Lancet* **2020**, *396* (10261), 1491–1503. [https://doi.org/10.1016/S0140-6736\(20\)32014-6](https://doi.org/10.1016/S0140-6736(20)32014-6).
- (144) Ward, B. J.; Gobeil, P.; Séguin, A.; Atkins, J.; Boulay, I.; Charbonneau, P.-Y.; Couture, M.; D’Aoust, M.-A.; Dhaliwall, J.; Finkle, C.; et al. Phase 1 Trial of a Candidate Recombinant Virus-Like Particle Vaccine for Covid-19 Disease Produced in Plants. *medRxiv* **2020**. <https://doi.org/doi.org/10.1101/2020.11.04.20226282>.
- (145) European Medicines Agency. Cervarix : EPAR - Scientific Discussion [https://www.ema.europa.eu/en/documents/scientific-discussion/cervarix-epar-scientific-discussion\\_en.pdf](https://www.ema.europa.eu/en/documents/scientific-discussion/cervarix-epar-scientific-discussion_en.pdf) (accessed Dec 20, 2020).
- (146) European Medicines Agency. Gardasil 9 : EPAR - Product Information - EMA/CHMP/76591/2015 [https://www.ema.europa.eu/en/documents/assessment-report/gardasil-9-epar-public-assessment-report\\_en.pdf](https://www.ema.europa.eu/en/documents/assessment-report/gardasil-9-epar-public-assessment-report_en.pdf) (accessed Dec 20, 2020).
- (147) Gu, Y.; Wei, M.; Wang, D.; Li, Z.; Xie, M.; Pan, H.; Wu, T.; Zhang, J.; Li, S.; Xia, N. Characterization of an Escherichia Coli-Derived Human Papillomavirus Type 16 and 18 Bivalent Vaccine. *Vaccine* **2017**, *35* (35), 4637–4645. <https://doi.org/10.1016/j.vaccine.2017.06.084>.
- (148) Qiao, Y. L.; Wu, T.; Li, R. C.; Hu, Y. M.; Wei, L. H.; Li, C. G.; Chen, W.; Huang, S. J.; Zhao, F. H.; Li, M. Q.; et al. Efficacy, Safety, and Immunogenicity of an Escherichia Coli-Produced Bivalent Human Papillomavirus Vaccine: An Interim Analysis of a Randomized Clinical Trial. *J. Natl. Cancer Inst.* **2020**, *112* (2), 145–153. <https://doi.org/10.1093/jnci/djz074>.
- (149) U.S. Food and Drug Administration. Summary for basis of Approval - ENGERIX-B <https://wayback.archive-it.org/7993/20170404184231/https://www.fda.gov/downloads/BiologicsBloodVaccines/Vaccines/ApprovedProducts/UCM110155.pdf> (accessed Dec 20, 2020).
- (150) European Medicines Agency. Fendrix : EPAR - Scientific Discussion [https://www.ema.europa.eu/en/documents/scientific-discussion/fendrix-epar-scientific-discussion\\_en.pdf](https://www.ema.europa.eu/en/documents/scientific-discussion/fendrix-epar-scientific-discussion_en.pdf) (accessed Dec 20, 2020).
- (151) McAleer, W. J.; Buynak, E. B.; Maigetter, R. Z.; Wampler, D. E.; Miller, W. J.; Hilleman, M. R. Human Hepatitis B Vaccine from Recombinant Yeast. *Nature* **1984**, *307* (5947), 178–180. <https://doi.org/10.1038/307178a0>.
- (152) Hilleman, M. R. Yeast Recombinant Hepatitis B Vaccine. *Infection* **1987**, *15* (1), 3–7. <https://doi.org/10.1007/BF01646107>.

- (153) Li, S. W.; Zhang, J.; Li, Y. M.; Ou, S. H.; Huang, G. Y.; He, Z. Q.; Ge, S. X.; Xian, Y. L.; Pang, S. Q.; Ng, M. H.; et al. A Bacterially Expressed Particulate Hepatitis E Vaccine: Antigenicity, Immunogenicity and Protectivity on Primates. *Vaccine* **2005**, *23* (22), 2893–2901. <https://doi.org/10.1016/j.vaccine.2004.11.064>.
- (154) Wu, T.; Li, S. W.; Zhang, J.; Ng, M. H.; Xia, N. S.; Zhao, Q. Hepatitis E Vaccine Development: A 14-Year Odyssey. *Hum. Vaccines Immunother.* **2012**, *8* (6), 823–827. <https://doi.org/10.4161/hv.20042>.
- (155) Zhu, F. C.; Zhang, J.; Zhang, X. F.; Zhou, C.; Wang, Z. Z.; Huang, S. J.; Wang, H.; Yang, C. L.; Jiang, H. M.; Cai, J. P.; et al. Efficacy and Safety of a Recombinant Hepatitis e Vaccine in Healthy Adults: A Large-Scale, Randomised, Double-Blind Placebo-Controlled, Phase 3 Trial. *Lancet* **2010**, *376* (9744), 895–902. [https://doi.org/10.1016/S0140-6736\(10\)61030-6](https://doi.org/10.1016/S0140-6736(10)61030-6).
- (156) Wei, M.; Wang, D.; Li, Z.; Song, S.; Kong, X.; Mo, X.; Yang, Y.; He, M.; Li, Z.; Huang, B.; et al. N-Terminal Truncations on L1 Proteins of Human Papillomaviruses Promote Their Soluble Expression in Escherichia Coli and Self-Assembly in Vitro. *Emerg. Microbes Infect.* **2018**, *7* (1), 1–12. <https://doi.org/10.1038/s41426-018-0158-2>.
- (157) Keech, C.; Albert, G.; Cho, I.; Robertson, A.; Reed, P.; Neal, S.; Plested, J. S.; Zhu, M.; Cloney-Clark, S.; Zhou, H.; et al. Phase 1–2 Trial of a SARS-CoV-2 Recombinant Spike Protein Nanoparticle Vaccine. *N. Engl. J. Med.* **2020**, *383* (24), 2320–2332. <https://doi.org/10.1056/NEJMoa2026920>.
- (158) Smith, G.; Liu, Y.; Flyer, D.; Massare, M. J.; Zhou, B.; Patel, N.; Ellingsworth, L.; Lewis, M.; Cummings, J. F.; Glenn, G. Novel Hemagglutinin Nanoparticle Influenza Vaccine with Matrix-M™ Adjuvant Induces Hemagglutination Inhibition, Neutralizing, and Protective Responses in Ferrets against Homologous and Drifted A(H3N2) Subtypes. *Vaccine* **2017**, *35* (40), 5366–5372. <https://doi.org/10.1016/j.vaccine.2017.08.021>.
- (159) Portnoff, A. D.; Patel, N.; Massare, M. J.; Zhou, H.; Tian, J.-H.; Zhou, B.; Shinde, V.; Glenn, G. M.; Smith, G. Influenza Hemagglutinin Nanoparticle Vaccine Elicits Broadly Neutralizing Antibodies against Structurally Distinct Domains of H3N2 HA. *Vaccines* **2020**, *8* (1), 99. <https://doi.org/10.3390/vaccines8010099>.
- (160) Glenn, G. M.; Smith, G.; Fries, L.; Raghunandan, R.; Lu, H.; Zhou, B.; Thomas, D. N.; Hickman, S. P.; Kpamegan, E.; Boddapati, S.; et al. Safety and Immunogenicity of a Sf9 Insect Cell-Derived Respiratory Syncytial Virus Fusion Protein Nanoparticle Vaccine. *Vaccine* **2013**, *31* (3), 524–532. <https://doi.org/10.1016/j.vaccine.2012.11.009>.

## 7 References

- (161) Fries, L.; Shinde, V.; Stoddard, J. J.; Thomas, D. N.; Kpamegan, E.; Lu, H.; Smith, G.; Hickman, S. P.; Piedra, P.; Glenn, G. M. Immunogenicity and Safety of a Respiratory Syncytial Virus Fusion Protein (RSV F) Nanoparticle Vaccine in Older Adults. *Immun. Ageing* **2017**, *14* (1), 8. <https://doi.org/10.1186/s12979-017-0090-7>.
- (162) Steinmetz, N. F. Viral Nanoparticles as Platforms for Next-Generation Therapeutics and Imaging Devices. *Nanomedicine Nanotechnology, Biol. Med.* **2010**, *6* (5), 634–641. <https://doi.org/10.1016/j.nano.2010.04.005>.
- (163) Rohovie, M. J.; Nagasawa, M.; Swartz, J. R. Virus-like Particles: Next-Generation Nanoparticles for Targeted Therapeutic Delivery. *Bioeng. Transl. Med.* **2017**, *2* (1), 43–57. <https://doi.org/10.1002/btm2.10049>.
- (164) Bajaj, S.; Banerjee, M. Engineering Virus Capsids Into Biomedical Delivery Vehicles: Structural Engineering Problems in Nanoscale. *J. Biomed. Nanotechnol.* **2015**, *11* (1), 53–69. <https://doi.org/10.1166/jbn.2015.1959>.
- (165) Kimchi-Sarfaty, C.; Ben-Nun-Shaul, O.; Rund, D.; Oppenheim, A.; Gottesman, M. M. In Vitro -Packaged SV40 Pseudovirions as Highly Efficient Vectors for Gene Transfer. *Hum. Gene Ther.* **2002**, *13* (2), 299–310. <https://doi.org/10.1089/10430340252769815>.
- (166) Kimchi-Sarfaty, C.; Vieira, W. D.; Dodds, D.; Sherman, A.; Kreitman, R. J.; Shinar, S.; Gottesman, M. M. SV40 Pseudovirion Gene Delivery of a Toxin to Treat Human Adenocarcinomas in Mice. *Cancer Gene Ther.* **2006**, *13* (7), 648–657. <https://doi.org/10.1038/sj.cgt.7700943>.
- (167) Galaway, F. A.; Stockley, P. G. MS2 Viruslike Particles: A Robust, Semisynthetic Targeted Drug Delivery Platform. *Mol. Pharm.* **2013**, *10* (1), 59–68. <https://doi.org/10.1021/mp3003368>.
- (168) Yildiz, I.; Shukla, S.; Steinmetz, N. F. Applications of Viral Nanoparticles in Medicine. *Curr. Opin. Biotechnol.* **2011**, *22* (6), 901–908. <https://doi.org/10.1016/j.copbio.2011.04.020>.
- (169) Barwal, I.; Kumar, R.; Kateriya, S.; Dinda, A. K.; Yadav, S. C. Targeted Delivery System for Cancer Cells Consist of Multiple Ligands Conjugated Genetically Modified CCMV Capsid on Doxorubicin GNPs Complex. *Sci. Rep.* **2016**, *6* (1), 37096. <https://doi.org/10.1038/srep37096>.
- (170) Peyret, H.; Gehin, A.; Thuenemann, E. C.; Blond, D.; El Turabi, A.; Beales, L.; Clarke, D.; Gilbert, R. J. C.; Fry, E. E.; Stuart, D. I.; et al. Tandem Fusion of Hepatitis B Core Antigen Allows Assembly of Virus-like Particles in Bacteria and Plants with Enhanced Capacity to

- Accommodate Foreign Proteins. *PLoS One* **2015**, *10* (4), 1–20. <https://doi.org/10.1371/journal.pone.0120751>.
- (171) Ren, Y.; Wong, S. M.; Lim, L.-Y. Folic Acid-Conjugated Protein Cages of a Plant Virus: A Novel Delivery Platform for Doxorubicin. *Bioconjug. Chem.* **2007**, *18* (3), 836–843. <https://doi.org/10.1021/bc060361p>.
- (172) Chung, Y. H.; Cai, H.; Steinmetz, N. F. Viral Nanoparticles for Drug Delivery, Imaging, Immunotherapy, and Theranostic Applications. *Adv. Drug Deliv. Rev.* **2020**, No. January. <https://doi.org/10.1016/j.addr.2020.06.024>.
- (173) Wojta-Stremayr, D.; Pickl, W. F. Fluorosomes: Fluorescent Virus-like Nanoparticles That Represent a Convenient Tool to Visualize Receptor-Ligand Interactions. *Sensors (Switzerland)* **2013**, *13* (7), 8722–8749. <https://doi.org/10.3390/s130708722>.
- (174) Sakin, V.; Paci, G.; Lemke, E. A.; Müller, B. Labeling of Virus Components for Advanced, Quantitative Imaging Analyses. *FEBS Lett.* **2016**, *590* (13), 1896–1914. <https://doi.org/10.1002/1873-3468.12131>.
- (175) Li, F.; Zhang, Z.-P.; Peng, J.; Cui, Z.-Q.; Pang, D.-W.; Li, K.; Wei, H.-P.; Zhou, Y.-F.; Wen, J.-K.; Zhang, X.-E. Imaging Viral Behavior in Mammalian Cells with Self-Assembled Capsid-Quantum-Dot Hybrid Particles. *Small* **2009**, *5* (6), 718–726. <https://doi.org/10.1002/sml.200801303>.
- (176) Chen, C.; Daniel, M.-C.; Quinkert, Z. T.; De, M.; Stein, B.; Bowman, V. D.; Chipman, P. R.; Rotello, V. M.; Kao, C. C.; Dragnea, B. Nanoparticle-Templated Assembly of Viral Protein Cages. *Nano Lett.* **2006**, *6* (4), 611–615. <https://doi.org/10.1021/nl0600878>.
- (177) Goicochea, N. L.; De, M.; Rotello, V. M.; Mukhopadhyay, S.; Dragnea, B. Core-like Particles of an Enveloped Animal Virus Can Self-Assemble Efficiently on Artificial Templates. *Nano Lett.* **2007**, *7* (8), 2281–2290. <https://doi.org/10.1021/nl070860e>.
- (178) Enomoto, T.; Kawano, M.; Fukuda, H.; Sawada, W.; Inoue, T.; Haw, K. C.; Kita, Y.; Sakamoto, S.; Yamaguchi, Y.; Imai, T.; et al. Viral Protein-Coating of Magnetic Nanoparticles Using Simian Virus 40 VP1. *J. Biotechnol.* **2013**, *167* (1), 8–15. <https://doi.org/10.1016/j.jbiotec.2013.06.005>.
- (179) Colella, P.; Ronzitti, G.; Mingozzi, F. Emerging Issues in AAV-Mediated In Vivo Gene Therapy. **2018**, *8* (March), 87–104. <https://doi.org/10.1016/j.omtm.2017.11.007>.
- (180) Burgess, R. R. Chapter 17 Refolding Solubilized Inclusion Body Proteins. In *Methods in Enzymology*; Elsevier Inc., 2009; Vol. 463, pp 259–282. <https://doi.org/10.1016/S0076->

- 6879(09)63017-2.
- (181) Wobus, C. E.; Hügler-Dörr, B.; Girod, A.; Petersen, G.; Hallek, M.; Kleinschmidt, J. a. Monoclonal Antibodies against the Adeno-Associated Virus Type 2 (AAV-2) Capsid: Epitope Mapping and Identification of Capsid Domains Involved in AAV-2-Cell Interaction and Neutralization of AAV-2 Infection. *J. Virol.* **2000**, *74* (19), 9281–9293.
- (182) Salganik, M.; Venkatakrisnan, B.; Bennett, A.; Lins, B.; Yarbrough, J.; Muzyczka, N.; Agbandje-McKenna, M.; McKenna, R. Evidence for PH-Dependent Protease Activity in the Adeno-Associated Virus Capsid. *J. Virol.* **2012**, *86* (21), 11877–11885. <https://doi.org/10.1128/JVI.01717-12>.
- (183) Lavelle, L.; Gingery, M.; Phillips, M.; Gelbart, W. M.; Knobler, C. M.; Cadena-Nava, R. D.; Vega-Acosta, J. R.; Pinedo-Torres, L. A.; Ruiz-Garcia, J. Phase Diagram of Self-Assembled Viral Capsid Protein Polymorphs. *J. Phys. Chem. B* **2009**, *113* (12), 3813–3819.
- (184) Joo, K.; Fang, Y.; Liu, Y.; Xiao, L.; Gu, Z.; Tai, A.; Lee, C.; Tang, Y.; Wang, P. Enhanced Real-Time Monitoring of Adeno-Associated Virus Trafficking by Virus-Quantum Dot Conjugates. *ACS Nano* **2011**, *5* (5), 3523–3535. <https://doi.org/10.1021/nn102651p>.
- (185) Wang, Q.; Firman, J.; Wu, Z.; Pokiniewski, K. A.; Valencia, C. A.; Wang, H.; Wei, H.; Zhuang, Z.; Liu, L.; Wunder, S. L.; et al. High-Density Recombinant Adeno-Associated Viral Particles Are Competent Vectors for *In Vivo* Transduction. *Hum. Gene Ther.* **2016**, *27* (12), 971–981. <https://doi.org/10.1089/hum.2016.055>.
- (186) Teschner, J. Improvement of RAAV Production by Analysis of Capsid Modification, Producer Cell Line Generation and a Novel Affinity Chromatography, Bielefeld University, 2020. <https://doi.org/doi.org/10.4119/unibi/2942828>.
- (187) Chen, H. Comparative Observation of the Recombinant Adeno-Associated Virus 2 Using Transmission Electron Microscopy and Atomic Force Microscopy. *Microsc. Microanal.* **2007**, *13* (5), 384–389. <https://doi.org/10.1017/S1431927607070808>.
- (188) Summerford, C.; Samulski, R. J. Membrane-Associated Heparan Sulfate Proteoglycan Is a Receptor for Adeno-Associated Virus Type 2 Virions. *J. Virol.* **1998**, *72* (2), 1438–1445.
- (189) Nicklin, S. a; Buening, H.; Dishart, K. L.; de Alwis, M.; Girod, A.; Hacker, U.; Thrasher, a J.; Ali, R. R.; Hallek, M.; Baker, a H. Efficient and Selective AAV2-Mediated Gene Transfer Directed to Human Vascular Endothelial Cells. *Mol. Ther.* **2001**, *4* (3), 174–181. <https://doi.org/10.1006/mthe.2001.0424>.
- (190) Zhou, S.; Hansen, J.; Srivastava, A.; Mah, C.; Dwarki, V.; Qing, K. Human Fibroblast Growth

- Factor Receptor 1 Is a Co-Receptor for Infection by Adeno-Associated Virus 2. *Nat. Med.* **2002**, 5 (1), 71–77. <https://doi.org/10.1038/4758>.
- (191) Iwabuchi, K.; Daida, H.; Matsumoto, K.; Oshimi, K.; Watanabe, M.; Kashiwakura, Y.; Tamayose, K.; Shimada, T.; Nakamura, T.; Hirai, Y. Hepatocyte Growth Factor Receptor Is a Coreceptor for Adeno-Associated Virus Type 2 Infection. *J. Virol.* **2004**, 79 (1), 609–614. <https://doi.org/10.1128/jvi.79.1.609-614.2005>.
- (192) Pillay, S.; Meyer, N. L.; Puschnik, A. S.; Davulcu, O.; Diep, J.; Ishikawa, Y.; Jae, L. T.; Wosen, J. E.; Nagamine, C. M.; Chapman, M. S.; et al. An Essential Receptor for Adeno-Associated Virus Infection. *Nature* **2016**, 530 (7588), 108–112. <https://doi.org/10.1038/nature16465>.
- (193) Bartlett, J. S.; Wilcher, R.; Samulski, R. J. Infectious Entry Pathway of Adeno-Associated Virus and Adeno-Associated Virus Vectors. *J. Virol.* **2000**, 74 (6), 2777–2785. <https://doi.org/10.1128/JVI.74.6.2777-2785.2000>.
- (194) Grieger, J. C.; Snowdy, S.; Samulski, R. J. Separate Basic Region Motifs within the Adeno-Associated Virus Capsid Proteins Are Essential for Infectivity and Assembly. *J. Virol.* **2006**, 80 (11), 5199–5210. <https://doi.org/10.1128/JVI.02723-05>.
- (195) Popa-Wagner, R.; Reuss, M.; Weimer, M.; Kann, M.; Kleinschmidt, J. A.; Florin, L.; Porwal, M. Impact of VP1-Specific Protein Sequence Motifs on Adeno-Associated Virus Type 2 Intracellular Trafficking and Nuclear Entry. *J. Virol.* **2012**, 86 (17), 9163–9174. <https://doi.org/10.1128/jvi.00282-12>.
- (196) Tse, L. V.; Moller-Tank, S.; Meganck, R. M.; Asokan, A. Mapping and Engineering Functional Domains of the Assembly-Activating Protein of Adeno-Associated Viruses. *J. Virol.* **2018**, 92 (14), e00393-18. <https://doi.org/10.1128/JVI.00393-18>.
- (197) Maurer, A. C.; Cepeda Diaz, A. K.; Vandenberghe, L. H. Residues on Adeno-Associated Virus Capsid Lumen Dictate Interactions and Compatibility with the Assembly-Activating Protein. *J. Virol.* **2019**, 93 (7). <https://doi.org/10.1128/JVI.02013-18>.
- (198) Shi, W.; Arnold, G. S.; Bartlett, J. S. Insertional Mutagenesis of the Adeno-Associated Virus Type 2 (AAV2) Capsid Gene and Generation of AAV2 Vectors Targeted to Alternative Cell-Surface Receptors. *Hum. Gene Ther.* **2001**, 12 (14), 1697–1711. <https://doi.org/10.1089/104303401750476212>.
- (199) Nieto, K.; Salvetti, A. AAV Vectors Vaccines against Infectious Diseases. *Front. Immunol.* **2014**, 5 (5), 1–9. <https://doi.org/10.3389/fimmu.2014.00005>.
- (200) Nieto, K.; Weghofer, M.; Sehr, P.; Ritter, M.; Sedlmeier, S.; Karanam, B.; Seitz, H.; Müller,

## 7 References

- M.; Kellner, M.; Hörer, M.; et al. Development of AAVLP(HPV16/31L2) Particles as Broadly Protective HPV Vaccine Candidate. *PLoS One* **2012**, *7* (6), e39741. <https://doi.org/10.1371/journal.pone.0039741>.
- (201) Zhang, H.; Xie, J.; Dmitriev, I.; Kashentseva, E.; Curiel, D. T.; Hsu, H.; Mountz, J. D. Addition of Six-His-Tagged Peptide to the C Terminus of Adeno-Associated Virus VP3 Does Not Affect Viral Tropism or Production. *J. Virol.* **2002**, *76* (23), 12023–12031. <https://doi.org/10.1128/JVI.76.23.12023>.
- (202) Wu, P.; Xiao, W.; Conlon, T.; Hughes, J.; Agbandje-McKenna, M.; Ferkol, T.; Flotte, T.; Muzyczka, N. Mutational Analysis of the Adeno-Associated Virus Type 2 (AAV2) Capsid Gene and Construction of AAV2 Vectors with Altered Tropism. *J. Virol.* **2000**, *74* (18), 8635–8647. <https://doi.org/10.1128/JVI.74.18.8635-8647.2000>.
- (203) Rybicki, E. P. Plant-Based Vaccines against Viruses. *Viol. J.* **2014**, *11* (1), 1–20. <https://doi.org/10.1186/s12985-014-0205-0>.
- (204) Le, D. T.; Radukic, M. T.; Müller, K. M. AAV Capsid Assembly Using Escherichia Coli. *Mol. Ther.* **2020**, *28* (4), 79–79.
- (205) Schellman, J. A. Temperature, Stability, and the Hydrophobic Interaction. *Biophys. J.* **1997**, *73* (6), 2960–2964. [https://doi.org/10.1016/S0006-3495\(97\)78324-3](https://doi.org/10.1016/S0006-3495(97)78324-3).
- (206) Baldwin, R. L. Temperature Dependence of the Hydrophobic Interaction in Protein Folding. *Proc. Natl. Acad. Sci.* **1986**, *83* (21), 8069–8072. <https://doi.org/10.1073/pnas.83.21.8069>.
- (207) Kuck, D.; Kern, A.; Kleinschmidt, J. A. Development of AAV Serotype-Specific ELISAs Using Novel Monoclonal Antibodies. *J. Virol. Methods* **2007**, *140* (1–2), 17–24. <https://doi.org/10.1016/j.jviromet.2006.10.005>.
- (208) Nass, S. A.; Mattingly, M. A.; Woodcock, D. A.; Burnham, B. L.; Ardinger, J. A.; Osmond, S. E.; Frederick, A. M.; Scaria, A.; Cheng, S. H.; O’Riordan, C. R. Universal Method for the Purification of Recombinant AAV Vectors of Differing Serotypes. *Mol. Ther. - Methods Clin. Dev.* **2018**, *9* (June), 33–46. <https://doi.org/10.1016/j.omtm.2017.12.004>.
- (209) Bernaud, J.; Rossi, A.; Fis, A.; Gardette, L.; Aillot, L.; Büning, H.; Castelnovo, M.; Salvetti, A.; Faivre-Moskalenko, C. Characterization of AAV Vector Particle Stability at the Single-Capsid Level. *J. Biol. Phys.* **2018**, *44* (2), 181–194. <https://doi.org/10.1007/s10867-018-9488-5>.
- (210) Khabou, H.; Desrosiers, M.; Winckler, C.; Fouquet, S.; Auregan, G.; Bemelmans, A. P.; Sahel, J. A.; Dalkara, D. Insight into the Mechanisms of Enhanced Retinal Transduction by the Engineered AAV2 Capsid Variant -7m8. *Biotechnol. Bioeng.* **2016**, *113* (12), 2712–2724.

- <https://doi.org/10.1002/bit.26031>.
- (211) Arnold, G. S.; Sasser, A. K.; Stachler, M. D.; Bartlett, J. S. Metabolic Biotinylation Provides a Unique Platform for the Purification and Targeting of Multiple AAV Vector Serotypes. *Mol. Ther.* **2006**, *14* (1), 97–106. <https://doi.org/10.1016/j.ymthe.2006.02.014>.
- (212) Keiser, N. W.; Yan, Z.; Zhang, Y.; Lei-Butters, D. C. M.; Engelhardt, J. F. Unique Characteristics of AAV1, 2, and 5 Viral Entry, Intracellular Trafficking, and Nuclear Import Define Transduction Efficiency in HeLa Cells. *Hum. Gene Ther.* **2011**, *22* (11), 1433–1444. <https://doi.org/10.1089/hum.2011.044>.
- (213) Bantel-Schaal, U.; Hub, B.; Kartenbeck, J. Endocytosis of Adeno-Associated Virus Type 5 Leads to Accumulation of Virus Particles in the Golgi Compartment. *J. Virol.* **2002**, *76* (5), 2340–2349. <https://doi.org/10.1128/jvi.76.5.2340-2349.2002>.
- (214) Kaludov, N.; Brown, K. E.; Walters, R. W.; Zabner, J.; Chiorini, J. A. Adeno-Associated Virus Serotype 4 (AAV4) and AAV5 Both Require Sialic Acid Binding for Hemagglutination and Efficient Transduction but Differ in Sialic Acid Linkage Specificity. *J. Virol.* **2001**, *75* (15), 6884–6893. <https://doi.org/10.1128/jvi.75.15.6884-6893.2001>.
- (215) Di Pasquale, G.; Davidson, B. L.; Stein, C. S.; Martins, I.; Scudiero, D.; Monks, A.; Chiorini, J. A. Identification of PDGFR as a Receptor for AAV-5 Transduction. *Nat. Med.* **2003**, *9* (10), 1306–1312. <https://doi.org/10.1038/nm929>.
- (216) Zhang, R.; Xu, G.; Cao, L.; Sun, Z.; He, Y.; Cui, M.; Sun, Y.; Li, S.; Li, H.; Qin, L.; et al. Divergent Engagements between Adeno-Associated Viruses with Their Cellular Receptor AAVR. *Nat. Commun.* **2019**, *10* (1), 3760. <https://doi.org/10.1038/s41467-019-11668-x>.
- (217) Grosse, S.; Penaud-Budloo, M.; Herrmann, A.-K.; Börner, K.; Fakhiri, J.; Laketa, V.; Krämer, C.; Wiedtke, E.; Gunkel, M.; Ménard, L.; et al. Relevance of Assembly-Activating Protein for Adeno-Associated Virus Vector Production and Capsid Protein Stability in Mammalian and Insect Cells. *J. Virol.* **2017**, *91* (20), e01198-17. <https://doi.org/10.1128/JVI.01198-17>.
- (218) Le, D. T.; Behrsing, O.; Rothschild, C.; Radukic, M. T.; Arndt, K. M.; Mueller, K. M. AAV Capsid Proteins Fused with SARS-CoV-2 RBD or RBM: Expression in E. Coli, In-Vitro Assembly, and Characterization. *Mol. Ther.* **2021**, *4*, Suppl.1 (29), 357.
- (219) Wang, Q.; Zhang, Y.; Wu, L.; Niu, S.; Song, C.; Zhang, Z.; Lu, G.; Qiao, C.; Hu, Y.; Yuen, K.-Y.; et al. Structural and Functional Basis of SARS-CoV-2 Entry by Using Human ACE2. *Cell* **2020**, *181* (4), 894-904.e9. <https://doi.org/10.1016/j.cell.2020.03.045>.
- (220) Wang, Y.; Wang, L.; Cao, H.; Liu, C. SARS-CoV-2 S1 Is Superior to the RBD as a COVID-19

## 7 References

- Subunit Vaccine Antigen. *J. Med. Virol.* **2020**, jmv.26320. <https://doi.org/10.1002/jmv.26320>.
- (221) Lan, J.; Ge, J.; Yu, J.; Shan, S.; Zhou, H.; Fan, S.; Zhang, Q.; Shi, X.; Wang, Q.; Zhang, L.; et al. Structure of the SARS-CoV-2 Spike Receptor-Binding Domain Bound to the ACE2 Receptor. *Nature* **2020**, *581* (7807), 215–220. <https://doi.org/10.1038/s41586-020-2180-5>.
- (222) Feiner, R. C.; Teschner, J.; Teschner, K. E.; Radukic, M. T.; Baumann, T.; Hagen, S.; Hannappel, Y.; Biere, N.; Anselmetti, D.; Arndt, K. M.; et al. RAAV Engineering for Capsid-Protein Enzyme Insertions and Mosaicism Reveals Resilience to Mutational, Structural and Thermal Perturbations. *Int. J. Mol. Sci.* **2019**, *20* (22), 5702. <https://doi.org/10.3390/ijms20225702>.
- (223) Pédelacq, J.-D.; Cabantous, S.; Tran, T.; Terwilliger, T. C.; Waldo, G. S. Engineering and Characterization of a Superfolder Green Fluorescent Protein. *Nat. Biotechnol.* **2006**, *24* (1), 79–88. <https://doi.org/10.1038/nbt1172>.
- (224) Moore, M. J.; Dorfman, T.; Li, W.; Wong, S. K.; Li, Y.; Kuhn, J. H.; Coderre, J.; Vasilieva, N.; Han, Z.; Greenough, T. C.; et al. Retroviruses Pseudotyped with the Severe Acute Respiratory Syndrome Coronavirus Spike Protein Efficiently Infect Cells Expressing Angiotensin-Converting Enzyme 2. *J. Virol.* **2004**, *78* (19), 10628–10635. <https://doi.org/10.1128/JVI.78.19.10628-10635.2004>.
- (225) Zepeda-Cervantes, J.; Ramírez-Jarquín, J. O.; Vaca, L. Interaction Between Virus-Like Particles (VLPs) and Pattern Recognition Receptors (PRRs) From Dendritic Cells (DCs): Toward Better Engineering of VLPs. *Front. Immunol.* **2020**, *11* (June), 1–22. <https://doi.org/10.3389/fimmu.2020.01100>.
- (226) Boisgérault, F.; Morón, G.; Leclerc, C. Virus-like Particles: A New Family of Delivery Systems. *Expert Rev. Vaccines* **2002**, *1* (1), 101–109. <https://doi.org/10.1586/14760584.1.1.101>.
- (227) Apostólico, J. D. S.; Lunardelli, V. A. S.; Coirada, F. C.; Boscardin, S. B.; Rosa, D. S. Adjuvants: Classification, Modus Operandi , and Licensing. *J. Immunol. Res.* **2016**, *2016* (Article ID 1459394), 1–16. <https://doi.org/10.1155/2016/1459394>.
- (228) Ju, B.; Zhang, Q.; Ge, J.; Wang, R.; Sun, J.; Ge, X.; Yu, J.; Shan, S.; Zhou, B.; Song, S.; et al. Human Neutralizing Antibodies Elicited by SARS-CoV-2 Infection. *Nature* **2020**, *584* (7819), 115–119. <https://doi.org/10.1038/s41586-020-2380-z>.
- (229) Shi, R.; Shan, C.; Duan, X.; Chen, Z.; Liu, P.; Song, J.; Song, T.; Bi, X.; Han, C.; Wu, L.; et al. A Human Neutralizing Antibody Targets the Receptor-Binding Site of SARS-CoV-2. *Nature*

- 2020**, 584 (7819), 120–124. <https://doi.org/10.1038/s41586-020-2381-y>.
- (230) Tan, C. W.; Chia, W. N.; Qin, X.; Liu, P.; Chen, M. I.-C.; Tiu, C.; Hu, Z.; Chen, V. C.-W.; Young, B. E.; Sia, W. R.; et al. A SARS-CoV-2 Surrogate Virus Neutralization Test Based on Antibody-Mediated Blockage of ACE2–Spike Protein–Protein Interaction. *Nat. Biotechnol.* **2020**, 38 (9), 1073–1078. <https://doi.org/10.1038/s41587-020-0631-z>.
- (231) Watanabe, Y.; Allen, J. D.; Wrapp, D.; McLellan, J. S.; Crispin, M. Site-Specific Glycan Analysis of the SARS-CoV-2 Spike. *Science (80-. )*. **2020**, 369 (6501), eabb9983. <https://doi.org/10.1126/science.abb9983>.
- (232) Li, Q.; Wu, J.; Nie, J.; Zhang, L.; Hao, H.; Liu, S.; Zhao, C.; Zhang, Q.; Liu, H.; Nie, L.; et al. The Impact of Mutations in SARS-CoV-2 Spike on Viral Infectivity and Antigenicity. *Cell* **2020**, 182 (5), 1284-1294.e9. <https://doi.org/10.1016/j.cell.2020.07.012>.
- (233) Dai, L.; Gao, G. F. Viral Targets for Vaccines against COVID-19. *Nat. Rev. Immunol.* **2020**. <https://doi.org/10.1038/s41577-020-00480-0>.
- (234) Roldão, A.; Mellado, M. C. M.; Castilho, L. R.; Carrondo, M. J. T.; Alves, P. M. Virus-like Particles in Vaccine Development. *Expert Rev. Vaccines* **2010**, 9 (10), 1149–1176. <https://doi.org/10.1586/erv.10.115>.
- (235) Gavor, E.; Choong, Y. K.; Er, S. Y.; Sivaraman, H.; Sivaraman, J. Structural Basis of SARS-CoV-2 and SARS-CoV Antibody Interactions. *Trends Immunol.* **2020**, 41 (11), 1006–1022. <https://doi.org/10.1016/j.it.2020.09.004>.
- (236) Louis Jeune, V.; Joergensen, J. A.; Hajjar, R. J.; Weber, T. Pre-Existing Anti-Adeno-Associated Virus Antibodies as a Challenge in AAV Gene Therapy. *Hum. Gene Ther. Methods* **2013**, 24 (2), 59–67. <https://doi.org/10.1089/hgtb.2012.243>.
- (237) Requião, R. D.; Carneiro, R. L.; Moreira, M. H.; Ribeiro-Alves, M.; Rossetto, S.; Palhano, F. L.; Domitrovic, T. Viruses with Different Genome Types Adopt a Similar Strategy to Pack Nucleic Acids Based on Positively Charged Protein Domains. *Sci. Rep.* **2020**, 10 (1), 5470. <https://doi.org/10.1038/s41598-020-62328-w>.
- (238) Hajitou, A.; Trepel, M.; Lilley, C. E.; Soghomonyan, S.; Alauddin, M. M.; Marini, F. C.; Restel, B. H.; Ozawa, M. G.; Moya, C. A.; Rangel, R.; et al. A Hybrid Vector for Ligand-Directed Tumor Targeting and Molecular Imaging. *Cell* **2006**, 125 (2), 385–398. <https://doi.org/10.1016/j.cell.2006.02.042>.
- (239) Ellis, B. L.; Hirsch, M. L.; Barker, J. C.; Connelly, J. P.; Steininger, R. J.; Porteus, M. H.; Porteus, M. H. A Survey of Ex Vivo/in Vitro Transduction Efficiency of Mammalian Primary

## 7 References

- Cells and Cell Lines with Nine Natural Adeno-Associated Virus (AAV1-9) and One Engineered Adeno-Associated Virus Serotype. *Virology*. **2013**, *10* (1), 74. <https://doi.org/10.1186/1743-422X-10-74>.
- (240) Mével, M.; Bouzelha, M.; Leray, A.; Pacouret, S.; Guilbaud, M.; Penaud-Budloo, M.; Alvarez-Dorta, D.; Dubreil, L.; Gouin, S. G.; Combal, J. P.; et al. Chemical Modification of the Adeno-Associated Virus Capsid to Improve Gene Delivery. *Chem. Sci.* **2020**, *11* (4), 1122–1131. <https://doi.org/10.1039/C9SC04189C>.
- (241) Chang, A. Y.; Chau, V. W.; Landas, J. A.; Yvonne. Preparation of Calcium Competent Escherichia Coli and Heat-Shock Transformation. *JEMl methods* **2017**, *1* (June), 22–25.
- (242) Dower, W. J.; Miller, J. F.; Ragsdale, C. W. High Efficiency Transformation of E.Coli by High Voltage Electroporation. *Nucleic Acids Res.* **1988**, *16* (13), 6127–6145. <https://doi.org/10.1093/nar/16.13.6127>.
- (243) Hoefer. User manual SE 260 <http://photos.labwrench.com/equipmentManuals/8176-3198.pdf>.
- (244) Chevallet, M.; Luche, S.; Rabilloud, T. Silver Staining of Proteins in Polyacrylamide Gels. *Nat. Protoc.* **2006**, *1* (4), 1852–1858. <https://doi.org/10.1038/nprot.2006.288>.
- (245) Kingston, R. E.; Chen, C. A.; Rose, J. K. Calcium Phosphate Transfection. *Curr. Protoc. Mol. Biol.* **2003**, *63* (1), 9.1.1-9.1.11. <https://doi.org/10.1002/0471142727.mb0901s63>.
- (246) Agilent Technologies. AAV Helper-Free System Instruction Manual <https://www.agilent.com/cs/library/usermanuals/Public/240071.pdf> (accessed Aug 13, 2019).
- (247) Teschner, K. E. Optimization of RAAV Mediated Targeted Suicide Gene Therapy, RAAV Manufacturing and Downstream Processing, Bielefeld University, 2020. <https://doi.org/doi.org/10.4119/unibi/2942830>.

## 8. Appendix

### 8.1. Supplementary information to section 4.1.

In section 4.1, we presented the results of AAV2 capsid protein expression using a pET expression system in *E. coli* BL21(DE3). In parallel, we also tested other expression systems using *E. coli*. A weaker lac promoter (pJKME plasmid,<sup>1</sup> derived from pAK400 plasmid,<sup>2</sup> **Figure S1a**) and *E. coli* RV308 as host were chosen. Two different temperatures (18°C and 37°C) were used for protein expression in *E. coli* and a western blot analysis was then performed with the B1 antibody for VP protein detection. As a result, we expressed AAV2 VP3 protein in inclusion bodies at both expression temperatures as described in **Figure S1b**.

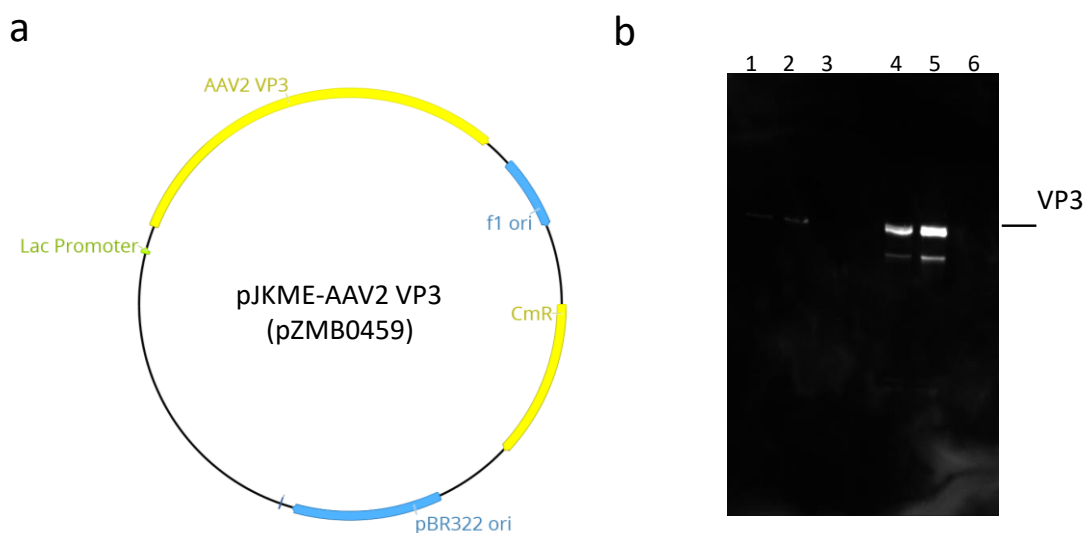


**Figure S1.** Expression of AAV2 VP3 in *E. coli* RV308 using plasmid pJKME. (a) Plasmid map of pJKME-AAV2 VP3. (b) Western blot analysis of VP3 expression at 18°C and 37°C; lane 1, whole-cell protein of *E. coli* RV308 post-induction with IPTG at 18°C; lane 2, insoluble fraction of intracellular protein post-induction with IPTG at 18°C; lane 3, soluble fraction of intracellular protein post-induction with IPTG at 18°C; lane 4, whole-cell protein of *E. coli* RV308 post-induction with IPTG at 37°C; lane 5, insoluble fraction of intracellular protein post-induction with IPTG at 37°C, soluble fraction of intracellular protein post-induction with IPTG at 37°C.

At the same time, the *E. coli* “leaky mutant” JW1667-5 strain ( $\Delta lpp-752:kan$ ), which lacks the *lpp* gene to enhance the permeability of the outer membrane,<sup>3</sup> was also tested for secretion of AAV2 VP3 protein into a culture medium. AAV2 VP3 gene was cloned into the pJKME plasmid with the *pelB* leader sequence at 5’ (**Figure S2a**). Protein expression was carried out at 25°C and a western blot with the B1 antibody was used to analyze the expression. **Figure S2b** shows that no VP3 protein was detected in the *E. coli* culture medium, however, the protein was found as inclusion bodies in *E. coli*. Therefore, to express secreted AAV2 VP3 protein in the *E. coli* culture, further constructs and expression conditions need to be tested in the future.

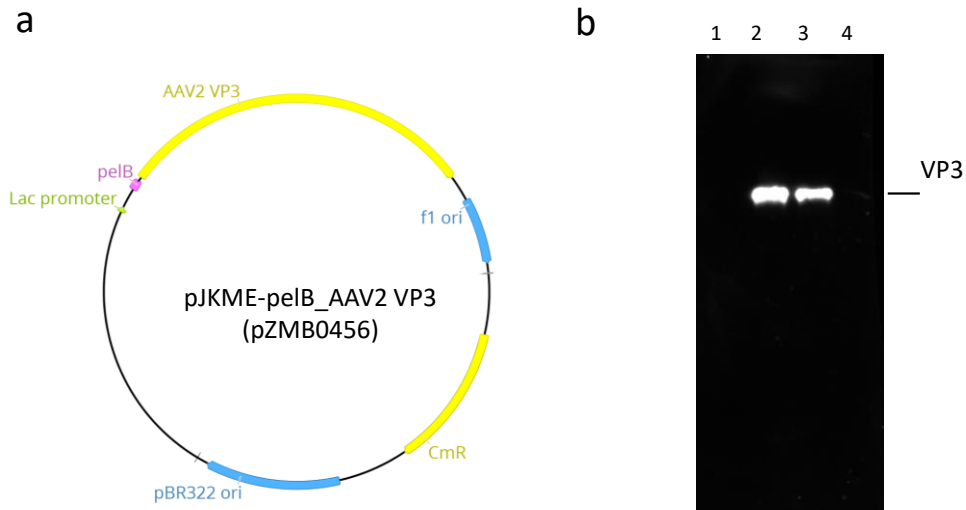


Figure S2. Expression of AAV2 VP3 in *E. coli* JW1667-5 using plasmid pJKME. (a) Plasmid map of pJKME-pebB\_AAV2 VP3. (b) Western blot analysis of VP3wt expression at 25°C; lane 1, protein in LB medium precipitated by  $(\text{NH}_4)_2\text{SO}_4$ ; lane 2, whole-cell protein of *E. coli* post-induction with IPTG; lane 3, insoluble fraction of intracellular protein post-induction; lane 4, soluble fraction of intracellular protein post-induction.

The inclusion body yield produced in these systems is much lower than that of the pET expression system presented in section 4.1, therefore, we chose the pET system for inclusion body production for further experiments.

## 8.2. Supplementary information to section 4.2

In section 4.2, we presented the result of expression and concomitant assembly of AAV5 VLPs inside *E. coli*. Here, we describe *in vitro* assembly methods for AAV5 VLP production by VP3 protein expression, purification and *in vitro* capsid assembly.

AAV5 VP3 can be expressed and formed AAV5 VLPs in *E. coli* at 18°C expression temperature (Figure 10). However, most soluble AAV5 VP3 protein still remains in unassembled form in *E. coli*. We cloned a His<sub>6</sub> tag at 5' of AAV5 VP3 gene in a pET vector and expressed protein in *E. coli*. After expression, we used IMAC to purify the His<sub>6</sub>-VP3 protein. Figure S3a indicates that we successfully purified soluble VP3 protein. After that, VP3 protein in an IMAC elution buffer (Table 5) was concentrated with an Amicon® Ultra-4 centrifugal filter with 10 kDa MWCO and exchanged into a high salt buffer of 1 M NaCl, and then dialyzed into an assembly buffer of 20 mM Tris-HCl, 125 mM NaCl, pH 8.0. Reduced and oxidized L-Glutathione (3 mM GSH/0.3 mM GSSG) were also added to the assembly buffer that might help to form correct disulfide bridges. After dialysis, the samples were collected and assessed by an indirect ELISA with ADK5a antibody that specifically binds to assembled AAV5. Figure S3b indicates a small number of AAV5 VLPs after assembly as shown by a low ELISA signal. Therefore, the *in vitro* assembly of the soluble AAV5 VP3 needs to be further optimized in the future.

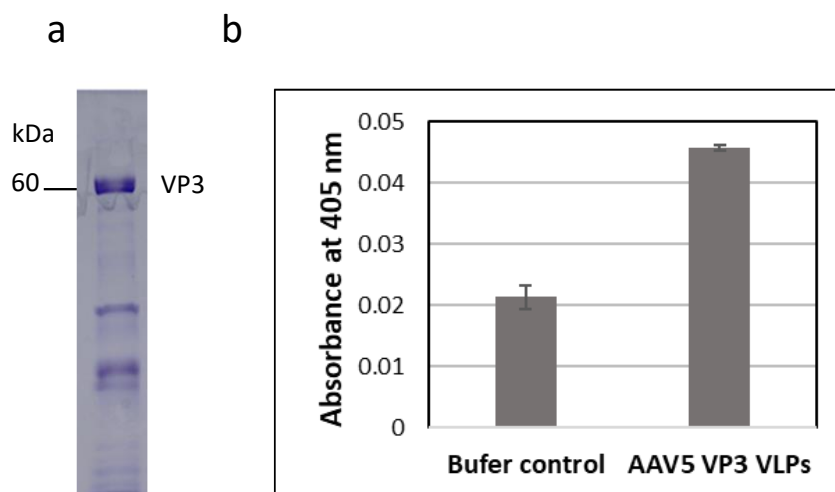


Figure S3. Purification of soluble AAV5 VP3 protein, *in vitro* assembly and detection of AAV5 VLPs using ELISA. (a) SDS-PAGE of purified VP3. (b) ELISA probed with anti-AAV5 (intact capsid) antibody (ADK5a).

At the same time, since AAV5 VP3 protein also formed inclusion bodies when expressed at 37°C in *E. coli* (Figure 10), we purified the protein in the form of inclusion bodies and performed *in vitro* assembly of VLPs. The AAV5 VP3 inclusion bodies were dissolved in the IEX buffer A with 8 M urea (Table 5) and purified via anion-exchange chromatography (Q Sepharose resin). Figure S4a indicates that VP3 protein was successfully purified. For *in vitro* assembly, as described for AAV2 VP3 assembly, AAV5 VP3 protein in the 8 M urea buffer was exchanged to a buffer of 5 M GuHCl, then dialyzed into an assembly buffer of PBS containing 0.2 M L-arginine. After dialysis, ELISA with the AAV5 VP3 assembled capsid antibody (ADK5a) was used to detect the VLPs. As a result, VP3 VLP formation was confirmed (Figure S4b). This finding offers an *in vitro* method to produce AAV5 VP3 VLPs besides the reported *in vivo* VLP production method described in section 4.2.

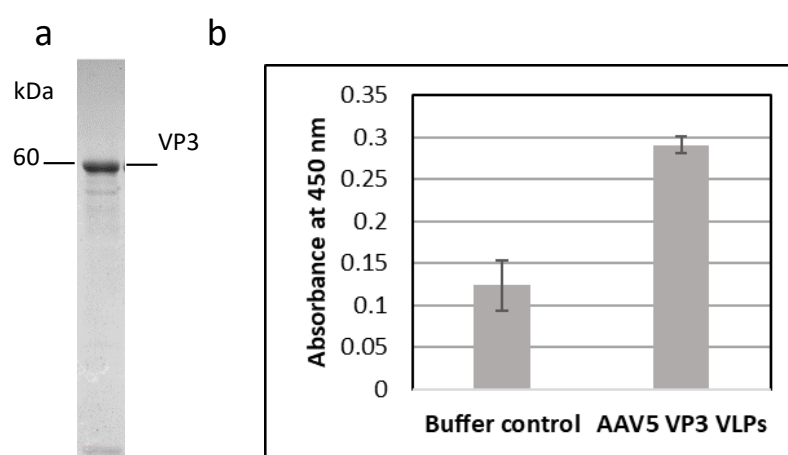


Figure S4. Purification of AAV5 VP3 inclusion body, *in vitro* assembly and detection of AAV5 VLPs using ELISA. (a) SDS-PAGE of purified VP3. (b) ELISA probed with anti-AAV5 (intact capsid) antibody (ADK5a).

## References

- (1) Speck, J.; Hecky, J.; Tam, H. K.; Arndt, K. M.; Einsle, O.; Müller, K. M. Exploring the Molecular Linkage of Protein Stability Traits for Enzyme Optimization by Iterative Truncation and Evolution. *Biochemistry* **2012**, 51 (24), 4850–4867. <https://doi.org/10.1021/bi2018738>.
- (2) Krebber, A.; Bornhauser, S.; Burmester, J.; Honegger, A.; Willuda, J.; Bosshard, H. R.; Plückthun, A. Reliable Cloning of Functional Antibody Variable Domains from Hybridomas and Spleen Cell Repertoires Employing a Reengineered Phage Display System. *J. Immunol. Methods* **1997**, 201 (1), 35–55. [https://doi.org/10.1016/S0022-1759\(96\)00208-6](https://doi.org/10.1016/S0022-1759(96)00208-6).
- (3) Müller, J. M.; Wetzel, D.; Flaschel, E.; Friehs, K.; Risse, J. M. Constitutive Production and Efficient Secretion of Soluble Full-Length Streptavidin by an Escherichia Coli “Leaky Mutant.” *J. Biotechnol.* **2016**. <https://doi.org/10.1016/j.jbiotec.2016.01.032>.

## 8.3. Appendix: Publications

Title:

**Adeno-associated virus capsid protein expression in *Escherichia coli* and chemically defined capsid assembly**

Authors:

Dinh To Le, Marco T. Radukic, Kristian M. Müller

OPEN

# Adeno-associated virus capsid protein expression in *Escherichia coli* and chemically defined capsid assembly

Dinh To Le, Marco T. Radukic<sup>ID</sup> & Kristian M. Müller<sup>ID</sup>\*

Research and clinical applications of recombinant adeno-associated virus (rAAV) significantly increased in recent years alongside regulatory approvals of rAAV gene therapy products. To date, all rAAV vectors as well as AAV empty capsids are produced in eukaryotic cells. We explored a new route to generate AAV capsids with the aim to analyze capsid assembly in a chemically defined setting and pave the way for new production methods and applications based on AAV virus-like particles (VLPs). We generated these empty capsids by bacterial expression and subsequent concomitant protein refolding and VLP formation. AAV serotype 2 structural protein VP3 was expressed in *Escherichia coli*. VLPs formed as demonstrated by dynamic light scattering, atomic force microscopy, and ELISA. Furthermore, VLPs internalized into human HeLa cells. To extend the application range of the VLPs, we tested peptide insertions, at the genetic level, in a surface loop (amino acid position 587) or at the C-terminus of VP3 and these variants also formed VLPs. VLPs developed without assembly-activating protein (AAP), but adding purified recombinant AAP to the refolding process increased capsid yield. Our findings offer a new route to understand AAV assembly biology and open a toolbox for AAV production strategies that might enable capsid display for vaccination and matching of capsids with cargoes at large scale and low cost.

AAV is a member of the family of *Parvoviridae* genus *Dependoparvovirus* and consists of a single-stranded DNA (ssDNA) genome of 4.7 kb packed in a non-enveloped capsid of 60 proteins arranged in a T = 1 icosahedral symmetry. AAV serotype 2 (AAV2) is the best-studied member of the genus which comprises currently 13 human and primate serotypes<sup>1</sup>. The genome of AAV2 consists of two open-reading-frame (ORF) cassettes flanked by inverted terminal repeat (ITR) sequences. In the typical genome depiction, the left ORF cassette codes for four non-structural Rep proteins (Rep 78, Rep 68, Rep 52, and Rep 40), which are responsible for AAV DNA replication, transcriptional regulation, site-specific integration and packaging of DNA into the capsid<sup>2-5</sup>. The right ORF cassette codes for three capsid proteins VP1, VP2 and VP3 (VP proteins) with apparent molecular masses of 87 kDa, 73 kDa, and 62 kDa, respectively<sup>6</sup>. These proteins, which only differ in their N-terminus, are produced by alternative splicing and leaky scanning from one reading frame to achieve a molar ratio of VP1:VP2:VP3 = 1:1:10<sup>7</sup>. VP3 is the main structural protein and can form VP3-only capsids<sup>8</sup>. The right ORF cassette also codes in a different reading frame for the assembly-activating protein (AAP), which promotes capsid assembly by increasing capsid protein stability and VP-VP interactions<sup>9,10</sup>. The AAP of AAV2 (AAP2) also plays a role in transporting the capsid proteins to the nucleolus for assembly<sup>11</sup>. Notably, while the capsids of AAV4, AAV5 and AAV11 can assemble without AAP, the other AAV serotypes from 1–12 including AAV2 critically require AAP to form capsids<sup>12</sup>.

Virus-like particles (VLPs) assemble from structural proteins of viruses. They lack a genome and are thus non-replicating particles. In recent years, these particles attracted great interest for targeted therapeutic delivery and vaccination<sup>13-15</sup>. Previous studies showed that AAV empty capsids produced in HEK-293 cells can be modified to present epitopes for vaccination<sup>16,17</sup>. Moreover, the concept of AAV VLP production using a yeast expression system was introduced<sup>18</sup>.

Cellular and Molecular Biotechnology, Faculty of Technology, Bielefeld University, Bielefeld, Germany. \*email: [kristian@syntbio.net](mailto:kristian@syntbio.net)

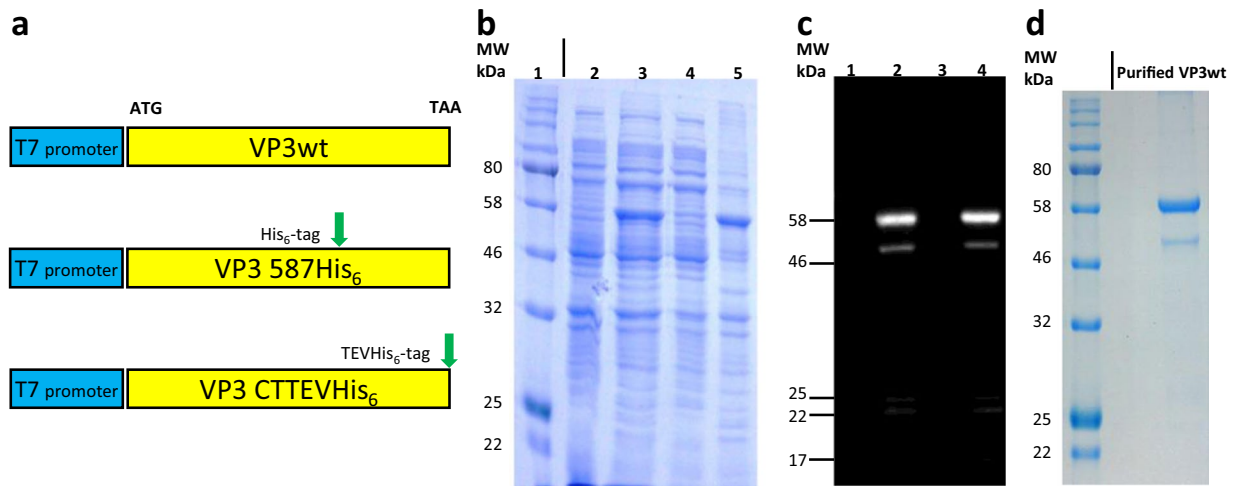


**Figure 1.** Expression of VP3wt protein in *E. coli*. (a) Schematic representation of VP3wt protein expression constructs downstream of a T7 promoter. Either a His-tag coding sequence was incorporated at the aa 587 coding position or a TEV\_cleavage\_site-His-tag coding sequence was cloned 3' of the VP3wt gene. (b) Coomassie stained SDS-PAGE of VP3wt expression; lane 1, protein standard; lane 2, whole-cell protein of *E. coli* BL21 (DE3) before induction; lane 3, whole-cell protein 18 h post-induction with IPTG; lane 4, soluble fraction of intracellular protein 18 h post-induction; lane 5, insoluble fraction of intracellular protein. (c) Western blot analysis; lane 1–4, samples corresponding to lane 2–5 (b) detected with B1 antibody. (d) SDS-PAGE of VP3wt protein after IEX purification. The black vertical line divides two different crops of the same gel. Full-length gels and blot are presented in Supplementary Fig. S1a–c.

AAV vectors have had increasing successes in recent clinical gene therapy trials. Among the AAV serotypes, AAV2 is a preferred model and its clinical suitability is highlighted by the approval as a vector in the drug Luxturna (Voretigene neparvovec) for the treatment of patients with an inherited form of vision loss by the Food and Drug Administration (FDA)<sup>19</sup>. Moreover, the drug Glybera (Alipogene tiparvovec) based on AAV1 was approved by the European Medicines Agency (EMA) in 2012<sup>20</sup> and Zolgensma (Onasemnogene abeparvovec) based on AAV9 was approved by the FDA in 2019<sup>21</sup>. Mammalian cell (HEK-293) or insect cell (Sf9) based systems are the two most commonly used methods to produce rAAV. Despite their success, they also pose disadvantages. HEK-293 cell culture is difficult to scale, specifically when using adherent cells, post-translational modifications of rAAV lead to charge heterogeneity<sup>22</sup>, and foremost process- and product-related impurities occur<sup>23</sup>. Production in Sf9 cells has drawbacks related to the genetic instability of baculovirus stocks during the expansion phase, the difficulty to produce infectious AAV particles with a correct capsid protein ratio and the requirement to remove baculoviruses and its components<sup>24,25</sup>.

A rising number of therapeutic AAV applications requiring high AAV vector doses, such as tumor therapy<sup>26</sup>, present a challenge to current production methods. Clinical trials report dosing of  $10^{12}$ – $10^{13}$  AAV genome copies per kg of body weight for liver transduction gene therapy<sup>27</sup> and about  $10^{14}$  genome copies/kg for targeting organs without porous capillary networks<sup>28</sup> thus reaching acceptable cost limits of current production techniques. In this light, the less expensive host yeast has been explored for production. However, low vector yields hinder commercial deployment<sup>29</sup>. The production of AAV empty capsids in bacteria could be the first step of a new strategy for rAAV production, if later *in vitro* encapsidation of genomes becomes possible.

*E. coli*, the most important host for molecular biology, has been used successfully for the production of virus-like particles<sup>13,14</sup>. Notably, although distant from the original host, heterologous production of primate erythroparvovirus 1 (human parvovirus B19) and canine parvovirus VLPs, which also belong to family Parvoviridae, has been described in *E. coli*<sup>30,31</sup>.

With the long-term perspective to develop a novel method for rAAV production based on a prokaryotic host and the short-term goal to study AAV VLPs production in bacteria and analyze epitope presentation, we established AAV VP expression in *E. coli* and subsequent VLP formation. High-level expression of AAV2 VP3 capsid protein in *E. coli* and, for the first time, chemically-defined, concomitant refolding and assembly of VP3 protein into AAV capsids was achieved. Biological functionality of capsids was demonstrated by anti-capsid ELISA and imaging of cellular uptake.

## Results

**Expression and purification of VP3 proteins.** AAV2 VP3 wild type (VP3wt) protein is known to form VP3-only capsids<sup>8</sup>. Hence, the codon usage of the VP3wt gene was optimized for *E. coli* and cloned as a synthetic gene into a pET vector downstream of a T7 promoter without an additional tag (Fig. 1a). We tested different expression conditions in shake flasks with the BL21(DE3) host, such as temperature (37 °C, 25 °C and 18 °C), OD at induction (OD<sub>600</sub> of 0.6, 1.5 and 2.5) and duration of cultivation after induction (6 h, 18 h) to obtain soluble protein. However, only inclusion bodies were obtained due to suspected folding problems and growth-limiting effects of VP3wt protein to *E. coli*. Another expression system, which was subsequently evaluated, with a weaker

lac promoter and *E. coli* RV308 as host also yielded inclusion bodies (Supplementary Fig. S1d). Consequently, we settled with overexpression with the T7 system in inclusion body form at 18 °C and induction of expression at an OD<sub>600</sub> of 1.5 for 18 h (Fig. 1b, lane 5). The identity of the VP3 protein was confirmed by Western blot analysis using the antibody B1. Interestingly, in addition to a strong band at the expected size of VP3wt (theoretical mass 60.06 kDa), the B1 antibody identified four weaker and smaller bands. This suggests that VP3wt is unstable during expression (Fig. 1c, lane 2 and lane 4). Capsid proteins were then solubilized under denaturing condition (8 M Urea) and purified by denaturing anion-exchange chromatography (IEX). SDS-PAGE analysis of purified protein showed a major protein band at about 60 kDa which is in agreement with the theoretical mass of VP3wt (Fig. 1d). The purified protein yield with one degradation band around 50 kDa was around 10 mg per liter of culture with an estimated final purity of the correct-mass protein of 79% (by SDS-PAGE).

**Assembly and characterization of VLPs.** We used VP3wt proteins in denaturing buffer as the starting material for refolding and concomitant *in vitro* assembly to VLPs. In other studies, capsid formation from denatured protein was initiated by the removal of denaturant<sup>30,32</sup>. To test this strategy, the VP3wt sample, which was concentrated and re-buffered in denaturing buffer with 5 M guanidine/HCl and 1 mM DTT as reducing agent, was dialyzed against PBS buffer containing 0.2 mol/l L-arginine at different pH conditions (pH 6, pH 7.5, pH 8.5, and pH 9). Significant amounts of VP3wt protein precipitated at pH 6 and pH 7.5. At pH 8.5 and pH 9, however, precipitation decreased. At these pH values, after removal of aggregates by centrifugation and filtration, the yield of soluble protein was around 36% at pH 8.5 and 70% at pH 9. Since particles aggregated when going back to the neutral pH (Supplementary Fig. S1e), the samples were used at pH 9 for further characterization.

First, the presence of VLPs and/or their intermediate forms was analyzed by dynamic light scattering (DLS) at pH 9. The dialyzed VP3wt sample showed a mean hydrodynamic diameter of 37.7 nm and a polydispersity of 0.22 indicating homogeneity and the assembly of VLPs (Fig. 2a). Note that the hydrodynamic size is always greater than the physical size, and that this result is consistent with the hydrodynamic size of rAAV measured by DLS from other reports (34.4 nm or 38.2 nm)<sup>33,34</sup>.

Next, the VP3wt VLP conformation was assessed by ELISA with the A20 monoclonal antibody (mAb), which only binds to assembled AAV2 capsids<sup>35</sup>. Parallel to the A20 antibody, we also used a recombinant A20 single-chain Fv fragment Fc fusion antibody variant (A20 scFv-Fc) cloned in our lab and produced in HEK-293 cells (K. Teschner *et al.*, in preparation). The ELISA signals indicated correctly assembled VLPs (Fig. 2b). We compared the ELISA result to a sample of rAAV2 with known capsid concentration and estimated the ratio of correctly assembled particles to be 1 VLP per 5000 theoretical VLPs based on VP3wt concentration (i.e. protein concentration divided by 60). The total yield from 0.23 mg denatured protein was  $5 \times 10^9$  correctly assembled VLPs in 1.5 ml.

The physical size and height profile of the particles were measured by atomic force microscopy (AFM). Recombinant AAV2 produced in HEK-293 cells was used for comparison. The shape and diameter of rAAV2 and VP3wt VLPs were similar, spherical and around 22 nm in diameter (Fig. 2c–f), which is expected for AAV<sup>36</sup>. In the AFM images of the *in-vitro* assembly also particles of a smaller diameter and higher-order aggregates were observed (Supplementary Fig. S2b).

**Cellular uptake of VP3wt VLPs.** We used HeLa cells to evaluate cellular uptake and thereby biological activity of VP3wt VLPs, as these cells are known to have a high density of AAV2's primary receptor heparan sulfate proteoglycan<sup>37</sup>. In this experiment, HeLa cells were incubated with rAAV2 or VP3wt VLPs, fixed, permeabilized and the A20 antibody as well as a fluorescent secondary antibody (red fluorescent signal) were added for detection with fluorescence microscopy (Fig. 3). No red fluorescent background signal was seen in the buffer control treated with the detection antibody (Fig. 3a). The distribution of rAAV2 was shifted towards the nucleus (Fig. 3b), while VP3wt VLPs were widely distributed in the cytoplasm, potentially in endosomes (Fig. 3c). We attribute this to the known nuclear translocation role of VP1, however, most of rAAV2 particles were still located in the cytoplasm after 2 h. This result indicates that VP3wt VLPs are biologically active and can internalize into cells.

**Effect of AAP2 on *in vitro* assembly.** AAP2 plays a critical role in AAV2 assembly. To investigate the impact of AAP2 on the production of AAV2 VLPs *in vitro*, we expressed AAP2 in *E. coli*. For the purpose of detection and purification, we added a C-terminal His-tag (Fig. 4a), as a modification at this position does not interfere with AAP function<sup>38</sup>. As for VP3, we tested various expression temperatures, such as 37 °C, 25 °C and 18 °C, to acquire AAP2 in soluble form. At 18 °C, AAP2 was expressed as a soluble protein, however, most proteins degraded during expression (Supplementary Fig. S5). Therefore, we settled with an inclusion body production at 37 °C and convenient purification by immobilized metal ion affinity chromatography (IMAC) under denaturing condition (Fig. 4b). Under these conditions, AAP was stable. We observed an apparent molecular weight of AAP2 of about 28 kDa, which is consistent with AAP2 produced in HEK-293 cells<sup>12</sup>. AAP2 was then added to the *in-vitro* assembly reaction in the presence of 5 M guanidine with VP3wt:AAP2 ratios of 1:2 or 2.5:1 and the refolding and assembly was performed as described. After dialysis, analysis by ELISA revealed that even though VP3wt can form capsids on its own, AAP2 enhanced the *in-vitro* assembly (Fig. 4c). Specifically, at a ratio of VP3wt:AAP2 of 1:2, the ELISA signal of VLP particles was 1.9 times greater than that of the VP3wt-only assembly reaction. This suggests that the yield of *in vitro* assembly increases in the presence of AAP2.

**Surface modification but not C-terminal extension is compatible with capsid antibody A20 mAb detection.** Incorporation of peptides into the capsid is an important strategy in AAV retargeting<sup>39</sup> and also gains interest in vaccine development<sup>16,17</sup>. To evaluate the effect of small peptide insertions on *in vitro* assembly, we chose two sites for modification. We genetically incorporated either a tag containing a TEV protease cleavage

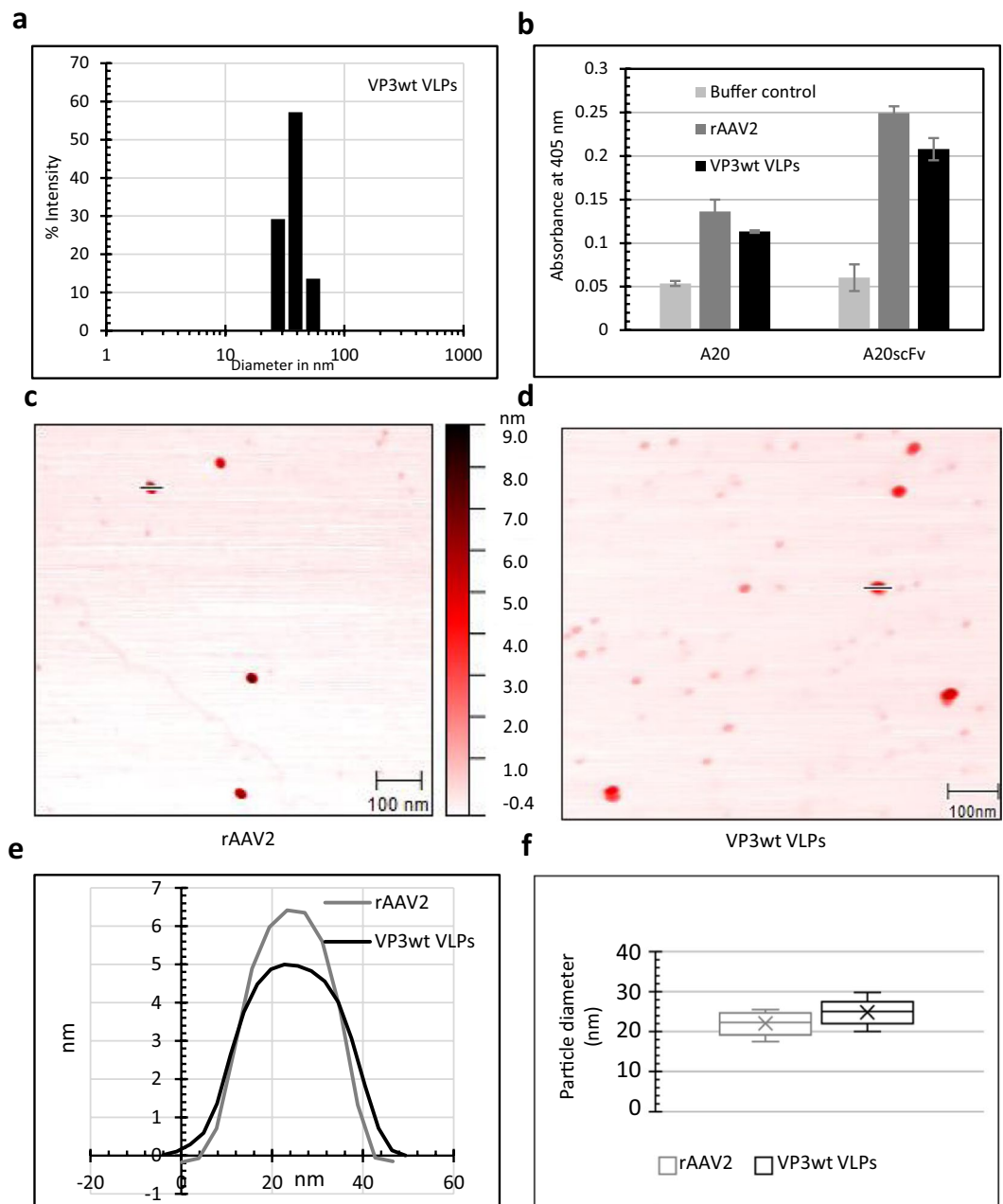


**Figure 2.** Characterization of VP3wt VLPs. **(a)** Size distribution of VP3wt VLP determined by DLS at pH 9.0. **(b)** ELISA probed with anti-intact-capsid AAV2 antibodies (A20 mAb or A20 scFv-Fc); samples were rAAV2 particles ( $1.6 \times 10^9$  particles/ml) and VP3wt VLPs ( $50 \mu\text{g/ml}$ ). **(c,d)** AFM images of rAAV2 and VP3wt VLPs, respectively. Scale bars are 100 nm. **(e)** AFM height profiles of rAAV2 and VP3wt VLPs. **(f)** Box plot of the size distribution of rAAV2 particles and VP3wt VLPs determined by AFM ( $n = 9$ , mean  $\pm$  SD, box from first to third quartile, cross median marker). Full AFM images are presented in Supplementary Fig. S2a,b.

site followed by a His-tag at the C-terminus (VP3 CTTEVHis<sub>6</sub>) or a His-tag into the 587-loop (VP3 587His<sub>6</sub>) of VP3wt protein (Fig. 5a,e). The two sites were previously described to tolerate insertions *in vivo*<sup>39,40</sup>. We found that neither insertion of the tag at the C-terminus nor the 587-loop affected protein expression in *E. coli*. *In vitro* assembly of both modified proteins formed VLPs according to DLS and AFM measurements (Fig. 5b,c,f,g).

In ELISA, the anti-capsid A20 antibody did recognize VP3 587His<sub>6</sub> particles as did the A20 scFv-Fc recombinant antibody construct (Fig. 5d) indicating wt-identical VLP assembly. Interestingly, ELISA results also showed that the A20 monoclonal antibody did not bind to VP3 CTTEVHis<sub>6</sub> VLPs although particles were present (Fig. 5h). In contrast, the A20 scFv-Fc readily recognized VP3 CTTEVHis<sub>6</sub> VLPs. These findings suggest a more flexible binding mode of this antibody construct. The results show that the 587-loop of VP3 is a potential position for capsid modification of particles assembled in a chemically-defined reaction.

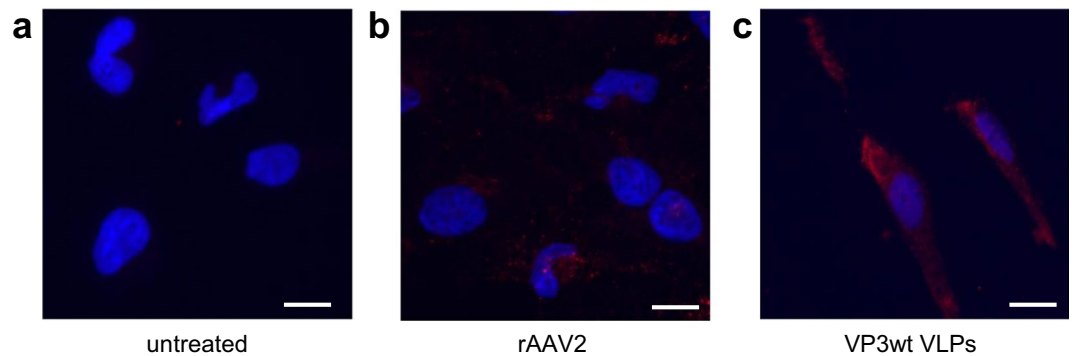


**Figure 3.** Fluorescent microscopy images of internalization. HeLa cells were incubated with either (a) medium, (b) rAAV2 ( $3 \times 10^4$  particles/cell) or (c) VP3wt VLPs (final concentration of  $50 \mu\text{g/ml}$ ) at  $37^\circ\text{C}$ . After 2 h, cells were fixed, permeabilized and stained with the A20 antibody followed by a DyLight 594 conjugated secondary antibody (red) as well as with DAPI (blue) and imaged with a  $40\times$  objective. Scale bars are  $10 \mu\text{m}$ . Full images are presented in Supplementary Fig. S3.

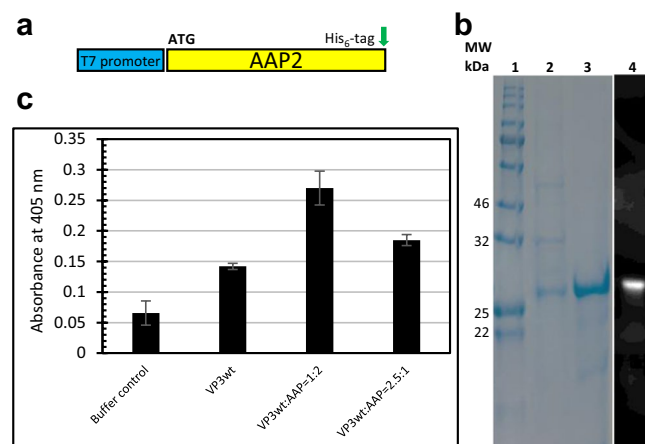


**Figure 4.** Impact of AAP2 on *in vitro* assembly. (a) Schematic representation of AAP2 expression construct. A His-tag coding sequence was added 3' of the AAP2 gene. (b) Coomassie SDS-PAGE; (1) protein standard; (2) insoluble fraction of intracellular protein before purification; (3) IMAC purified protein; (4) Western blot of the insoluble fraction detected with anti-His-tag antibody. (c) ELISA after *in vitro* assembly using the same final protein concentration ( $50 \mu\text{g/ml}$ ) with different ratios of VP3wt:AAP2. Full-length gel and blot are presented in Supplementary Fig. S4.

## Discussion

AAV emerged as the most prominent candidate for gene therapy approaches. However, the several steps of AAV capsid assembly still remain unclear. AAV assembly has been proposed to occur in two steps. Empty capsids form and are then filled with its single-stranded DNA genome<sup>5</sup>. Hence, production of empty capsids from *E. coli* might not only help to elucidate the AAV biology aspect in capsid assembly, but also provide a feasible strategy for future AAV production. Production of rAAV2 capsids *in vitro* was first reported by Steinbach *et al.*<sup>41</sup>. The group used the recombinant baculovirus strategy to separately express and purify capsid proteins. AAV2 capsids then formed only in the presence of HeLa cell extract. In our study, capsid proteins were produced in *E. coli* and capsids formed in a chemically defined assembly reaction. To our knowledge, this is the first experimental evidence for true *in vitro*, cell-free assembly of AAV capsids.

*E. coli* remains one of the most attractive hosts to produce recombinant proteins because of well-established protocols and low cost. Due to the high level of expression in *E. coli*, heterologous proteins tend to aggregate and form inclusion bodies with a lack of biological activity. For proteins that can be refolded *in vitro*, however, especially for toxic or unstable proteins or proteins with potential protease activity, inclusion body formation can be advantageous due to the high volumetric yield and easy purification<sup>42</sup>. In addition, viral particles forming in *E. coli* might encapsidate bacterial polymers, such as DNA or RNA, which are then difficult to remove and not desired for human application. In our study, VP3 protein expression blocked *E. coli* growth at physiological temperatures and no useful amounts of VP3 were obtained in soluble form even at low temperatures. However, VP3 was effectively expressed in inclusion bodies and subsequently easily purified by a one-step purification, either IEX or IMAC. This was our preferred method. We confirmed the presence of VP3 during expression with the B1

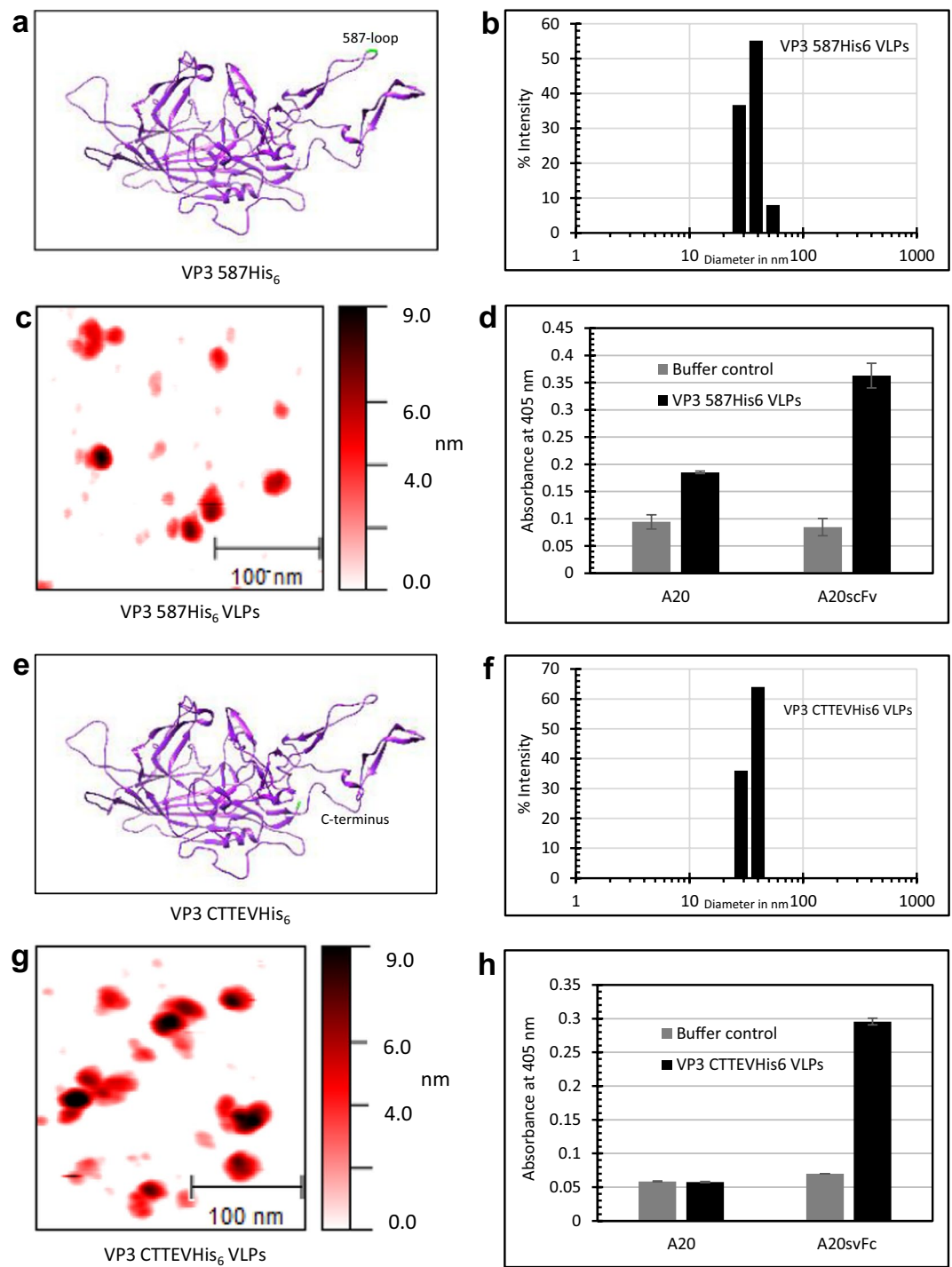


**Figure 5.** The effect of incorporation of a small peptide, either into the 587-loop or at the C-terminus of VP3wt, on *in vitro* assembly. **(a,e)** Representations of VP3wt protein structure (PDB ID: 1LP3) with highlighted 587-loop and C-terminus. **(b,f)** DLS size distribution of VP3 587His<sub>6</sub> VLPs ( $35.7 \pm 7.5$  nm) and VP3 CTTEVHis<sub>6</sub> VLPs ( $35.9 \pm 5.5$  nm). **(c,g)** AFM images of VP3 587His<sub>6</sub> VLPs and VP3 CTTEVHis<sub>6</sub> VLPs. Scale bars are 100 nm. **(d,h)** ELISA of modified VLPs using either A20 mAb or A20 scFv-Fc antibody for detection. Full AFM images are presented in Supplementary Fig. S2c,d.

antibody, which recognizes a C-terminal epitope of VP3<sup>35</sup>. Next to the major VP3 band, additional lower molecular weight bands were detected in Western blots. We suppose that VP3 is proteolytically degraded, possibly by an intrinsic protease activity as found in AAV2 particles<sup>43</sup>, or cleaved by *E. coli* proteases.

*In vitro* assembly of icosahedral VLPs is a complex process, which depends on various factors such as temperature, pH, ionic strength and the presence of additives<sup>30,31,41</sup>. In the current study, we used PBS containing 0.2 M L-arginine with different pH values to optimize the assembly reaction. L-arginine aids to form VLPs *in*

*vitro* due to its ability to increase protein solubility and prevent aggregation of intermediate forms<sup>44</sup>. In previous studies, the pH showed significant impact on *in vitro* assembly of VLPs<sup>31,32</sup>. In the present study, the majority of VP3wt protein precipitated at pH 6 and pH 7.5. This can be explained with the theoretical isoelectric point of VP3 of pH 6.40 (ProtParam ExPASy Webtool) to 6.88 (Geneious R9 Software). To enhance the solubility of particles, we chose basic conditions with pH 8.5 and pH 9 for further study. We found a suitable assembly condition to be PBS containing 0.2 M L- arginine at pH 9. This indicates that charge plays a significant role during *in vitro* assembly. Furthermore, VP3wt contains five free cysteines, some located in proximity and at the inter-protein interface<sup>45</sup>, which likely need to get buried during folding and assembly to avoid oxidation and/or crosslinking. This is particularly critical for the thiolate anions present at levels above pH 8. We used DTT as reducing agent in the denaturing buffer but not the dialysis buffer. Keeping a reducing agent for the first dialysis steps might further reduce aggregation.

We characterized our assembly results by DLS and observed an average diameter in line with the expected hydrodynamic diameter. AFM imaging (Figs. 2c,d; 5c,g) showed particles with proper shape and diameter. In addition, we found other particles with a smaller diameter, which we attribute to assembly intermediates. The mechanism of capsid assembly of icosahedral virus is known to involve the formation of intermediate forms, and our observation correlates with those obtained for *in vitro* production of other icosahedral capsids<sup>30,46</sup>. Also, larger structures are visible, which might have formed during the drying procedure on the mica support.

VP3wt assembled capsids were also confirmed by ELISA, for which we used the well-established A20 antibody that specifically recognizes a conformational epitope on the AAV2 capsid exterior<sup>35</sup>. Additionally, we routinely used an A20 single-chain Fv-Fc variant for capsid detection, which gave comparable results. However, the structural requirement seemed to be less strict.

AAV2 binds to permissive cells using heparan sulfate proteoglycan (HSPG)<sup>47</sup> and then a universal AAV receptor, which was identified with high-affinity to multiple AAV serotypes including AAV2<sup>48</sup>. These receptor-virus interfaces all lie within the VP3-only capsid. After attachment to the cell membrane, AAV2 internalizes by receptor-mediated endocytosis. Endosomal escape and nuclear entry, the next steps in infection, are attributed to the VP1 capsid protein<sup>49,50</sup>. Therefore, VP3wt VLPs should be able to enter cells that express the corresponding receptors but should not be able to translocate to the nucleus. We show that 2 h after transduction with the given buffer conditions, VP3wt VLPs internalized and distributed granular in the cytosol without nuclear preference, which is compatible with expectations of endosomal confinement. rAAV2 from mammalian production showed a similar appearance albeit with a shift towards the nucleus. These observations are consistent with a previously described distribution of rAAV2 and rAAV2 with deleted VP1 after infection of HeLa cells<sup>51</sup>, which supports the finding of biological activity of our VLPs. Further work will elucidate the internalization pathway of the particles.

Moreover, our study provides evidence that AAV2 VP3 proteins can form capsids *in vitro*, even in the complete absence of AAP2. AAP2 likely acts as a chaperone and/or a scaffold that directly or indirectly binds the luminal surface of VP proteins and plays a role in VP stability and in VP oligomerization during assembly<sup>10,52</sup>. However, the exact mode of action of AAP2 in AAV2 assembly remains unclear. Our initial results of AAP2-free assembly agree with the previous report from Steinbach *et al.*<sup>41</sup>, although the authors of this study used HeLa cell extract for assembly. Here, by using a chemically defined reaction, we present direct evidence that the ability to form a capsid is entirely a property of VP3. To further investigate the role of AAP2 in capsid assembly, we expressed it in *E. coli* as inclusion bodies. Subsequent addition of solubilized AAP to our assembly reaction resulted in a 1.9-fold increase of mAb A20 positive particles over the AAP2-free assembly reaction. Although the complexity of the experiment provides a challenge for interpretation, the result indicates that AAP2 directly aids in capsid assembly, next to its before described function in VP stabilization by inhibition of proteasomal, lysosomal or autophagosomal degradation and nuclear translocation<sup>10,11</sup>.

Finally, we explored possibilities to assemble capsids from modified VP3 proteins. Our loop and C-terminal insertions did not interfere with *in vitro* assembly as detected by DLS and AFM and gave VLP yields comparable to that of wild type VP3. As the capsid is known to tolerate these modifications *in vivo*<sup>39,40,53</sup>, our result hints that the *in-vitro* assembly process in general reflects the cellular process. Since the loop-region is exposed on the capsid surface, this opens the possibility to produce VLPs with modified tropism. Furthermore, these modified VLPs could be used to display functional proteins and act as antigen carriers for vaccination as described before for other virus particles<sup>14,15</sup>. However, we note that VLPs with VP3 C-terminal modification were detectable only by the A20 scFv-Fc, but not by the monoclonal IgG3-class A20 antibody. The broader binding of the single-chain construct can possibly be attributed to its general structural flexibility, allowing binding of slightly distorted capsids. One group found that a VP3 C-terminal His-tag is compatible with biological function<sup>40</sup> and another found that the tag interferes with capsid assembly *in vivo*<sup>54</sup>. From our data, we can conclude that a C-terminal His-tag is compatible with forming particles, which are very similar in shape and diameter to wt capsids, but show subtle structural differences revealed by A20 mAb recognition.

In summary, the current study shows that AAV2 VP3 proteins can be expressed in *E. coli*, and that these proteins are able to form AAV2 capsids in a defined *in-vitro* reaction. This work provides a tool to assess capsid assembly of AAV under controlled conditions. At the same time, it opens the door for *in vitro* AAV capsid production with wide applications in vaccine development, cellular delivery of small-molecule drugs and possibly genetic payloads in gene therapy. Further studies will improve the assembly yield and elucidate the mechanisms of *in vitro* assembly.

## Methods

**Expression and purification of proteins.** VP3wt was expressed in *E. coli* BL21(DE3) from a chemically synthesized, codon-optimized sequence (GeneArt/ThermoFisher Scientific, gene and amino acid sequence given in Supplementary Information subsection 2.1 and 2.2) inserted into the *NdeI* and *XhoI* sites of pET24b (Novagen/Merck). Transformed *E. coli* was cultured in LB medium containing Kanamycin (50 µg/ml) at 37 °C to an OD<sub>600</sub> of

1.5, then isopropyl  $\beta$ -D-thiogalactopyranoside (IPTG) was added to a concentration of 0.4 mM, and the culture was incubated at 18 °C for additional 18 h. Cells were harvested at  $5,000 \times g$ , 4 °C for 15 min. Pelleted cells were re-suspended in a lysis buffer (50 mM  $\text{NaH}_2\text{PO}_4$ , 300 mM NaCl, pH 8) supplemented with 1 mg/ml lysozyme and lysed by sonication on ice (Branson Sonifier 250 with micro tip, power setting 70%, constant duty, 10 cycles, 30 s each). The recombinant proteins formed inclusion bodies, therefore, cell debris and inclusion bodies were collected by centrifugation at  $10,000 \times g$ , 4 °C for 20 min. The inclusion bodies were washed three times with lysis buffer. The remaining pellet was solubilized in ion-exchange chromatography (IEX) buffer A (20 mM Tris-HCl, 8 M Urea, pH 8). A 2 ml Q Sepharose resin (GE Healthcare) packed column was equilibrated with IEX Buffer A. The column was then loaded with sample and washed with IEX Buffer A. Bound proteins were eluted with a gradient of IEX Buffer B (20 mM Tris-HCl, 1 M NaCl, 8 M Urea, pH 8). Fractions containing target proteins were collected and concentrated with centrifugal filter units with a 30 kDa molecular weight cut-off. In this step, the buffer was changed to another denaturing buffer (5 M GuHCl, 20 mM Tris-HCl, 0.15 M NaCl, 1 mM EDTA, 1 mM DTT, pH 8).

Other VP3 constructs were designed to additionally code for either a TEV protease cleavage site-His<sub>6</sub>-tag fused to the C-terminus or a His<sub>6</sub>-tag at the amino acid position 587 (gene and amino acid sequences given in Supplementary Information subsection 2.3 to 2.6). The protein expression methods were used as described above. Protein AAP2 was also constructed into vector pET24b with a His<sub>6</sub>-tag at the C-terminus. This protein was expressed with 0.4 mM IPTG induction at 37 °C for 4 h and purified by immobilized metal-ion affinity chromatography (IMAC). Briefly, a column with 2 ml of Ni-NTA Agarose (Macherey-Nagel) was equilibrated with IMAC buffer A (50 mM  $\text{NaH}_2\text{PO}_4$ , 300 mM NaCl, 10 mM imidazole, 8 M Urea, pH 8), then sample was loaded and washed with five column volumes of IMAC buffer A containing 7% IMAC buffer B (50 mM  $\text{NaH}_2\text{PO}_4$ , 300 mM NaCl, 250 mM imidazole, 8 M Urea, pH 8). Afterwards, bound proteins were eluted with 100% IMAC buffer B.

**SDS-PAGE and western blot.** Samples of protein were separated on a 12% polyacrylamide (12% T, 0.4% C) with a 4% collection gel, followed by semi-dry transfer to nitrocellulose membranes (88018, ThermoFisher Scientific, 0.45  $\mu\text{m}$ ). After blocking with 10% (w/v) non-fat dry milk (Applichem) in TBS buffer (500 mM Tris-HCl, 1.5 M NaCl, pH 7.5), the membranes were incubated 1 h at room temperature with either anti-AAV VP1/VP2/VP3 mouse monoclonal, B1 antibody (1: 100 dilution) (Progen) for detecting VP3 proteins or anti-His-tag antibody (Tetra-His, Qiagen) for detecting AAP2 protein. Detection was achieved using anti-mouse antibody coupled to horseradish peroxidase (Goat anti-Mouse IgG (H + L) Secondary Antibody, HRP, 1: 2500 dilution) (31430, ThermoFisher Scientific), SuperSignal™ West Pico PLUS Chemiluminescent Substrate (34580, ThermoFisher Scientific) and a Fusion FX camera system (Vilber).

**In vitro assembly of VLPs.** Capsid assembly was carried out by dialyzing 1.5 mL of VP3 proteins (0.15 mg/mL) in solubilization buffer five times against 100 mL of phosphate buffered saline (PBS) (500 mM NaCl, 100 mM KCl, 10 mM  $\text{Na}_2\text{HPO}_4$ , 10 mM  $\text{KH}_2\text{PO}_4$ , pH 9) containing 0.2 M L- arginine, at 4 °C, changing buffer every 12 h over a 60-h period. To investigate the effect of AAP2 on *in vitro* assembly, purified VP3 protein (0.15 mg/ml) was mixed with a varying concentration of purified AAP2 (a VP3:AAP2 ratio of 1:2 or 2.5:1). Afterwards, capsid assembly was performed as mentioned above.

**DLS, AFM Characterization of VLPs.** Dynamic light scattering (DLS) was performed on a DynaPro99 (Wyatt Technology) instrument. Samples were filtered through 0.22  $\mu\text{m}$  PVDF syringe filters (Millipore) and centrifuged at  $18,000 \times g$  for 30 min before measurement. Measurements for each sample were averages of at least 20 acquisitions.

Atomic Force Microscopy (AFM) measurements of rAAV2 and VLPs were carried out using a Multimode 8 AFM (Bruker) with Tap300Al-G cantilevers (BudgetSensors) in tapping mode in air. Samples after filtration and centrifugation were spotted onto freshly cleaved mica and incubated for one minute. The mica was then briefly rinsed with water and dried under a gentle nitrogen flow. The analysis of the AFM images was performed with Gwyddion 2.49 software. The diameter of visualized particles was measured at half maximum particle height. The rAAV used as control was provided by K. Teschner and was produced using a three plasmid system in HEK-293 cells and purified by affinity chromatography.

**ELISA.** VLPs were detected by ELISA with anti-AAV2 (intact particle) mouse monoclonal, A20 antibody or its single-chain derivative A20 scFv-Fc. MaxiSorp 96 well-plates (Nunc) were coated with VLPs (50  $\mu\text{g}/\text{ml}$ ) or rAAV2 ( $1.6 \times 10^9$  AAV2/ml) for 1 h at 37 °C and afterwards blocked with 0.8% BSA for 1 h. Samples were incubated with A20 antibody (Progen, 1: 250 dilution), or A20 scFv-Fc (produced by our working group, 1: 250 dilution, manuscript in preparation) for another 1 h at 37 °C. Anti-mouse-HRP (31430, ThermoFisher Scientific) or anti-human-HRP (ThermoFisher Scientific) (1: 2000, 1 h incubation at 37 °C) was used for detection. Following every incubation step, the plate was washed three times with 0.05% Tween in blocking buffer. Lastly, samples were developed with 1 g/L 2,2'-Azinobis [3-ethylbenzothiazoline-6-sulfonic acid]-diammonium salt (ABTS), and optical density was measured by a microplate reader (BioTek) at 405 nm.

**Cellular uptake of VP3wt VLPs.** To study cellular uptake of VLPs, HeLa cells were seeded on poly-L-lysine-coated 12-mm glass coverslips placed in a 24-well plate at a density of  $3 \times 10^4$  cells/well in DMEM 10% FCS and allowed to adhere overnight. Then, VP3wt VLPs (50  $\mu\text{g}/\text{ml}$ , estimated  $1.4 \times 10^4$  particles/cell) and rAAV2 ( $3 \times 10^4$  particles/cell) were added and incubated for 2 h. Following three washes with PBS, cells were fixed with 4% paraformaldehyde for 15 min at room temperature. The cells were then permeabilized with 0.2% Triton X-100 in PBS buffer for 5 min. Afterwards, the permeabilized cells were blocked in 1% BSA in PBS buffer for 30 min at room temperature. The cells were incubated with primary antibody (A20 antibody, Progen (1:40)) overnight at 4 °C, followed by incubation with the second antibody (Goat anti-Mouse IgG (H + L) Secondary

Antibody, DyLight 594, 35510, ThermoFisher Scientific (1:500)) for 1 h at room temperature. After three washes in PBS, the cells were incubated in 10  $\mu$ M 4',6-diamidino-2-phenylindole (DAPI) for 10 min at room temperature. Coverslips were then mounted on glass slides with mounting medium (Mowiol-Dabco) and cells were imaged on a Leica DMI6000 B microscope.

Received: 4 July 2019; Accepted: 20 November 2019;

Published online: 09 December 2019

## References

- Agbandje-McKenna, M. *et al.* Molecular Characterization of the Heparin-Dependent Transduction Domain on the Capsid of a Novel Adeno-Associated Virus Isolate, AAV(VR-942). *J. Virol.* **82**, 8911–8916 (2008).
- Ward, P., Elias, P. & Linden, R. M. Rescue of the adeno-associated virus genome from a plasmid vector: evidence for rescue by replication. *J. Virol.* **77**, 11480–11490 (2003).
- Pereira, D. J., McCarty, D. M. & Muzyczka, N. The adeno-associated virus (AAV) Rep protein acts as both a repressor and an activator to regulate AAV transcription during a productive infection. *J. Virol.* **71**, 1079–1088 (1997).
- Surosky, R. T. *et al.* Adeno-associated virus Rep proteins target DNA sequences to a unique locus in the human genome. *J. Virol.* **71**, 7951–7959 (1997).
- King, J. A., Dubielzig, R., Grimm, D. & Kleinschmidt, J. A. DNA helicase-mediated packaging of adeno-associated virus type 2 genomes into preformed capsids. *EMBO J.* **20**, 3282–3291 (2001).
- Rose, J. A., Maizel, J. V., Inman, J. K. & Shatkin, A. J. Structural proteins of adenovirus-associated viruses. *J. Virol.* **8**, 766–770 (1971).
- Becerra, S. P., Kocot, F., Fabisch, P. & Rose, J. A. Synthesis of adeno-associated virus structural proteins requires both alternative mRNA splicing and alternative initiations from a single transcript. *J. Virol.* **62**, 2745–2754 (1988).
- Sonntag, F. *et al.* The assembly-activating protein promotes capsid assembly of different adeno-associated virus serotypes. *J. Virol.* **85**, 12686–12697 (2011).
- Sonntag, F., Schmidt, K. & Kleinschmidt, J. A. A viral assembly factor promotes AAV2 capsid formation in the nucleolus. *Proc. Natl. Acad. Sci. USA* **107**, 10220–10225 (2010).
- Maurer, A. C. *et al.* The Assembly-Activating Protein Promotes Stability and Interactions between AAV's Viral Proteins to Nucleate Capsid Assembly. *Cell Rep.* **23**, 1817–1830 (2018).
- Nakai, H. *et al.* Identification and Characterization of Nuclear and Nucleolar Localization Signals in the Adeno-Associated Virus Serotype 2 Assembly-Activating Protein. *J. Virol.* **89**, 3038–3048 (2015).
- Earley, L. F. *et al.* Adeno-associated Virus (AAV) Assembly-Activating Protein Is Not an Essential Requirement for Capsid Assembly of AAV Serotypes 4, 5, and 11. *J. Virol.* **91**, e01980–16 (2017).
- Rohovie, M. J., Nagasawa, M. & Swartz, J. R. Virus-like particles: Next-generation nanoparticles for targeted therapeutic delivery. *Bioeng. Transl. Med.* **2**, 43–57 (2017).
- Huang, X., Wang, X., Zhang, J., Xia, N. & Zhao, Q. Escherichia coli-derived virus-like particles in vaccine development. *npj Vaccines* **2**, 3 (2017).
- Rybicki, E. P. Plant-based vaccines against viruses. *Virol. J.* **11**, 1–20 (2014).
- Nieto, K. & Salvetti, A. AAV vectors vaccines against infectious diseases. *Front. Immunol.* **5**, 1–9 (2014).
- Nieto, K. *et al.* Development of AAVLP(HPV16/31L2) particles as broadly protective HPV vaccine candidate. *PLoS One* **7**, e39741 (2012).
- Backovic, A. *et al.* Capsid protein expression and adeno-associated virus like particles assembly in *Saccharomyces cerevisiae*. *Microb. Cell Fact.* **11**, 124 (2012).
- Spark Therapeutics. Briefing Document: FDA Advisory Committee Meeting, Luxturna™ (voretigene neparovec). FDA, Silver Spring, MD, USA (2017).
- Ylä-Herttua, S. Endgame: Glybera Finally Recommended for Approval as the First Gene Therapy Drug in the European Union. *Mol. Ther.* **20**, 1831–1832 (2012).
- FDA. FDA approves innovative gene therapy to treat pediatric patients with spinal muscular atrophy, a rare disease and leading genetic cause of infant mortality. (2019). Available at: <https://www.fda.gov/news-events/press-announcements/fda-approves-innovative-gene-therapy-treat-pediatric-patients-spinal-muscular-atrophy-rare-disease>. (Accessed: 6th June 2019).
- Giles, A. R. *et al.* Deamidation of Amino Acids on the Surface of Adeno-Associated Virus Capsids Leads to Charge Heterogeneity and Altered Vector Function. *Mol. Ther.* **26**, 2848–2862 (2018).
- Wright, J. F. Product-Related Impurities in Clinical-Grade Recombinant AAV Vectors: Characterization and Risk Assessment. *Biomedicines* **2**, 80–97 (2014).
- Kohlbrenner, E. *et al.* Successful production of pseudotyped rAAV vectors using a modified baculovirus expression system. *Mol. Ther.* **12**, 1217–1225 (2005).
- Clément, N. & Grieger, J. C. Manufacturing of recombinant adeno-associated viral vectors for clinical trials. *Mol. Ther. - Methods Clin. Dev.* **3**, 16002 (2016).
- Hagen, S. *et al.* Modular adeno-associated virus (rAAV) vectors used for cellular virus-directed enzyme prodrug therapy. *Sci. Rep.* **4**, 3759 (2014).
- Miesbach, W. *et al.* Gene therapy with adeno-associated virus vector 5–human factor IX in adults with hemophilia B. *Blood* **131**, 1022–1031 (2018).
- ClinicalTrials.gov, Bethesda (MD): National Library of Medicine (US). 2000 -. National Clinical Trials Identifier: 03199469, 02122952. <https://clinicaltrials.gov>. (Accessed: 6th June 2019).
- Barajas, D. *et al.* Generation of infectious recombinant Adeno-associated virus in *Saccharomyces cerevisiae*. *PLoS One* **12**, e0173010 (2017).
- Sánchez-Rodríguez, S. P. *et al.* Enhanced assembly and colloidal stabilization of primate erythroparvovirus 1 virus-like particles for improved surface engineering. *Acta Biomater.* **35**, 206–214 (2016).
- Jin, X. *et al.* Self-assembly of virus-like particles of canine parvovirus capsid protein expressed from *Escherichia coli* and application as virus-like particle vaccine. *Appl. Microbiol. Biotechnol.* **98**, 3529–3538 (2014).
- Lavelle, L. *et al.* Phase diagram of self-assembled viral capsid protein polymorphs. *J. Phys. Chem. B* **113**, 3813–3819 (2009).
- Joo, K. *et al.* Enhanced real-time monitoring of adeno-associated virus trafficking by virus-quantum dot conjugates. *ACS Nano* **5**, 3523–3535 (2011).
- Wang, Q. *et al.* High-Density Recombinant Adeno-Associated Viral Particles are Competent Vectors for *In Vivo* Transduction. *Hum. Gene Ther.* **27**, 971–981 (2016).
- Wobus, C. E. *et al.* Monoclonal antibodies against the adeno-associated virus type 2 (AAV-2) capsid: epitope mapping and identification of capsid domains involved in AAV-2-cell interaction and neutralization of AAV-2 infection. *J. Virol.* **74**, 9281–9293 (2000).
- Chen, H. Comparative observation of the recombinant adeno-associated virus 2 using transmission electron microscopy and atomic force microscopy. *Microsc. Microanal.* **13**, 384–389 (2007).

37. Summerford, C. & Samulski, R. J. Membrane-associated heparan sulfate proteoglycan is a receptor for adeno-associated virus type 2 virions. *J. Virol.* **72**, 1438–1445 (1998).
38. Tse, L. V., Moller-Tank, S., Meganck, R. M. & Asokan, A. Mapping and Engineering Functional Domains of the Assembly-Activating Protein of Adeno-associated Viruses. *J. Virol.* **92**, e00393–18 (2018).
39. Shi, W., Arnold, G. S. & Bartlett, J. S. Insertional mutagenesis of the adeno-associated virus type 2 (AAV2) capsid gene and generation of AAV2 vectors targeted to alternative cell-surface receptors. *Hum. Gene Ther.* **12**, 1697–1711 (2001).
40. Zhang, H. *et al.* Addition of six-His-tagged peptide to the C terminus of adeno-associated virus VP3 does not affect viral tropism or production. *J. Virol.* **76**, 12023–12031 (2002).
41. Steinbach, S., Wistuba, A., Bock, T. & Kleinschmidt, J. A. Assembly of adeno-associated virus type 2 capsids *in vitro*. *J. Gen. Virol.* **78**, 1453–1462 (1997).
42. Burgess, R. R. Refolding Solubilized Inclusion Body Proteins. in *Methods in Enzymology* **463**, 259–282 (Elsevier Inc., 2009).
43. Salganik, M. *et al.* Evidence for pH-Dependent Protease Activity in the Adeno-Associated Virus Capsid. *J. Virol.* **86**, 11877–11885 (2012).
44. Ohtake, S., Kita, Y. & Arakawa, T. Interactions of formulation excipients with proteins in solution and in the dried state. *Adv. Drug Deliv. Rev.* **63**, 1053–1073 (2011).
45. Xie, Q. *et al.* The atomic structure of adeno-associated virus (AAV-2), a vector for human gene therapy. *Proc. Natl. Acad. Sci. USA* **99**, 10405–10410 (2002).
46. Medrano, M. *et al.* Imaging and Quantitation of a Succession of Transient Intermediates Reveal the Reversible Self-Assembly Pathway of a Simple Icosahedral Virus Capsid. *J. Am. Chem. Soc.* **138**, 15385–15396 (2016).
47. Nicklin, S. A. *et al.* Efficient and selective AAV2-mediated gene transfer directed to human vascular endothelial cells. *Mol. Ther.* **4**, 174–181 (2001).
48. Pillay, S. *et al.* An essential receptor for adeno-associated virus infection. *Nature* **530**, 108–112 (2016).
49. Bartlett, J. S., Wilcher, R. & Samulski, R. J. Infectious entry pathway of adeno-associated virus and adeno-associated virus vectors. *J. Virol.* **74**, 2777–2785 (2000).
50. Grieger, J. C., Snowdy, S. & Samulski, R. J. Separate basic region motifs within the adeno-associated virus capsid proteins are essential for infectivity and assembly. *J. Virol.* **80**, 5199–5210 (2006).
51. Popa-Wagner, R. *et al.* Impact of VP1-Specific Protein Sequence Motifs on Adeno-Associated Virus Type 2 Intracellular Trafficking and Nuclear Entry. *J. Virol.* **86**, 9163–9174 (2012).
52. Maurer, A. C., Cepeda Diaz, A. K. & Vandenberghe, L. H. Residues on Adeno-associated Virus Capsid Lumen Dictate Interactions and Compatibility with the Assembly-Activating Protein. *J. Virol.* **93** (2019).
53. Feiner, R. C. *et al.* rAAV Engineering for Capsid-Protein Enzyme Insertions and Mosaicism Reveals Resilience to Mutational, Structural and Thermal Perturbations. *Int. J. Mol. Sci.* **20**, 5702 (2019).
54. Wu, P. *et al.* Mutational analysis of the adeno-associated virus type 2 (AAV2) capsid gene and construction of AAV2 vectors with altered tropism. *J. Virol.* **74**, 8635–8647 (2000).

## Acknowledgements

We acknowledge support for the Article Processing Charge by the Deutsche Forschungsgemeinschaft and the Open Access Publication Fund of Bielefeld University. D.T.L. acknowledges support by DAAD (Deutscher Akademischer Austauschdienst) for providing a PhD fellowship (Personal ref. no.: 91651068). We thank Kathrin Teschner and Julian Teschner for kindly providing rAAV2wt and A20 scFv-Fc antibody. We also want to thank Ann-Christin Moritzer (Structural Biochemistry, Department of Chemistry, Bielefeld University) for helping in DLS measurements, and Dario Anselmetti (Experimental Biophysics and Applied Nanoscience, Physics Department, Bielefeld University) for helping in AFM measurements.

## Author contributions

D.T.L., M.R. and K.M. conceived the study. D.T.L. performed the experiments (except for A.F.M. measurement), prepared figures, and wrote the initial manuscript. M.R. conducted A.F.M. measurements. M.R. and K.M. edited the manuscript. K.M. supervised the project. All authors discussed the experiments, read and approved the final manuscript.

## Competing interests

The authors declare no competing interests.

## Additional information

**Supplementary information** is available for this paper at <https://doi.org/10.1038/s41598-019-54928-y>.

**Correspondence** and requests for materials should be addressed to K.M.M.

**Reprints and permissions information** is available at [www.nature.com/reprints](http://www.nature.com/reprints).

**Publisher's note** Springer Nature remains neutral with regard to jurisdictional claims in published maps and institutional affiliations.



**Open Access** This article is licensed under a Creative Commons Attribution 4.0 International License, which permits use, sharing, adaptation, distribution and reproduction in any medium or format, as long as you give appropriate credit to the original author(s) and the source, provide a link to the Creative Commons license, and indicate if changes were made. The images or other third party material in this article are included in the article's Creative Commons license, unless indicated otherwise in a credit line to the material. If material is not included in the article's Creative Commons license and your intended use is not permitted by statutory regulation or exceeds the permitted use, you will need to obtain permission directly from the copyright holder. To view a copy of this license, visit <http://creativecommons.org/licenses/by/4.0/>.

© The Author(s) 2019

## Supplementary information

# Adeno-associated virus capsid protein expression in *Escherichia coli* and chemically defined capsid assembly

Dinh To Le<sup>1</sup>, Marco T. Radukic<sup>1</sup>, Kristian M. Müller<sup>1\*</sup>

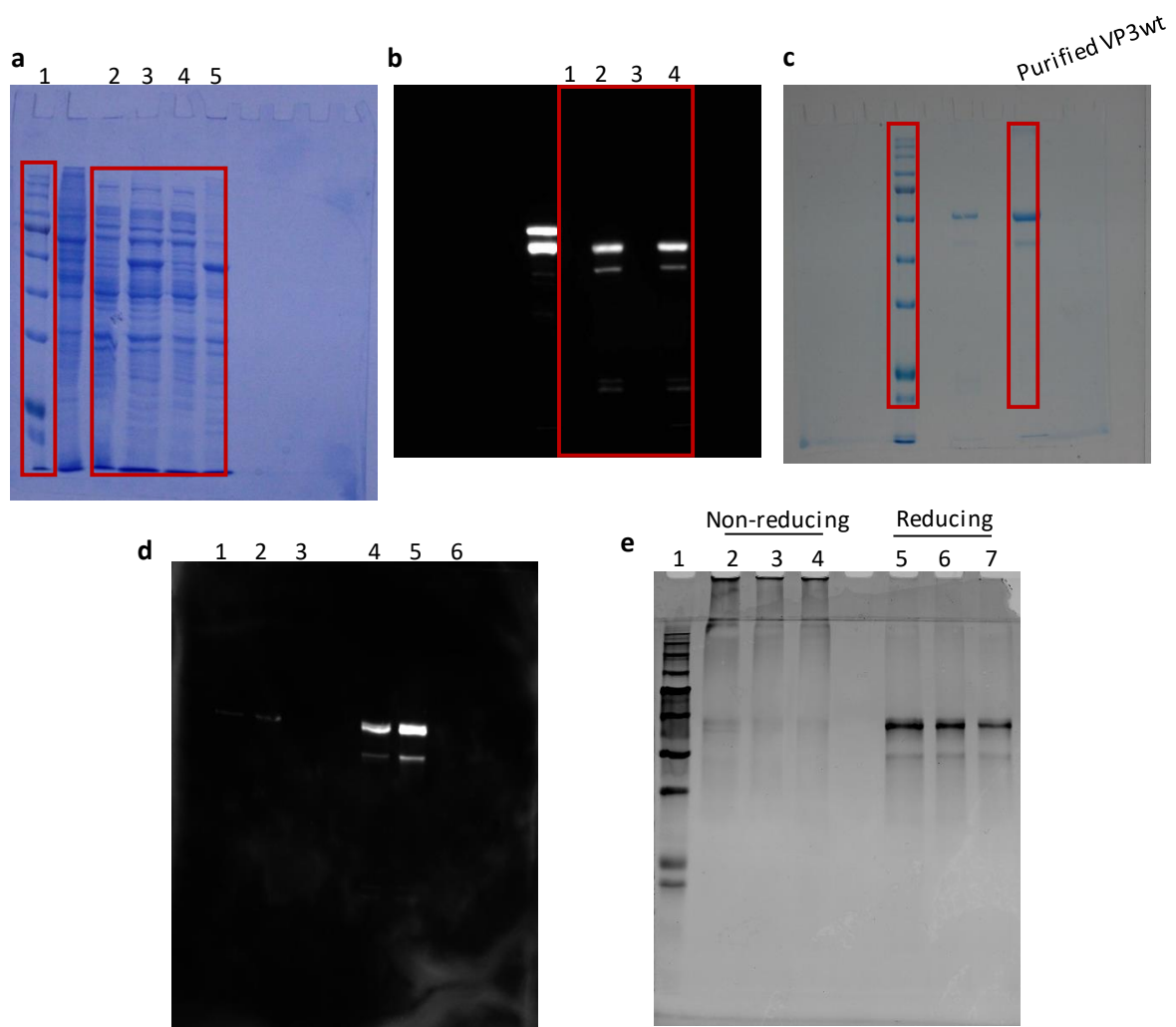
<sup>1</sup> Cellular and Molecular Biotechnology, Faculty of Technology, Bielefeld University, Bielefeld, Germany

\* Corresponding author: Kristian M. Müller, Cellular and Molecular Biotechnology, Bielefeld University, Universitätsstraße 25, 33615 Bielefeld, Germany; Email: kristian@syntbio.net

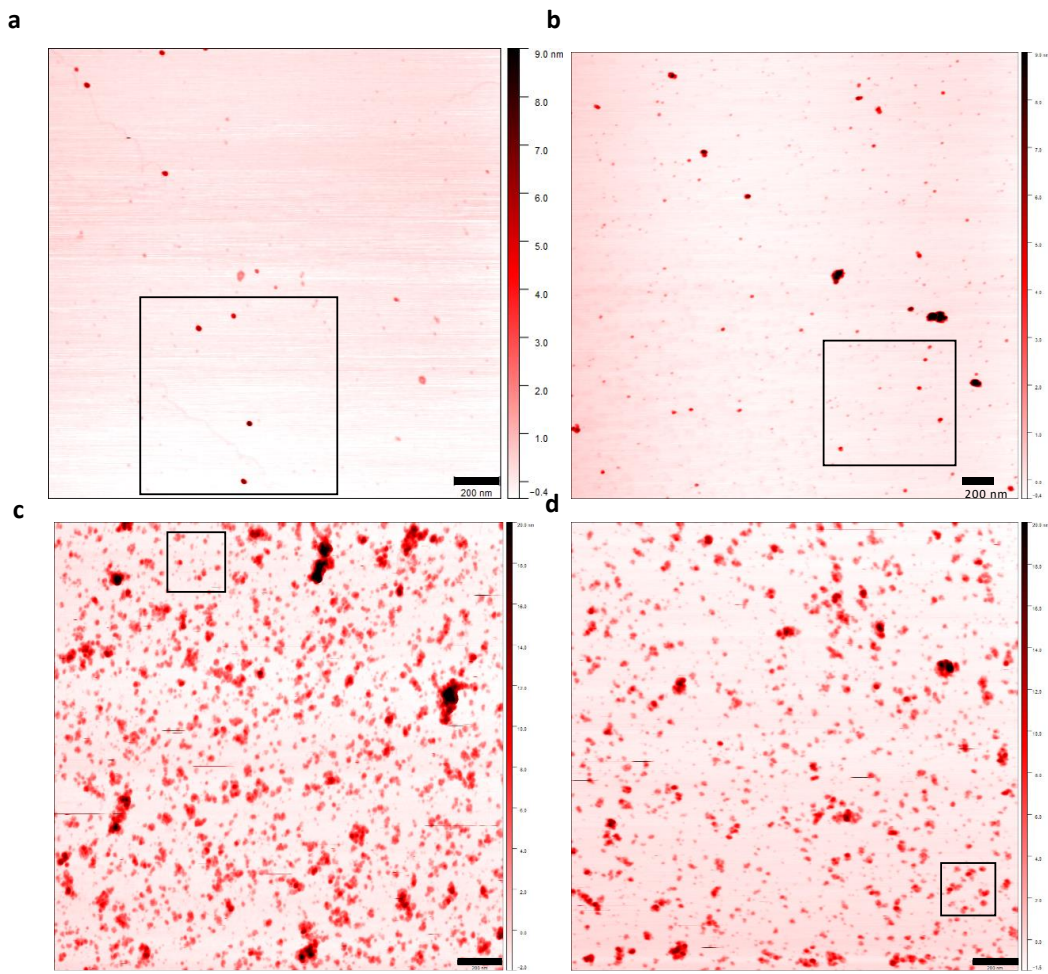
## SI contents

1	Supplementary figures .....	2
2	VP3 sequences.....	5
2.1	VP3wt coding sequence .....	5
2.2	VP3wt amino acid sequence .....	6
2.3	VP3 587His <sub>6</sub> coding sequence .....	6
2.4	VP3 587His <sub>6</sub> amino acid sequence.....	6
2.5	VP3 CTTEVHis <sub>6</sub> coding sequence .....	7
2.6	VP3 CTTEVHis <sub>6</sub> amino acid sequence .....	7

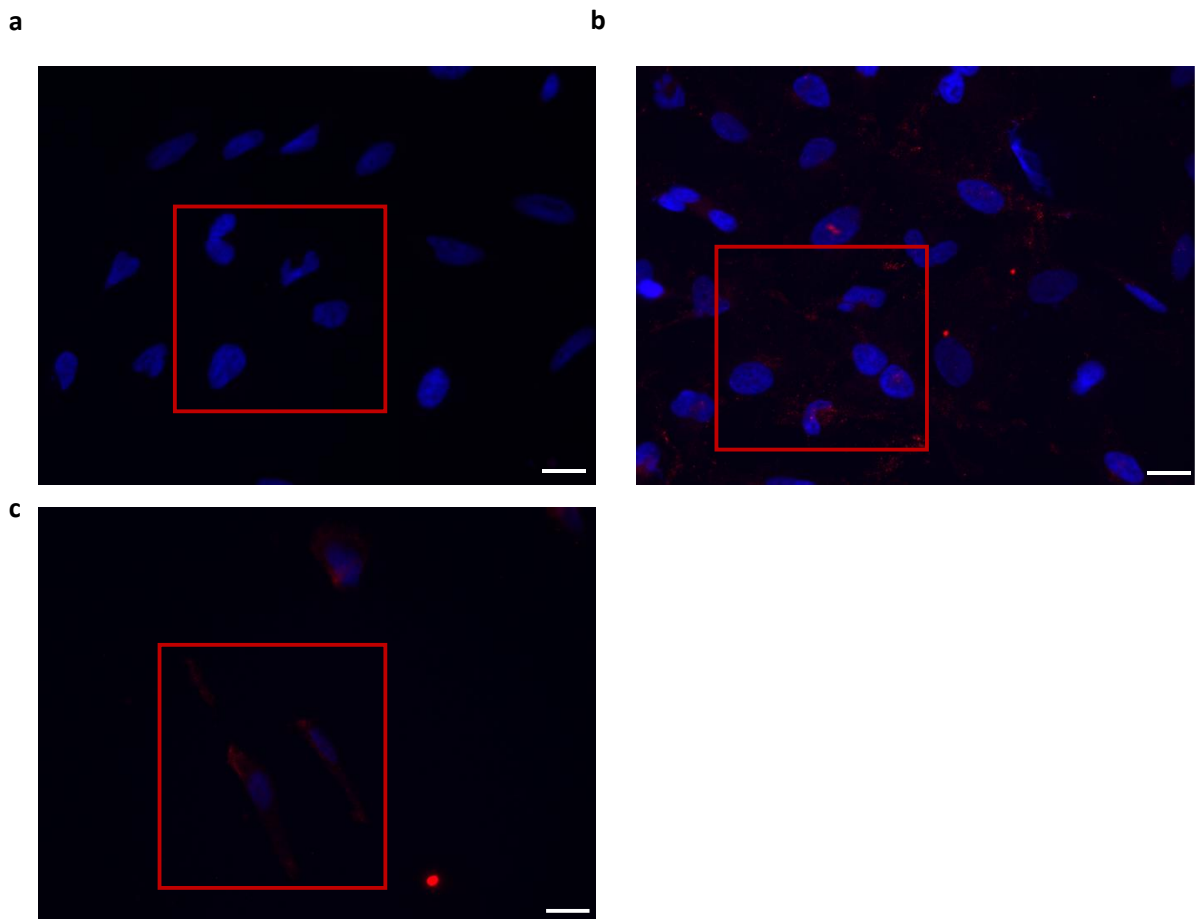
## 1 Supplementary figures



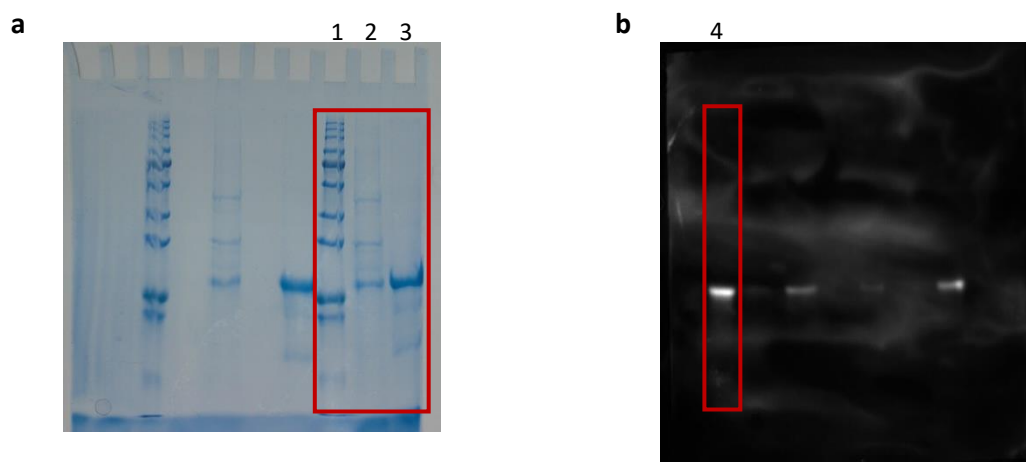
**Supplementary Figure S1:** Full-length gels and blots. (a), (b), (c) correspond to Fig. 1b, c, d in the manuscript. The red rectangles indicate cropped parts of the gels and blot. (d) Western blot analysis of VP3wt expression using plasmid pAK100 in *E. coli* RV308 at 18°C and 37°C; lane 1, whole-cell protein of *E. coli* RV308 post-induction with IPTG at 18°C; lane 2, insoluble fraction of intracellular protein post-induction with IPTG at 18°C; lane 3, soluble fraction of intracellular protein post-induction with IPTG at 18°C; lane 4, whole-cell protein of *E. coli* RV308 post-induction with IPTG at 37°C; lane 5, insoluble fraction of intracellular protein post-induction with IPTG at 37°C; lane 6, soluble fraction of intracellular protein post-induction with IPTG at 37°C. (e) Non-reducing and reducing SDS-PAGE of particles at pH 9 and samples after changing from pH 9 to pH 7.4 (before and after removal of aggregates); lane 1, protein standard; lane 2, particles at pH 9 in non-reducing condition; lane 3, 4, samples after change from pH 9 to pH 7.4, before and after removal of aggregates by centrifugation in non-reducing condition, respectively; lane 5, particles at pH 9 in reducing condition, lane 6 and 7, samples after changing from pH 9 to pH 7.4, before and after removal of aggregates by centrifugation in reducing conditions, respectively. We assume that the significant disulfide crosslinking seen in the gel occurs during sample boiling in SDS under non-reducing conditions.



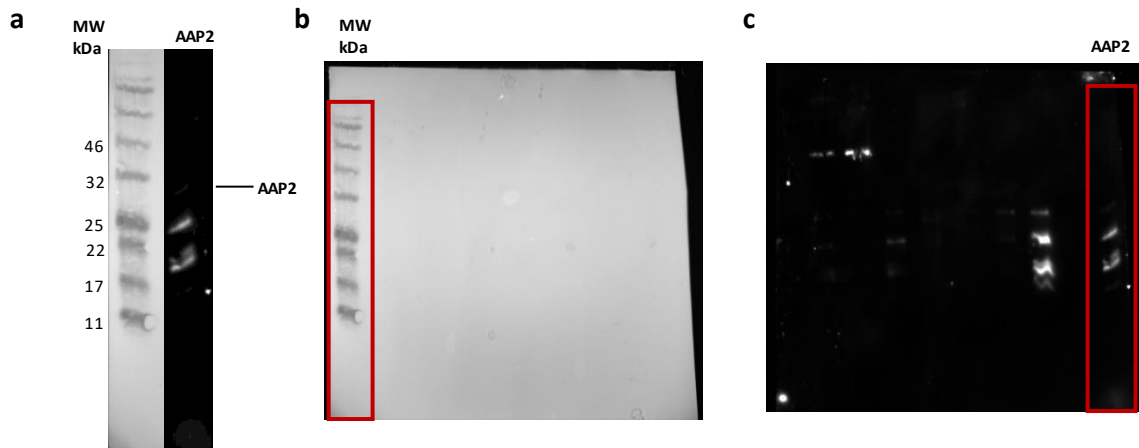
**Supplementary Figure S2:** Atomic force micrographs of (a) rAAV2, (b) VP3wt VLPs, (c) VP3 587His<sub>6</sub> VLPs (c) and (d) VP3 CTTEVHis<sub>6</sub> VLPs. The scale bars indicate 200 nm. (a), (b) correspond to Fig. 2c, d in the manuscript; (c), (d) correspond to Fig. 5c, g in the manuscript. The black squares indicate cropped parts of the images.



**Supplementary Figure S3:** Fluorescent microscopy of HeLa cells treated with rAAV2 or VP3wt VLPs. (a) untreated; (b) rAAV2; (c) VP3wt VLPs. All images show the overlay of rAAV2 or VP3wt VLPs (red) and nuclei (blue) channels. The scale bars indicate 25  $\mu\text{m}$ . (a), (b), (c) correspond to Fig. 3a, b, c in the manuscript. The red squares indicate cropped parts of the images.



**Supplementary Figure S4:** Full-length gel and blot of AAP2 expression in *E. coli* at 37°C. (a), (b) correspond to Fig. 4b in the manuscript. The red rectangles indicate cropped parts of the gel and blot.



**Supplementary Figure S5:** (a) Expression of AAP2 in *E. coli* at 18°C. The AAP2-degraded bands were detected by anti-His tag antibody. (b), (c) Full-length blots of AAP2 expression in *E. coli* at 18°C. The red rectangles indicate cropped parts of the blots.

## 2 VP3 sequences

### 2.1 VP3wt coding sequence

```

ATGGCAACCGTTCAGGCGCGCAATGGCAGATAATAATGAAGGTGCAGATGGTGTGGTAATAGCAGCGGT
AATTGGCATTGTGATAGCACCTGGATGGGTGATCGTGTATTACCACAAGCACCCGTACCTGGGCACTGCCGA
CCTATAATAACCATCTGTATAAACAATTAGCAGCCAGAGCGGTGCAAGCAATGATAATCATTATTTTGGTTAT
AGCACCCCGTGGGGCTATTTTGATTTAATCGTTTTCACTGCCATTTAGTCCGCGTGATTGGCAGCGTCTGATT
AATAACAATTGGGGTTTTCGTCCGAAACGCCTGAACTTTAACTGTTAATATCCAGGTGAAAGAAGTGACCCA
GAACGACGGCACCACCATTGCAAATAATCTGACCAGCACCGTTCAGGTTTTTACCGATAGCGAATATCAGC
TGCCTTATGTTCTGGGTAGCGCACATCAGGGTGTCTGCCACCGTTTTCCGGCAGATGTTTTATGGTTCGCGAG
TATGGTTATCTGACCCTGAATAATGGTAGCCAGGCAGTTGGTCGTAGCAGCTTTTATTGTCTGGAATATTTTCC
GAGCCAGATGCTGCGTACCGGTAATAACTTTACCTTAGCTATACCTTTGAGGATGTGCCGTTTCATAGCAGCT
ATGCACATAGCCAGAGCCTGGATCGTCTGATGAATCCGCTGATTGATCAGTATCTGTATTATCTGAGCCGTACC
AATACACCGAGCGGTACAACCACACAGAGCCGTCTGCAATTTAGTCAGGCAGGCGCAAGCGATATTCGTGATC
AGAGCCGTAATTGGCTGCCTGGTCCGTGTTATCGTCAGCAGCGTGTTAGCAAAACCAGCGCAGATAACAATAA
CAGCGAATATAGTTGGACCGGTGCCACCAATATCATCTGAATGGTCGTGATAGCCTGGTTAATCCGGGTCTCT
GCAATGGCCAGCCATAAAGATGATGAAGAAAAATTCTTTCCGCAGAGTGGCGTCTGATTTTTGGTAAACAGG
GTAGCGAAAAAACCAACGTGGATATCGAAAAAGTGATGATCACCGATGAAGAAGAGATTCGTACCACCAATC
CGTTTGGCAGCGAACAGTATGGTAGCGTTAGCACCAATCTGCAACGTGGTAATCGTCAGGCAGCAACCGCAG
ATGTTAATACCCAGGGTGTCTGCCTGGTATGGTTTGGCAGGATCGTGATGTTTATCTGCAAGGTCCGATTTGG
GCAAAAATTCGCATACCGATGGTCATTTTCATCCGAGTCCGCTGATGGGTGGTTTTGGTCTGAAACATCCGCC
TCCGAGATTCTGATTAAGAATACTCCGGTTCGGCAAATCCGAGCACCACTTTAGCGCAGCAAAATTTGCCA
GCTTTATTACCCAGTATAGTACCGGTCAGGTTAGCGTTGAAATTGAATGGGAACTGCAAAAAGAAAAACAGCAA
ACGTTGGAATCCGAAATTCAGTATACCAGCAACTATAACAAAAGCGTGAACGTGGATTTTACCGTGGATACC
AATGGTGTTTATAGCGAACCGCGTCCGATTGGCACCCGCTATCTGACACGTAATCTGTAA

```

## 2.2 VP3wt amino acid sequence

MATGSGAPMADNNEGADGVGNSSGNWHCDSTWMGDRVITSTRTWALPTYNNHLYKQISSQSGASNDNHYF  
GYSTPWGYFDNRFHCHFSRPDWQRLINNNWGRPKRLNFKLFNIQVKEVTQNDGTTIANLSTVQVFTDSEY  
QLPYVLGSAHQGLPPFPADVFMVPQYGYLTLNNGSQAVGRSSFYCLEYFPSQMLRTGNNFTFSYTFEDVPFHSSY  
AHSQSLDRLMNPLIDQYLYLSRTNTPSGTTTQSRQLQFSQAGASDIRDQSRNWLPGPCYRQQRVSKTSADNNNSEY  
SWTGATKYHLNGRDSLVPNGPAMASHKDDEEKFFPQSGVLIFGKQGSEKTNVDIEKVMITDEEEIRTTNPVATEQY  
GSVSTNLQRGNRQAATADVNTQGVLPGMVWQDRDVYLQGPWAKIPHTDGHFHPSPLMGGFGLKHPPPQILIK  
NTPVPANPSTTFSAAKFASFITQYSTGQVSVEIEWELQKENSKRWNPEIQYTSNYNKSVINVDFTVDTNGVYSEPRPI  
GTRYLTRNL

## 2.3 VP3 587His<sub>6</sub> coding sequence

the 587-loop insertion of His<sub>6</sub> is in boldface

ATGGCAACCGTTCAGGCGCGCCAATGGCAGATAATAATGAAGGTGCAGATGGTGTGGTAATAGCAGCGGT  
AATTGGCATTGTGATAGCACCTGGATGGGTGATCGTGTATTACCACAAGCACCCGTACCTGGGCACTGCCGA  
CCTATAATAACCATCTGTATAAACAATAGCAGCCAGAGCGGTGCAAGCAATGATAATCATTATTTGGTTAT  
AGCACCCCGTGGGGCTATTTGATTTAATCGTTTTACTGCCATTCAGTCCGCGTGATTGGCAGCGTCTGATT  
AATAACAATTGGGTTTTCTGCCGAAACGCCTGAACTTAACTGTTAATATCCAGGTGAAAGAAGTGACCCA  
GAACGACGGCACCACCATTGCAATAATCTGACCAGCACCGTTCAGGTTTTTACCGATAGCGAATATCAGC  
TGCCTTATGTTCTGGGTAGCGCACATCAGGGTGTCTGCCACCGTTTCCGGCAGATGTTTTATGGTTCCGCG  
TATGGTTATCTGACCCTGAATAATGGTAGCCAGGCAGTTGGTCGTAGCAGCTTTTATTGTCTGGAATATTTCC  
GAGCCAGATGCTGCGTACCGGTAATAACTTTACCTTAGCTATACCTTGAGGATGTGCCGTTTCATAGCAGCT  
ATGCACATAGCCAGAGCCTGGATCGTCTGATGAATCCGCTGATTGATCAGTATCTGTATTATCTGAGCCGTACC  
AATACACCGAGCGGTACAACCACACAGAGCCGTCTGCAATTTAGTCAGGCAGGCGCAAGCGATATTCGTGATC  
AGAGCCGTAATTGGCTGCCTGGTCCGTGTTATCGTCAGCAGCGTGTAGCAAACCAGCGCAGATAACAATAA  
CAGCGAATATAGTTGGACCGGTGCCACCAATATCATCTGAATGGTCGTGATAGCCTGGTTAATCCGGGTCT  
GCAATGGCCAGCCATAAAGATGATGAAGAAAAATTCTTCCGCAGAGTGGCGTTCTGATTTTTGGTAAACAGG  
GTAGCGAAAAACCAACGTGGATATCGAAAAAGTGATGATCACCGATGAAGAAGAGATTCGTACCACCAATC  
CGGTTGCGACCGAACAGTATGGTAGCGTTAGCACCAATCTGCAACGTGGTAAT**CATCATCACCATCATCATCG**  
TCAGGCAGCAACCGCAGATGTTAATACCAGGGTGTCTGCCTGGTATGGTTTGGCAGGATCGTGATGTTTAT  
CTGCAAGGTCCGATTTGGGCAAAAATTCCGCATACCGATGGTCATTTTCATCCGAGTCCGCTGATGGGTGGTTT  
TGGTCTGAAACATCCGCTCCGCAGATTCTGATTAAGAATACTCCGGTCCGGCAAAATCCGAGCACCACCTTA  
GCGCAGCAAAAATTGCCAGCTTATTACCCAGTATAGTACCGGTCAGGTTAGCGTTGAAATTGAATGGGAACT  
GCAAAAAGAAAACAGCAAACGTTGGAATCCGGAAATTAGTATACCAGCAACTATAACAAAAGCGTGAACGT  
GGATTTTACCGTGGATACCAATGGTGTATAGCGAACCGCGTCCGATTGGCACCCGCTATCTGACACGTAATC  
TGTA

## 2.4 VP3 587His<sub>6</sub> amino acid sequence

MATGSGAPMADNNEGADGVGNSSGNWHCDSTWMGDRVITSTRTWALPTYNNHLYKQISSQSGASNDNHYF  
GYSTPWGYFDNRFHCHFSRPDWQRLINNNWGRPKRLNFKLFNIQVKEVTQNDGTTIANLSTVQVFTDSEY  
QLPYVLGSAHQGLPPFPADVFMVPQYGYLTLNNGSQAVGRSSFYCLEYFPSQMLRTGNNFTFSYTFEDVPFHSSY  
AHSQSLDRLMNPLIDQYLYLSRTNTPSGTTTQSRQLQFSQAGASDIRDQSRNWLPGPCYRQQRVSKTSADNNNSEY  
SWTGATKYHLNGRDSLVPNGPAMASHKDDEEKFFPQSGVLIFGKQGSEKTNVDIEKVMITDEEEIRTTNPVATEQY  
GSVSTNLQRGN**HHHHHR**QAATADVNTQGVLPGMVWQDRDVYLQGPWAKIPHTDGHFHPSPLMGGFGLKH

PPPQILIKNTPVPANPSTTFSAAKFASFITQYSTGQVSVEIEWELQKENSKRWNPEIQYTSNYNKSVINVDFTVDTNG  
VYSEPRPIGTRYLTRNL

## 2.5 VP3 CTTEVHis<sub>6</sub> coding sequence

the C-terminal extension is in boldface

ATGGCAACCGGTT CAGGCGCGCCAATGGCAGATAATAATGAAGGTGCAGATGGTGTGGTAATAGCAGCGGT  
AATTGGCATTGTGATAGCACCTGGATGGGTGATCGTGTTATTACCACAAGCACCCGTACCTGGGCACTGCCGA  
CCTATAATAACCATCTGTATAAACAATTAGCAGCCAGAGCGGTGCAAGCAATGATAATCATTATTTTGGTTAT  
AGCACCCCGTGGGGCTATTTGATTTAATCGTTTTCACTGCCATTTAGTCCGCGTGATTGGCAGCGTCTGATT  
AATAACAATTGGGGTTTTCGTCCGAAACGCCTGAACTTTAACTGTTAATATCCAGGTGAAAGAAGTGACCCA  
GAACGACGGCACCACCATTGCAAATAATCTGACCAGCACCGTTCAGGTTTTTACCGATAGCGAATATCAGC  
TGCCTTATGTTCTGGGTAGCGCACATCAGGGTGTCTGCCACCGTTTTCCGGCAGATGTTTTATGGTTCCGCGAG  
TATGGTTATCTGACCCTGAATAATGGTAGCCAGGCAGTTGGTCGTAGCAGCTTTTATTGTCTGGAATATTTTCC  
GAGCCAGATGCTGCGTACCGGTAATAACTTTACCTTAGCTATACCTTTGAGGATGTGCCGTTTCATAGCAGCT  
ATGCACATAGCCAGAGCCTGGATCGTCTGATGAATCCGCTGATTGATCAGTATCTGTATTATCTGAGCCGTACC  
AATACACCGAGCGGTACAACCACACAGAGCCGTCTGCAATTTAGTCAGGCAGGCGCAAGCGATATTCGTGATC  
AGAGCCGTAATTGGCTGCCTGGTCCGTGTTATCGTCAGCAGCGTGTTAGCAAACCAGCGCAGATAACAATAA  
CAGCGAATATAGTTGGACCGGTGCCACCAAATATCATCTGAATGGTCGTGATAGCCTGGTTAATCCGGGTCTCT  
GCAATGGCCAGCCATAAAGATGATGAAGAAAAATTCTTTCCGCAGAGTGGCGTTCTGATTTTTGGTAAACAGG  
GTAGCGAAAAACCAACGTGGATATCGAAAAAGTGATGATCACCGATGAAGAAGAGATTCGTACCACCAATC  
CGGTTGCGACCGAACAGTATGGTAGCGTTAGCACCAATCTGCAACGTGGTAATCGTCAGGCAGCAACCGCAG  
ATGTTAATACCCAGGGTGTCTGCCTGGTATGGTTTGGCAGGATCGTGATGTTTATCTGCAAGGTCCGATTTGG  
GCAAAAATTCGCATACCGATGGTCATTTTCATCCGAGTCCGCTGATGGGTGGTTTTGGTCTGAAACATCCGCC  
TCCGCAGATTCTGATTAAGAATACTCCGGTTCGGCAAATCCGAGCACCACTTTAGCGCAGCAAAAATTTGCCA  
GCTTTATTACCCAGTATAGTACCGGTCAGGTTAGCGTTGAAATTGAATGGGAACTGCAAAAAGAAAAACAGCAA  
ACGTTGGAATCCGAAAATTCAGTATACCAGCAACTATAACAAAAGCGTGAACGTGGATTTTACCGTGGATACC  
AATGGTGTATATAGCGAACCGCGTCCGATTGGCACCCGCTATCTGACACGTAATCTGGGTCAGTTTTATCTGAA  
**TGAACATCATCACCATCATCATTAA**

## 2.6 VP3 CTTEVHis<sub>6</sub> amino acid sequence

MATGSGAPMADNNEGADGVGNSSGNWHCDSTWMGDRVITSTRTWALPTYNNHLYKQISSQSGASNDNHFY  
GYSTPWGYFDFNRFHCHFSRPDWQRLINNNWGFPRKRLNFKLFNIQVKEVTQNDGTTTIANNLTSTVQVFTDSEY  
QLPYVLGSAHQGLPPFPADVFMVPQYGYLTLNNGSQAVGRSSFYCLEYFPSQMLRTGNNFTFSYTFEDVPPFHSSY  
AHSQSLDRLMNPLIDQYLYLSRTNTPSGTTTQSRLQFSQAGASDIRDQSRNWLPGPCYRQQRVSKTSADNNNSEY  
SWTGATKYHLNDRSLVNP GPAMASHKDDEEKFFPQSGVLIFGKQGSEKTNVDIEKVMITDEEEIRTNPVATEQY  
GSVSTNLQRGNRQAATADVNTQGVLPGMVWQDRDVYLQGPWIWAKIPHTDGHFHPSPLMGGFGLKHPPPQILIK  
NTPVPANPSTTFSAAKFASFITQYSTGQVSVEIEWELQKENSKRWNPEIQYTSNYNKSVINVDFTVDTNGVYSEPRPI  
GTRYLTRNL**GQFYLNHHHHHH**

Title:

**AAV Capsid Assembly Using *Escherichia coli***

Authors:

Dinh To Le, Marco T. Radukic, Kristian M. Müller

or validation. Moreover, visualizing the distribution of many variants while preserving spatial context will offer insights into AAV biology, which can include entry mechanisms as well as cell- and tissue-type associated expression.

### 156. SMRT Sequencing Allows High-Throughput Analysis of a Whole Capsid Shuffled AAV Capsid Library Following CNS Selection in Mice and NHPs

Widler Casy<sup>1</sup>, Xin Chen<sup>1</sup>, Thomas Dong<sup>1</sup>, Yuhui Hu<sup>1</sup>, Mohammed Kanchwala<sup>1</sup>, Chao Xing<sup>1</sup>, Stephen Braun<sup>2</sup>, Bruce Bunnell<sup>2</sup>, Steven Gray<sup>1</sup>

<sup>1</sup>Pediatrics, University of Texas Southwestern Medical Center, Dallas, TX, <sup>2</sup>Tulane National Primate Research Center, New Orleans, LA

The outcomes from AAV capsid engineering efforts since its discovery have been both encouraging and promising, but it remains a major challenge to engineer AAVs that are seamlessly compatible across mouse and non-human primate (NHP) species. The use of AAV variant libraries coupled with various selection strategies has become an increasingly useful strategy to generate novel AAV variants with enhanced properties. However, analysis of capsids recover post-selection has been hampered by the inability to accurately sequence the entire capsid gene in a high-throughput manner. As a result, many library approaches are shifting to small changes in the capsid such as peptide insertions or barcodes, which can be sequenced quickly and easily. This has restricted the diversity of capsids in libraries, shifting the field away from whole capsid shuffled libraries. We suggest that this could restrict libraries to select for relatively incremental changes in vector tropism. To overcome this and enable the use of whole-capsid changes to be evaluated, we employed single molecule real-time (SMRT) sequencing analysis for a high throughput evaluation of recovered whole AAV capsid genes. SMRT sequencing has the advantage of sequencing the entire capsid gene in a single read with high accuracy, enabling sequencing the entire shuffled capsid rather than only an insert region or barcode. We hypothesized that paralleled AAV whole capsid shuffling and directed evolution in both mice and NHPs have the propensity to yield AAVs that are compatible across mice and NHPs and that will be serologically distinct from natural AAVs. As first steps to test this hypothesis, we have developed a new approach which consists of AAV whole capsid shuffling and directed evolution in mice and NHPs conducted in parallel. The AAV library was subjective to mainly target tissues of the central nervous system (CNS) in these animals following intrathecal (IT) injection. SMRT sequencing was able to identify over 15 thousand distinct whole AAV capsid sequences present in the library. After the first round of IT injection of this library in mice, SMRT sequencing analysis of the AAV genomes that were recovered post injection showed that 65 new capsids were recovered from mouse brain and 31 new capsids were recovered from mouse spinal cord. IT injection of this library in NHPs revealed that hundreds of unique AAVs from the library were able to target the brain while over a thousand unique AAV variants targeted the spinal cord. In depth analysis of the sequencing data revealed that several of the AAVs that targeted the mouse brain were also able to target regions of NHP brain. Currently, we are screening the viruses that are present at the highest frequency in mouse and NHP brains

by packaging them with GFP followed by IT injection in mice. The analysis of selected library clones thus far demonstrates the utility of SMRT sequencing for high-content screening of whole capsid shuffled libraries, which was previously limited to analysis by capsid gene subcloning and Sanger sequencing. This approach should expand the options for library-based AAV capsid development beyond barcoded analysis and/or peptide insertion libraries.

### 157. AAV Capsid Assembly Using *Escherichia Coli*

DINH TO LE

Cellular and Molecular Biotechnology, Bielefeld University, Bielefeld, Germany

Virus-like particles (VLPs) have been used for numerous therapeutic applications, especially in vaccination and drug delivery. While the recombinant adeno-associated virus (rAAV) has emerged as a leading candidate in gene therapy with approved products, rAAV production in HEK-293 or insect cells still remains a challenge. We established and analyzed AAV VLP production using *E. coli* cells. Such VLPs could be used as a bio-nanoparticles and also serve as a starting material for DNA encapsidation for production of rAAV type moieties. To do this, first the widely used serotype-AAV2 was chosen. The codon usage of the AAV2 VP3, the main structural capsid protein, coding gene was optimized, cloned into a pET vector, expressed effectively in inclusion bodies in *E. coli* and purified by ion-exchange chromatography. AAV2 VLPs were obtained by a chemically defined refolding reaction. Specifically, the purified protein in a denaturing buffer with 5 M GuHCl was dialyzed against an assembly buffer containing 2 M L-arginine for 60 h. In addition, we also tested for an assembly-activating-protein (AAP)-independent AAV serotype. VP3 capsid protein of AAV serotype 5, the most genetically divergent AAV serotype among known 13 human and non-human primate serotypes, was successfully expressed in soluble form and able to develop AAV5 VLPs inside *E. coli*. The correct formation of AAV2 and AAV5 VLPs was confirmed by ELISA with anti-intact-AAV antibodies and imaging by atomic force microscopy. The biological transduction functionality was confirmed with an internalization assay into human HeLa cells. Furthermore, to increase VLP production and assess the effect of AAP on capsid assembly, we expressed and purified AAP2 and added the protein to the *in-vitro* assembly reaction of AAV2 VP3. For AAV5 VLPs, due to the formation of capsid within *E. coli*, we co-transformed AAP5 and AAV5 VP3 genes into *E. coli* cells using two pET vectors harboring different antibiotic resistance genes. The results showed that AAP2 directly aided AAV2 VLPs formation and that AAP5 supported AAV5 capsid assembly inside *E. coli*. To our knowledge, this is the first report of AAV VLP production within a chemically defined reaction or inside *E. coli* cells. Even though the VLP production needs to be optimized in the future, our finding opens an opportunity to explore AAV VLPs in biomedical applications and paves the way to investigate rAAV production using *E. coli*.

Title:

**Expression and concomitant assembly of adeno-associated virus-like particles in  
*Escherichia coli***

Authors:

Dinh To Le, Marco T. Radukic, Kathrin Teschner, Lukas Becker, Kristian M. Müller

# Expression and concomitant assembly of adeno-associated virus-like particles in *Escherichia coli*

Dinh To Le<sup>‡</sup>, Marco T. Radukic<sup>‡</sup>, Kathrin Teschner<sup>‡</sup>, Lukas Becker<sup>‡</sup>, Kristian M. Müller<sup>‡,\*</sup>

<sup>‡</sup>Cellular and Molecular Biotechnology, Faculty of Technology, Bielefeld University, Bielefeld, Germany

## Supporting Information

**ABSTRACT:** Virus-like particles (VLPs) have been used for numerous pharmaceutical applications, especially in vaccination and drug delivery. The recombinant adeno-associated virus (rAAV), known as a leading candidate in gene therapy, has also been produced in mammalian cells for vaccine development. Here, we established a new direct method to produce AAV VLPs using *E. coli*. VP3 capsid proteins of AAV serotype 5 (AAV5) were expressed and formed VLPs inside *E. coli* during expression. The VLPs were purified and the correct formation was confirmed by ELISA with an intact-capsid antibody and imaging by atomic force microscopy. The biological functionality was proven with an internalization assay on HeLa cells. Furthermore, co-expression of the assembly-activating protein of AAV5 and the capsid protein in *E. coli* led to an increase in capsid formation. This is the first evidence that AAV VLPs are produced in *E. coli* opening an opportunity to explore AAV VLPs in biomedical applications.

Virus-like particles (VLPs) are non-infectious nanoparticles formed by assembly of protein monomers, which have been widely used in various applications including vaccine development with many products on the market,<sup>1</sup> drug delivery,<sup>2</sup> and materials science.<sup>3</sup> In addition, VLPs also offer a platform for genetic payloads in gene therapy.<sup>2</sup> These particles have been produced using different expression hosts, such as mammalian cells, insect cells, yeast and bacteria. Among them, bacteria, in particular, *E. coli* has been frequently used in VLP production due to its low cost and high yield.<sup>4</sup>

Adeno-associated virus (AAV) is a non-enveloped, single-stranded DNA (ssDNA) virus of 20-25 nm in diameter and a member of the *Parvoviridae* family genus *Dependoparvovirus*. The AAV genome is divided into two open-reading-frame (ORF) cassettes (namely, Rep and Cap). The Cap ORF cassette encodes the three capsid proteins (VP1, VP2 and VP3) that only differ in their N-terminus. The VP3 capsid protein is the structural protein and able to form VP3-only capsids.<sup>5</sup> In addition, the Cap ORF cassette also codes for an assembly-activating protein (AAP) to promote capsid assembly.<sup>6</sup> Interestingly, among 13 known human and non-human primate AAV serotypes, AAV5 is the most genetically divergent AAV and its capsid can assemble without AAP.<sup>7,8</sup>

AAV is a promising candidate in biomedical applications because of its lack of pathogenicity and low immunogenicity. In recent studies, AAV VLPs have been produced for vaccination by displaying different epitopes.<sup>9-11</sup> Production of AAV VLPs was achieved by different approaches, including capsid protein expression and concomitant assembly in yeast,<sup>12</sup> HEK293 cells<sup>10</sup> or even by *in vitro* assembly of capsid proteins.<sup>13,14</sup> Moreover, recombinant AAV (rAAV) vectors have emerged as a favorable system in gene therapy with products approved by the U.S. Food and Drug Administration (FDA) and European Medicines Agency (EMA) and many ongoing clinical trials worldwide.<sup>15</sup> Currently, rAAV is produced in HEK293 and *Spodoptera frugiperda* Sf9 cells, which still remains challenging.<sup>16</sup> AAV assembly has been proposed as initial capsid

formation followed by ssDNA genome filling into preformed capsid.<sup>17</sup> Thus, to produce rAAV for gene therapy, AAV VLPs could be used as a starting material for loading DNA.

In our study, we expressed VP3 protein of AAV5 and assembled VLPs directly in *E. coli*. Co-expression of AAP5 and capsid proteins in *E. coli* significantly improved VLP production. This work thereby provides a new approach to produce AAV VLPs.

## RESULTS AND DISCUSSION

### Expression of AAV5 VP3 proteins

As AAV is able to form capsids with only VP3 proteins,<sup>5</sup> we optimized the codon usage of the AAV5 VP3 (VP3) gene for *E. coli* expression and cloned it into a pET vector (**Figure 1a**). To assess the protein expression level, we tested two different expression temperatures (at 37°C and 18°C) and performed a western blot analysis with the B1 antibody, which recognizes unassembled VP proteins. As a result, VP3 protein was observed with an apparent mass of about 60 kDa at both 37°C and 18°C, which is consistent with its theoretical molecular weight (59.55 kDa, Geneious 9.1.8) (**Figure 1b**). At 37°C, VP3 protein mainly formed inclusion bodies (**Figure 1b**, lane 1, 2, 3), conversely, VP3 protein was highly soluble at 18°C (**Figure 1b**, lane 4, 5, 6). We attribute this to the impact of temperature to reduce protein misfolding during expression in *E. coli*. It is known that aggregation during protein folding is favored at higher temperatures due to the temperature dependence of hydrophobic interaction.<sup>18,19</sup> Interestingly, in addition to the full-size VP3 protein band, other bands with lower molecular weight were also detected by the antibody. The B1 antibody specifically recognizes an epitope at the C-terminus of AAV capsid proteins,<sup>20</sup> indicating that AAV5 VP3 protein was not stable during expression. This occurrence is possibly due to either an intrinsic protease activity of the protein or *E. coli* protease activity, a phenomenon we also observed during AAV2 VP3 expression in *E. coli*.<sup>14</sup>

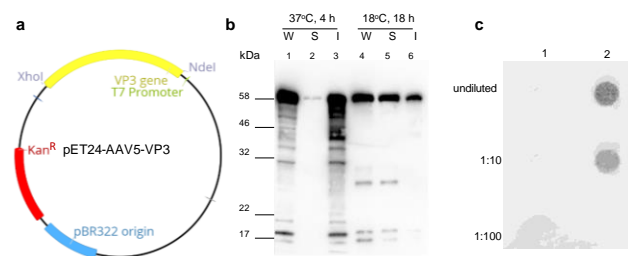


**Figure 1.** Expression of AAVS VP3 protein in *E. coli*. (a) Plasmid map of pET24-AAV5-VP3. (b) Western blot analysis of VP3 expression with B1 antibody (whole-cell proteins (W), soluble fraction (S) and insoluble fraction (I) of intracellular proteins); Lane 1, 2, 3: expression for 4 h at 37°C; Lane 4, 5, 6: expression for 18 h at 18°C. (c) Dot blot of *E. coli* cell extracts with anti-AAV5 (intact capsid) antibody (ADK5a); lane 1, untransformed *E. coli*

BL21(DE3) cell extracts; lane 2, *E. coli* BL21(DE3) containing pET24-AAV5-VP3 vector cell extracts.

Since a large part of the VP3 protein was soluble with the 18°C expression protocol, we analyzed whether VLPs spontaneously formed during capsid protein expression. To detect VLPs in the supernatant lysed *E. coli* extract, we performed a dot blot assay using an anti-intact-AAV5 antibody (ADK5a), which only binds AAV5-assembled capsids but not unassembled capsid proteins.<sup>21</sup> The results presented in **Figure 1c** indicate the presence of VLPs in *E. coli* harboring the pET24-AAV5-VP3 vector after induction and expression (**Figure 1c**, lane 2), while there was no particle detected in the control sample of cell extracts from untransformed *E. coli* (**Figure 1c**, lane 1).

### Purification and characterization of VLPs

We next tested to purify the assembled particles by POROS AAVX affinity resin which contains a single-domain [<sub>VIH</sub>H] antibody fragment known for AAV-capsid specific binding.<sup>22</sup> The SDS-PAGE of

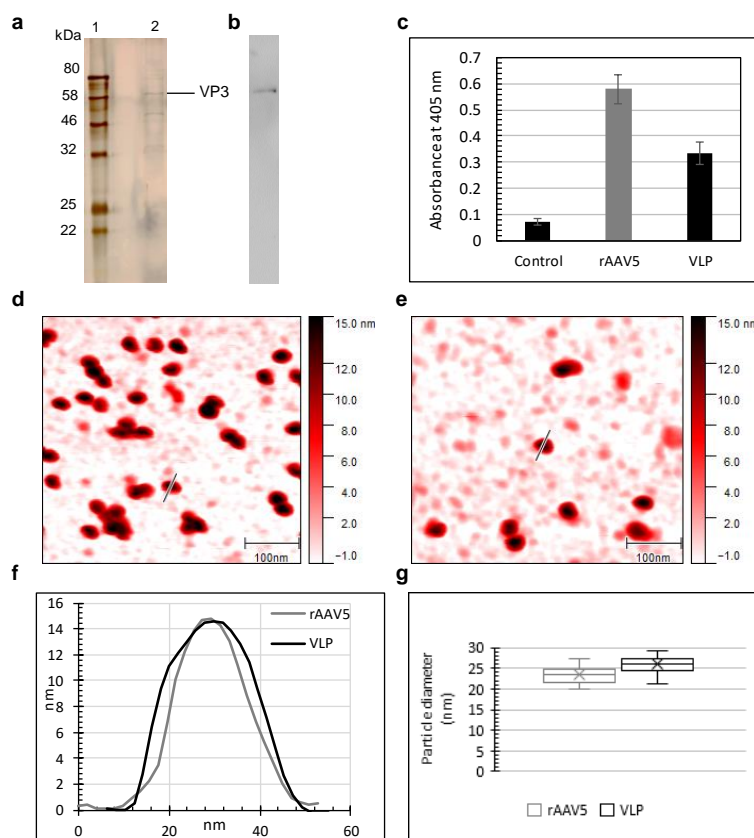


**Figure 2.** Purification and characterization of AAVS VLPs. (a) SDS-PAGE of purified VLPs; Lane 1, protein ladder; Lane 2, sample after purification by POROS AAVX resin column. (b) Western blot analysis of sample after purification (Figure 2a (lane 2)) with B1 antibody. (c) ELISA probed with anti-AAV5 (intact capsid) antibody (ADK5a). (d) AFM image of rAAV5 produced in HEK293. (e) AFM image of VLPs produced in *E. coli*. (f) Height profile of rAAV5 and VLPs. (g) Box plot of the size distribution of rAAV5 and VLPs determined by AFM ( $n = 20$ , mean  $\pm$  SD, box from first to third quartile, cross median marker).

the purified sample displayed a band with the expected size of VP3 protein (**Figure 2a**, lane 2), which was also identified by the B1 antibody (**Figure 2b**), even though other contaminating proteins remained.

To detect the purified VLPs, we performed an ELISA with the ADK5a antibody. Besides the VLPs, we used rAAV5 produced in HEK293 cells and also purified by POROS AAVX resin as control. Our ELISA data shown in **Figure 2c** reaffirmed the presence of AAV5 VLPs after purification. Furthermore, we used atomic force microscopy (AFM) to analyze the size and morphology of the purified particles. We found homogeneous particles with a size of about 25 nm and a height of around 15 nm in both rAAV5 and VLP samples (**Figure 2d, e, f, g**). This is characteristic of AAV particles and consistent with a previous report.<sup>23</sup> Notably, the previous reports demonstrated that the insertion of a peptide into a surface loop of AAV5 capsid did not interfere capsid formation in HEK293 production.<sup>24,25</sup> Thus, the AAV5 capsids produced in *E. coli* can be used to display an antigen of interest for vaccine development.

Moreover, to detect possible encapsidation of host nucleic acid polymers (DNA/RNA) during VLP production in *E. coli*, an agarose gel electrophoresis of heated rAAV5 and VLPs was performed. After staining with SYBR Gold, no nucleic acid polymers were found inside VLPs, while a DNA band, potentially rAAV5 genomes, was detected within rAAV5 (**Figure S1**). Within the limits of this analysis, we conclude that capsids should mostly be empty and this finding offers the prospect of loading of genetic materials into the empty VLPs either within *E. coli* cells or in an *in-vitro* reaction.

### Internalization of VLPs

We used human HeLa cells to assess the cellular uptake of VLPs and thereby their biological activity. HeLa cells were incubated with rAAV5 and AAV5 VLPs, fixed, permeabilized and stained with the ADK5a antibody and a fluorescent coupling secondary antibody. After 2 h of incubation, both rAAV5 and VLPs were found inside the cells (**Figure 3b, c**), while no signal was detectable in the buffer control (**Figure 3a**). The particle distribution after 2h-incubation is in line with the previous reports of rAAV5 internalization into HeLa cells.<sup>26,27</sup> AAV5 enters into the cell by receptor-mediated endocytosis. The particles initially bind to  $\alpha 2-3$  sialic acid on the cell surface as a primary receptor,<sup>28</sup> then interact with the platelet-derived growth factor receptor (PDGFR)<sup>29</sup> and the polycystic kidney disease 1 (PKD1) domain of the AAV receptor.<sup>30,31</sup> Since the recognized domains of AAV5 are present on the VP3-only capsid exterior, VP3-only AAV5 capsids are able to internalize into cells. This finding demonstrated the biological activity of VLPs and offers an application of VLPs in drug delivery into human cells.

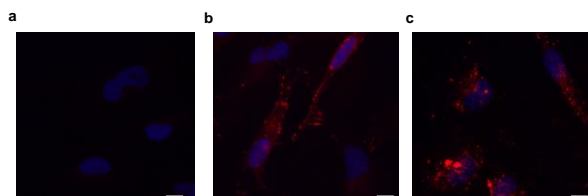


**Figure 3.** Internalization of rAAV5 and VLPs. HeLa cells were treated with (a) buffer, (b) rAAV5 or (c) VLPs. Samples were stained with the ADK5a antibody followed by a Dylight 594 conjugated secondary antibody (red) and DAPI (blue). Scale bars are 10  $\mu$ m.

### Co-expression of VP3 protein and AAP5

rAAV5 is able to form capsids in the absence of AAP5 in HEK293 cells, although the supply of AAP5 *in trans* improves rAAV production significantly.<sup>8</sup> Therefore, we cloned AAP5 with a His<sub>6</sub>-tag coding sequence 3' of the gene into another pET vector with the different antibiotic resistance gene (pET21-AAP5, **Figure 4a**) and co-transformed *E. coli* with this vector and pET24-AAV5-VP3 vector (**Figure 1a**). The addition of a tag at the C-terminus of the AAP protein has previously been shown not to interfere with AAP function,<sup>32</sup> and allows the detection of AAP5 expression. AAP5 was successfully co-expressed with VP3 in *E. coli* as proven by western blot analysis (**Figure 4b, c**). Notably, in addition to the experimentally expected band of AAP5 (about 33 kDa),<sup>8</sup> degraded fragments were also visible (**Figure 4b**), which is in agreement with a previous report of AAP5 expression in HEK293 cells.<sup>33</sup> Furthermore, the expression of VP3 protein in *E. coli* expressing also AAP5 was lower compared to VP3 expression in *E. coli* harboring VP3 only (**Figure 4c**). However, even though a reduced amount of VP3 protein was observed, the assembled particles significantly increased in the co-expression system as shown by western blot analysis with the B1 antibody of POROS-AAVX purified particles (**Figure 4d**) and about 3.6-fold by sandwich ELISA with PKD1 as a capture agent (produced in *E. coli*, **Figure S2**) and the ADK5a antibody as detection antibody (**Figure 4e**). This is the first evidence that AAP5 helps to improve the capsid production in *E. coli* and hints again on the fundamental chaperone activity of AAP, which was reported during AAV capsid production using mammalian cells,<sup>6</sup> yeast<sup>34</sup> and *in vitro* assembly.<sup>14</sup>

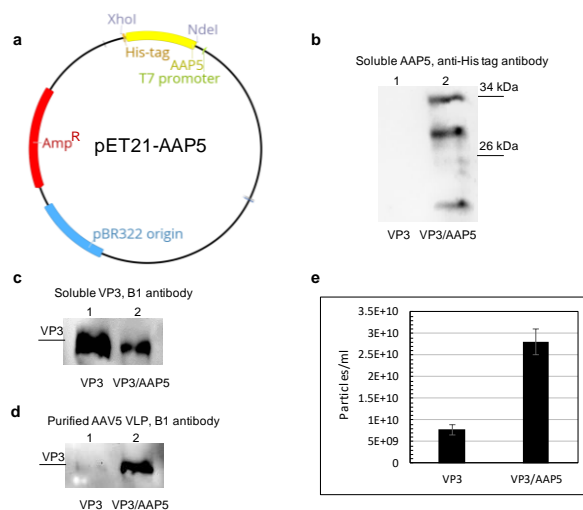


**Figure 4.** Co-expression of AAP5 and VP3 in *E. coli*. (a) Plasmid map of pET21-AAP5. A His<sub>6</sub>-tag was inserted at the C-terminus of AAP5. (b) Western blot with the anti-His-tag antibody of the soluble fraction of intracellular proteins after induction and expression;

lane 1, *E. coli* harboring pET24-AAV5-VP3; lane 2, *E. coli* harboring pET24-AAV5-VP3 and pET21-AAP5. (c) Western blot of the soluble fraction of intracellular proteins with the B1 antibody after induction and expression; lane 1, *E. coli* harboring pET24-AAV5-VP3; lane 2, *E. coli* harboring pET24-AAV5-VP3 and pET21-AAP5. (d) Western blot of the purified VLP samples with the B1 antibody; lane 1, *E. coli* harboring pET24-AAV5-VP3; lane 2, *E. coli* harboring pET24-AAV5-VP3 and pET21-AAP5. (e) Number of purified VLPs estimated by sandwich ELISA using PKD1 protein and the ADK5a antibody with qPCR-titered rAAV5 from HEK293-production taken as reference.

In summary, we report here a new, feasible method to produce AAV5 VLPs, based on the straightforward expression of capsid proteins in *E. coli* and subsequent direct purification of VLPs from the soluble protein fraction. Capsid proteins showed the ability to form VLPs within *E. coli*. Moreover, the co-expression of the assembly-activating protein AAP5 and capsid protein VP3 using two plasmids with different antibiotic-resistance genes was successfully achieved and led to an increased particle production. In addition, we presented a new sandwich ELISA method using PKD1 domain of AAV receptor as a capture agent and AKD5a antibody that can be used to detect or titer AAV5 VLPs and rAAV5. Even though the VLP production needs to be optimized in the future, our study paves the way for AAV VLPs production using *E. coli* for different biomedical applications and emphasizes *E. coli* as a possible host for future production of transduction-competent AAV.

## MATERIALS AND METHODS

### Cloning and expression of AAV5 VP3 protein in *E. coli*

The AAV5 VP3 coding sequence was codon-optimized, chemically synthesized (GeneArt/ThermoFisher Scientific, DNA sequence given in **Supplementary Information 5.1**) and cloned into the bacterial expression vector pET24b (Novagen/Merck) via *NdeI* and *XhoI* sites. Transformed *E. coli* was cultured in LB medium containing 50 µg/ml kanamycin at 37°C until OD<sub>600</sub> reached 1.5. Then, IPTG was added to a final concentration of 0.4 mM and the 1-liter medium was incubated in an orbital shaker with a speed of 170 rpm at either 37°C for 4 h or 18°C for 18 h.

### Co-expression of VP3 and AAP5 in *E. coli*

The AAP5 coding sequence (PCR-amplified from a Rep2Cap5 vector, sequence given in **Supplementary Information 5.2**) was cloned into vector pET21a (Novagen/Merck). pET21-AAP5 and pET24-AAV5-VP3 were co-transferred into *E. coli* BL21(DE3) and plated onto LB agar media containing 50 µg/ml kanamycin and 100 µg/ml ampicillin. The co-expression of proteins was performed as described above (post-induction at 18°C, in LB medium containing kanamycin and ampicillin).

### Purification of VLPs

*E. coli* cells were harvested at 5,000×g, 4°C for 10 min. Pelleted cells were washed, resuspended in PBS buffer and disrupted with a French press at 1,000 psi. Afterwards, soluble proteins were obtained by centrifugation at 20,000×g, 4°C for 20 min. Proteins were then precipitated from this solution by ammonium sulfate (12.52 g

per 40 ml of sample, on ice 1 h) and VLPs were purified from the pellet with POROS™ CaptureSelect™ AAVX Affinity resin (A36739, ThermoFisher Scientific). Briefly, a 0.5 ml resin packed column was equilibrated with 5 ml 1 × PBS buffer (137 mM NaCl, 2.6 mM KCl, 10 mM Na<sub>2</sub>HPO<sub>4</sub>, 1.8 mM KH<sub>2</sub>PO<sub>4</sub>) plus 0.1 M NaCl, pH 7.4 at 1 ml/min. The column was then loaded with the sample and washed with 10 ml equilibration buffer at 1 ml/min. Bound particles were eluted using 5 ml citric acid (100 mM, pH 2) and neutralized with 1 M Tris-HCl (pH 8.7), concentrated and changed to 500 µl Hank's Balanced Salt Solution (HBSS) buffer with a centrifugal filter unit of 100 kDa molecular weight cut-off.

### rAAV5 production

As a control for VLPs produced in *E. coli*, we produced rAAV5 in HEK293 cells with a three-plasmid system. Briefly, HEK293 cells were seeded with a density of 3 × 10<sup>6</sup> cells per 10 cm dish and cultivated overnight. Cells were then transfected with 15 µg of total DNA per dish including Rep2Cap5 plasmid, pHelper plasmid and ITR-containing plasmid with a molar ratio of 1:1:1 using calcium phosphate. After 3-day incubation, the cells were harvested and lysed by three freeze-thaw cycles. rAAV5 was then purified using a POROS AAVX column as described above.

### SDS-PAGE and Western Blot

Samples of protein were separated on a 12% polyacrylamide with 4% stacking gel. Protein staining was either performed with silver nitrate or Coomassie, or protein was transferred onto a nitrocellulose membrane (88018, ThermoFisher Scientific) for western blot analysis. The membrane was then blocked with 10% (w/v) non-fat dry milk powder (Applichem) in TBS buffer, and incubated with either B1 antibody (1: 100 dilution, 61058, Progen) for VP3 protein detection or anti-His-tag antibody (1: 2,000 dilution, Tetra-His, 34670, Qjagen) for AAP5 detection for 1 h at room temperature. To detect the proteins, Goat anti-mouse IgG (H+L), HRP conjugated secondary antibody (1: 2,500 dilution, 31430, ThermoFisher Scientific) and SuperSignal™ West Pico PLUS Chemiluminescent Substrate (34580, ThermoFisher Scientific) were used. Images were acquired with a Fusion FX camera system (Vilber).

### Dot blot assay

Nitrocellulose membrane (88018, ThermoFisher Scientific) was submerged in TBS buffer and mounted onto a dot blot apparatus (Bio-Rad). *E. coli* cell extracts were diluted (10 and 100 times) in TBS buffer to 250 µl and applied to the membrane with a flow rate of 250 µl per 45 seconds. Afterwards, the membrane was removed from the apparatus and washed with TBS buffer for 10 min. The following steps were performed as described above for western blot analysis.

### ELISA

To detect AAV5 VLPs, VLP and rAAV5 samples (7.14 × 10<sup>9</sup> particles/ml) were captured onto a Nunc MaxiSorp 96 well plate at 4°C overnight and an anti-AAV5 mouse monoclonal antibody (intact-particle, ADK5a antibody, 610148, Progen) was used for detection. The wells were blocked with 0.8% BSA in PBS for 1 h, followed by

incubation with the ADK5a antibody (1: 250 dilution, in blocking buffer) for 1 h at room temperature. The secondary antibody was an anti-mouse-HRP conjugate (31430, ThermoFisher Scientific, 1: 2,000 dilution). Then, 1 g/L 2,2'-326 Azinobis [3-ethylbenzothiazoline-6-sulfonic acid]-diammonium salt (ABTS) was added and incubated for 30 min. Optical density was measured by a microplate reader (PowerWaveHT, BioTek) at 405 nm.

We also used a sandwich ELISA with recombinant PKD1 domain of the AAV receptor (recombinant PKD1 production protocol given in **Supplementary Figure S2**) for capture and an anti-AAV5 mouse monoclonal (ADK5a) antibody for detection to titer AAV5 VLPs. Briefly, PKD1 (200 ng/well) was applied to a Nunc MaxiSorp 96 well plate and incubated at 4°C overnight. Then, 0.8% BSA was used to block the wells before adding AAV5 VLPs and ADK5a antibody, respectively. Further steps of the ELISA were performed as mentioned above.

### AFM measurement of particles

A multimode 8 AFM (Bruker) with Tap300AI-G cantilevers (BudgetSensors) in tapping mode in air was used to measure the particles. Briefly, particles with a concentration of about  $5 \times 10^{12}$  particles/ml in HBSS buffer were spotted onto freshly cleaved mica and incubated for three minutes. Then, wash the mica with distilled water and dry it under a gentle nitrogen flow. The AFM images and particle height profiles were generated using Gwyddion 2.49 software.

### Internalization of rAAV5 and VLPs

Internalization of VLPs was studied using human HeLa cells. First, HeLa cells were seeded on a L-lysine-coated coverslip (1.2 cm diameter) placed in 24-well plates with a density of  $3 \times 10^4$  cells/well overnight. Then, the cells were incubated with rAAV5 or VLPs (about  $10^5$  particles/cell) for 2 h at 37°C, followed by fixation with 4% paraformaldehyde and permeabilization with 1% Triton X-100. BSA 1% was applied for blocking for 30 min and the ADK5a antibody in blocking buffer was added and incubated at 4°C overnight. For detection, a fluorescently label antibody (Goat anti-Mouse IgG (H+L) Secondary Antibody, Dylight 594, 35510, ThermoFisher Scientific, 1:500) was used. After washing, the cells were incubated with 4',6-diamidino-2-phenylindole (DAPI) for 10 min at room temperature and the coverslips were mounted on glass slides, followed by image acquisition on a Leica DMI6000 B microscopy, 40x objective.

### ASSOCIATED CONTENT

#### Supporting Information

Figure S1: Agarose gel electrophoresis of heated rAAV5 and VLPs, Figure S2: Expression and purification of PKD1. Strain, plasmids, primers and DNA sequences used in this study are given.

### AUTHOR INFORMATION

#### Corresponding author

\*: Email: kristian@syntbio.net

### ORCID

Dinh To Le: 0000-0002-9383-4199

Marco T. Radukic: 0000-0001-8721-966X

Kristian M. Müller: 0000-0002-7914-0625

### Author Contributions

D.T.L., M.T.R. and K.M.M. conceived the study. D.T.L. performed the experiments, drew the figures and wrote the initial manuscript. M.T.R. performed AFM measurements. K.T. produced PKD1 protein for ELISA. L.B. performed the preliminary protein expression in *E. coli*. K.M.M. supervised the project. All authors read and approved the final manuscript.

### Notes

The authors declare no competing interests.

### ACKNOWLEDGMENTS

We thank Dr. Molly Strom (The Sainsbury Wellcome Centre for Neural Circuits and Behaviour, University College London, UK) for kindly providing the Rep2Cap5 vector for rAAV5 production in HEK293 cells. DTL acknowledges support by DAAD (Deutscher Akademischer Austauschdienst) for providing a PhD fellowship (Personal ref. no.: 91651068).

### ABBREVIATIONS

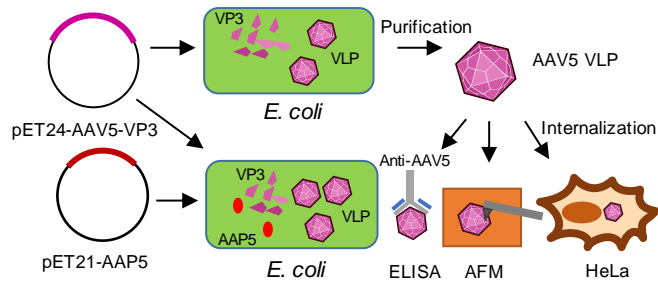
VLPs, virus-like particles; rAAV, recombinant adeno-associated virus; IPTG, isopropyl  $\beta$ -D-thiogalactopyranoside; SDS-PAGE, sodium dodecyl sulfate polyacrylamide gel electrophoresis; AFM, atomic force microscopy; ELISA, enzyme-linked immunosorbent assay; BSA, Bovine serum albumin; PKD1, polycystic kidney disease 1; PBS, phosphate-buffered saline; HBSS, Hank's balanced salt solution; TBS, tris-buffered saline.

### REFERENCES

- (1) Roldão, A., Mellado, M. C. M., Castilho, L. R., Carrondo, M. J. T., and Alves, P. M. (2010) Virus-like particles in vaccine development. *Expert Rev. Vaccines* 9, 1149–1176.
- (2) Rohovie, M. J., Nagasawa, M., and Swartz, J. R. (2017) Virus-like particles: Next-generation nanoparticles for targeted therapeutic delivery. *Bioeng. Transl. Med.* 2, 43–57.
- (3) Lee, S. Y., Lim, J. S., and Harris, M. T. (2012) Synthesis and application of virus-based hybrid nanomaterials. *Biotechnol. Bioeng.* 109, 16–30.
- (4) Huang, X., Wang, X., Zhang, J., Xia, N., and Zhao, Q. (2017) Escherichia coli-derived virus-like particles in vaccine development. *npj Vaccines* 2, 3.
- (5) Sonntag, F., Köther, K., Schmidt, K., Weghofer, M., Raupp, C., Nieto, K., Kuck, A., Gerlach, B., Böttcher, B., Müller, O. J., Lux, K., Hörer, M., and Kleinschmidt, J. A. (2011) The Assembly-Activating Protein Promotes Capsid Assembly of Different Adeno-Associated Virus Serotypes  $\gamma$ . *J. Virol.* 85, 12686–12697.
- (6) Sonntag, F., Schmidt, K., and Kleinschmidt, J. A. (2010) A viral

- assembly factor promotes AAV2 capsid formation in the nucleolus. *Proc. Natl. Acad. Sci. U. S. A.* 107, 10220–10225.
- (7) Gao, G., Vandenbergh, L. H., Alvira, M. R., Lu, Y., Calcedo, R., Zhou, X., and Wilson, J. M. (2004) Clades of Adeno-Associated Viruses Are Widely Disseminated in Human Tissues. *J. Virol.* 78, 6381–6388.
- (8) Earley, L. F., Powers, J. M., Adachi, K., Baumgart, J. T., Meyer, N. L., Xie, Q., Chapman, M. S., and Nakai, H. (2017) Adeno-associated Virus (AAV) Assembly-Activating Protein Is Not an Essential Requirement for Capsid Assembly of AAV Serotypes 4, 5, and 11. *J. Virol.* 91, e01980-16.
- (9) Singer, J., Manzano-Szalai, K., Fazekas, J., Thell, K., Bentley-Lukschal, A., Stremnitzer, C., Roth-Walter, F., Weghofer, M., Ritter, M., Tossi, K. P., Hörer, M., Michaelis, U., and Jensen-Jarolim, E. (2016) Proof of concept study with an HER-2 mimotope anticancer vaccine deduced from a novel AAV-mimotope library platform. *Oncoimmunology* 5, 1–11.
- (10) Nieto, K., Weghofer, M., Sehr, P., Ritter, M., Sedlmeier, S., Karanam, B., Seitz, H., Müller, M., Kellner, M., Hörer, M., Michaelis, U., Roden, R. B. S., Gissmann, L., and Kleinschmidt, J. A. (2012) Development of AAVLP(HPV16/31L2) particles as broadly protective HPV vaccine candidate. *PLoS One* 7, e39741.
- (11) Nieto, K., and Salvetti, A. (2014) AAV vectors vaccines against infectious diseases. *Front. Immunol.* 5, 1–9.
- (12) Backovic, A., Cervelli, T., Salvetti, A., Zentilin, L., Giacca, M., and Galli, A. (2012) Capsid protein expression and adeno-associated virus like particles assembly in *Saccharomyces cerevisiae*. *Microb. Cell Fact.* 11, 124.
- (13) Steinbach, S., Wistuba, A., Bock, T., and Kleinschmidt, J. A. (1997) Assembly of adeno-associated virus type 2 capsids in vitro. *J. Gen. Virol.* 78, 1453–1462.
- (14) Le, D. T., Radukic, M. T., and Müller, K. M. (2019) Adeno-associated virus capsid protein expression in *Escherichia coli* and chemically defined capsid assembly. *Sci. Rep.* 9, 19631.
- (15) Wang, D., Tai, P. W. L., and Gao, G. (2019) Adeno-associated virus vector as a platform for gene therapy delivery. *Nat. Rev. Drug Discov.* 18, 358–378.
- (16) Clément, N., and Grieger, J. C. (2016) Manufacturing of recombinant adeno-associated viral vectors for clinical trials. *Mol. Ther. - Methods Clin. Dev.* 3, 16002.
- (17) King, J. A., Dubielzig, R., Grimm, D., and Kleinschmidt, J. A. (2001) DNA helicase-mediated packaging of adeno-associated virus type 2 genomes into preformed capsids. *EMBO J.* 20, 3282–3291.
- (18) Schellman, J. A. (1997) Temperature, stability, and the hydrophobic interaction. *Biophys. J.* 73, 2960–2964.
- (19) Baldwin, R. L. (1986) Temperature dependence of the hydrophobic interaction in protein folding. *Proc. Natl. Acad. Sci.* 83, 8069–8072.
- (20) Wobus, C. E., Hügler-Dörr, B., Girod, A., Petersen, G., Hallek, M., and Kleinschmidt, J. A. (2000) Monoclonal antibodies against the adeno-associated virus type 2 (AAV-2) capsid: epitope mapping and identification of capsid domains involved in AAV-2-cell interaction and neutralization of AAV-2 infection. *J. Virol.* 74, 9281–9293.
- (21) Kuck, D., Kern, A., and Kleinschmidt, J. A. (2007) Development of AAV serotype-specific ELISAs using novel monoclonal antibodies. *J. Virol. Methods* 140, 17–24.
- (22) Nass, S. A., Mattingly, M. A., Woodcock, D. A., Burnham, B. L., Ardinger, J. A., Osmond, S. E., Frederick, A. M., Scaria, A., Cheng, S. H., and O’Riordan, C. R. (2018) Universal Method for the Purification of Recombinant AAV Vectors of Differing Serotypes. *Mol. Ther. - Methods Clin. Dev.* 9, 33–46.
- (23) Bernaud, J., Rossi, A., Fis, A., Gardette, L., Aillot, L., Büning, H., Castelnovo, M., Salvetti, A., and Faivre-Moskalenko, C. (2018) Characterization of AAV vector particle stability at the single-capsid level. *J. Biol. Phys.* 44, 181–194.
- (24) Khabou, H., Desrosiers, M., Winckler, C., Fouquet, S., Auregan, G., Bemelmans, A. P., Sahel, J. A., and Dalkara, D. (2016) Insight into the mechanisms of enhanced retinal transduction by the engineered AAV2 capsid variant -7m8. *Biotechnol. Bioeng.* 113, 2712–2724.
- (25) Arnold, G. S., Sasser, A. K., Stachler, M. D., and Bartlett, J. S. (2006) Metabolic Biotinylation Provides a Unique Platform for the Purification and Targeting of Multiple AAV Vector Serotypes. *Mol. Ther.* 14, 97–106.
- (26) Keiser, N. W., Yan, Z., Zhang, Y., Lei-Butters, D. C. M., and Engelhardt, J. F. (2011) Unique Characteristics of AAV1, 2, and 5 Viral Entry, Intracellular Trafficking, and Nuclear Import Define Transduction Efficiency in HeLa Cells. *Hum. Gene Ther.* 22, 1433–1444.
- (27) Bantel-Schaal, U., Hub, B., and Kartenbeck, J. (2002) Endocytosis of Adeno-Associated Virus Type 5 Leads to Accumulation of Virus Particles in the Golgi Compartment. *J. Virol.* 76, 2340–2349.
- (28) Kaludov, N., Brown, K. E., Walters, R. W., Zabner, J., and Chiorini, J. A. (2001) Adeno-Associated Virus Serotype 4 (AAV4) and AAV5 Both Require Sialic Acid Binding for Hemagglutination and Efficient Transduction but Differ in Sialic Acid Linkage Specificity. *J. Virol.* 75, 6884–6893.
- (29) Di Pasquale, G., Davidson, B. L., Stein, C. S., Martins, I., Scudiero, D., Monks, A., and Chiorini, J. A. (2003) Identification of PDGFR as a receptor for AAV-5 transduction. *Nat. Med.* 9, 1306–1312.
- (30) Pillay, S., Meyer, N. L., Puschnik, A. S., Davulcu, O., Diep, J., Ishikawa, Y., Jae, L. T., Wosen, J. E., Nagamine, C. M., Chapman, M. S., and Carette, J. E. (2016) An essential receptor for adeno-associated virus infection. *Nature* 530, 108–112.
- (31) Zhang, R., Xu, G., Cao, L., Sun, Z., He, Y., Cui, M., Sun, Y., Li, S., Li, H., Qin, L., Hu, M., Yuan, Z., Rao, Z., Ding, W., Rao, Z., and Lou, Z. (2019) Divergent engagements between adeno-associated viruses with their cellular receptor AAVR. *Nat. Commun.* 10, 3760.
- (32) Tse, L. V., Moller-Tank, S., Meganck, R. M., and Asokan, A. (2018) Mapping and Engineering Functional Domains of the Assembly-Activating Protein of Adeno-associated Viruses. *J. Virol.* 92, e00393-18.
- (33) Grosse, S., Penaud-Budloo, M., Herrmann, A.-K., Börner, K., Fakhiri, J., Laketa, V., Krämer, C., Wiedtke, E., Gunkel, M., Ménard, L., Ayuso, E., and Grimm, D. (2017) Relevance of Assembly-Activating Protein for Adeno-associated Virus Vector Production and Capsid Protein Stability in Mammalian and Insect Cells. *J. Virol.* 91, e01198-17.
- (34) Barajas, D., Aponte-Ubillus, J. J., Akeefe, H., Cinek, T., Peltier, J., and Gold, D. (2017) Generation of infectious recombinant Adeno-associated

virus in *Saccharomyces cerevisiae*. *PLoS One* 12, e0173010.



For Table of Contents Only

---

1 **Supplementary material:**  
 2 **Expression and concomitant assembly of adeno-associated virus-**  
 3 **like particles in *Escherichia coli***  
 4

5 Dinh To Le<sup>‡</sup>, Marco T. Radukic<sup>‡</sup>, Kathrin Teschner<sup>‡</sup>, Lukas Becker<sup>‡</sup>, Kristian M. Müller<sup>‡\*</sup>

6 <sup>‡</sup> Cellular and Molecular Biotechnology, Faculty of Technology, Bielefeld University, Bielefeld, Germany

7 <sup>\*</sup>Correspondence: Kristian M. Müller, email: kristian@syntbio.net

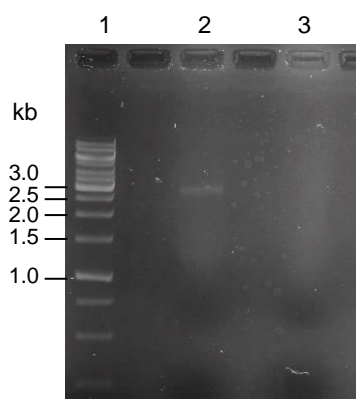
8 **CONTENTS**

9	1. Agarose gel electrophoresis of heated rAAV5 and AAV5 VLPs.....	2
10	2. Expression and purification of PKD1 in <i>E. coli</i> .....	2
11	3. Strain and plasmids used in this study.....	3
12	4. Primer sequences.....	3
13	5. DNA sequences.....	3
14	5.1 AAV5 VP3 DNA coding sequence.....	3
15	5.2 AAV5 DNA coding sequence with His <sub>6</sub> -tag.....	4

16

17

18 **1. Agarose gel electrophoresis of heated rAAV5 and AAV5 VLPs**

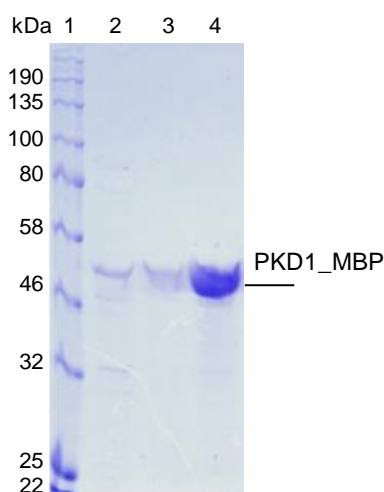


19

20 **Figure S1.** Agarose gel electrophoresis (rAAV5 and VLPs were heated at 95°C for 10 min, run in 1% Agarose gel, TAE  
 21 buffer and stained by SYBR Gold nucleic acid gel stain (S11494, ThermoFisher Scientific). Lane 1: DNA ladder; lane 2:  
 22 rAAV5 ( $4 \times 10^{10}$  rAAV particles/well); lane 3: VLPs ( $4 \times 10^{10}$  VLPs/well).

23 **2. Expression and purification of PKD1 in *E. coli***

24 PKD1 genetically fused to the maltose-binding protein (MBP) and a C-terminal His<sub>6</sub>-tag was cloned into a  
 25 pET24b vector and the pET24-PKD1\_MBP vector was then introduced into *E. coli* BL21(DE3) cells. Protein  
 26 expression was induced with IPTG (0.1 mM) and the protein was expressed for 4 h at 37°C. The cells were  
 27 harvested by centrifugation at 8,000×g for 10 min and lysed with a French Press at 1,000 psi. Afterwards, the  
 28 sample was centrifuged at 20,000×g for 5 min and the protein of interest was purified by Ni-NTA column from  
 29 the supernatant. Briefly, samples were applied onto a 1 ml Ni-NTA column equilibrated with IMAC buffer A  
 30 (500 mM NaCl, 50 mM Tris, 10 mM Imidazole, pH 8.0). Then, the column was washed with IMAC buffer A  
 31 containing 7% IMAC buffer B (500 mM NaCl, 50 mM Tris, 500 mM Imidazole, pH 8) and eluted with 100%  
 32 IMAC buffer B.



33

34 **Figure S2.** Expression and purification of PKD1. Lane 1: protein ladder; lane 2: Proteins before purification; lane 3: Wash  
 35 fraction; lane 4: Proteins after purification.

36

37 **3. Strain and plasmids used in this study**

Strain/plasmids	Description	Ref.
<i>E. coli</i> BL21 (DE3)	<i>F<sup>-</sup> ompT hsdSB(rB<sup>-</sup>mB<sup>-</sup>) gal dcm (DE3)</i>	Fermentation Technology Group, Bielefeld University, Germany
pET24b		Novagen/Merck
pET21a		Novagen/Merck
pET24-AAV5-VP3	AAV5 VP3 was inserted into pET24b via <i>NdeI</i> and <i>XhoI</i>	This study
pET21-AAP5	AAP5 was inserted into pET21a via <i>NdeI</i> and <i>XhoI</i>	This study
pET24-PKD1_MBP	PKD1_MBP was inserted into pET24b via <i>NdeI</i> and <i>BamHI</i>	This study

38

39 **4. Primer sequences**

40

Name	Sequence	Description
VP3_Seq1	CCACGATGCGTCCGGCGTAG	Sequencing primers of VP3
VP3_Seq2	CGTATGTTGTTGGCAATGG	
VP3_Seq3	CAGCCTGCAAATCCGGGTAC	
AAP5_F	ATATAATATACATATGGACCCAGCGGATCCC AG	Forward primer to amplify AAP5
AAP5_R	ATATACTCGAGTTAATGATGATGGTGATGAT GGCGTCGCGTAACCGTACTGC	Revert primer to amplify AAP5
AAP5_Seq	CCACGATGCGTCCGGCGTAG	Sequencing primer of AAP5

41

42 **5. DNA sequences**

## 43 5.1 AAV5 VP3 DNA coding sequence

44 ATGTCTGCAGGTGGTGGTGGTCCGCTGGGTGATAATAATCAGGGTGCAGATGGTGTGGTA  
45 ATGCAAGCGGTGATTGGCATTGTGATAGCACCTGGATGGGTGATCGTGTTGTTACCAAAGC  
46 ACCCGTACCTGGGTTCTGCCGAGCTATAATAACCATCAGTATCGTGAAATCAAAGCGGTAG  
47 CGTTGATGGTAGCAATGCAAATGCATATTTGGTTATAGCACCCCGTGGGGCTATTTGATT  
48 TTAATCGTTTTCATAGCCATTGGAGTCCTCGCGATTGGCAGCGTCTGATTAATAACTATTGG  
49 GGTTTTCGTCCGCGTAGCCTGCGTGTTAAAATCTTTAATATCCAGGTGAAAGAGGTGACCGT  
50 TCAGGATAGCACCACCACAATTGCAAATAATCTGACCAGCACCGTGCAGGTTTTTACCGATG  
51 ATGATTATCAACTGCCGTATGTTGTTGGCAATGGCACCGAAGGTTGTCTGCCTGCATTTCCG  
52 CCTCAGGTGTTTACCCTGCCGCAGTATGGTTATGCAACCCTGAATCGTGATAATACCGAAAA  
53 TCCGACCGAACGTAGCAGCTTTTTTGCCTGGAATATTTTCCGAGCAAATGCTGCGTACCG  
54 GCAACAATTTGAGTTCACCTATAACTTTGAAGAAGTGCCGTTTACAGCAGCTTTGCACCG  
55 AGCCAGAACCTGTTTAAACTGGCAAATCCGCTGGTTGATCAGTATCTGTATCGTTTTGTTAG

56 CACCAATAATACCGGTGGTGTGCAGTTTAAACAAAATCTGGCAGGTCGTTATGCCAACACCT  
57 AAAAAATTGGTTTCCGGGTCCGATGGGTTCGTACCCAAGGTTGGAATTTAGGTAGCGGTGTT  
58 AATCGTGCAAGCGTTAGCGCATTGCAACCACCAATCGTATGGAAGTGAAGGTGCAAGCTA  
59 TCAGGTTCCCTCCGCAGCCGAATGGTATGACCAATAATCTGCAAGGTAGCAATACCTATGCAC  
60 TGGAAAATACCATGATCTTTAATTCCCAGCCTGCAAATCCGGGTACAACCGCAACCTATCTG  
61 GAAGGTAATATGCTGATTACCAGCGAAAGCGAAACCCAGCCGGTTAATCGCGTTGCATATAA  
62 TGTTGGTGGTCAGATGGCAACAAATAATCAGAGCAGTACCACCGCACCGGCAACCGGCACAT  
63 ATAACCTGCAAGAAATTGTTCCGGGTAGCGTTTGGATGGAACGTGATGTTTATTTACAGGGT  
64 CCGATTTGGGCAAAAATCCGGAAACCGGTGCACATTTTCATCCGAGTCCGGCAATGGGTGG  
65 TTTTGGTCTGAAACATCCGCCTCCGATGATGCTGATCAAAAATACACCGGTTCCGGGAAATA  
66 TTACCAGCTTTAGTGATGTTCCGGTGTCCAGCTTTATTACCCAGTATAGCACCGGTCAGGTT  
67 ACCGTTGAAATGGAATGGGAACGAAAAAAGAAAACAGCAAACGTTGGAACCCGGAAATTCAG  
68 TATACCAACAATTATAACGATCCGCAGTTTGTGGATTTTGCACCGGATAGTACCGGTGAATA  
69 TCGTACCACACGTCCGATTGGCACCCGTTATCTGACCCGTCCGCTGTAA

70 5.2 AAP5 DNA coding sequence with His<sub>6</sub>-tag

71 ATGGACCCAGCGGATCCCAGCAGCTGCAAATCCCAGCCCAACCAGCCTCAAGTTTGGGAGCT  
72 GATACAATGTCTGCGGGAGGTGGCGGCCCATTTGGGCGACAATAACCAAGGTGCCGATGGAG  
73 TGGGCAATGCCTCGGGAGATTGGCATTGCGATTCCACGTGGATGGGGGACAGAGTCGTCAC  
74 CAAGTCCACCCGAACCTGGGTGCTGCCAGCTACAACAACCACCAGTACCGAGAGATCAAAA  
75 GCGGCTCCGTCGACGGAAGCAACGCCAACGCCTACTTTGGATACAGCACCCCTGGGGGTA  
76 CTTTGACTTTAACCGCTTCCACAGCCACTGGAGCCCCGAGACTGGCAAAGACTCATCAACA  
77 ACTACTGGGGCTTCAGACCCCGGTCCCTCAGAGTCAAAAATCTTCAACATTCAAGTCAAAGAG  
78 GTCACGGTGCAGGACTCCACCACCACCATCGCCAACAACCTCACCTCCACCGTCCAAGTGTT  
79 TACGGACGACGACTACCAGCTGCCCTACGTTCGTCGGCAACGGGACCGAGGGATGCCTGCCG  
80 GCCTTCCCTCCGCAGGTCTTTACGCTGCCGCAGTACGGTTACGCGACGCCATCATCACCAT  
81 CATCATTA

Title:

**AAV capsid proteins fused with SARS-CoV-2 RBD or RBM: Expression in *E. coli*,  
*in-vitro* assembly, and characterization**

Authors:

Dinh To Le, Olaf Behrsing, Claire Rothschild, Marco T. Radukic, Katja M. Arndt, Kristian M. Müller

similar mean levels of VG and hOTCco mRNA on days 84 and 140 in all four groups. These data are consistent with ISH and IHC results. Most animals showed positive ELISPOT responses to a capsid peptide pool (AAV8-C), with weak, transient responses in PBMCs on day 70, and stronger positive response in liver lymphocytes on day 140. Few/weak ELISPOT responses were observed in the liver to the transgene peptide pools and none were observed in PBMCs. In summary, there were no apparent differences between female and males cynomolgous macaques in immunologic parameters or in DTX301 effectivity.

### 735. AAV Capsid Proteins Fused with SARS-CoV-2 RBD or RBM: Expression in *E. coli*, *In-Vitro* Assembly, and Characterization

Dinh To Le<sup>1</sup>, Olaf Behrsing<sup>2</sup>, Claire Rothschild<sup>1</sup>, Marco T. Radukic<sup>1</sup>, Katja M. Arndt<sup>2</sup>, Kristian M. Müller<sup>1</sup>

<sup>1</sup>Cellular and Molecular Biotechnology, Bielefeld University, Bielefeld, Germany; <sup>2</sup>Molecular Biotechnology, Institute for Biochemistry and Biology, University of Potsdam, Potsdam, Germany

In the current COVID-19 pandemic, the SARS-CoV-2 virus has infected over a hundred million people and contributed to millions of deaths. The SARS-CoV-2 spike protein, in particular its receptor-binding domain (RBD) containing the receptor-binding motif (RBM), mediates virus binding to the cellular receptor angiotensin-converting enzyme 2 (ACE2) and subsequent viral internalization. Therefore, RBD and RBM are lead candidates for SARS-CoV-2 subunit vaccine development. Virus-like particles (VLPs) have been widely used for vaccine development due to their ability to induce a strong immune response and adeno-associated virus-like particles (AAV VLPs) produced in mammalian cells have been tested as a scaffold for presenting antigens. However, mammalian cell culture is expensive and particles may contain cellular components. Recently, we reported that AAV2 VP3 capsid proteins produced in *E. coli* can be assembled to AAV2 VLPs *in vitro*. In the current work, we explore the potential of *in-vitro* AAV2 VLPs for coronavirus vaccine development. SARS-CoV-2 RBD and RBM were incorporated into the 587-loop of AAV2 VP3 proteins and these fusion proteins were expressed in *E. coli* using T7 promoter (pET) plasmids. The proteins formed inclusion bodies in *E. coli* and were successfully purified under denaturing conditions of 8 M urea. Refolding and concomitant *in vitro* assembly of VP3\_RBD VLPs or VP3\_RBM VLPs was attained by serially dialyzing initial denatured proteins against different buffers containing 4, 2, 1, 0.5, and finally 0 M urea. After dialysis, atomic force microscopy (AFM) of AAV2 VP3\_RBD and VP3\_RBM samples identified particles with the expected size. This hints that the incorporation of RBD or RBM into the 587-loop is compatible with *in vitro* AAV2 VLP capsid assembly, though irregular aggregates and smaller structures, potentially single and intermediate assemblies, were also recorded. In ELISAs, an RBD conformation-specific antibody readily recognized coated protein samples indicating at least partial correct folding of VP3\_RBD. Next, mice were immunized and boosted with VP3\_RBM and VP3\_RBD VLPs mixed with adjuvants, and serum was collected at various timepoints. The immune response was examined by ELISA with coated antigens (VP3\_RBD and VP3\_RBM VLPs) as well as GFP\_RBD produced in 293-F cells as a control for SARS-CoV-2 specificity. Immunization of mice with the motif VP3\_RBM VLPs resulted in a high level of the desired RBD-specific antibodies and a low level of VP3

VLP-directed antibodies. Unexpectedly, the domain VP3\_RBD VLPs induced a low level of RBD-specific antibodies, but an intermediate level of VP3 VLP antibodies. Taken together our data suggest that *in vitro* AAV VLPs bear potential as vaccine scaffolds and that AAV VLP production using *E. coli* lends itself as a versatile strategy for vaccines and drug delivery.

### 736. Presence of Pre-Existing Anti-Adeno-Associated Virus (AAV) Serotype 5 Neutralizing Antibodies (NABs) in Serum of Huntington Disease (HD) Patients Was Not Associated with Detectable Anti-AAV5 Nabs in Cerebrospinal Fluid (CSF)

Anna Majowicz<sup>1</sup>, Floris van Waes<sup>1</sup>, Astrid Valles<sup>1</sup>, Sander van Deventer<sup>1</sup>, Mette Gilling<sup>2</sup>, Anka Ehrhardt<sup>3</sup>, Pavlina Konstantinova<sup>1</sup>, Valerie Sier-Ferreira<sup>1</sup>

<sup>1</sup>uniQure N.V, Amsterdam, Netherlands; <sup>2</sup>Enroll-HD Platform Team, European Huntington's Disease Network (EHDN), University Hospital of Ulm, Ulm, Germany; <sup>3</sup>CHDI Foundation, Princeton, NJ

**Background** AAV-based therapies are under investigation in early clinical trials for several neurodegenerative diseases. We have previously reported that serum anti-AAV5 NABs titers up to 340 in humans and as high as 1030 in primates did not interfere with the therapeutic efficacy of intravenously administered AAV5 vector. However, it remains unclear whether naturally acquired pre-existing systemic immunity to AAV would impact the therapeutic efficacy of AAV vectors delivery to the Central Nervous System (CNS). This knowledge is of importance for the interpretation of AAV-based gene therapies for Huntington Disease (HD), since the blood-brain barrier in HD patients might be compromised. To address such concern the prevalence of NABs against AAV serotype 5 was correlated between matched serum and CSF samples obtained from a same individual, either HD patients at different stages of the disease or healthy controls participating in HDClarity. **Methods** Serum and plasma samples from HD patients and healthy donors were analyzed for the presence of anti-AAV5 NABs with the use of luciferase-based assay. The sensitivity (lowest sample dilution) of the assay was set at 50. Consequently, CSF samples were obtained from all HD patients and healthy donors that tested positive for serum/plasma anti-AAV5 NABs and 3 that tested negative (controls) to analyze for presence of CSF anti-AAV5 NABs. **Results** Overall, serum anti-AAV5 NABs were not associated with detectable NABs in CSF; remarkably, this was true even in the presence of the highest serum titers (5364 in HD patient, 5129 in healthy donor). In HD patients, 37 (21.5%) of 172 serum samples had detectable anti-AAV5 NABs titers; none (0%) of the 37 HD patients had detectable anti-AAV5 NABs titers in CSF above threshold. Similarly, in healthy controls, 12 (18.2%) of 66 serum samples had a detectable anti-AAV5 NABs titer; none (0%) of those 12 donors had detectable anti-AAV5 NABs titers in CSF. **Conclusion** Pre-existing serum anti-AAV5 antibodies have not impacted clinical efficacy of intravenous AAV5 therapies. The current analysis of HDClarity samples suggest patients with detectable serum NABs do not have CSF NABs. Therefore, we conclude that there is minimal risk for reduced therapeutic efficacy of intrathecal or intraparenchymal administration of therapeutic AAV5 vectors by pre-existing serum or CSF AAV5 NABs in HD patients.

Title:

***In vitro* assembly of virus-like particles and their applications**

Authors:

Dinh To Le, Kristian M. Müller

Review

# In Vitro Assembly of Virus-Like Particles and Their Applications

Dinh To Le and Kristian M. Müller \* 

Cellular and Molecular Biotechnology, Faculty of Technology, Bielefeld University, 33615 Bielefeld, Germany; dinh\_to.le@uni-bielefeld.de

\* Correspondence: kristian@syntbio.net; Tel.: +49-521-106-6323

**Abstract:** Virus-like particles (VLPs) are increasingly used for vaccine development and drug delivery. Assembly of VLPs from purified monomers in a chemically defined reaction is advantageous compared to in vivo assembly, because it avoids encapsidation of host-derived components and enables loading with added cargoes. This review provides an overview of ex cella VLP production methods focusing on capsid protein production, factors that impact the in vitro assembly, and approaches to characterize in vitro VLPs. The uses of in vitro produced VLPs as vaccines and for therapeutic delivery are also reported.

**Keywords:** capsid protein; in vitro assembly; virus-like particle; VLP-based vaccines; drug delivery



**Citation:** Le, D.T.; Müller, K.M. In Vitro Assembly of Virus-Like Particles and Their Applications. *Life* **2021**, *11*, 334. <https://doi.org/10.3390/life11040334>

Academic Editors: Adam Taylor and Marko Noerenberg

Received: 23 December 2020

Accepted: 7 April 2021

Published: 10 April 2021

**Publisher's Note:** MDPI stays neutral with regard to jurisdictional claims in published maps and institutional affiliations.



**Copyright:** © 2021 by the authors. Licensee MDPI, Basel, Switzerland. This article is an open access article distributed under the terms and conditions of the Creative Commons Attribution (CC BY) license (<https://creativecommons.org/licenses/by/4.0/>).

## 1. Introduction

Virus-like particles (VLPs) are highly structured protein complexes that resemble a native virus capsid. VLPs typically represent gene-less virus shells but in a wider definition encompass any type of capsid-derived nanoparticle. VLPs assemble from single or multiple structural capsid proteins inside appropriate production hosts, which is often termed in vivo assembly, as the host is seen as a single-cell organism, or in defined, cell-free conditions, also termed in vitro assembly. VLPs in general can be either enveloped or non-enveloped [1], whereby in vitro assembly typically leads to protein-only shells. Due to the lack of viral genomes, these particles are non-replicative but typically retain the transduction potential of the parental viruses, which may be used for nanoparticle delivery systems [2].

In vivo-produced VLPs have been exploited for different biomedical applications, such as vaccines, drug delivery and nanomaterials [3–5]. However, in this production strategy, capsid proteins are expressed and concomitantly assembled into VLPs inside the host cells, which may encapsidate host-related contaminations and thus impede VLP use [6,7].

Along with progress in understanding virus assembly requirements, in vitro VLP production based on various viruses had been established. For the in vitro assembly, the capsid proteins are expressed and purified from expression hosts or cell-free protein synthesis systems (CFPS), or the proteins are obtained from in vivo VLPs via a disassembly procedure. This avoids trapping host-derived impurities, a potential source for unwanted immune response. Next, the capsid proteins are incubated under defined chemical conditions which promote VLP assembly. Compared to the in vivo VLPs, the in vitro technology offers the possibility to mix different capsid proteins or epitopes within a particle, for example resulting in a vaccine candidate for different viral genotypes [8,9]. For therapeutic delivery applications, the in vitro technology also enables the possibility to mix and match as well as control the amounts of different payloads during the capsid assembly reaction [4].

There are a few literature reviews on VLPs that focus on production [10] and various applications [3–5,11], but these do not discriminate between in vivo and in vitro VLPs. Here, we focus on in vitro produced VLPs covering the three domains: capsid-protein production, in vitro VLP formation and VLP characterization. We report in vitro VLP

assembly protocols that have been applied in the context of vaccine development and drug delivery.

## 2. In Vitro Assembly of Virus-Like Particles (VLPs)

### 2.1. Capsid Protein Production

To prepare protein monomers for a cell-free capsid assembly under defined and controllable conditions, viral capsid protein can be obtained either by expression and purification of non-assembled proteins or via a disassembly procedure from in vivo generated and purified VLPs. The choice of the hosts for capsid protein expression significantly affects all further steps. *E. coli* is a preferred host for high capsid-protein expression [12]. Depending on the viral protein structure and expression method, proteins are either expressed in soluble form, which is normally favorable for capsid assembly, or as aggregates forming inclusion bodies within *E. coli*. To increase the soluble protein yield during expression, different factors such as the choice of the *E. coli* strain, expression vector, codon usage, expression temperature, induction condition and medium can be optimized [10,13]. Furthermore, tags have been fused to viral protein termini at the genetic level to aid protein folding and/or purification. Taking into account that the additional tag may interfere with capsid formation, a protease cleavage site can be added and used prior to assembly [14–16]. If proteins tend to form inclusion bodies in *E. coli* owing to incorrect folding, this expression strategy may be exploited with a strong promoter to produce high yields per dry mass and ease initial purification. The inclusion bodies can be easily separated from the cell debris and solubilized using strong denaturants like 6 M guanidinium HCl or 6–8 M urea [17–21].

Other favorable hosts for capsid protein production are Sf9 insect cells in combination with baculovirus vectors and yeast. Both organisms are amenable to scale up and offer the advantage of eukaryotic post-translational protein modification [22–24]. Lastly, cell-free protein synthesis systems have also been used to produce viral capsid proteins in defined transcription/translation reactions. This method allows for a direct control of capsid protein expression and VLP assembly conditions and enables production of toxic and insoluble proteins [25–28].

If VLPs assemble spontaneously inside the expression hosts, they may contain undesired compounds. To obtain protein subunits from VLPs formed inside the host cell, different disassembly methods exist. Bacteriophage MS2 VLPs produced in *E. coli* were disassembled at low pH, while human papillomavirus (HPV) VLPs obtained from insect cells were dissociated with carbonate buffer at pH 9.6 [29,30]. Cowpea chlorotic mottle virus (CCMV) particles assembled in plants were denatured in a neutral buffer with high salt concentration [31–33]. Urea is commonly used to disassemble the formed VLPs. Bacteriophage Q $\beta$  VLPs were disassembled in 6 M urea [34], whereas 2.5 M urea were sufficient to denature hepatitis B core protein (HBc) VLPs [35]. Reducing and chelating agents can also be used in VLP disassembly [30,36–41].

### 2.2. Factors Impacting In Vitro Assembly

The capsid self-assembly is driven by Brownian motion and interactions between subunits as well as subunits and other viral or non-viral components to minimize free energy in higher structures. The capsid assembly is proposed to occur in three steps. First, a capsid oligomer nucleus is formed from capsid proteins in the so-called nucleation phase. Afterwards, building blocks (a protein monomer, or capsid oligomers) are added to the nucleus during the growth phase. Finally, the last building block is inserted to complete the capsid [42–44]. The assembly process is complicated and highly dependent on the viral protein structure and the experimental conditions. Conceptually, VLP formation in the first place is governed by general rules applicable to protein folding and stability while considering aggregation [45]. We present here the main factors that affect in vitro assembly (Figure 1).

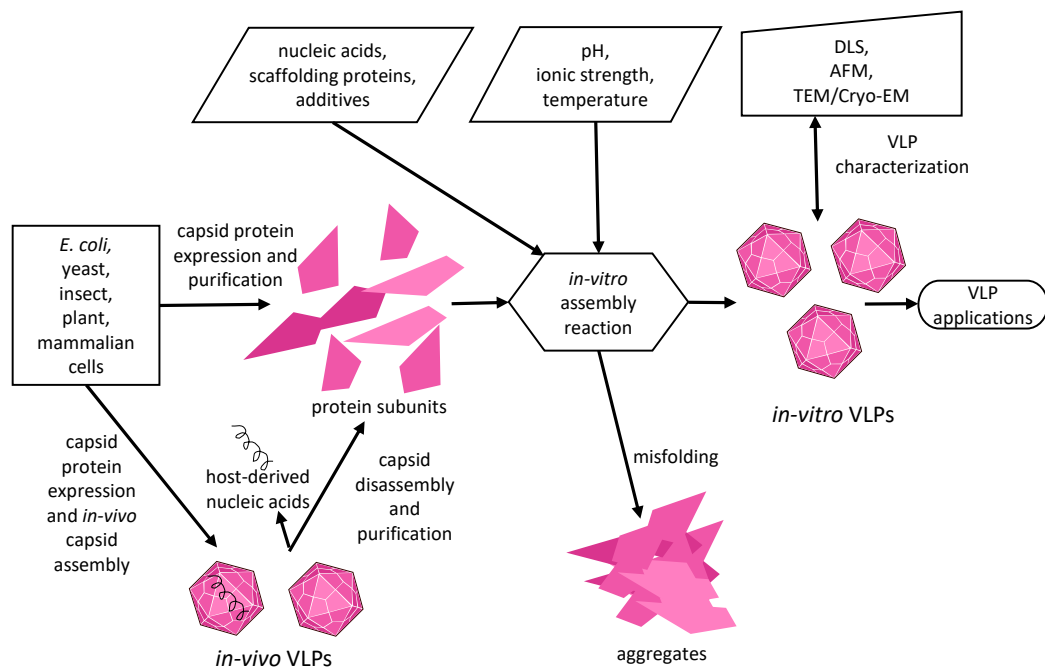


**Figure 1.** Schematic representation of in vitro virus-like particle (VLP) assembly. Capsid protein production methods, factors impacting on VLP in vitro assembly and typical methods to characterize VLPs are presented.

### 2.2.1. pH, Ionic Strength, and Temperature

pH plays an important role for in vitro assembly since it affects the capsid-protein charge. Most in-vitro assembly reactions were optimized at a physiological pH [15,18,46]. Interestingly, some particles assemble at acidic or alkaline pH. In vitro assembly studies of CCMV showed that the attraction between capsid proteins was optimal at about pH 5 and decreased sharply with increasing pH [47]. Rotavirus (RV) VLPs formed in vitro at an acidic pH [21]. Our in vitro assembly results from adeno-associated virus serotype 2 (AAV2), however, indicated that an alkaline pH (pH 9) was most suitable to avoid aggregates and promote VLP formation [19].

Ionic strength is another main factor for capsid assembly in vitro. Salts interact with charges on the protein surface, influence the water shell, disfavor hydrophobic exposure and ultimately affect protein stability [48]. To optimize in vitro capsid-assembly reactions, ionic strength needs to be optimized along with the change of pH [15,18,46], which can be presented as phase diagrams of the protein assembly [49].

The effect of temperature on the capsid assembly also deserves evaluation. Low temperatures are normally favorable as they reduce protein aggregation and chemical degradation. For example, the in vitro assembly of primate erythroparvovirus 1 (B19) at 4 °C showed a better yield at 4 °C than at 37 °C [18]. Contrarily, near-physiological temperatures promoted the Rous Sarcoma virus capsid formation in vitro [50]. Another report on hepatitis virus assembly revealed that subunit exchange with assembled capsid shells was generally slow but slightly elevated at lower temperature [51].

### 2.2.2. Nucleic Acids, Scaffolding Protein, and Additives

The in vitro assembly of some capsids was highly influenced by the presence of nucleic acids. CCMV, a single-stranded RNA virus, is a well-studied model. Garmann et al. demonstrated that the assembly of CCMV depends on balanced capsid protein (CP)–CP interactions relative to CP–RNA interactions [52]. Furthermore, a high CP/RNA mass ratio is required to assemble CCMV VLPs [53]. Recently, CCMV capsid proteins were shown to encapsidate both single-stranded DNA (ssDNA) in typical spherical assemblies and double-stranded DNA (dsDNA) in rod-like VLPs [54]. Other RNA viruses also require nucleic acids

for in vitro assembly. The assembly of Gag proteins into human immunodeficiency virus (HIV1) VLPs in a defined system was directly supported by RNA [55]. Similarly, the in-vitro assembly of hepatitis C virus (HCV) nucleocapsid-like particles required structured RNA as reported by Kunkel et al. [56]. Bacteriophage MS2 was also assembled in vitro in the presence of nucleic acids [29]. The assembly of beak and feather disease virus (BFDV), a member of the circular ssDNA circovirus family, is regulated by its ssDNA genomes. The highly positive charged N-terminal arginine-rich motif of capsid proteins interacted with ssDNA during in vitro capsid assembly [57]. VLPs derived from simian virus 40 (SV40), a dsDNA virus, also needed DNA for efficient in vitro assembly [58]. Nonetheless, it should be considered that the additional nucleic acids within the in vitro VLPs might interfere with VLP applications. For example, nucleic acid can modulate the immune response by activating pattern recognition receptor (PRR) [6].

Scaffolding proteins are not a component of a mature capsid. These proteins assist during capsid formation. Providing a scaffolding protein to an in vitro capsid assembly in many cases increases the yield of fully assembled capsids. Our data on in vitro assembly of AAV2 showed that the addition of assembly-activating protein (AAP, an AAV scaffolding protein) helped to improve AAV2 capsid formation [19]. The assembly of different bacteriophages was highly dependent on scaffolding proteins, which promoted the polymerization of the major capsid protein [59–63]. The herpes simplex virus procapsid assembly reaction from purified major capsid proteins has been reported by Newcomb et al. to require a scaffolding protein and to form small procapsids at low concentrations of the scaffolding protein [64].

Small molecule additives can be used to aid capsid assembly. L-arginine improved the solubility of assembled VLPs by preventing aggregation during protein refolding [19,65]. In a study performed by Lampel et al., chemical chaperones, such as methylamines enhanced HIV-1 in vitro assembly [66]. Other reagents can be combined with capsid proteins during in vitro assembly leading to new hybrid materials. For example, CCMV capsid proteins have been explored in combination with different supramolecular templates. Organo Pt (II) complexes formed spherical or rod-like structures that were combined with the capsid proteins to form likewise shaped CCMV VLPs [67]. Micelles and DNA micelles were packaged inside CCMV VLPs that offer new drug-delivery systems, especially for hydrophobic drugs [68,69]. Polymers were also incorporated into CCMV VLPs during in vitro assembly [70,71].

### 2.3. VLP Characterization

To analyze the formed in vitro VLPs, different biochemical and biophysical methods can be applied. Standard methods are sodium dodecyl sulfate-polyacrylamide gel electrophoresis (SDS-PAGE) to determine size and purity, Western blot to confirm the identity, and ultraviolet (UV) spectroscopy with light scattering compensation, which monitors amino acids (phenylalanine, tyrosine and tryptophan) and nucleotides with an absorbance spectrum of about 240–300 nm, to determine concentrations [36,72,73]. Other protein quantitation methods, such as the bicinchoninic acid (BCA) assay and Bradford assay have been also used [18,36,74]. Size exclusion chromatography and dynamic light scattering (DLS) are widely used to characterize the size of VLPs [19,75–77]. The latter method provides the heterogeneity of the VLP samples and the mean hydrodynamic diameter of particles, which is normally greater than the physical diameter. Stability has been assessed using techniques such as differential scanning fluorimetry [78]. Structural integrity has been verified by circular dichroism spectroscopy (CD) and Fourier-transform infrared (FT-IR) spectroscopy [79]. The nucleic–capsid protein interactions have been determined by gel retardation assay, optical tweezers (OT) and acoustic force spectroscopy (AFS) [53,58]. VLP morphology and possible intermediate aggregates formed during an in-vitro assembly reaction can be visualized using transmission electron microscopy (TEM) or atomic force microscopy (AFM). TEM can also be used to distinguish between empty and encapsulated VLPs [52,59] and AFM can assess the VLP height profile [19,80,81]. A VLP high-resolution

structure can be determined using Cryo-EM [52] or crystallography [82]. Mass spectrometry has been used to identify VLP composition [76]. If available, an assembled particle antibody helps to confirm VLP conformation in enzyme-linked immunosorbent assays (ELISAs) [19].

Understanding capsid self-assembly pathways will help to tailor the mechanisms of virus infection and replication for therapeutic applications. Different methods have been used to characterize intermediate assemblies and the assembly pathways of virus capsids, such as electron microscopy [83–86], X-ray crystallography [57], atomic force microscopy [57,58,85], small-angle X-ray scattering [87–92], mass spectrometry [93–95], size-exclusion chromatography [84], resistive-pulse sensing [84,96], interferometric scattering microscopy [97], single-molecule fluorescence correlation spectroscopy [98], optical tweezers in combination with confocal fluorescence microscopy and acoustic force spectroscopy [58,99]. Recently, high-speed atomic force microscopy (HS-AFM), a powerful single-molecule technique for real-time visualization of biomolecules in dynamic action [100], has been used to visualize self-assembly of HIV capsid protein lattice [81]. This physical virology technique will enable real-time capsid assembly studies of other viruses in the future.

### 3. Application of In Vitro-Assembled VLPs

#### 3.1. Vaccine Development

VLPs are composed of protein monomer units in a repetitively ordered structure with a size range of 20–200 nm in diameter that is appropriate for vaccination [11]. VLPs are able to induce a strong immune response, which was described by Jennings et al. and Mohsen et al. [6,101]. A VLP derived from a pathogenic virus may be used to elicit an immune response directly to the parental virus, or function as a scaffold to present heterologous epitopes. Compared to subunit peptides or proteins, VLPs provide the possibility to present epitopes in a natural conformation that benefits an anti-viral B- and T-cell immune response. Moreover, due to the highly repetitive epitope presentation, VLPs can induce a strong B cell response even without adjuvants [102–104]. Another advantage is that a foreign epitope can be chemically or genetically incorporated onto the VLP surface, offering a flexible platform to create different vaccine candidates [105–108].

A few VLP-based vaccines have a long and very successful tradition in the clinic and recently several new candidates progressed to the clinic. These vaccine candidates have been produced in vivo or by an in vitro system [3]. Compared to in vivo VLP production, which potentially may be contaminated with host-derived components resulting in unpredictable immune responses that require an additional quality control effort [6], a cell-free VLP technology offers better control during production. A list of developed and approved vaccine candidates is presented in Table 1.

**Table 1.** In vitro produced VLP-based vaccines on the market or in development.

Vaccine Candidate	Host	VLP <sup>a</sup> Platform	Vaccine Antigen Proteins	Assembly Method	Development Stage	Ref.
Cervarix (GlaxoSmithKline)	Insect cell	HPV-L1	HPV 16 and 18 L1	Multi-step purification	Approved	[109]
Gardasil (Merck Sharp and Dohme)	Yeast	HPV-L1	HPV 6/11/16/18 L1	VLP disassembly using DTT/Reassembly by DTT removal	Approved	[79]
Gardasil-9 (Merck Sharp and Dohme)	Yeast	HPV L1	HPV 6/11/16/18/31/33/45/52/58 L1	VLP disassembly using DTT/Reassembly by DTT removal	Approved	[110]
Cecolin <sup>®</sup> (Innovax)	<i>E. coli</i>	HPV L1	HPV16 and 18 L1	Protein purification and reducing agent removal	Approved (China)	[8,111]

Table 1. Cont.

Vaccine Candidate	Host	VLP <sup>a</sup> Platform	Vaccine Antigen Proteins	Assembly Method	Development Stage	Ref.
HPV 9-valent (Innovax)	<i>E. coli</i>	HPV L1	HPV 6/11/16/18/31/33/45/52/58 L1	Protein purification and reducing agent removal	Phase 2 NCT03935204	[9]
Hecolin® (Innovax)	<i>E. coli</i>	HEV p239	HEV truncated E2, 239 a.a.	Multi-step purification	Approved (China)	[78,112–114]
HEV	<i>E. coli</i>	HEV p495	HEV E2, 495 a.a.	Protein was dialyzed into 50 mM phosphate buffer with 0.5 M NaCl, pH 6.5	Preclinical evaluation	[115]
ENGERIX-B/Fendrix (GlaxoSmithKline)	Yeast	HBsAg	HBV HBsAg	Multi-step purification	Approved	[116,117]
Recombivax (Merck Sharp and Dohme)	Yeast	HBsAg	HBV HBsAg	Multi-step purification	Approved	[118,119]
Hepatitis B	Cell-free synthesis system	HBcAg	HBV truncated HBcAg	30 µL CFPS product was dialyzed against 100 mM HEPES and 200 mM NaCl, pH 7 1 mL CFPS product was dialyzed against 10 mM BisTris and 0.385 M NaCl, pH 5.5	Preclinical evaluation	[27]
SARS-CoV-2 (NVX-CoV2373, Novavax)	Sf9 cell	S-trimer nanoparticle	SARS-CoV-2 Spike	Removal of the detergent (Tergitol™ NP-9) during protein purification	Phase 3 NCT04611802	[77,120]
MERS-CoV and SARS-CoV (Novavax)	Sf9 cell	S nanoparticle	MERS-CoV/SARS-CoV Spike	Removal of the detergent (Tergitol™ NP-9) during protein purification	Preclinical evaluation	[121]
Influenza (NanoFlu™, Novavax)	Sf9 cell	HA nanoparticle	Influenza virus HA	Removal of the detergent (Tergitol™ NP-9) during protein purification	Phase 1/2 NCT04120194	[122,123]
RSV (Novavax)	Sf9 cell	F nanoparticle	RSV F	Removal of the detergent (Tergitol™ NP-9) during protein purification	Phase 1 NCT03026348	[23,124,125]
RSV	<i>E. coli</i>	B19 VP2	Two peptides derived from RSV F	Denatured proteins in 5 M GuHCl were dialyzed into PBS buffer at 4 °C for 36 h	Preclinical evaluation	[126]
CPV	<i>E. coli</i>	CPV VP2	CPV VP2	Fusion proteins (SUMO tag fused to capsid protein) were cleaved by SUMO protease and dialyzed into 50 mM Tris-HCl, 150 mM NaCl, pH 7	Preclinical evaluation	[15]

<sup>a</sup> B19: Erythroparvovirus 1; CPV: Canine parvovirus; HBcAg: Hepatitis B core antigen; HBsAg: the surface antigen of the Hepatitis B virus; HBV: Hepatitis B virus; HEV: Hepatitis E Virus; HPV: Human papillomavirus; MERS: Middle East respiratory syndrome coronavirus; RSV: Respiratory syncytial virus; SARS: Severe acute respiratory syndrome coronavirus; SARS-CoV-2: Severe acute respiratory syndrome coronavirus type 2; HEPES: 2-[4-(2-hydroxyethyl)piperazin-1-yl]ethanesulfonic acid.

Human papillomavirus (HPV) is a major cause of cervical cancer and associates with many human diseases [127]. HPV capsids are composed of two capsid proteins, L1 and L2, assembled in a  $T = 7$  icosahedral structure (about 60 nm in diameter) [128]. L1 is a structural protein and able to form HPV VLPs [129]. To date, there are four HPV vaccines on the market, which use L1-VLP platforms [3].

The HPV vaccine Cervarix, which is manufactured by GlaxoSmithKline and partially based on technology from MedImmune/AstraZeneca, was approved in 2007 in the European Union (EU) and other countries and 2009 in the USA. It contains two monovalent antigen bulks of C-terminally truncated versions of the major capsid proteins L1 of either serotype 16 or 18. The proteins are produced in cells derived from the *Trichoplusia ni* (Hi-5) insect cell line with recombinant baculoviruses encoding the L1 proteins. The proteins are released by osmotic shock and upon a multi-step purification by filtration and chromatography the proteins assemble into spherical particles, which are mixed and formulated with adjuvant. The final product dose contains 20 µg HPV 16 L1 protein, 20 µg HPV 18 L1 protein, 500 µg aluminium hydroxide, 50 µg 3-O-desacyl-4'-monophosphoryl lipid A (MPL) and 0.624 mg  $\text{NaH}_2\text{PO}_4 \cdot 2\text{H}_2\text{O}$  [109].

The HPV vaccine Gardasil, which is produced by Merck Sharp and Dohme and was approved in the USA in 2010, contains the HPV L1 protein from serotypes 6, 11, 16, and 18. The vaccine Gardasil 9 (9-valent vaccine), which was approved in the USA in 2014, additionally contains the HPV L1 proteins of serotypes of 31, 33, 45, 52, and 58. The proteins are individually produced in the yeast from *Saccharomyces cerevisiae* transformed with the pGAL110 expression vector coding for the respective proteins. Cells are harvested by filtration, frozen and then VLPs are released by homogenization. For some L1 types (31, 33, 45, 52, 58), a protease inhibitor is added. Purification comprises cross-flow membrane filtration for debris removal, cation exchange chromatography for host cell protein removal, and hydroxyapatite chromatography for polishing and enrichment of monodisperse VLPs. For all but type L1 serotype 18, the VLPs are disassembled using dithiothreitol (DTT) and reassembled by removing DTT, which improves VLP structure and stability. A final buffer exchange yields the final aqueous products which are then adsorbed onto the adjuvant amorphous aluminium hydroxyphosphate sulfate by in-line mixing. The individual products are then mixed by sequentially adding them to a tank with buffer and alum adjuvant, settling and decanting. The final 0.5 mL aqueous dose Gardasil 9 contains 30 µg L1 6, 40 µg L1 11, 60 µg L1 16, 40 µg L1 18, and 20 µg of L1 31, 33, 45, 52, 58 as well as 500 µg aluminium (adjuvant as amorphous aluminium hydroxyphosphate sulfate), 9.56 mg NaCl (for stability), 0.78 mg L-histidine (for buffering), 50 µg polysorbate 80 (for VLP stability and prevention of aggregation or surface adsorption), 35 µg Na-borate (for buffering) [79,110].

As a biosimilar, the company Inovax produced Cecolin, a bivalent HPV16 and HPV18 vaccine, by expressing the respective L1 proteins in *E. coli* and maintaining them in soluble pentamer form under a reducing condition (20 mM DTT). The HPV VLPs were formed by removal of the reductant during protein purification [8]. The vaccine production in *E. coli* offers a low manufacturing cost and easy scale-up compared to other licensed products [111]. Similarly, Inovax produced an HPV9-valent vaccine candidate (HPV 6/11/16/18/31/33/45/52 and 58), which is currently in phase 2 clinical trial [9]. As a result of protein expression in *E. coli*, lipopolysaccharide (LPS) might contaminate into VLPs that can enhance immune responses and cause pyrogenic and shock reactions in mammals. To reduce LPS contamination, different methods, such as size exclusion chromatography, affinity chromatography, binding to polymyxin and treatment with Triton X-114 have been used [130].

Hepatitis E virus (HEV), which can be quasi-enveloped, is the most acute hepatitis cause in both developing and developed countries [131,132]. A 7.5-kb HEV genome comprises three overlapping open reading frames encapsidated into a  $T = 3$  symmetry capsid of 27–34 nm in diameter [133,134]. The open reading frame 2 (ORF2) codes for viral capsid proteins, which were produced in *E. coli* or insect cells as recombinant HEV vaccine candidates [135]. Hecolin, a licensed HEV vaccine in China, is an HEV cell-free

assembly product [113]. p239 truncated capsid protein (239 amino acid (a.a.) of a full-length capsid protein with 660 a.a.) was obtained from *E. coli* and assembled into VLPs of 20–30 nm diameter via multiple purification steps [78,112]. Another HEV vaccine candidate is currently under preclinical evaluation using p495 protein (495 a.a. truncated capsid protein) expressed in *E. coli* to form in vitro HEV VLPs [115].

Also surface antigens from enveloped viruses have been used in mostly defined assembly reactions. The surface antigen of the hepatitis B virus (HBV) which causes chronic infection of about 3.5% world population [136] named HBsAg was recombinantly produced in yeast. In a first version, the S gene of HBV was cloned in a plasmid and expressed in *Saccharomyces cerevisiae* strain DC5. Purification steps comprised cell disruption, diafiltration, size exclusion chromatography, ion-exchange chromatography, a CsCl ultracentrifugation followed by a final size exclusion chromatography. In the absence of chemical treatment, HBsAg formed spheres of about 20–22 nm containing non-glycosylated HBsAg and a lipid matrix consisting mainly of phospholipids [116,117]. This vaccine is marketed by GlaxoSmithKline as ENGERIX B, which was approved in 1986 in the EU as the first recombinant vaccine, and with added MPL adjuvant as Fendrix, which was approved in 2005. A similar product also produced in yeast is Recombivax HB from Merck [118,119]. The malaria vaccine Mosquirix from GlaxoSmithKline, which is also named RTS,S/AS01 and was approved in the EU in 2015, is produced by coexpression in yeast of the HBsAg with a fusion protein of HBsAg with the pre-erythrocytic circumsporozoite protein (CSP) of the *Plasmodium falciparum* malaria parasite. In this case, the mixed particles formed already during expression [137]. Hence, for these multi-subunit particles formed by surface antigens of enveloped viruses, which do not resemble typical capsids but defined aggregates, the differentiation between in-cell versus in-buffer VLP assembly is fluid. Compared to in vivo VLPs, the in vitro manufacturing process is defined by additional steps to reassemble VLPs outside the cells. In some cases, a dedicated assembly step is missing, because the in vitro VLP assembly occurs during steps ascribed to purification (Assembly method, Table 1). Such combined purification and assembly may reduce downstream processing costs. In other cases, few mutations may shift assembly between in vivo and in vitro.

Recently, the company Novavax developed the NVX-CoV2373 vaccine candidate (currently in phase 3 clinical trial) for preventing severe acute respiratory syndrome coronavirus 2 (SARS-CoV-2) infection, the virus which spread from China around the globe in 2020 causing the coronavirus disease 2019 (COVID-19) pandemic with millions of infections and deaths [120,138]. The SARS-CoV-2 spike protein (S protein), which is responsible for receptor binding and virus entry [139] was expressed in Sf9 insect cells using a baculovirus expression system. The protein was then obtained from the plasma membranes with a buffer containing NP-9 detergent. The 27.2 nm nanoparticles, potentially S-trimers anchored within polysorbate 80 (PS80) detergent cores, formed during protein purification and, concomitantly, detergent removal [77]. This strategy was also used to develop vaccine candidates against other coronaviruses (SARS, Middle East respiratory syndrome (MERS)) [121] and other pathogens including Influenza virus [122,123] and respiratory syncytial virus (RSV) [23,124,125].

Other vaccine candidates with different in-vitro assembly conditions are under preclinical evaluation. The C-terminally truncated hepatitis B core antigen (HBcAg) was produced using *E. coli*-based cell-free protein synthesis reaction and assembled into HBV VLPs [27]. The primate erythroparvovirus 1 (B19) VLPs presenting the peptides derived from F proteins of RSV virus were tested as an RSV vaccine candidate. The chimeric proteins were expressed in inclusion bodies in *E. coli*, and the VLPs were formed by dialyzing of the proteins from a denaturing buffer (5 M GuHCl) to PBS buffer [126]. A vaccine candidate for canine parvovirus (CPV) disease was also produced via an in vitro cell-free reaction. Xu et al. reported that CPV capsid protein (VP2) fused to a SUMO-tag was acquired from *E. coli* in soluble form. The CPV VLPs were developed during SUMO tag removal and dialysis of the capsid proteins into a physiological buffer [15].

### 3.2. Therapeutic Delivery

VLPs are attractive candidates to deliver drugs, small molecules or nucleic acids due to their biocompatibility, biodegradability and targeted delivery [4,140]. Different cargo-loading strategies have been explored with both in vivo and in vitro VLPs [141]. Here, we focus on different in vitro packaging approaches, which occur via disassembly/reassembly of VLPs or during in vitro assembly of purified proteins into VLPs. The in vitro encapsulation mainly relies on the interactions between loading cargoes and viral capsid proteins and differs among VLPs (Table 2). With small molecules not interfering with the assembly, concentration-dependent stochastic loading by engulfment during assembly is also feasible [142].

**Table 2.** In vitro VLP delivery platforms.

VLP <sup>a</sup> Platform	Expression System	Cargo and Loading Method	Targeting	Assembly Method	Ref.
MS2	<i>E. coli</i>	Chemotherapeutic drugs (DOX), siRNA cocktails, protein toxins Conjugated to RNA	Hepatocellular carcinoma using SP94 peptide	VLP disassembly in glacial acetic acid/Reassembly and packaging: capsid proteins in 10 mM acetic acid, 50 mM NaCl, pH 4 were incubated with RNA in 50 mM Tris-HCl pH 8.5 buffer	[29]
MS2	<i>E. coli</i>	siRNA Genetic fusion to TR step loop	HeLa cells using human transferrin	VLP disassembly in glacial acetic acid/Reassembly and packaging in 40 mM ammonium acetate, pH 6 buffer	[143]
MS2	<i>E. coli</i>	Alkaline phosphatase Electrostatic interaction to capsid protein	-	VLP disassembly in glacial acetic acid/Reassembly and protein packaging in 50 mM Tris, 100 mM NaCl, 250 mM Trimethylamine <i>N</i> -oxide buffer	[76]
P22	<i>E. coli</i>	Streptavidin, Ferritin cages, CelB Genetic fusion to a scaffold protein (SP)	-	VLP disassembly in 3 M GuHCl/Reassembly and protein packaging by adjusting the mixture of coat proteins (CP) and fusion proteins to 1.5 M GuHCl, and dialyzing to the buffer of 50 mM Tris-HCl, 25 mM NaCl, 2 mM EDTA, 3 mM $\beta$ -mercaptoethanol, 1% glycerol	[144,145]
Q $\beta$	<i>E. coli</i>	Fluorescent protein (GFP)	-	Q $\beta$ VLPs disassembly in 20 mM Tris-HCl, 50 mM NaCl, 6 M urea, 10 mM DTT, and dialyzed against 10 mM acetic acid and 50 mM NaCl/Reassembly and GFP packaging in 50 mM NaCl, 20 mM Tris-HCl, pH 7.5	[34]
HBc	<i>E. coli</i>	DOX Insertion of hydrophobic peptide to capsid protein to confine DOX	Tumor-targeting peptide RGD	VLP disassembly in 2.5 M urea, 150 mM NaCl, 50 mM Tris-HCl/Reassembly and DOX packaging in the buffer of 50 mM Tris-HCl, 150 mM NaCl, 10% glycerol, 1% glycine, pH 8	[35]
SV40	Sf9	DNA plasmid (up to 17.7 kb) Interaction between capsid protein and dsDNA	-	VLP disassembly in the presence of DTT, EDTA, EGTA/Reassembly and DNA packaging in the buffer containing MgCl <sub>2</sub> , CaCl <sub>2</sub> (ATP)	[41,146,147]

Table 2. Cont.

VLP <sup>a</sup> Platform	Expression System	Cargo and Loading Method	Targeting	Assembly Method	Ref.
JC virus	Yeast	RNAi	IL 10	Purified JC-VLPs were mixed with shRNA in a capsid buffer (150 mM NaCl, 10 mM Tris-HCl, 10 mM CaCl <sub>2</sub> ) then diluted with distilled water (an osmotic shock)	[148]
HPV	Sf21/HEK 293 cell	DNA plasmid (up to 8 kb) Interaction between capsid protein and dsDNA	-	VLP disassembly in the presence of DTT (EGTA)/Reassembly and DNA packaging in the buffer containing CaCl <sub>2</sub> , (ATP)	[37–39]
CCMV	Plant	ssDNA, dsDNA Electrostatic interaction to capsid protein	-	VLP disassembly in 5× assembly buffer (250 mM Tris-HCl containing 250 mM NaCl, 50 mM KCl, 25 mM MgCl <sub>2</sub> , pH 7.2)/Reassembly and DNA packaging by adding the mixture of capsid protein and DNA to 1× assembly buffer	[54]
CCMV	Plant/ <i>E. coli</i>	siRNA, mRNA, Enzyme (HRP) Electrostatic interaction to capsid protein	FOXA1 using siRNA	VLP disassembly in the high salt concentration, neutral pH buffer/Reassembly and cargoes packaging by dialyzing to the first assembly buffer (50 mM Tris pH 7.2, 50 mM NaCl, 10 mM KCl, 5 mM MgCl <sub>2</sub> , 1 mM DTT), then the second buffer (50 mM NaCH <sub>3</sub> COO, 8 mM Mg(CH <sub>3</sub> COO) <sub>2</sub> , pH 4.5)	[31–33]
CMV	Plant	DNA, protein, fluorophore Electrostatic interaction with capsid protein	-	VLP disassembly by LiCl/Reassembly and packaging by dialyzing against an assembly buffer (20 mM Tris-HCl, 80 mM KCl, 1 mM DTT, 1 mM MgCl <sub>2</sub> , pH 7.2)	[149]
CCMV	<i>E. coli</i>	DOX Conjugated to capsid proteins	Cancer cells using folic acid	Purified proteins were dialyzed to the buffer of 0.1 M NaCH <sub>3</sub> COO, 0.1 M NaCl, pH 4.8	[150]
MPyV	<i>E. coli</i>	GFP, m-Ruby3 protein Genetic fusion to capsid protein	-	Purified proteins-linked capsomeres were dialyzed to 20 mM Tris, 0.5 M (NH <sub>4</sub> ) <sub>2</sub> SO <sub>4</sub> , 1 mM CaCl <sub>2</sub> , 5% glycerol buffer	[75]
RV	<i>E. coli</i>	DOX Conjugated to capsid protein	Hepatoma cells using lactobionic acid	Purified, denatured capsid proteins (in urea) were dialyzed to CH <sub>3</sub> COOH/CH <sub>3</sub> COONa buffer at pH 4.5	[21]
SV40	Sf9	Magnetic nano-particles (MNPs) Electrostatic interaction between capsid protein and MNPs	EGF receptor	VP1 capsid proteins of SV40 were produced in Sf9 cells, pentamers were purified and assembled around magnetic nano-particles in MOPS buffer (20 mM MOPS-NaOH, 150 mM NaCl, 2 mM CaCl <sub>2</sub> , pH 7.0)	[151]
SV40	<i>E. coli</i>	Quantum dots (QDs) Direct association between His-tag in VP1 protein and Zn <sup>2+</sup> on the QDs surface	-	VP1 capsid proteins with a His-tag were produced in <i>E. coli</i> , purified VP1 pentamers and QDs were mixed and dialyzed against an assembly buffer (10 mM Tris-HCl, 1 mM CaCl <sub>2</sub> , 250 mM NaCl, 5% glycerol, pH 7.2)	[152]

Table 2. Cont.

VLP <sup>a</sup> Platform	Expression System	Cargo and Loading Method	Targeting	Assembly Method	Ref.
BMV	Plant	Gold nanoparticles Electrostatic interaction with capsid protein	-	Purified BMV proteins and gold particles were mixed in TKM buffer (10 mM Tris-HCl, 1 M KCl, 5 mM MgCl <sub>2</sub> , pH 7.4 and dialyzed against an assembly buffer (50 mM Tris-HCl, 50 mM NaCl, 10 mM KCl, 5 mM MgCl <sub>2</sub> , pH 7.4), then against SAMA buffer (50 mM NaOAc, 8 mM Mg(OAc) <sub>2</sub> , pH 4.5)	[153]
RRV	<i>E. coli</i>	Gold nanoparticles Electrostatic interaction with capsid protein	-	Purified capsid proteins and functionalized GNPs were mixed and dialyzed against an assembly buffer (20 mM Tris-HCl, 50 mM NaCl, 10 mM KCl, 5 mM MgCl <sub>2</sub> , pH 7.4)	[154]

<sup>a</sup> BMV: Brome mosaic virus; CCMV: Cowpea chlorotic mottle virus; CMV: cucumber mosaic virus; HBc: Hepatitis B core; JC: John Cunningham virus/human polyomavirus 2; MPyV: Murine polyomavirus; MS2: Bacteriophage MS2; P22: Bacteriophage P22; Qβ: Bacteriophage Qβ; RRV: Ross River virus; RV: Rotavirus; SV40: Simian virus 40; DOX: doxycycline; EDTA: ethylenediaminetetraacetic acid.

During protein expression, some capsid proteins tend to assemble VLPs inside the hosts. To remove potential host-related impurities and encapsulate cargoes, the disassembly and reassembly of VLPs are needed. The use of bacteriophage MS2 VLPs in cargo delivery was reported by different groups. Generally, MS2 capsid proteins were produced and formed 27.5 nm MS2 VLPs in *E. coli*. The VLPs were subsequently purified and disassembled in glacial acetic acid. Since MS2 VLPs are able to reassemble and encapsulate negatively charged cargoes in vitro at neutral pH, drugs, proteins or siRNA were loaded into the capsids for therapeutic delivery [29,76,143]. Targeting peptides were covalently linked to the capsid surfaces to specifically deliver the drugs to cells presenting the cognate receptor [29,143]. With a similar approach, Douglas et al. described a method to package a protein inside bacteriophage P22, which was performed by mixing of the cargo protein fused to a scaffold protein and bacteriophage P22 capsid proteins in a mild denaturing condition buffer (1.5 M GuHCl), followed by dialysis against a neutral buffer [144,145]. Another bacteriophage, Qβ has been used to encapsidate a fluorescent protein [34]. Hepatitis B core protein (HBc) VLPs were also exploited for drug delivery. The HBc VLPs assembled in *E. coli*, were denatured with urea, and reassembly and drug encapsulation was achieved by dialysis of the denatured proteins with a neutral buffer. The RGD peptide was genetically incorporated to HBc VLPs to target tumors [35]. In vitro VLPs were also explored in gene delivery. SV40 and HPV VLPs were produced in insect or mammalian cells. The particles were disassembled in the presence of reducing and chelating agents, DNA plasmids were then packaged inside the VLPs and delivered to target cells [37–39,41,146,147]. Human polyomavirus 2 (JC) VLPs produced in yeast have been used to deliver RNAi, which was loaded via an osmotic shock [148].

CCMV VLPs are widely tested for therapeutic delivery due to their pH-dependent capsid assembly [155]. CCMV VLPs were produced in plant cells, the particles were then disassembled in a high-salt concentration buffer at neutral pH. Reassembly and packaging followed by adding cargoes and dialyzing into an acidic buffer (at pH 4.5–4.8) [31–33], which can be used to package RNA replicons [156], or a neutral buffer which has been used with DNA cargoes [54]. CCMV VLPs were also produced using *E. coli* by expressing soluble capsid proteins, followed by purification and assembly in the presence of cargoes. To target subcutaneous cancers, folic acid (FA) was conjugated to CCMV capsid proteins [32,150]. Other VLPs obtained by in-vitro assembly were also tested for loading and drug delivery. Murine polyomavirus (MPyV) capsomeres fused to a desired protein were expressed in *E. coli* and the purified capsomeres were dialyzed resulting in the formation of VLPs

containing the guest protein for delivery [75]. Zhao et al. described a method to deliver the chemotherapy drug doxorubicin (DOX) using rotavirus (RV). RV structural protein VP6 formed inclusion bodies during expression in *E. coli*, and the protein was then purified under denaturing condition (8 M urea). DOX was conjugated to denatured VP proteins and the assembly of VLPs occurred during protein dialysis into a low pH buffer [21].

For diagnostic purposes such as magnetic resonance imaging (MRI), magnetic nanoparticles can also be coated with capsid proteins and additionally endowed with a targeting function. VP1<sup>ΔC589</sup>, VP1<sup>wt</sup> or VP1<sup>N138C</sup> of SV40 were produced in Sf9 cells and pentamers were purified and assembled around magnetic nano-particles in MOPS (3-Morpholinopropane-1-sulfonic acid) buffer. The latter two particles were crosslinked with epidermal growth factor (EGF) for the targeting of EGFR expressing cells using heterobifunctional crosslinkers with N-hydroxysuccinimide and maleimide groups [151]. Similarly, SV40 VLPs produced in *E. coli* have been used to encapsulate quantum dots for imaging [152]. Brome mosaic virus (BMV) and Ross River virus (RRV) particles were also explored for medical imaging. The purified capsid proteins were mixed with functionalized gold nanoparticles (GNPs) and dialyzed against an assembly buffer. The encapsulation was regulated by the electrostatic interactions between capsid proteins and gold nanoparticles, followed by the capsid protein–capsid protein interactions [153,154].

#### 4. Conclusions

VLPs have been widely exploited for vaccine development and therapeutic delivery with success in the clinic and promising preclinical evaluations. In vitro VLP production technology has emerged as a versatile technology besides the in vivo method. The formation of VLPs under controllable and defined conditions enables the technology to create multi-vaccine candidates by combining different antigens within a particle while avoiding the unpredictable immune response related to possible host-related contaminations. In vitro assembly of VLPs also offers a feasible tool to control the packaging amount and cargo components for therapeutic delivery.

In vitro VLP assembly is a complex process and differs among viral capsids. Even though many in-vitro VLPs have been produced, it is still unclear whether all virus capsids are amenable to ex cella production. Many factors need to be optimized for each candidate to assemble VLPs in vitro, improve assembly yields, and enable large-scale production. Cell-free protein synthesis in combination with in vitro VLP assembly bears potential for the generation of various synthetic biology products at a smaller scale. In vitro VLPs have been widely used as VLP-based protein vaccines. When in vitro nucleic acid encapsidation becomes more accessible, in vitro VLPs might also become an efficient and safe technology for vector VLP vaccines, which deliver an antigen-coding sequence, or for gene therapy vectors for treating diseases. Also for other therapeutic delivery strategies, recent advances provided mostly a proof of concept. Further work is needed to fully tap the potential of in vitro VLPs, but the future looks bright.

**Author Contributions:** Conceptualization, D.T.L. and K.M.M.; writing—original draft preparation, D.T.L.; writing—review and editing, K.M.M.; All authors have read and agreed to the published version of the manuscript.

**Funding:** We acknowledge support for the publication costs by the Open Access Publication Fund of Bielefeld University. D.T.L. acknowledges support by DAAD (Deutscher Akademischer Austauschdienst) for providing a PhD fellowship (Personal ref. no.: 91651068).

**Institutional Review Board Statement:** Not applicable.

**Informed Consent Statement:** Not applicable.

**Data Availability Statement:** Not applicable.

**Conflicts of Interest:** The authors declare no conflict of interest.

## References

1. Lua, L.H.L.; Connors, N.K.; Sainsbury, F.; Chuan, Y.P.; Wibowo, N.; Middelberg, A.P.J. Bioengineering virus-like particles as vaccines. *Biotechnol. Bioeng.* **2014**, *111*, 425–440. [[CrossRef](#)] [[PubMed](#)]
2. Jeevanandam, J.; Barhoum, A.; Chan, Y.S.; Dufresne, A.; Danquah, M.K. Review on nanoparticles and nanostructured materials: History, sources, toxicity and regulations. *Beilstein J. Nanotechnol.* **2018**, *9*, 1050–1074. [[CrossRef](#)]
3. Qian, C.; Liu, X.; Xu, Q.; Wang, Z.; Chen, J.; Li, T.; Zheng, Q.; Yu, H.; Gu, Y.; Li, S.; et al. Recent Progress on the Versatility of Virus-Like Particles. *Vaccines* **2020**, *8*, 139. [[CrossRef](#)] [[PubMed](#)]
4. Rohovie, M.J.; Nagasawa, M.; Swartz, J.R. Virus-like particles: Next-generation nanoparticles for targeted therapeutic delivery. *Bioeng. Transl. Med.* **2017**, *2*, 43–57. [[CrossRef](#)] [[PubMed](#)]
5. Lee, S.Y.; Lim, J.S.; Harris, M.T. Synthesis and application of virus-based hybrid nanomaterials. *Biotechnol. Bioeng.* **2012**, *109*, 16–30. [[CrossRef](#)] [[PubMed](#)]
6. Mohsen, M.; Gomes, A.; Vogel, M.; Bachmann, M. Interaction of Viral Capsid-Derived Virus-Like Particles (VLPs) with the Innate Immune System. *Vaccines* **2018**, *6*, 37. [[CrossRef](#)] [[PubMed](#)]
7. Vicente, T.; Mota, J.P.B.; Peixoto, C.; Alves, P.M.; Carrondo, M.J.T. Rational design and optimization of downstream processes of virus particles for biopharmaceutical applications: Current advances. *Biotechnol. Adv.* **2011**, *29*, 869–878. [[CrossRef](#)]
8. Gu, Y.; Wei, M.; Wang, D.; Li, Z.; Xie, M.; Pan, H.; Wu, T.; Zhang, J.; Li, S.; Xia, N. Characterization of an Escherichia coli-derived human papillomavirus type 16 and 18 bivalent vaccine. *Vaccine* **2017**, *35*, 4637–4645. [[CrossRef](#)] [[PubMed](#)]
9. Wei, M.; Wang, D.; Li, Z.; Song, S.; Kong, X.; Mo, X.; Yang, Y.; He, M.; Li, Z.; Huang, B.; et al. N-terminal truncations on L1 proteins of human papillomaviruses promote their soluble expression in Escherichia coli and self-assembly in vitro. *Emerg. Microbes Infect.* **2018**, *7*, 1–12. [[CrossRef](#)]
10. Zeltins, A. Construction and characterization of virus-like particles: A review. *Mol. Biotechnol.* **2013**, *53*, 92–107. [[CrossRef](#)]
11. Roldão, A.; Mellado, M.C.M.; Castilho, L.R.; Carrondo, M.J.T.; Alves, P.M. Virus-like particles in vaccine development. *Expert Rev. Vaccines* **2010**, *9*, 1149–1176. [[CrossRef](#)] [[PubMed](#)]
12. Huang, X.; Wang, X.; Zhang, J.; Xia, N.; Zhao, Q. Escherichia coli-derived virus-like particles in vaccine development. *npj Vaccines* **2017**, *2*, 3. [[CrossRef](#)] [[PubMed](#)]
13. Ladd Effio, C.; Baumann, P.; Weigel, C.; Vormittag, P.; Middelberg, A.; Hubbuch, J. High-throughput process development of an alternative platform for the production of virus-like particles in Escherichia coli. *J. Biotechnol.* **2016**, *219*, 7–19. [[CrossRef](#)]
14. Bajaj, S.; Banerjee, M. In vitro assembly of polymorphic virus-like particles from the capsid protein of a nodavirus. *Virology* **2016**, *496*, 106–115. [[CrossRef](#)] [[PubMed](#)]
15. Xu, J.; Guo, H.-C.C.; Wei, Y.-Q.Q.; Dong, H.; Han, S.-C.C.; Ao, D.; Sun, D.-H.H.; Wang, H.-M.M.; Cao, S.-Z.Z.; Sun, S.-Q.Q.; et al. Self-assembly of virus-like particles of canine parvovirus capsid protein expressed from Escherichia coli and application as virus-like particle vaccine. *Appl. Microbiol. Biotechnol.* **2014**, *98*, 3529–3538. [[CrossRef](#)] [[PubMed](#)]
16. Guo, H.; Zhu, J.; Tan, Y.; Li, C.; Chen, Z.; Sun, S.; Liu, G. Self-assembly of virus-like particles of rabbit hemorrhagic disease virus capsid protein expressed in Escherichia coli and their immunogenicity in rabbits. *Antiviral Res.* **2016**, *131*, 85–91. [[CrossRef](#)]
17. Yazdani, R.; Shams-Bakhsh, M.; Hassani-Mehraban, A.; Arab, S.S.; Thelen, N.; Thiry, M.; Crommen, J.; Fillet, M.; Jacobs, N.; Brans, A.; et al. Production and characterization of virus-like particles of grapevine fanleaf virus presenting L2 epitope of human papillomavirus minor capsid protein. *BMC Biotechnol.* **2019**, *19*, 81. [[CrossRef](#)]
18. Sánchez-Rodríguez, S.P.; Münch-Anguiano, L.; Echeverría, O.; Vázquez-Nin, G.; Mora-Pale, M.; Dordick, J.S.; Bustos-Jaimes, I. Human parvovirus B19 virus-like particles: In vitro assembly and stability. *Biochimie* **2012**, *94*, 870–878. [[CrossRef](#)]
19. Le, D.T.; Radukic, M.T.; Müller, K.M. Adeno-associated virus capsid protein expression in Escherichia coli and chemically defined capsid assembly. *Sci. Rep.* **2019**, *9*, 19631. [[CrossRef](#)]
20. Bin Mohamed Suffian, I.F.; Garcia-Maya, M.; Brown, P.; Bui, T.; Nishimura, Y.; Palermo, A.R.B.M.J.; Ogino, C.; Kondo, A.; Al-Jamal, K.T. Yield Optimisation of Hepatitis B Virus Core Particles in E. coli Expression System for Drug Delivery Applications. *Sci. Rep.* **2017**, *7*, 43160. [[CrossRef](#)]
21. Zhang, L.; Zhang, J.; Zhang, Z.; Chen, Y.; Zhao, Q.; Chen, W. Self-Assembled Virus-Like Particles from Rotavirus Structural Protein VP6 for Targeted Drug Delivery. *Bioconjug. Chem.* **2011**, *22*, 346–352. [[CrossRef](#)]
22. Steinbach, S.; Wistuba, A.; Bock, T.; Kleinschmidt, J.A. Assembly of adeno-associated virus type 2 capsids in vitro. *J. Gen. Virol.* **1997**, *78*, 1453–1462. [[CrossRef](#)] [[PubMed](#)]
23. Smith, G.; Raghunandan, R.; Wu, Y.; Liu, Y.; Massare, M.; Nathan, M.; Zhou, B.; Lu, H.; Boddapati, S.; Li, J.; et al. Respiratory Syncytial Virus Fusion Glycoprotein Expressed in Insect Cells Form Protein Nanoparticles That Induce Protective Immunity in Cotton Rats. *PLoS ONE* **2012**, *7*, e50852. [[CrossRef](#)]
24. Acosta-Rivero, N.; Rodriguez, A.; Musacchio, A.; Falcón, V.; Suarez, V.M.; Martinez, G.; Guerra, I.; Paz-Lago, D.; Morera, Y.; De La Rosa, M.C.; et al. In vitro assembly into virus-like particles is an intrinsic quality of Pichia pastoris derived HCV core protein. *Biochem. Biophys. Res. Commun.* **2004**, *325*, 68–74. [[CrossRef](#)] [[PubMed](#)]
25. Tinafar, A.; Jaenes, K.; Pardee, K. Synthetic Biology Goes Cell-Free. *BMC Biol.* **2019**, *17*, 64. [[CrossRef](#)]
26. Bundy, B.C.; Swartz, J.R. Efficient disulfide bond formation in virus-like particles. *J. Biotechnol.* **2011**, *154*, 230–239. [[CrossRef](#)]
27. Bundy, B.C.; Franciszkowicz, M.J.; Swartz, J.R. Escherichia coli-based cell-free synthesis of virus-like particles. *Biotechnol. Bioeng.* **2008**, *100*, 28–37. [[CrossRef](#)]

28. Spice, A.J.; Aw, R.; Bracewell, D.G.; Polizzi, K.M. Synthesis and Assembly of Hepatitis B Virus-Like Particles in a *Pichia pastoris* Cell-Free System. *Front. Bioeng. Biotechnol.* **2020**, *8*, 72. [[CrossRef](#)]
29. Ashley, C.E.; Carnes, E.C.; Phillips, G.K.; Durfee, P.N.; Buley, M.D.; Lino, C.A.; Padilla, D.P.; Phillips, B.; Carter, M.B.; Willman, C.L.; et al. Cell-specific delivery of diverse cargos by bacteriophage MS2 virus-like particles. *ACS Nano* **2011**, *5*, 5729–5745. [[CrossRef](#)] [[PubMed](#)]
30. McCarthy, M.P.; White, W.I.; Palmer-Hill, F.; Koenig, S.; Suzich, J.A. Quantitative Disassembly and Reassembly of Human Papillomavirus Type 11 Virus like Particles In Vitro. *J. Virol.* **1998**, *72*, 32–41. [[CrossRef](#)]
31. Villagrana-Escareño, M.V.; Reynaga-Hernández, E.; Galicia-Cruz, O.G.; Durán-Meza, A.L.; De la Cruz-González, V.; Hernández-Carballo, C.Y.; Ruíz-García, J. VLPs Derived from the CCMV Plant Virus Can Directly Transfect and Deliver Heterologous Genes for Translation into Mammalian Cells. *Biomed Res. Int.* **2019**, *2019*, 4630891. [[CrossRef](#)] [[PubMed](#)]
32. Lam, P.; Steinmetz, N.F. Delivery of siRNA therapeutics using cowpea chlorotic mottle virus-like particles. *Biomater. Sci.* **2019**, *7*, 3138–3142. [[CrossRef](#)] [[PubMed](#)]
33. Comellas-Aragonès, M.; Engelkamp, H.; Claessen, V.I.; Sommerdijk, N.A.J.M.; Rowan, A.E.; Christianen, P.C.M.; Maan, J.C.; Verduin, B.J.M.; Cornelissen, J.J.L.M.; Nolte, R.J.M. A virus-based single-enzyme nanoreactor. *Nat. Nanotechnol.* **2007**, *2*, 635–639. [[CrossRef](#)]
34. Fang, P.Y.; Ramos, L.M.G.; Holguin, S.Y.; Hsiao, C.; Bowman, J.C.; Yang, H.W.; Williams, L.D. Functional RNAs: Combined assembly and packaging in VLPs. *Nucleic Acids Res.* **2016**, *45*, 3519–3527. [[CrossRef](#)]
35. Ren, L.; Zhang, X.; Bi, S.; Shan, W.; Ye, S.; Hu, B.; Wu, Y.; Lv, X.; Zhang, D.; Zhou, X. Modularized peptides modified Hbc virus-like particles for encapsulation and tumor-targeted delivery of doxorubicin. *Nanomedicine Nanotechnology, Biol. Med.* **2017**, *14*, 725–734. [[CrossRef](#)]
36. Lee, E.B.; Kim, J.-H.; Hur, W.; Choi, J.E.; Kim, S.M.; Park, D.J.; Kang, B.-Y.; Lee, G.W.; Yoon, S.K. Liver-specific Gene Delivery Using Engineered Virus-Like Particles of Hepatitis E Virus. *Sci. Rep.* **2019**, *9*, 1616. [[CrossRef](#)]
37. Cerqueira, C.; Pang, Y.-Y.S.; Day, P.M.; Thompson, C.D.; Buck, C.B.; Lowy, D.R.; Schiller, J.T. A Cell-Free Assembly System for Generating Infectious Human Papillomavirus 16 Capsids Implicates a Size Discrimination Mechanism for Preferential Viral Genome Packaging. *J. Virol.* **2016**, *90*, 1096–1107. [[CrossRef](#)]
38. Cerqueira, C.; Thompson, C.D.; Day, P.M.; Pang, Y.-Y.S.; Lowy, D.R.; Schiller, J.T. Efficient Production of Papillomavirus Gene Delivery Vectors in Defined In Vitro Reactions. *Mol. Ther.-Methods Clin. Dev.* **2017**, *5*, 165–179. [[CrossRef](#)] [[PubMed](#)]
39. Touze, A.; Coursaget, P. In vitro gene transfer using human papillomavirus-like particles. *Nucleic Acids Res.* **1998**, *26*, 1317–1323. [[CrossRef](#)]
40. Colomar, M.C.; Degoumois-Sahli, C.; Beard, P. Opening and refolding of simian virus 40 and in vitro packaging of foreign DNA. *J. Virol.* **1993**, *67*, 2779–2786. [[CrossRef](#)] [[PubMed](#)]
41. Sandalon, Z.; Dalyot-Herman, N.; Oppenheim, A.B.; Oppenheim, A. In Vitro Assembly of SV40 Virions and Pseudovirions: Vector Development for Gene Therapy. *Hum. Gene Ther.* **1997**, *8*, 843–849. [[CrossRef](#)]
42. Perlmutter, J.D.; Hagan, M.F. Mechanisms of virus assembly. *Annu. Rev. Phys. Chem.* **2015**, *66*, 217–239. [[CrossRef](#)]
43. Hagan, M.F. Modeling Viral Capsid Assembly. In *Advances in Chemical Physics*; Rice, S.A., Dinner, A.R., Eds.; John Wiley & Sons, Inc.: Hoboken, NJ, USA, 2014; pp. 1–68. ISBN 6176321972.
44. Hagan, M.F.; Elrad, O.M. Understanding the Concentration Dependence of Viral Capsid Assembly Kinetics—The Origin of the Lag Time and Identifying the Critical Nucleus Size. *Biophys. J.* **2010**, *98*, 1065–1074. [[CrossRef](#)]
45. Chi, E.Y.; Krishnan, S.; Randolph, T.W.; Carpenter, J.F. Physical stability of proteins in aqueous solution: Mechanism and driving forces in nonnative protein aggregation. *Pharm. Res.* **2003**, *20*, 1325–1336. [[CrossRef](#)]
46. Barklis, E.; Alfadhli, A.; McQuaw, C.; Yalamuri, S.; Still, A.; Barklis, R.L.; Kukull, B.; López, C.S. Characterization of the In Vitro HIV-1 Capsid Assembly Pathway. *J. Mol. Biol.* **2009**, *387*, 376–389. [[CrossRef](#)]
47. Johnson, J.M.; Tang, J.; Nyame, Y.; Willits, D.; Young, M.J.; Zlotnick, A. Regulating self-assembly of spherical oligomers. *Nano Lett.* **2005**, *5*, 765–770. [[CrossRef](#)] [[PubMed](#)]
48. Dominy, B.N.; Perl, D.; Schmid, F.X.; Brooks, C.L. The effects of ionic strength on protein stability: The cold shock protein family. *J. Mol. Biol.* **2002**, *319*, 541–554. [[CrossRef](#)]
49. Lavelle, L.; Gingery, M.; Phillips, M.; Gelbart, W.M.; Knobler, C.M.; Cadena-Nava, R.D.; Vega-Acosta, J.R.; Pinedo-Torres, L.A.; Ruiz-Garcia, J. Phase diagram of self-assembled viral capsid protein polymorphs. *J. Phys. Chem. B* **2009**, *113*, 3813–3819. [[CrossRef](#)]
50. Jaballah, S.A.; Bailey, G.D.; Desfosses, A.; Hyun, J.; Mitra, A.K.; Kingston, R.L. In vitro assembly of the Rous Sarcoma Virus capsid protein into hexamer tubes at physiological temperature. *Sci. Rep.* **2017**, *7*, 2913. [[CrossRef](#)] [[PubMed](#)]
51. Uetrecht, C.; Watts, N.R.; Stahl, S.J.; Wingfield, P.T.; Steven, A.C.; Heck, A.J.R. Subunit exchange rates in Hepatitis B virus capsids are geometry- and temperature-dependent. *Phys. Chem. Chem. Phys.* **2010**, *12*, 13368–13371. [[CrossRef](#)]
52. Comas-Garcia, M.; Knobler, C.M.; Gelbart, W.M.; Gopal, A.; Garmann, R.F. The Assembly Pathway of an Icosahedral Single-Stranded RNA Virus Depends on the Strength of Inter-Subunit Attractions. *J. Mol. Biol.* **2013**, *426*, 1050–1060. [[CrossRef](#)]
53. Gelbart, W.M.; Garmann, R.F.; Cadena-Nava, R.D.; Comas-Garcia, M.; Knobler, C.M.; Rao, A.L.N. Self-Assembly of Viral Capsid Protein and RNA Molecules of Different Sizes: Requirement for a Specific High Protein/RNA Mass Ratio. *J. Virol.* **2011**, *86*, 3318–3326. [[CrossRef](#)]

54. de Ruiter, M.V.; van der Hee, R.M.; Driessen, A.J.M.; Keurhorst, E.D.; Hamid, M.; Cornelissen, J.J.L.M. Polymorphic assembly of virus-capsid proteins around DNA and the cellular uptake of the resulting particles. *J. Control. Release* **2019**, *307*, 342–354. [[CrossRef](#)]
55. Comas-Garcia, M.; Kroupa, T.; Datta, S.A.K.; Harvin, D.P.; Hu, W.-S.; Rein, A. Efficient support of virus-like particle assembly by the HIV-1 packaging signal. *Elife* **2018**, *7*, e38438. [[CrossRef](#)] [[PubMed](#)]
56. Kunkel, M.; Lorinczi, M.; Rijnbrand, R.; Lemon, S.M.; Watowich, S.J. Self-Assembly of Nucleocapsid-Like Particles from Recombinant Hepatitis C Virus Core Protein. *J. Virol.* **2001**, *75*, 2119–2129. [[CrossRef](#)] [[PubMed](#)]
57. Sarker, S.; Terrón, M.C.; Khandokar, Y.; Aragão, D.; Hardy, J.M.; Radjainia, M.; Jiménez-Zaragoza, M.; de Pablo, P.J.; Coulibaly, F.; Luque, D.; et al. Structural insights into the assembly and regulation of distinct viral capsid complexes. *Nat. Commun.* **2016**, *7*, 13014. [[CrossRef](#)]
58. van Rosmalen, M.G.M.; Kamsma, D.; Biebricher, A.S.; Li, C.; Zlotnick, A.; Roos, W.H.; Wuite, G.J.L. Revealing in real-time a multistep assembly mechanism for SV40 virus-like particles. *Sci. Adv.* **2020**, *6*, eaaz1639. [[CrossRef](#)] [[PubMed](#)]
59. Medina, E.M.; Andrews, B.T.; Nakatani, E.; Catalano, C.E. The bacteriophage lambda gpNu3 scaffolding protein is an intrinsically disordered and biologically functional procapsid assembly catalyst. *J. Mol. Biol.* **2011**, *412*, 723–736. [[CrossRef](#)]
60. Motwani, T.; Lokareddy, R.K.; Dunbar, C.A.; Cortines, J.R.; Jarrold, M.F.; Cingolani, G.; Teschke, C.M. A viral scaffolding protein triggers portal ring oligomerization and incorporation during procapsid assembly. *Sci. Adv.* **2017**, *3*, e1700423. [[CrossRef](#)] [[PubMed](#)]
61. Wang, S.; Palasingam, P.; Nøkling, R.H.; Lindqvist, B.H.; Dokland, T. In vitro assembly of bacteriophage P4 procapsids from purified capsid and scaffolding proteins. *Virology* **2000**, *275*, 133–144. [[CrossRef](#)] [[PubMed](#)]
62. Cerritelli, M.E.; Studier, F.W. Assembly of T7 capsids from independently expressed and purified head protein and scaffolding protein. *J. Mol. Biol.* **1996**, *258*, 286–298. [[CrossRef](#)]
63. Fu, C.; Morais, M.C.; Battisti, A.J.; Rossmann, M.G.; Prevelige, P.E. Molecular Dissection of Ø29 Scaffolding Protein Function in an in Vitro Assembly System. *J. Mol. Biol.* **2007**, *366*, 1161–1173. [[CrossRef](#)] [[PubMed](#)]
64. Newcomb, W.W.; Homa, F.L.; Thomsen, D.R.; Brown, J.C. In vitro assembly of the herpes simplex virus procapsid: Formation of small procapsids at reduced scaffolding protein concentration. *J. Struct. Biol.* **2001**, *133*, 23–31. [[CrossRef](#)] [[PubMed](#)]
65. Sánchez-Rodríguez, S.P.; Morán-García, A. del C.; Bolonduro, O.; Dordick, J.S.; Bustos-Jaimes, I. Enhanced assembly and colloidal stabilization of primate erythroparvovirus 1 virus-like particles for improved surface engineering. *Acta Biomater.* **2016**, *35*, 206–214. [[CrossRef](#)]
66. Lampel, A.; Bram, Y.; Levy-Sakin, M.; Bacharach, E.; Gazit, E. The Effect of Chemical Chaperones on the Assembly and Stability of HIV-1 Capsid Protein. *PLoS ONE* **2013**, *8*, 25–29. [[CrossRef](#)] [[PubMed](#)]
67. Sinn, S.; Yang, L.; Biedermann, F.; Wang, D.; Kübel, C.; Cornelissen, J.J.L.M.; De Cola, L. Templated Formation of Luminescent Virus-like Particles by Tailor-Made Pt(II) Amphiphiles. *J. Am. Chem. Soc.* **2018**, *140*, 2355–2362. [[CrossRef](#)] [[PubMed](#)]
68. Millán, J.G.; Brasch, M.; Anaya-Plaza, E.; De La Escosura, A.; Velders, A.H.; Reinhoudt, D.N.; Torres, T.; Koay, M.S.T.; Cornelissen, J.J.L.M. Self-assembly triggered by self-assembly: Optically active, paramagnetic micelles encapsulated in protein cage nanoparticles. *J. Inorg. Biochem.* **2014**, *136*, 140–146. [[CrossRef](#)] [[PubMed](#)]
69. Kwak, M.; Minten, I.J.; Anaya, D.M.; Musser, A.J.; Brasch, M.; Nolte, R.J.M.; Müllen, K.; Cornelissen, J.J.L.M.; Herrmann, A. Virus-like particles templated by DNA micelles: A general method for loading virus nanocarriers. *J. Am. Chem. Soc.* **2010**, *132*, 7834–7835. [[CrossRef](#)] [[PubMed](#)]
70. Comellas-Aragonès, M.; de la Escosura, A.; Dirks, A.T.J.; van der Ham, A.; Fustè-Cuñè, A.; Cornelissen, J.J.L.M.; Nolte, R.J.M. Controlled Integration of Polymers into Viral Capsids. *Biomacromolecules* **2009**, *10*, 3141–3147. [[CrossRef](#)]
71. Sikkema, F.D.; Comellas-Aragonès, M.; Fokkink, R.G.; Verduin, B.J.M.; Cornelissen, J.J.L.M.; Nolte, R.J.M. Monodisperse polymer-virus hybrid nanoparticles. *Org. Biomol. Chem.* **2007**, *5*, 54–57. [[CrossRef](#)]
72. Mach, H.; Middaugh, C.R.; Lewis, R.V. Statistical determination of the average values of the extinction coefficients of tryptophan and tyrosine in native proteins. *Anal. Biochem.* **1992**, *200*, 74–80. [[CrossRef](#)]
73. Mach, H.; Middaugh, C.R. Simultaneous Monitoring of the Environment of Tryptophan, Tyrosine, and Phenylalanine Residues in Proteins by Near-Ultraviolet Second-Derivative Spectroscopy. *Anal. Biochem.* **1994**, *222*, 323–331. [[CrossRef](#)] [[PubMed](#)]
74. Walker, J.M. The Bicinchoninic Acid (BCA) Assay for Protein Quantitation. *Methods Mol. Biol.* **1994**, *32*, 5–8. [[CrossRef](#)]
75. Dashti, N.H.; Abidin, R.S.; Sainsbury, F. Programmable in Vitro Coencapsulation of Guest Proteins for Intracellular Delivery by Virus-like Particles. *ACS Nano* **2018**, *12*, 4615–4623. [[CrossRef](#)] [[PubMed](#)]
76. Glasgow, J.E.; Capehart, S.L.; Francis, M.B.; Tullman-Ercek, D. Osmolyte-mediated encapsulation of proteins inside MS2 viral capsids. *ACS Nano* **2012**, *6*, 8658–8664. [[CrossRef](#)] [[PubMed](#)]
77. Termini, E.; Description, F.P.; Street, D.; Id, B.S.; Schedule, E.; Code, F.F.; Funds, F.; Code, S.F.; Funds, S.; Funds, L.; et al. SARS-CoV-2 spike glycoprotein vaccine candidate NVX-CoV2373 elicits immunogenicity in baboons and protection in mice. *bioRxiv* **2020**. [[CrossRef](#)]
78. Zhang, X.; Wei, M.; Pan, H.; Lin, Z.; Wang, K.; Weng, Z.; Zhu, Y.; Xin, L.; Zhang, J.; Li, S.; et al. Robust manufacturing and comprehensive characterization of recombinant hepatitis E virus-like particles in Hecolin<sup>®</sup>. *Vaccine* **2014**, *32*, 4039–4050. [[CrossRef](#)] [[PubMed](#)]
79. European Medicines Agency Gardasil: EPAR—Scientific discussion. Available online: [https://www.ema.europa.eu/en/documents/scientific-discussion/gardasil-epar-scientific-discussion\\_en.pdf](https://www.ema.europa.eu/en/documents/scientific-discussion/gardasil-epar-scientific-discussion_en.pdf) (accessed on 20 December 2020).

80. Zhao, Q.; Allen, M.J.; Wang, Y.; Wang, B.; Wang, N.; Shi, L.; Sitrin, R.D. Disassembly and reassembly improves morphology and thermal stability of human papillomavirus type 16 virus-like particles. *Nanomed. Nanotechnol. Biol. Med.* **2012**, *8*, 1182–1189. [[CrossRef](#)]
81. Valbuena, A.; Maity, S.; Mateu, M.G.; Roos, W.H. Visualization of Single Molecules Building a Viral Capsid Protein Lattice through Stochastic Pathways. *ACS Nano* **2020**, *14*, 8724–8734. [[CrossRef](#)]
82. Ashcroft, A.E. Mass spectrometry-based studies of virus assembly. *Curr. Opin. Virol.* **2019**, *36*, 17–24. [[CrossRef](#)]
83. Prevelige, P.E.; Thomas, D.; King, J. Nucleation and growth phases in the polymerization of coat and scaffolding subunits into icosahedral procapsid shells. *Biophys. J.* **1993**, *64*, 824–835. [[CrossRef](#)]
84. Li, C.; Kneller, A.R.; Jacobson, S.C.; Zlotnick, A. Single Particle Observation of SV40 VP1 Polyanion-Induced Assembly Shows That Substrate Size and Structure Modulate Capsid Geometry. *ACS Chem. Biol.* **2017**, *12*, 1327–1334. [[CrossRef](#)] [[PubMed](#)]
85. Medrano, M.; Fuertes, M.Á.; Valbuena, A.; Carrillo, P.J.P.; Rodríguez-Huete, A.; Mateu, M.G. Imaging and Quantitation of a Succession of Transient Intermediates Reveal the Reversible Self-Assembly Pathway of a Simple Icosahedral Virus Capsid. *J. Am. Chem. Soc.* **2016**, *138*, 15385–15396. [[CrossRef](#)]
86. Ignatiou, A.; Brasilès, S.; El Sadek Fadel, M.; Bürger, J.; Mielke, T.; Topf, M.; Tavares, P.; Orlova, E.V. Structural transitions during the scaffolding-driven assembly of a viral capsid. *Nat. Commun.* **2019**, *10*, 4840. [[CrossRef](#)] [[PubMed](#)]
87. Khaykelson, D.; Raviv, U. Studying viruses using solution X-ray scattering. *Biophys. Rev.* **2020**, *12*, 41–48. [[CrossRef](#)] [[PubMed](#)]
88. Tuma, R.; Tsuruta, H.; French, K.H.; Prevelige, P.E. Detection of Intermediates and Kinetic Control during Assembly of Bacteriophage P22 Procapsid. *J. Mol. Biol.* **2008**, *381*, 1395–1406. [[CrossRef](#)] [[PubMed](#)]
89. Tresset, G.; Le Coeur, C.; Bryche, J.-F.; Tatou, M.; Zeghal, M.; Charpilienne, A.; Poncet, D.; Constantin, D.; Bressanelli, S. Norovirus Capsid Proteins Self-Assemble through Biphasic Kinetics via Long-Lived Stave-like Intermediates. *J. Am. Chem. Soc.* **2013**, *135*, 15373–15381. [[CrossRef](#)] [[PubMed](#)]
90. Asor, R.; Selzer, L.; Schlicksup, C.J.; Zhao, Z.; Zlotnick, A.; Raviv, U. Assembly Reactions of Hepatitis B Capsid Protein into Capsid Nanoparticles Follow a Narrow Path through a Complex Reaction Landscape. *ACS Nano* **2019**, *13*, 7610–7626. [[CrossRef](#)]
91. Chevreuril, M.; Law-Hine, D.; Chen, J.; Bressanelli, S.; Combet, S.; Constantin, D.; Degrouard, J.; Möller, J.; Zeghal, M.; Tresset, G. Nonequilibrium self-assembly dynamics of icosahedral viral capsids packaging genome or polyelectrolyte. *Nat. Commun.* **2018**, *9*, 3071. [[CrossRef](#)] [[PubMed](#)]
92. Panahandeh, S.; Li, S.; Marichal, L.; Leite Rubim, R.; Tresset, G.; Zandi, R. How a Virus Circumvents Energy Barriers to Form Symmetric Shells. *ACS Nano* **2020**, *14*, 3170–3180. [[CrossRef](#)] [[PubMed](#)]
93. Uetrecht, C.; Barbu, I.M.; Shoemaker, G.K.; van Duijn, E.; Heck, A.J.R. Interrogating viral capsid assembly with ion mobility–mass spectrometry. *Nat. Chem.* **2011**, *3*, 126–132. [[CrossRef](#)] [[PubMed](#)]
94. Lutomski, C.A.; Lykтей, N.A.; Pierson, E.E.; Zhao, Z.; Zlotnick, A.; Jarrold, M.F. Multiple Pathways in Capsid Assembly. *J. Am. Chem. Soc.* **2018**, *140*, 5784–5790. [[CrossRef](#)] [[PubMed](#)]
95. Shoemaker, G.K.; van Duijn, E.; Crawford, S.E.; Uetrecht, C.; Baclayon, M.; Roos, W.H.; Wuite, G.J.L.; Estes, M.K.; Prasad, B.V.V.; Heck, A.J.R. Norwalk Virus Assembly and Stability Monitored by Mass Spectrometry. *Mol. Cell. Proteomics* **2010**, *9*, 1742–1751. [[CrossRef](#)]
96. Harms, Z.D.; Selzer, L.; Zlotnick, A.; Jacobson, S.C. Monitoring Assembly of Virus Capsids with Nanofluidic Devices. *ACS Nano* **2015**, *9*, 9087–9096. [[CrossRef](#)]
97. Garmann, R.F.; Goldfain, A.M.; Manoharan, V.N. Measurements of the self-assembly kinetics of individual viral capsids around their RNA genome. *Proc. Natl. Acad. Sci.* **2019**, *116*, 22485–22490. [[CrossRef](#)]
98. Borodavka, A.; Tuma, R.; Stockley, P.G. Evidence that viral RNAs have evolved for efficient, two-stage packaging. *Proc. Natl. Acad. Sci. USA* **2012**, *109*, 15769–15774. [[CrossRef](#)]
99. Marchetti, M.; Kamsma, D.; Cazares Vargas, E.; Hernandez García, A.; van der Schoot, P.; de Vries, R.; Wuite, G.J.L.; Roos, W.H. Real-Time Assembly of Viruslike Nucleocapsids Elucidated at the Single-Particle Level. *Nano Lett.* **2019**, *19*, 5746–5753. [[CrossRef](#)]
100. Uchihashi, T.; Scheuring, S. Applications of high-speed atomic force microscopy to real-time visualization of dynamic biomolecular processes. *Biochim. Biophys. Acta-Gen. Subj.* **2018**, *1862*, 229–240. [[CrossRef](#)]
101. Jennings, G.T.; Bachmann, M.F. The coming of age of virus-like particle vaccines. *Biol. Chem.* **2008**, *389*, 521–536. [[CrossRef](#)]
102. Jegerlehner, A.; Storni, T.; Lipowsky, G.; Schmid, M.; Pumpens, P.; Bachmann, M.F. Regulation of IgG antibody responses by epitope density and CD21-mediated costimulation. *Eur. J. Immunol.* **2002**, *32*, 3305–3314. [[CrossRef](#)]
103. Chackerian, B.; Lenz, P.; Lowy, D.R.; Schiller, J.T. Determinants of Autoantibody Induction by Conjugated Papillomavirus Virus-Like Particles. *J. Immunol.* **2002**, *169*, 6120–6126. [[CrossRef](#)]
104. Zabel, F.; Mohanan, D.; Bessa, J.; Link, A.; Fettelschoss, A.; Saudan, P.; Kündig, T.M.; Bachmann, M.F. Viral Particles Drive Rapid Differentiation of Memory B Cells into Secondary Plasma Cells Producing Increased Levels of Antibodies. *J. Immunol.* **2014**, *192*, 5499–5508. [[CrossRef](#)] [[PubMed](#)]
105. Peacey, M.; Wilson, S.; Baird, M.A.; Ward, V.K. Versatile RHDV virus-like particles: Incorporation of antigens by genetic modification and chemical conjugation. *Biotechnol. Bioeng.* **2007**, *98*, 968–977. [[CrossRef](#)] [[PubMed](#)]
106. Billaud, J.-N.; Peterson, D.; Barr, M.; Chen, A.; Sallberg, M.; Garduno, F.; Goldstein, P.; McDowell, W.; Hughes, J.; Jones, J.; et al. Combinatorial Approach to Hepadnavirus-Like Particle Vaccine Design. *J. Virol.* **2005**, *79*, 13656–13666. [[CrossRef](#)]

107. Marini, A.; Zhou, Y.; Li, Y.; Taylor, I.J.; Leneghan, D.B.; Jin, J.; Zanic, M.; Mekhaieel, D.; Long, C.A.; Miura, K.; et al. A Universal Plug-and-Display Vaccine Carrier Based on HBsAg VLP to Maximize Effective Antibody Response. *Front. Immunol.* **2019**, *10*, 02931. [CrossRef] [PubMed]
108. Zha, L.; Zhao, H.; Mohsen, M.O.; Hong, L.; Zhou, Y.; Li, Z.; Yao, C.; Guo, L.; Chen, H.; Liu, X.; et al. Development of a COVID-19 vaccine based on the receptor binding domain displayed on virus-like particles. *bioRxiv* **2020**. [CrossRef]
109. European Medicines Agency Cervarix: EPAR—Scientific Discussion. Available online: [https://www.ema.europa.eu/en/documents/scientific-discussion/cervarix-epar-scientific-discussion\\_en.pdf](https://www.ema.europa.eu/en/documents/scientific-discussion/cervarix-epar-scientific-discussion_en.pdf) (accessed on 20 December 2020).
110. European Medicines Agency Gardasil 9: EPAR - Product Information-EMA/CHMP/76591/2015. Available online: [https://www.ema.europa.eu/en/documents/assessment-report/gardasil-9-epar-public-assessment-report\\_en.pdf](https://www.ema.europa.eu/en/documents/assessment-report/gardasil-9-epar-public-assessment-report_en.pdf) (accessed on 20 December 2020).
111. Qiao, Y.L.; Wu, T.; Li, R.C.; Hu, Y.M.; Wei, L.H.; Li, C.G.; Chen, W.; Huang, S.J.; Zhao, F.H.; Li, M.Q.; et al. Efficacy, Safety, and Immunogenicity of an Escherichia coli-Produced Bivalent Human Papillomavirus Vaccine: An Interim Analysis of a Randomized Clinical Trial. *J. Natl. Cancer Inst.* **2020**, *112*, 145–153. [CrossRef]
112. Li, S.W.; Zhang, J.; Li, Y.M.; Ou, S.H.; Huang, G.Y.; He, Z.Q.; Ge, S.X.; Xian, Y.L.; Pang, S.Q.; Ng, M.H.; et al. A bacterially expressed particulate hepatitis E vaccine: Antigenicity, immunogenicity and protectivity on primates. *Vaccine* **2005**, *23*, 2893–2901. [CrossRef] [PubMed]
113. Wu, T.; Li, S.W.; Zhang, J.; Ng, M.H.; Xia, N.S.; Zhao, Q. Hepatitis E vaccine development: A 14-year odyssey. *Hum. Vaccines Immunother.* **2012**, *8*, 823–827. [CrossRef] [PubMed]
114. Zhu, F.C.; Zhang, J.; Zhang, X.F.; Zhou, C.; Wang, Z.Z.; Huang, S.J.; Wang, H.; Yang, C.L.; Jiang, H.M.; Cai, J.P.; et al. Efficacy and safety of a recombinant hepatitis e vaccine in healthy adults: A large-scale, randomised, double-blind placebo-controlled, phase 3 trial. *Lancet* **2010**, *376*, 895–902. [CrossRef]
115. Zheng, M.; Jiang, J.; Zhang, X.; Wang, N.; Wang, K.; Li, Q.; Li, T.; Lin, Q.; Wang, Y.; Yu, H.; et al. Characterization of capsid protein (p495) of hepatitis E virus expressed in Escherichia coli and assembling into particles in vitro. *Vaccine* **2018**, *36*, 2104–2111. [CrossRef]
116. U.S. Food and Drug Administration Summary for Basis of Approval-ENGERIX-B. Available online: <https://wayback.archive-it.org/7993/20170404184231/https://www.fda.gov/downloads/BiologicsBloodVaccines/Vaccines/ApprovedProducts/UCM110155.pdf> (accessed on 20 December 2020).
117. European Medicines Agency Fendrix: EPAR-Scientific Discussion. Available online: [https://www.ema.europa.eu/en/documents/scientific-discussion/fendrix-epar-scientific-discussion\\_en.pdf](https://www.ema.europa.eu/en/documents/scientific-discussion/fendrix-epar-scientific-discussion_en.pdf) (accessed on 20 December 2020).
118. McAleer, W.J.; Buynak, E.B.; Maigetter, R.Z.; Wampler, D.E.; Miller, W.J.; Hilleman, M.R. Human hepatitis B vaccine from recombinant yeast. *Nature* **1984**, *307*, 178–180. [CrossRef] [PubMed]
119. Hilleman, M.R. Yeast recombinant hepatitis B vaccine. *Infection* **1987**, *15*, 3–7. [CrossRef] [PubMed]
120. Keech, C.; Albert, G.; Cho, I.; Robertson, A.; Reed, P.; Neal, S.; Plested, J.S.; Zhu, M.; Cloney-Clark, S.; Zhou, H.; et al. Phase 1–2 Trial of a SARS-CoV-2 Recombinant Spike Protein Nanoparticle Vaccine. *N. Engl. J. Med.* **2020**, *383*, 2320–2332. [CrossRef]
121. Coleman, C.M.; Liu, Y.V.; Mu, H.; Taylor, J.K.; Massare, M.; Flyer, D.C.; Glenn, G.M.; Smith, G.E.; Frieman, M.B. Purified coronavirus spike protein nanoparticles induce coronavirus neutralizing antibodies in mice. *Vaccine* **2014**, *32*, 3169–3174. [CrossRef] [PubMed]
122. Smith, G.; Liu, Y.; Flyer, D.; Massare, M.J.; Zhou, B.; Patel, N.; Ellingsworth, L.; Lewis, M.; Cummings, J.F.; Glenn, G. Novel hemagglutinin nanoparticle influenza vaccine with Matrix-M<sup>TM</sup> adjuvant induces hemagglutination inhibition, neutralizing, and protective responses in ferrets against homologous and drifted A(H3N2) subtypes. *Vaccine* **2017**, *35*, 5366–5372. [CrossRef]
123. Portnoff, A.D.; Patel, N.; Massare, M.J.; Zhou, H.; Tian, J.-H.; Zhou, B.; Shinde, V.; Glenn, G.M.; Smith, G. Influenza Hemagglutinin Nanoparticle Vaccine Elicits Broadly Neutralizing Antibodies against Structurally Distinct Domains of H3N2 HA. *Vaccines* **2020**, *8*, 99. [CrossRef] [PubMed]
124. Glenn, G.M.; Smith, G.; Fries, L.; Raghunandan, R.; Lu, H.; Zhou, B.; Thomas, D.N.; Hickman, S.P.; Kpamegan, E.; Boddapati, S.; et al. Safety and immunogenicity of a Sf9 insect cell-derived respiratory syncytial virus fusion protein nanoparticle vaccine. *Vaccine* **2013**, *31*, 524–532. [CrossRef] [PubMed]
125. Fries, L.; Shinde, V.; Stoddard, J.J.; Thomas, D.N.; Kpamegan, E.; Lu, H.; Smith, G.; Hickman, S.P.; Piedra, P.; Glenn, G.M. Immunogenicity and safety of a respiratory syncytial virus fusion protein (RSV F) nanoparticle vaccine in older adults. *Immun. Ageing* **2017**, *14*, 8. [CrossRef]
126. del Carmen Morán-García, A.; Rivera-Toledo, E.; Echeverría, O.; Vázquez-Nin, G.; Gómez, B.; Bustos-Jaimes, I. Peptide presentation on primate erythroparvovirus 1 virus-like particles: In vitro assembly, stability and immunological properties. *Virus Res.* **2016**, *224*, 12–18. [CrossRef] [PubMed]
127. Ljubojevic, S.; Skerlev, M. HPV-associated diseases. *Clin. Dermatol.* **2014**, *32*, 227–234. [CrossRef] [PubMed]
128. Baker, T.S.; Newcomb, W.W.; Olson, N.H.; Cowser, L.M.; Olson, C.; Brown, J.C. Structures of bovine and human papillomaviruses. Analysis by cryoelectron microscopy and three-dimensional image reconstruction. *Biophys. J.* **1991**, *60*, 1445–1456. [CrossRef]
129. Neeper, M.P.; Hofmann, K.J.; Jansen, K.U. Expression of the major capsid protein of human papillomavirus type 11 in *Saccharomyces cerevisiae*. *Gene* **1996**, *180*, 1–6. [CrossRef]
130. Schädlich, L.; Senger, T.; Kirschning, C.J.; Müller, M.; Gissmann, L. Refining HPV 16 L1 purification from *E. coli*: Reducing endotoxin contaminations and their impact on immunogenicity. *Vaccine* **2009**, *27*, 1511–1522. [CrossRef]

131. Kamar, N.; Dalton, H.R.; Abravanel, F.; Izopet, J. Hepatitis E virus infection. *Clin. Microbiol. Rev.* **2014**, *27*, 116–138. [[CrossRef](#)]
132. Hoofnagle, J.H.; Nelson, K.E.; Purcell, R.H. Hepatitis E. *N. Engl. J. Med.* **2012**, *367*, 1237–1244. [[CrossRef](#)]
133. Tam, A.W.; Smith, M.M.; Guerra, M.E.; Huang, C.-C.; Bradley, D.W.; Fry, K.E.; Reyes, G.R. Hepatitis E virus (HEV): Molecular cloning and sequencing of the full-length viral genome. *Virology* **1991**, *185*, 120–131. [[CrossRef](#)]
134. Guu, T.S.Y.; Liu, Z.; Ye, Q.; Mata, D.A.; Li, K.; Yin, C.; Zhang, J.; Tao, Y.J. Structure of the hepatitis E virus-like particle suggests mechanisms for virus assembly and receptor binding. *Proc. Natl. Acad. Sci. USA* **2009**, *106*, 12992–12997. [[CrossRef](#)]
135. Emerson, S.U.; Purcell, R.H. Recombinant vaccines for hepatitis E. *Trends Mol. Med.* **2001**, *7*, 462–466. [[CrossRef](#)]
136. Yuen, M.-F.; Chen, D.-S.; Dusheiko, G.M.; Janssen, H.L.A.; Lau, D.T.Y.; Locarnini, S.A.; Peters, M.G.; Lai, C.-L. Hepatitis B virus infection. *Nat. Rev. Dis. Prim.* **2018**, *4*, 18035. [[CrossRef](#)] [[PubMed](#)]
137. European Medicines Agency Mosquirix: Public Assessment Report-EMA/CHMP/439337/2015. Available online: [https://www.ema.europa.eu/en/documents/medicine-outside-eu/mosquirix-public-assessment-report\\_en.pdf](https://www.ema.europa.eu/en/documents/medicine-outside-eu/mosquirix-public-assessment-report_en.pdf) (accessed on 20 December 2020).
138. Shin, M.D.; Shukla, S.; Chung, Y.H.; Beiss, V.; Chan, S.K.; Ortega-Rivera, O.A.; Wirth, D.M.; Chen, A.; Sack, M.; Pokorski, J.K.; et al. COVID-19 vaccine development and a potential nanomaterial path forward. *Nat. Nanotechnol.* **2020**, *15*, 646–655. [[CrossRef](#)]
139. Wrapp, D.; Wang, N.; Corbett, K.S.; Goldsmith, J.A.; Hsieh, C.-L.; Abiona, O.; Graham, B.S.; McLellan, J.S. Cryo-EM structure of the 2019-nCoV spike in the prefusion conformation. *Science* **2020**, *367*, 1260–1263. [[CrossRef](#)] [[PubMed](#)]
140. Steinmetz, N.F. Viral nanoparticles as platforms for next-generation therapeutics and imaging devices. *Nanomed. Nanotechnol. Biol. Med.* **2010**, *6*, 634–641. [[CrossRef](#)] [[PubMed](#)]
141. Bajaj, S.; Banerjee, M. Engineering Virus Capsids Into Biomedical Delivery Vehicles: Structural Engineering Problems in Nanoscale. *J. Biomed. Nanotechnol.* **2015**, *11*, 53–69. [[CrossRef](#)]
142. Schwarz, B.; Uchida, M.; Douglas, T. Biomedical and Catalytic Opportunities of Virus-Like Particles in Nanotechnology. *Adv. Virus Res.* **2017**, *97*, 1–60. [[CrossRef](#)]
143. Galaway, F.A.; Stockley, P.G. MS2 Viruslike Particles: A Robust, Semisynthetic Targeted Drug Delivery Platform. *Mol. Pharm.* **2013**, *10*, 59–68. [[CrossRef](#)]
144. Waghvani, H.K.; Uchida, M.; Fu, C.Y.; Lafrance, B.; Sharma, J.; McCoy, K.; Douglas, T. Virus-Like Particles (VLPs) as a Platform for Hierarchical Compartmentalization. *Biomacromolecules* **2020**, *21*, 2060–2072. [[CrossRef](#)]
145. Sharma, J.; Uchida, M.; Miettinen, H.M.; Douglas, T. Modular interior loading and exterior decoration of a virus-like particle. *Nanoscale* **2017**, *9*, 10420–10430. [[CrossRef](#)]
146. Kimchi-Sarfaty, C.; Ben-Nun-Shaul, O.; Rund, D.; Oppenheim, A.; Gottesman, M.M. In Vitro -Packaged SV40 Pseudovirions as Highly Efficient Vectors for Gene Transfer. *Hum. Gene Ther.* **2002**, *13*, 299–310. [[CrossRef](#)] [[PubMed](#)]
147. Kimchi-Sarfaty, C.; Vieira, W.D.; Dodds, D.; Sherman, A.; Kreitman, R.J.; Shinar, S.; Gottesman, M.M. SV40 Pseudovirion gene delivery of a toxin to treat human adenocarcinomas in mice. *Cancer Gene Ther.* **2006**, *13*, 648–657. [[CrossRef](#)]
148. Chou, M.-I.; Hsieh, Y.-F.; Wang, M.; Chang, J.; Chang, D.; Zouali, M.; Tsay, G.J. In vitro and in vivo targeted delivery of IL-10 interfering RNA by JC virus-like particles. *J. Biomed. Sci.* **2010**, *17*, 51. [[CrossRef](#)]
149. Lu, X.; Thompson, J.R.; Perry, K.L. Encapsulation of DNA, a protein and a fluorophore into virus-like particles by the capsid protein of cucumber mosaic virus. *J. Gen. Virol.* **2012**, *93*, 1120–1126. [[CrossRef](#)]
150. Barwal, I.; Kumar, R.; Kateriya, S.; Dinda, A.K.; Yadav, S.C. Targeted delivery system for cancer cells consist of multiple ligands conjugated genetically modified CCMV capsid on doxorubicin GNPs complex. *Sci. Rep.* **2016**, *6*, 37096. [[CrossRef](#)]
151. Enomoto, T.; Kawano, M.; Fukuda, H.; Sawada, W.; Inoue, T.; Haw, K.C.; Kita, Y.; Sakamoto, S.; Yamaguchi, Y.; Imai, T.; et al. Viral protein-coating of magnetic nanoparticles using simian virus 40 VP1. *J. Biotechnol.* **2013**, *167*, 8–15. [[CrossRef](#)] [[PubMed](#)]
152. Li, F.; Zhang, Z.-P.; Peng, J.; Cui, Z.-Q.; Pang, D.-W.; Li, K.; Wei, H.-P.; Zhou, Y.-F.; Wen, J.-K.; Zhang, X.-E. Imaging Viral Behavior in Mammalian Cells with Self-Assembled Capsid-Quantum-Dot Hybrid Particles. *Small* **2009**, *5*, 718–726. [[CrossRef](#)] [[PubMed](#)]
153. Chen, C.; Daniel, M.-C.; Quinkert, Z.T.; De, M.; Stein, B.; Bowman, V.D.; Chipman, P.R.; Rotello, V.M.; Kao, C.C.; Dragnea, B. Nanoparticle-Templated Assembly of Viral Protein Cages. *Nano Lett.* **2006**, *6*, 611–615. [[CrossRef](#)] [[PubMed](#)]
154. Goicochea, N.L.; De, M.; Rotello, V.M.; Mukhopadhyay, S.; Dragnea, B. Core-like Particles of an Enveloped Animal Virus Can Self-Assemble Efficiently on Artificial Templates. *Nano Lett.* **2007**, *7*, 2281–2290. [[CrossRef](#)]
155. Johnson, J.E.; Speir, J.A. Quasi-equivalent viruses: A paradigm for protein assemblies. *J. Mol. Biol.* **1997**, *269*, 665–675. [[CrossRef](#)]
156. Biddlecome, A.; Habte, H.H.; McGrath, K.M.; Sambanthamoorthy, S.; Wurm, M.; Sykora, M.M.; Knobler, C.M.; Lorenz, I.C.; Lasaro, M.; Elbers, K.; et al. Delivery of self-amplifying RNA vaccines in in vitro reconstituted virus-like particles. *PLoS ONE* **2019**, *14*, e0215031. [[CrossRef](#)]